

Proceedings to the 23<sup>rd</sup> Workshop  
**What Comes Beyond the  
Standard Models**

Bled, July 4–12, 2020

**[Virtual Workshop ]  
[July 6.–10. 2020]**

**Volume 2: Further Talks And  
Scientific Debuts**

Edited by

Norma Susana Mankoč Borštnik

Holger Bech Nielsen

Dragan Lukman

---

**The 23rd Workshop *What Comes Beyond the Standard Models*,  
4.– 12. July 2020, Bled  
[ Virtual Workshop, 6.–10. July 2020 ]  
Volume 2: Further Talks And Scientific Debuts**

**was organized by**

*Society of Mathematicians, Physicists and Astronomers of Slovenia*

**and sponsored by**

*Department of Physics, Faculty of Mathematics and Physics, University of Ljubljana*

*Society of Mathematicians, Physicists and Astronomers of Slovenia*

*Beyond Semiconductor (Matjaž Breskvar)*

*VIA (Virtual Institute of Astroparticle Physics), Paris*

*MDPI journal "Symmetry", Basel*

*MDPI journal "Physics", Basel*

*MDPI journal "Universe", Basel*

**Scientific Committee**

*John Ellis, King's College London / CERN*

*Roman Jackiw, MIT*

*Masao Ninomiya, Yukawa Institute for Theoretical Physics, Kyoto University*

**Organizing Committee**

*Norma Susana Mankoč Borštnik*

*Holger Bech Nielsen*

*Maxim Yu. Khlopov*

The Members of the Organizing Committee of the International Workshop "What Comes Beyond the Standard Models", Bled, Slovenia, state that the articles published in the Proceedings to the 23<sup>rd</sup> Workshop "What Comes Beyond the Standard Models", Bled, Slovenia are refereed at the Workshop in intense in-depth discussions.

## Workshops organized at Bled

- ▷ *What Comes Beyond the Standard Models*
  - (June 29–July 9, 1998), Vol. **0** (1999) No. 1
  - (July 22–31, 1999)
  - (July 17–31, 2000)
  - (July 16–28, 2001), Vol. **2** (2001) No. 2
  - (July 14–25, 2002), Vol. **3** (2002) No. 4
  - (July 18–28, 2003) Vol. **4** (2003) Nos. 2-3
  - (July 19–31, 2004), Vol. **5** (2004) No. 2
  - (July 19–29, 2005), Vol. **6** (2005) No. 2
  - (September 16–26, 2006), Vol. **7** (2006) No. 2
  - (July 17–27, 2007), Vol. **8** (2007) No. 2
  - (July 15–25, 2008), Vol. **9** (2008) No. 2
  - (July 14–24, 2009), Vol. **10** (2009) No. 2
  - (July 12–22, 2010), Vol. **11** (2010) No. 2
  - (July 11–21, 2011), Vol. **12** (2011) No. 2
  - (July 9–19, 2012), Vol. **13** (2012) No. 2
  - (July 14–21, 2013), Vol. **14** (2013) No. 2
  - (July 20–28, 2014), Vol. **15** (2014) No. 2
  - (July 11–19, 2015), Vol. **16** (2015) No. 2
  - (July 11–19, 2016), Vol. **17** (2016) No. 2
  - (July 9–17, 2017), Vol. **18** (2017) No. 2
  - (June 23–July 1, 2018), Vol. **19** (2018) No. 2
  - (July 6–14, 2019), Vol. **20** (2019) No. 2
  - (July 6–10, 2020), Vol. **21** (2020) No. 1
  - (July 6–10, 2020), Vol. **21** (2020) No. 2
- ▷ *Hadrons as Solitons* (July 6–17, 1999)
- ▷ *Few-Quark Problems* (July 8–15, 2000), Vol. **1** (2000) No. 1
- ▷ *Selected Few-Body Problems in Hadronic and Atomic Physics* (July 7–14, 2001), Vol. **2** (2001) No. 1
- ▷ *Quarks and Hadrons* (July 6–13, 2002), Vol. **3** (2002) No. 3
- ▷ *Effective Quark-Quark Interaction* (July 7–14, 2003), Vol. **4** (2003) No. 1
- ▷ *Quark Dynamics* (July 12–19, 2004), Vol. **5** (2004) No. 1
- ▷ *Exciting Hadrons* (July 11–18, 2005), Vol. **6** (2005) No. 1
- ▷ *Progress in Quark Models* (July 10–17, 2006), Vol. **7** (2006) No. 1
- ▷ *Hadron Structure and Lattice QCD* (July 9–16, 2007), Vol. **8** (2007) No. 1
- ▷ *Few-Quark States and the Continuum* (September 15–22, 2008), Vol. **9** (2008) No. 1
- ▷ *Problems in Multi-Quark States* (June 29–July 6, 2009), Vol. **10** (2009) No. 1
- ▷ *Dressing Hadrons* (July 4–11, 2010), Vol. **11** (2010) No. 1
- ▷ *Understanding hadronic spectra* (July 3–10, 2011), Vol. **12** (2011) No. 1
- ▷ *Hadronic Resonances* (July 1–8, 2012), Vol. **13** (2012) No. 1
- ▷ *Looking into Hadrons* (July 7–14, 2013), Vol. **14** (2013) No. 1
- ▷ *Quark Masses and Hadron Spectra* (July 6–13, 2014), Vol. **15** (2014) No. 1
- ▷ *Exploring Hadron Resonances* (July 5–11, 2015), Vol. **16** (2015) No. 1
- ▷ *Quarks, Hadrons, Matter* (July 3–10, 2016), Vol. **17** (2016) No. 1

#### IV

- ▷ *Advances in Hadronic Resonances* (July 2–9, 2017), Vol. **18** (2017) No. 1
- ▷ *Double-charm Baryons and Dimesons* (June 17–23, 2018), Vol. **19** (2018) No. 1
- ▷ *Electroweak Processes of Hadrons* (July 15–19, 2019), Vol. **20** (2019) No. 1
- ▷
  - *Statistical Mechanics of Complex Systems* (August 27–September 2, 2000)
  - *Studies of Elementary Steps of Radical Reactions in Atmospheric Chemistry* (August 25–28, 2001)

# Contents

Preface to Volume 2 in English and Slovenian Language .....	VII
Preface in English and Slovenian Language .....	XIII
Further Talks .....	1
<b>1 The Concept of Cosmological Inflation and the Origin of 3+1-dimensional Space-Time in a Universe Consisting of Conserved Vacuum Domains</b> <i>E. Dmitrieff</i> .....	1
<b>2 Neutrino Masses and Mixing Within a SU(3) Family Symmetry Model with Five Sterile Neutrinos</b> <i>A. Hernandez-Galeana</i> .....	11
<b>3 Dark Matter Macroscopic Pearls, 3.55 keV X-Ray Line, How Big ?</b> <i>H.B. Nielsen and C.D. Froggatt</i> .....	28
Scientific Debuts .....	75
<b>4 Problems of the Correspondence Principle for the Recombination Cross Section in Dark Plasma</b> <i>K. Belotsky, E. Esipova, D. Kalashnikov and A. Letunov</i> .....	77
<b>5 Neutrino Cooling Effect of Primordial Hot Areas in Dependence on its Size</b> <i>K.M. Belotsky, M.M. El Kasmi and S.G. Rubin</i> .....	84
<b>6 Consideration of a Loop Decay of Dark Matter Particle into Electron-Positron from Point of View of Possible FSR Suppression</b> <i>K. M. Belotsky and A.Kh. Kamaletdinov</i> .....	90
<b>7 Theoretical Indication of a Possible Asymmetry in Gamma-Radiation Between Andromeda Halo Hemispheres Due to Compton Scattering on Electrons From Their Hypothetical Sources in the Halo</b> <i>K.M. Belotsky, E.S. Shlepkina and M.L. Soloviev</i> .....	97
<b>8 Numerical Simulation of Dark Atom Interaction With Nuclei</b> <i>T.E. Bikbaev, M.Yu. Khlopov and A.G. Mayorov</i> .....	105

<b>9 Anihelium Flux From Antimatter Globular Cluster</b> <i>M.Yu. Khlopov, A.O. Kirichenko and A.G. Mayorov</i> . . . . .	118
<b>10 Domain Walls and Strings Formation in the Early Universe</b> <i>A.A. Kirillov and B. S. Murygin</i> . . . . .	128
<b>11 The Interaction of Domain Walls with Fermions in the Early Universe</b> <i>A.A. Kurakin and S.G. Rubin</i> . . . . .	134
<b>12 Cosmological Accumulation of Conserved Numbers in Kaluza-Klein Theories</b> <i>V.V. Nikulin</i> . . . . .	141
<b>13 Sub-Planckian Evolution of the Universe</b> <i>P.M. Petriakova</i> . . . . .	149
<b>14 The "Dark Disk" Model in the Light of DAMPE Experiment</b> <i>M.L. Solov'yov, M.A. Rakhimova and K.M. Belotsky</i> . . . . .	156
<b>15 Dynamical Evolution of a Cluster of Primordial Black Holes</b> <i>V.D. Stasenko and A. A. Kirillov</i> . . . . .	162
<b>Poem by Astri Kleppe</b> . . . . .	169
<b>16 Earth</b> <i>Astri Kleppe</i> . . . . .	171

## Preface to Volume 2 in English and Slovenian Language

The series of annual workshops on “What Comes Beyond the Standard Models?” started in 1998 with the idea of Norma and Holger for organizing a real workshop, in which participants would spend most of the time in discussions, confronting different approaches and ideas. Workshops have taken place in the picturesque town of Bled by the lake of the same name, surrounded by beautiful mountains and offering pleasant walks and mountaineering and very fruitful discussions.

This year 2020 we still had a workshop in July, but without personal conversations all day and late at night, even between very relaxing walks and mountaineering, due to COVID-19 pandemic. We have, however, a very long tradition of video-conferences (cosmovia), enabling discussions and explanations and exchanging informations and knowledge with laboratories all over the world. This enables us to have this year the total virtual workshop, resembling Bled workshops as much as possible.

The “cosmovia” way of workshop enabled more students to participate. Correspondingly the organizers decided to publish two volumes. In this second volume mostly students contributions and those contributions of invited speakers, which arrived the very last moment, are published. We inform the reader that the preface to Volume 1 contains a short information about topics from elementary fermion and boson fields and cosmology, presented and discussed in this year workshop. It appears in this volume after this preface.

In up to this year, the long presentations, with breaks and continuations over several days, followed by very detailed discussions, have led to very pedagogical presentations, clarifying the assumptions and the conclusions. Although “cosmovia” way of workshops worked optimally, enabling discussions almost day and night, internet discussions can not at all replace personal discussions. This year we have not succeeded to prepare the discussion section, representing the common work of participants initiated by discussions. The interactions among the participants were not efficient enough.

We present in what follows several questions, proposals and doubts, which remain unanswered during the workshop, or having not real response yet. We hope that all the participants — invited speakers and students — will try to participate in looking for the answers, new explanations, new ideas, proofs, doubts, questions, numerical evaluations, by exchanging emails up to the next year.

All the participants are welcome to add their own questions, proposals, doubts, etc. We shall publish the results of the common work during the year in the next year proceedings. We shall also take care that all the participants will receive questions, proposals, etc.

i. Many a contribution discusses the primordial black holes. This topic was triggered by gravitational wave signal, seemingly merging from black holes with masses of around 150 Solar masses or less.

The questions arises: i.a. What is the primordial time? In what position the universe was at the primordial time? With massless ordinary fermions and antifermions interacting with massless ordinary vector gauge fields, or with massive quarks and leptons and with all higher massive families included, as predicted by the spin-charge-family theory after the electroweak phase transition? The higher dimensions, if existing, remained compactified or the theories with higher dimensions, remaining compactified, are not the correct ones? i.b. What causes inflation? i.c. How does the inhomogeneity of the universe with ordinary matter generate the black holes?

ii. The spin-charge-family theory starts in  $d \geq (13 + 1)$  with gravity only — with the vielbeins and the two kinds of the spin connecting fields — manifesting in  $d = (3 + 1)$  all the known vector and scalar gauge fields and with massless family of fermions manifesting in  $(3 + 1)$  the families of quarks and leptons and predicting the fourth family to the existing three, the dark matter, the matter-antimatter asymmetry, the proton decay, new scalar fields, and many other prediction. This theory, starting with very simple starting action, needs no additional assumptions, no additional gauge groups, no additional gauge fields, scalar or vector ones, to explain observed properties of phenomena. Can the predictions be accurate enough to help experimentalists to measure them, like the mass of the fourth family of quarks and leptons, the properties of Yukawa couplings and higgs scalars? Do the proposals with additional groups and additional quarks and leptons relate the spin-charge-family theory? How do the Kaluza-Klein-like theories cause phase transitions if starting in  $d = \infty$  or any other dimension?

iii. What is the dark matter made of? iii.a The lowest of the four families, decoupled from the observed ones, like in the spin-charge-family theory, or they are dark stars with the properties of almost black holes? Or they are a new phase of the vacuum of ordinary quarks and antiquarks captured in bubbles? What interactions do make such bubbles possible? iii.b. What is the decay rate of the dark matter particles in any of the proposed dark matter model? Can any of proposals for dark matter explain the cosmic positron anomaly and all other cosmic measurements?

iv. What are indeed black holes? If there are singularities inside a black hole what is the status of fermions and fields inside the black hole? Do they make phase transitions into massless state within the black hole, loosing identity they have in  $d = (3 + 1)$ ? Do we really understand black holes inside the the horizon?

v. If the odd Clifford algebra explains the Dirac's second quantization postulates, what else can we learn out of the talk presented in this workshop? What consequences does the proposal bring for both standard models?

vi. Can one relate the model in which universe consists of closed packed vacuum domains and the models with proposed actions, presented in this workshop?

Having a poet among us we kindly asked her to offer us a poem. Thanks Astri, we publish for each volume one of your poems.  
May be our participants can up to next year translate your poems in the language of their countries.

Let us conclude this preface by thanking cordially and warmly to all the participants, present through the teleconferences at the Bled workshop, for their excellent presentations and also, in spite of all, for really fruitful discussions.

*Norma Mankoč Borštnik, Holger Bech Nielsen, Maxim Y. Khlopov,  
(the Organizing committee)*

*Norma Mankoč Borštnik, Holger Bech Nielsen, Dragan Lukman,  
(the Editors)*

*Ljubljana, December 2020*

## Predgovor k drugemu zvezku zbornika

Vsakoletne delavnice z naslovom „Kako preseči oba standardna modela, kozmološkega in elektrošibkega“ (“What Comes Beyond the Standard Models?”) sta postavila leta 1998 Norma in Holger z namenom, da bi udeleženci v izčrpnih diskusijah kritično soočali različne ideje in teorije. Delavnice domujejo v Plemljevi hiši na Bledu ob slikovitem jezeru, kjer prijetni sprehodi in pohodi na čudovite gore, ki kipijo nad mestom, ponujajo priložnosti in vzpodbudo za diskusije. Tudi to leto je bila delavnica v juliju, vendar nam je tokrat covid-19 onemogočil srečanje v Plemljevi hiši. Tudi diskutirali nismo med hojo okoli jezera ali med hribolazenjem. Vendar nam je dolgoletna izkušnja s “cosmovio” — videopovezavami z laboratoriji po svetu — omogočila, da je tudi letos stekla Blejska delavnica, tokrat prek interneta.

Uporaba sistema “Cosmovia” je omogočila udeležbo veliko večjemu številu študentov. Organizatorji so se zato odločili da zbornik delavnice izdajo v dveh delih. V tem drugem delu so v glavnem prispevki študentov, pa tudi prispevki, ki sodijo v prvi zbornik, a smo jih dobili v zadnjem trenutku. Predgovor k prvemu zvezku zbornika vsebuje kratek pregled vseh tem, o katerih je tekla beseda na letošnji delavnici, s področij osnovnih fermionskih in bozonskih polj in kozmologije. V tem zvezku sledi temu predgovoru predgovor prvega zvezka.

V dosedanjih delavnicah so dolge predstavitve del, s premori in nadaljevanji preko več dni, ki so jim sledile izčrpane diskusije, vodile do zelo pedagoških razlag, ki so pomagale razumeti predpostavke in zaključke prispevkov. Četudi je cosmovia poskrbela, da so diskusije tekle ves čas, tako kot je bilo na vseh delavnicah doslej, blejskih diskusij v živo diskusije po internetu niso mogle nadomestiti. To leto nam ni uspelo pripraviti razdelka z diskusijami, ki bi predstavile skupna dela udeležencev, ki so se začela z diskusijami. Razprave na daljavo niso bile dovolj učinkovite.

Zato ponujamo vprašanja, predloge in dvome, ki so med delavnico ostali neodgovorjeni, ali pa nanje ni bilo pravih odzivov. Upamo, da bodo vsi udeleženci — vabljeni predavatelji in študenti — poskusili sodelovati v iskanju odgovorov, novih razlag, idej, dokazov, dvomov, vprašanj in numeričnih izračunov, preko izmenjave elektronskih sporočil do naslednjega leta.

Vsi udeleženci so vabljeni, da dodajo svoja lastna vprašanja, predloge, dvome itd. Orgnizatorji jih bomo posredovali vsem. Nastala skupna dela pa bomo objavili v naslednjem zborniku.

i. Veliko je prispevkov na temo “prvotne črne luknje”, ki naj bi pojasnili izmerjene gravitacijske valove in ki se domnevno sproščajo pri zlitju črnih lukenj z masami okrog 150 sončevih mas.

Pojavijo se številna vprašanja: i.a. Kaj je “prvotni čas”, čas nastanka teh črnih

lukenj? V kakšnem stanju je bilo tedaj vesolje? Je to čas po elektrošibkem faznem prehodu vesolja, ali je bilo to pred tem faznim prehodom, ko so imeli (običajni) fermioni in antifermioni maso nič in so imela tudi vsa bozonska polja maso nič. Ali pa so pri nastanku teh črnih lukenj bili aktivni tudi stabilni hadroni masivnih kvarkov in leptonov druge gruče štirih družin, ki jih napove teorija spinov-nabojev-družin? So dimenzije, večje kot  $(3 + 1)$ , če obstajajo, ostale kompaktificirane, in ali so modeli z več kot  $(3 + 1)$  dimenzijami sploh ponudijo pravi opis našega vesolja? i.b. Kaj povzroča inflacijo? i.c. Kako nehomogenost vesolja z masivnimi kvarki in antikvarki ustvari črne luknje?

ii. Teorija spinov-nabojev-družin postavi preprosto akcijo, v kateri fermioni z maso nič interagirajo samo z gravitacijo v  $d \geq (13 + 1)$  — s tetradami in z dvema vrstama polj spinskih povezav — kar se v  $d = (3 + 1)$ -razsežnem prostoru času manifestira kot vsa poznana vektorska in skalarna umeritvena polja ter kot brezmasna družina fermionov, ki jih po elektrošibkem prehodu izmerimo kot masivne družine kvarkov in leptonov. Teorija napove obstoj četrte družine  $k$  znanim trem, temno snov, asimetrijo snov-antisnov, razpad protona, nova skalarna polja. Teorija, ki začne z zelo preprosto akcijo, ne potrebuje dodatnih prepostavk, dodatnih umeritvenih grup ali polj, skalarnih ali vektorskih za razlago opaženih lastnosti in pojavov. Ali lahko ponudi dovolj natančne napovedi, da bi eksperimenti potrdili napovedane mase četrte družine kvarkov in leptonov, lastnosti Yukawinih sklop-itev in higgsovega skalarja? Ali so predlogi z dodatnimi grupami in dodatnimi kvarki in leptoni povezani s teorijo spinov-nabojev-družin? Kaj sproži fazne prehode v teorijah Kaluza-Kleinovega tipa z  $d = \infty$  ali s kakšno drugo dimenzijo, denimo  $d = (13 + 1)$ ??

iii. Iz česa je temna snov? iii.a Ali je to najnižja od štirih družin, ki ni sklopljena z opaženimi, kot je to v teoriji spinov-nabojev-družin, ali pa so to temne zvezde, ki imajo lastnosti skoraj črnih lukenj? Ali je morda to nova faza vakuumu z običajnimi kvarki in antikvarki, ki so ujetih v mehurčkih? Katere lastnosti interakcij omogočajo obstoj takšnih mehurčkov? iii.b. Kakšna je stopnja razpada delcev temne snovi v predlaganih modelih? Ali lahko predlogi za temno snov pojasnijo anomalijo kozmičnih pozitronov?

iv. Kaj so v resnici črne luknje? Če so znotraj črnih lukenj singularnosti, kaj se zgodi s fermioni in polji znotraj črne luknje? Ali znotraj črne luknje preidejo v brezmasno stanje in izgubijo identiteto, ki jo imajo v  $d = (3 + 1)$ ? Ali v resnici razumemo črne luknje znotraj njihovega horizonta?

v. Če lahko Cliffordova algebra pojasni Diracove postulate za drugo kvantizacijo, kaj drugega se še lahko naučimo iz predavanj na tej delavnici? Kakšna spoznanja prinaša predstavljen predlog druge kvantizacije za oba standardna modela?

vi. Kako lahko vzporedimo predlog modela, da vesolje tvorijo vakuumske domene, ki so povsod goste, z modeli, ki gradijo na dinamiki fermionov in bozonov, ki jih določa akcija?

Prosili smo pesnico med nami, da popestri zbornik s pesmijo. Hvala Astri za obe pesmi, ki ju bodo morda udeleženci prevedli v jezik svoje dežele.

Naj zaključimo ta predgovor s prisrčno in toplo zahvalo vsem udeležencem, prisotnim preko videokonference, za njihova predavanja in še posebno za zelo plodne diskusije in kljub vsemu odlično vzdušje.

*Norma Mankoč Borštnik, Holger Bech Nielsen, Maxim Y. Khlopov,  
(Organizacijski odbor)*

*Norma Mankoč Borštnik, Holger Bech Nielsen, Dragan Lukman,  
(uredniki)*

*Ljubljana, grudna (decembra) 2020*

## Preface

The series of annual workshops on “What Comes Beyond the Standard Models?” started in 1998 with the idea of Norma and Holger for organizing a real workshop, in which participants would spend most of the time in discussions, confronting different approaches and ideas. Workshops have taken place in the picturesque town of Bled by the lake of the same name, surrounded by beautiful mountains and offering pleasant walks and mountaineering. This year 2020 we still had a workshop in July, but without personal conversations all day and late at night, even between very relaxing walks and mountaineering due to COVID-19 pandemic. We have, however, a very long tradition of videoconferences (cosmovia), enabling discussions and explanations with laboratories all over the world. This enables us to have this year the total virtual workshop, resembling Bled workshops as much as possible.

In our very open minded, friendly, cooperative, long, tough and demanding discussions several physicists and even some mathematicians have contributed. Most of topics presented and discussed in our Bled workshops concern the proposals how to explain physics beyond the so far accepted and experimentally confirmed both standard models — in elementary particle physics and cosmology — in order to understand the origin of assumptions of both standard models and be consequently able to propose new theories, models and to make predictions for future experiments.

Although most of participants are theoretical physicists, many of them with their own suggestions how to make the next step beyond the accepted models and theories, experts from experimental laboratories were and are very appreciated, helping a lot to understand what do measurements really tell and which kinds of predictions can best be tested.

The (long) presentations (with breaks and continuations over several days), followed by very detailed discussions, have been extremely useful, at least for the organizers. We hope and believe, however, that this is the case also for most of participants, including students. Many a time, namely, talks turned into very pedagogical presentations in order to clarify the assumptions and the detailed steps, analyzing the ideas, statements, proofs of statements and possible predictions, confronting participants’ proposals with the proposals in the literature or with proposals of the other participants, so that all possible weak points of the proposals, those from the literature as well as our own, showed up very clearly. The ideas therefore seem to develop in these years considerably faster than they would without our workshops.

This year neither the cosmological nor the particle physics experiments offered much new, as also has not happened in the last two years, which would offer new insight into the elementary particles and fields and also into cosmological events, although a lot of work and effort have been put in, and although there are some indications for the existence of the fourth family to the observed three, due to the fact that the existence of the fourth family might explain the existing experimental data better, what is mentioned in this proceedings, as we did in the last year proceedings. Also the newest analyses of the data from LHC and other experiments has not changed the situation much. Of particular interest is the observed gravitational waves signal triggered by black holes of around 150 solar masses. These measurements are of the central interest of many a contribution in this proceedings.

However, there are more and more cosmological evidences, which require the new step beyond the standard model of the elementary fermion and boson fields. Understanding the universe through the cosmological theories and theories of the elementary fermion and boson fields, have, namely, so far never been so dependent on common knowledge and experiments in both fields.

We are keeping expecting that new cosmological experiments and new experiments in laboratories together will help to resolve the open questions in both fields.

On both fields there appear proposals which should explain assumptions of these models. Most of them offer small steps beyond the existing models. The competition, who will have right, is open.

The new data might answer the question, whether laws of nature are elegant (as predicted by the spin-charge-family theory and also — up to the families — other Kaluza-Klein-like theories and the string theories) or “she is just using gauge groups when needed” (what many models assume, also some presented in this proceedings). Can the higgs scalars and the Yukawa couplings be guessed by small steps from the standard model case, or they originate in gravity in higher dimensions as also the vector and scalar gauge fields do?

Is there only gravity as the interacting field, which manifests in the low energy regime all the vector gauge fields as well as the scalar fields, those observed so far and those predicted by the spin-charge-family theory, with the scalar colour triplets included? Should correspondingly gravity be a quantized field like all the vector and the scalar gauge fields — possibly resulting from gravity — are?

Is masslessness of all the bosons and fermions, with scalar bosons included, essential, while masses appear at low energy region due to interactions and breaks of symmetries? Do the observed fermion charges indeed origin from spins of fermions in higher dimensions? What is then the dimension of space-time? Infinite, or it emerges from zero? One of contributions discusses also this problem. Does “nature use” odd Clifford algebra to describe fermions, what leads to anticommutation relations for second quantized fermions, explaining the Dirac’s postulates, making already the creation operators for single fermion state anticommuting?

What “forces” fermions to appear in families? How many families do we have and what is their relation to the observed ones? What are reasons for breaking symmetries — discrete, global and local? Is The Lorentz invariant really violated? Does

the symmetry between fermions and antifermions manifest also in the presence of gravity?

Do the baryons of the stable family, decoupled from the observed ones, and predicted by the spin-charge-family theory (or can follow from heterotic string model), contribute to the dark matter? Do new stable quarks constitute neutral particles like neutrons, or form negatively charged particles, bound with primordial helium in dark atoms? How close are the additional new fermions, added to quarks and leptons of the standard model "by hand", to the stable fifth family of the spin-charge-family theory? Are also the charged "nucleons" of OHe's atoms explainable with the stable nucleons of the fifth family? Is the dark matter explainable within the standard model? Or does the dark matter manifest in dark stars, which are a kind of black holes?

What are indeed the black holes? If they ought to be created in the primordial time during the inflation (early matter stages or phase transitions), what kind of fermions and antifermions should contribute to the creation of black holes, massless (that is before the electroweak transition) or massive? What did cause the inflation? If there are singularities inside a black hole what is the status of fermions and fields inside the black hole? Do they make phase transitions into massless state within the black hole, losing identity they have in  $d = (3 + 1)$ ? Do we really understand black holes inside the horizon?

We discussed these and many other open topics during Bled workshop 2020. Like it is the new idea of theory of strings, represented by particle objects, which do not develop in time.

The DAMA/LIBRA experiment convinced us again that the group in Gran Sasso do measure the dark matter particles scattering on the nuclei of their measuring apparatus. It is expected that sooner or later other laboratories will confirm the DAMA/LIBRA results. This has not yet happened and our discussions clarified the reasons for that.

Although cosmology served the discussions all the time (and we are very glad that we did have in spite of pandemic the 23<sup>rd</sup> workshop), it was not like previous workshops. Discussions were fiery and sharp, at least during some talks. But this was not our Bled workshop. Effective discussions require the personal presence of the debaters, as well as of the rest of participants, which interrupt the presentations with questions all the time. As students need personal discussions with a good teacher, Internet discussions can never replace the real one.

Let us point out that we still succeeded to discuss the open problems on present understanding of the elementary particle physics and cosmology in the fully online regime, trying to save the most important feature of Bled Workshops - their free streaming discussion resulting in the comprehensive view on the discussed phenomena and ideas.

And let us add that due to the on line presentations we have students participants, who otherwise would not be able to attend the Bled conference, the travel expenses are too high for them. Their presentations are published in the second part of the proceedings, together with the invited talks, which came at the very last moment. The organizers strongly hope that next year the covid-19 will be defeated, this is the hope for the whole world, for the young generation in particular and for all

of us, with the Bled workshop 2021 included. Let us meet at Bled! (This year's experience made us to think on more practical videoconferencing tools, like Zoom to facilitate extension of our discussions online.)

Since, as every year, also this year there has been not enough time to mature the discussions into the written contributions, only two months, authors can not really polish their contributions. Organizers hope that this is well compensated with fresh contents.

Questions and answers as well as lectures enabled by M. Yu. Khlopov via Virtual Institute of Astroparticle Physics ([viavca.in2p3.fr/site.html](http://viavca.in2p3.fr/site.html)) of APC have in ample discussions helped to resolve many dilemmas. Google Analytics, showing more than 242 thousand visits to this site from 154 countries, indicates world wide interest to the problems of physics beyond the Standard models, discussed at Bled Workshop. At XXIII Bled Workshop VIA streaming made possible to webcast practically all the talks.

The reader can find the records of all the talks delivered by cosmovia since Bled 2009 on [viavca.in2p3.fr/site.html](http://viavca.in2p3.fr/site.html) in Previous - Conferences.

Most of the talks can be found on the workshop homepage

<http://bsm.fmf.uni-lj.si/>.

Having a poet among us, we kindly asked Astri to contribute a poem for our proceedings. It is our pleasure that she did listen us and send two poems. We publish both, in each volume one.

Let us conclude this preface by thanking cordially and warmly to all the participants, present through the teleconferences at the Bled workshop, for their excellent presentations and also, in spite of all, for really fruitful discussions.

*Norma Mankoč Borštnik, Holger Bech Nielsen, Maxim Y. Khlopov,  
(the Organizing committee)*

*Norma Mankoč Borštnik, Holger Bech Nielsen, Dragan Lukman,  
(the Editors)*

*Ljubljana, December 2020*

## Predgovor (Preface in Slovenian Language)

Vsakoletne delavnice z naslovom „Kako preseči oba standardna modela, kozmološkega in elektrošibkega“ (“What Comes Beyond the Standard Models?”) sta postavila leta 1998 Norma in Holger z namenom, da bi udeleženci v izčrpnih diskusijah kritično soočali različne ideje in teorije. Delavnice domujejo v Plemljevi hiši na Bledu ob slikovitem jezeru, kjer prijetni sprehodi in pohodi na čudovite gore, ki kipijo nad mestom, ponujajo priložnosti in vzpodbudo za diskusije. Tudi to leto je bila delavnica v juliju, vendar nam je tokrat covid-19 onemogočil srečanje v Plemljevi hiši. Tudi diskutirali nismo med hojo okoli jezera ali med hribolazenjem. Vendar nam je dolgoletna iskušnja s “cosmovio” — videopovezavami z laboratoriji po svetu — omogočila, da je tudi letos stekla Blejska delavnica, tokrat prek interneta.

K našim zelo odprtim, prijateljskim, dolgim in zahtevnim diskusijam, polnim iskrivega sodelovanja, je prispevalo veliko fizikov in celo nekaj matematikov. V večini predavanj in razprav so udeleženci poskusili razumeti in pojasniti predpostavke obeh standardnih modelov, elektrošibkega in barvnega v fiziki osnovnih delcev ter kozmološkega, predpostavke in napovedi obeh modelov pa vskladiti z meritvami in opazovanji, da bi poiskali model, ki preseže oba standardna modela, kar bi omogočilo zanesljivejše napovedi za nove poskuse.

Čeprav je večina udeležencev teoretičnih fizikov, mnogi z lastnimi idejami kako narediti naslednji korak onkraj sprejetih modelov in teorij, so še posebej dobrodošli predstavniki eksperimentalnih laboratorijev, ki nam pomagajo v odprtih diskusijah razjasniti resnično sporočilo meritev in nam pomagajo razumeti kakšne napovedi so potrebne, da jih lahko s poskusi dovolj zanesljivo preverijo.

Organizatorji moramo priznati, da smo se na blejskih delavnicah v (dolgih) predstavitev (z odmori in nadaljevanji preko več dni), ki so jim sledile zelo podrobne diskusije, naučili veliko, morda več kot večina udeležencev. Upamo in verjamemo, da so veliko odnesli tudi študentje in večina udeležencev. Velikokrat so se predavanja spremenila v zelo pedagoške predstavitve, ki so pojasnile predpostavke in podrobne korake, soočile predstavljene predloge s predlogi v literaturi ali s predlogi ostalih udeležencev ter jasno pokazale, kje utegnejo tīčati šibke točke predlogov. Zdi se, da so se ideje v teh letih razvijale bistveno hitreje, zahvaljujoč prav tem delavnicam.

Tako kot v preteklih dveh letih tudi to leto niso eksperimenti v kozmologiji in fiziki osnovnih fermionskih in bozonskih polj ponudili rezultatov, ki bi omogočili nov vpogled v fiziko osnovnih delcev in polj, čeprav je bilo vanje vloženega veliko truda in četudi razberemo iz eksperimentov, da četrta družina  $k$  že izmerjenim trem mora biti, saj lahko s štirimi družinami lažje pojasnimo izmerjene podatke, kar je omenjeno tudi v tem zborniku.

Tudi zadnje analize rezultatov merjenj na LHC in drugih merilnikih niso pripomogle k boljšemu razumevanju naravnih zakonov v fiziki osnovnih delcev in kozmologiji. Posebno pozornost so vzbudile meritve gravitacijskih valov, ki so jih povzročile črne luknje z masami okoli 150 sončnih mas. Prav te meritve poskušajo razložiti nekateri prispevki v letošnjem zborniku.

Vse več je tudi kozmoloških meritev, za katere se zdi, da jih standardni model osnovnih fermionski in bozonskih polj ne more pojasniti. Še nikoli doslej niso bili predlogi za kozmološke teorije in iskanje nove teorije v fiziki osnovnih polj tako zelo soodvisne od poizkusov in razumevanja predpostavk na obeh področjih.

Pričakujemo, da bodo kozmološka merjenja in meritve v laboratorijih pomagala razrešiti odprta vprašanja na obeh področjih. Na obeh področjih je predlogov za novo teorijo čedalje več, vendar velika večina teh predlogov ponuja majhna odstopanja od standardnih modelov. Tekma, kdo ima prav, je odprta.

Nove meritve bodo morda kmalu ponudile odgovor na vprašanje, ali so naravni zakoni elegantni (kot napoveduje teorija spina-naboja-družin in tudi druge teorije Kaluze in Kleina, vendar brez družin in ne tako "udarno") ali pa "narava uporabi grupe, ki in ko jih ravno potrebuje" (kar predlaga velika večina modelov, tudi nekateri v tem zborniku). Ali je smotno pojav Higgsovega skalarnega polja in Yukawinih sklopitvev dodati k standardnemu modelu osnovnih delcev kot dodatno polje, ki ga zahtevajo poskusi, ali pa je v resnici skalarnih polj več, njihov izvor pa je gravitacijsko polje v razsežnostih  $d > (3 + 1)$ ?

So vsa osnovna fermionska in bozonska polj, tudi skalarna, brezmasna in je njihova masa, ki jo merimo pri nizkih energijah, posledica sil in zlomitve simetrij? Ali izvirajo naboji fermionov, ki jih izmerimo pri nizkih energijah, v spinih, ki jih ti fermioni nosijo v  $d > (3 + 1)$ ? Kaj tedaj prostor in čas v resnici pomenita? Sta neskončna, ali pa se rodita iz nič? Ali "narava uporabi" liho Clifordovo algebro za opis fermionov, kar zagotovi antikomutacijske relacije med kreacijskimi in anihilacijskimi operatorji že med enofermionskimi stanji, kar pojasni Diracove postulate za fermione v drugi kvantizaciji? Kaj "prisili" fermione, da se pojavijo v družinah? Koliko je družin kvarkov in leptonov in kako so povezani, če sploh, z izmerjenimi tremi družinami? Kaj povzroči zlomitev simetrij, diskretnih, globalnih, lokalnih? Ali je Lorentzova simetrija zlomljena in če je, pod kakšnimi pogoji se zlomi? Ali je simetrija med fermioni in antifermioni v gravitacijskem polju zlomljena?

Kaj so gradniki temne snovi? Ali so barioni družin, ki niso sklopljene z izmerjenimi družinami kvarkov in leptonov in jih napove teorija spina-nabojev-družin, del temne snovi v vesolju? Ali se lahko novi fermioni, ki jih dodajo k kvarkom in leptonom standardnega modela osnovnih fermionskih in bozonskih polj, dajo pojasniti s stabilnimi barioni, ki jih napove teorija spina-nabojev-družin? So tudi temna jedra atoma O-He-lija člani stabilne družine? Se da temna snov pojasniti s skupki kvarkov in leptonov standardnega modela? Ali pa k temni snovi prispevajo temne zvezde, ki imajo lastnosti črnih lukenj?

Kaj pa so v resnici črne luknje? Če so nastajale ob inflaciji, kakšni fermioni in antifermioni so sodelovali pri nastanku črnih lukenj, z maso nič (to je pred elektrošibkim faznim prehodom) ali z neničelnimi masami? Kaj je povzročilo inflacijo? Če ima črna luknja singularnost, kako se spremenijo lastnosti fermionov in an-

tifermionov znotraj črne luknje? Ali izgubijo lastnosti, ki so jih imeli v  $d = (3 + 1)$ -razsežnem prostoru? Ali razumemo, kaj se dogaja v črni luknji znotraj horizonta? Ta in še marsikatera druga vprašanja smo načeli v času Blejske delavnice 2020. Denimo kot to, da v novi teoriji strun, ki jo sestavljajo točkasti delci, čas sploh ne nastopa.

Meritve DAMA/LIBRA v Gran Sassu so nas znova prepričale, da so delci, ki se sipljejo na atomskih jedrih merilcev in ki skozi leto periodično spreminjajo svojo intenzivnost, delci temne snovi. Pričakujemo, da bo laboratorijem po svetu, ki poskušajo potrditi njihove meritve, prej ali slej to tudi uspelo. Vprašanja in odgovori so pomagali razumeti, zakaj nobenemu doslej potrditev še ni uspela.

Četudi je cosmovia poskrbela, da so diskusije tekle ves čas, tako kot je bilo na vseh delavnicah doslej, blejskih diskusij v živo diskusije po internetu niso mogle nadomestiti. Diskusije so bile ognjevit in ostre, vsaj pri nekaterih predavanjih, vendar potrebujejo učinkovite diskusije osebno prisotnost diskutantov in poslušalcev, ki z vprašanji poskrbijo, da je debata razumljiva vsem. Tudi študentom internet ne more nadomestiti dobrega učitelja.

Poudariti je potrebno, da nam je kljub temu uspela dokaj plodna diskusija o tem, kako dobro razumemo danes obe področji, fiziko osnovnih delcev in polj ter dinamiko našega vesolja. In dodajmo, da je delavnica preko interneta omogočila študentom aktivno in plodno sodelovanje, ki bi se ga v živo zaradi stroškov potovanja ne mogli udeležiti.

Študentski prispevki so zbrani v drugem zborniku Blejske delavnice, skupaj s prispevki vabljenih predavateljev, katerih prispevke smo prejeli zadnji trenutek. Organizatorji upamo, da bo naslednje leto virus premagan, naše upanje velja za ves svet, za mlado generacijo pa še posebej, pa tudi za Blejsko delavnico 2021, da bo stekla v živo na Bledu.

Ker je vsako leto le malo časa od delavnice do zaključka redakcije, manj kot dva meseca, avtorji ne morejo dovolj skrbno pripraviti svojih prispevkov, vendar upamo, da to nadomesti svezina prispevkov.

Bralec najde zapise vseh predavanj, objavljenih preko "cosmovia" od leta 2009, na [viauca.in2p3.fr/site.html](http://viauca.in2p3.fr/site.html) v povezavi Previous - Conferences. Večino predavanj najde bralec na spletni strani delavnice na <http://bsm.fmf.uni-lj.si/>.

Prosili smo Astri, da nam pošlje kako od svojih pesmi. Prijazno nam je ugodila in poslala dve. Objavljamo obe, v vsakem zborniku po eno.

Naj zaključimo ta predgovor s prisrčno in toplo zahvalo vsem udeležencem, prisotnim preko videokonference, za njihova predavanja in še posebno za zelo plodne diskusije in kljub vsemu odlično vzdušje.

*Norma Mankoč Borštnik, Holger Bech Nielsen, Maxim Y. Khlopov,  
(Organizacijski odbor)*

*Norma Mankoč Borštnik, Holger Bech Nielsen, Dragan Lukman,  
(uredniki)*

*Ljubljana, grudna (decembra) 2020*



## **Further Talks**

All talk contributions are arranged alphabetically with respect to the authors' names.





# 1 The Concept of Cosmological Inflation and the Origin of $3 + 1$ -dimensional Space-Time in a Universe Consisting of Conserved Vacuum Domains

E. Dmitrieff \*

Irkutsk State University

**Abstract.** We start from the assumption that the universe is a dense filling of small (Planck-scale or so) vacuum domains. Also we postulate that the total count of these domains is mostly conserved, but there are no strong restrictions on the coordination number of domains in their mutual packing. The dimensions count of such a universe is not predetermined but is defined by its characteristic coordination numbers.

We found out that under these conditions, the universe size, counted by inter-domain hops, falls down exponentially along with growth of dimension count, defined by the coordination number. The universe formed by hypercubic grid with more than 6 dimensions becomes microscopic and therefore causal connected.

Therefore the backward process of lowering the dimension count can be considered as a kind of exponential inflation that may start from two domains-sized universe, having hundreds of dimensions, and practically freeze down between 4 and 3 dimensions because of huge emergent sizes and local causality.

We explored dense packing in 2, 3 and 4 dimensions and found out that 4-dimensional flat torus with three ordinary and one maximally compactified dimensions pretends to be energetically optimal. So it can correspond to the true vacuum. The discreteness of domains does not allow the compactified dimension to collapse completely, so its length can not be less than two domains.

Our results show that such a spontaneous break of dimension symmetry in a tessellation of electrically charged domains slightly violates CP symmetry, leaving CPT symmetry conserved, and could explain the difference in properties of photons and gluons by corresponding symmetry break from 4 to  $3+1$  colors.

**Povzetek.** Avtor privzame, da vesolje sestavlja gosto pokritej majhnih (reda Planckove skale) vakuumskih območij, da se celotno število domen približno ohranja in da tudi njihova oblika in s tem "koordinacijska števila", ki določajo dimenzijo vesolja, niso strogo predpisani.

Avtor ugotovi, da pri teh pogojih velikost vesolja, ki je definirana s številom skokov med domenami, eksponentno pada z večanjem števila dimenzij. Vesolje, ki ga tvori hiperkubična mreža z več kot 6 dimenzijami, postane mikroskopsko in zato vzročno povezano.

Obraten proces, to je zniževanje dimenzij vesolja, vidi avtor kot eksponentno inflacijo vesolja, ki začne z dvema domenama in z nekaj sto dimenzijami in zamrzne med dimenzijama 3 in 4 kot zelo razsežno in lokalno vzročno povezano vesolje.

---

\* E-mail: elia@sr.isu.ru

V prispevku avtor predstavi gosto pakiranje domen v dimenzijah 2, 3 in 4 ter zaključi, da se zdi energijsko optimalen ploski 4-dimenzionalni torus s tremi običajnimi dimenzijami in eno maksimalno kompaktificirano. Zaradi diskretnosti domen se kompaktificirana dimenzija ne more zmanjšati na manj kot dve domeni.

Avtor oceni, da takšna spontana zlomitev dimenzij v teselaciji električno nabitih domen vodi k rahli kršitvi simetrije CP, ohranja pa simetrijo CPT. Zaključi, da njegov pristop morda pojasni zlomitev barvne simetrije na gluonsko in fotonsko.

Keywords: tessellation approach, dimension decay, cosmological inflation, causality, flat torus, satori

PACS: 02.40.Sf, 02.70.-c, 04.50.Gh, 04.60.Nc, 12.60.-i, 98.80.Bp, 98.80.Jk

## 1.1 Methodics

Speculating about physics and cosmology beyond Standard Models, we follow the concept of '*universe as a tessellation*'. The word *universe* here means an artificial mathematical and computational model. We build it, starting with a set of initial assumptions or axioms. Then, we explore the consequences and compare whether they have suitable correspondences in the real Universe.

### 1.1.1 Axioms

The assumptions that we start with in the tessellation approach, are the following:

1. **We treat the physical vacuum, and the universe as whole, as dense and (almost) regular filling of small vacuum domains.**

Here we neither assume existence of space or time of any kind, nor dimension count; neither of fluctuating fields of different types, nor of gravity, quanta, relativity, nor topology.

We just assume that there are domains, they are small enough to be particle's constituents, and they can neither completely overlap each other, nor mutually penetrate, so they form a sort of tessellation or bubble foam.

Each particular domain shares some walls with several other neighbor domains. These walls between domains emerge because domains do not overlap. However, *domain walls* with limited curvature could be postulated, instead of domains, as principal entities. In this case, domains would emerge on sides of walls.

2. **Vacuum domains have electrical charge either  $+\frac{\epsilon}{6}$  or  $-\frac{\epsilon}{6}$ .**

The magnitude is chosen to be  $\pm\frac{1}{6}e$ , to be able to reproduce the electrical charges and other quantum numbers of fundamental particles, as combinations of the domains.

According to the postulate, *each domain carry one bit* of information.

This assumption can be formulated with the dual way: Each domain carry one bit of information. So there are two kinds of domains.

The electrical charge of any sample taken emerges as a numerical difference between counts of domains of one kind and of another kind in this sample.

In case of principal walls in the first assumption, the second one would postulate that *some of walls are oriented*. Positive and negative domains emerge on different opposite sides of oriented wall.

### 1.1.2 Higgs field

Hereby, the scalar potential of the electric charge density, introduced above, pretends to be the real-valued Higgs-like field. It is non-zero almost everywhere, excepting walls. Inside domains, it keeps near or equal to either positive or negative constant with the same magnitude.

Suppose that two domains, either of equal charges, or of opposite charges, get closer to each other. So they would penetrate or overlap. Their electrical charge densities would interfere, and the electrical potential would fall or rise by the magnitude, getting away from the optimal constant.

According to the first assumption, these domains would pull back, towards the stable equilibrium point. We can treat it as rising of effective energy on both sides of positive and negative optimal values. So the function of effective energy must be at least fourth-power polynomial, looking like Higgs field  $V(\phi)$ .

Using the Higgs field vacuum expectation value, we estimate the domain size that appears to be about  $10^{-21}$  m.

### 1.1.3 Particles

We found out that these two assumptions are quite enough to represent all the known fundamental particles with correct quantum numbers [1].

While the pure vacuum is supposed to be a regular alternation of domain of both kinds, the cases of violations of periodicity could be treated as some particles.

In other words, particles are anti-structure defects of periodical tessellation, or bound states of them.

### 1.1.4 Particle formulas

Using equivalence between bits and domains, we can write particle formulas as clusters of several bits.

Note that these bit clusters are *not* bit *strings* that represent integers in computers. The mutual arrangement of bits is significant as well as mutual arrangement of defects among domains.

So the bit formulas for particles must be structural, like formulas of organic compounds in chemistry.

### 1.1.5 Non-particle excitations in tessellation

In addition to particle defects, other types of excitation can exist in this model, for example, in the form of compression, displacement, and torsion waves, which could be identified, for instance, with gravitational waves or dark matter.

### 1.1.6 Dimension count

Following the conception defined above, we introduce the space dimension count  $d$  as a function of count of walls, shared with domain's neighbors, average or exact.

If there are 2 neighbors, then the emergent space is one-dimensional; 3 to 6 neighbors is a characteristic of two-dimensional space. Three dimensions appear when there are 6 to 14 neighbors, four in case of 26 or some more.

So the dimension count is emergent, not fixed, determined by the average coordination number, that is a count of the nearest neighbors, that is a characteristic of particular tessellation.

In case of domains rearrangement, the coordination number, and therefore, the dimension count can change. Various configurations can have different effective energy, so some of them can be stable, meta-stable, or unstable. Non-stable domain configurations, rearranging into more stable ones with change of the neighbor count can also change the dimension count. It may be called the *dimension decay*.

### 1.1.7 Universe size

As a *distance* between two domains we consider the minimal count of inter-domain walls to be crossed on a way from one domain to another.

As the *universe size*  $L$  we treat the maximal distance between any pair of domains.

### 1.1.8 Assumption of domain count conservation

In current study, we introduce an additional assumption that **the total count of domains in the universe is strictly or mostly fixed**, i.e. processes of their formation and destruction are suppressed or absent and we can treat domain count as a constant.

We show that this assumption leads to the consequence, that the size of universe depend on the number of dimensions exponentially.

We suppose that the maximal number of dimensions can be achieved in the model having the topology of a multidimensional simplex: each domain would be a neighbor of all the others, so universe size would be 1.

But already in the case of a hypercube built from the same number of domains as the number of domains ( $10^{-21}$  m in size) in the Universe of about  $10^{10}$  light years, the maximum number of dimensions is only about 468, while such a 468-dimensional universe has a size of about  $10^{-20}$  m.

Rearrangement of domains with a decrease in dimension count leads to an increase in linear sizes, but only at 6 dimensions the universe becomes macroscopic, of the order of 0.1 mm.

A further decrease in dimensions is accompanied by an exponential increase in linear size to about 100 km at  $d = 5$  and to about 1000 astronomical units at  $d = 4$ .

In this step, there happens a loss of correlation between different parts of the universe, which, apparently, has been kept until this time: we have no reason to believe that the speed of oscillations that determines light speed in multidimensional structures should be significantly lower.

The last decay of 4-dimensional space into 3-dimensional, or compactification of one dimension with the formation of a flat torus, leads to the formation of a

universe of modern size. Further decay into the usual 3-dimensional, or 2- or 1-dimensional space, most likely, is energetically disadvantageous, since it is the four-dimensional space that offers the best saving of cross-domain walls with 26 neighbors.

## 1.2 Calculations

In a tessellation universe with some particular  $d$  there will be  $N$  repetitions of the elementary translation unit in each of  $d$  dimensions.

Suppose as first, that the  $N$ s are the same in all  $d$  dimensions, so it is a hypercube with the edge of  $N$  domains along it. Then, the total amount of domains

$$C = N^d \quad (1.1)$$

In case  $N$ s are different, i.e. there are  $N_0 \neq N_1$ , etc, the shape is a hyperrectangle, and

$$C = \prod_{n=0}^{d-1} N_n \quad (1.2)$$

But let us examine just the simplest and realistic hyper-cubic case.

Following the assumption that  $C = \text{const}$ , we evaluate this constant using the approximation of the Universe size  $L$  (20 billions light year):

First, we express universe size as a power of 2 (we use this basis because of simplicity of formulas for hypercubic grids):

$$L = 20 \times 10^9 \text{ years} \times 3 \cdot 10^8 \frac{\text{m}}{\text{s}} \times 365 \frac{1}{4} \times 24 \times 60 \times 60 \frac{\text{s}}{\text{year}} \approx 2 \cdot 10^{26} \text{ m} \approx 2^{87} \text{ m}. \quad (1.3)$$

And we use  $d = 3$  as a dimension count of our Universe.

The universe volume  $V_U$  thus will be of order  $L^3$ , i.e.

$$V_U \approx 2^{261} \text{ m}^3. \quad (1.4)$$

Also, we use the inter-domain size  $l$ , that is twice of the domain radius.

If domain sizes are at the Planck scale, it will be about

$$l_{\text{Planck}} = 10^{-34} \text{ m} \approx 2^{-113} \text{ m}. \quad (1.5)$$

If our hypothesis of the Higgs and Coloumb field Unity (HCU) is correct, the domains will be about

$$l_{\text{HCU}} = 10^{-21} \text{ m} \approx 2^{-70} \text{ m}. \quad (1.6)$$

So the volume of one domain is supposed to be

$$V_d = (10^{-34})^3 = 10^{-102} \text{ m}^3 \approx 2^{-339} \text{ m}^3 (\text{Planck}), \quad (1.7)$$

$$V_d = (10^{-21})^3 = 10^{-63} \text{ m}^3 \approx 2^{-209} \text{ m}^3 (\text{HCU}) \quad (1.8)$$

Then, dividing the universe volume by the domain volume, we get the domain count:

$$C_{\text{Planck}} = \frac{V_U}{V_d} = 2^{261+339} = 2^{600} (\text{Planck}), \quad (1.9)$$

$$C_{\text{HCU}} = \frac{V_U}{V_d} = 2^{261+209} = 2^{470} (\text{HCU}). \quad (1.10)$$

Since  $C$  is supposed to be conserved through  $d$ -changing decays, we can get  $N$  for any given dimension count  $d$ :

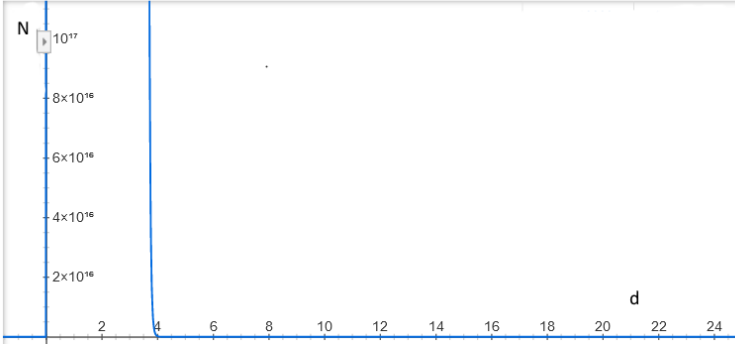
$$N = C^{\frac{1}{d}} \quad (1.11)$$

Multiplying with the domain diameter  $l$ , we get universe size:

$$L = N \times l = C^{\frac{1}{d}} \times l \quad (1.12)$$

For HCU domains with  $l = 2^{-70} \text{m}$  it gives

$$L = N \times l = 2^{\frac{470}{d}} \times 2^{-70} = 2^{\frac{470}{d}-70} (\text{m}). \quad (1.13)$$



Since  $N$  is discrete (it is a count of domains in particular direction), it can not be less than 2:  $N \geq 2$ . Thus,

$$N = C^{\frac{1}{d_{\max}}} = C_{\text{Planck}}^{\frac{1}{d_{\max}}} \geq 2 \rightarrow 2^{\frac{600}{d_{\max}}} > 2^1, \quad (1.14)$$

so  $d_{\max} \leq 600$  with Planck-size domains, or  $d_{\max} \leq 470$  with larger HCU domains.

In the extreme case, when  $d = d_{\max}$ , the universe would consist of *only one* translation unit, so it would be not periodical, it would not be a tessellation at all, but it would be just a single polytope.

However, it would be very good connected, all the parts would be correlated, since the sizes are small, there are at most 600 hops from any domain in the universe to anyone else, and the Euclidean distance is not greater than  $\sqrt{600} \approx 25$ .

All above is correct for hyper-cubic tessellations and polytopes. In case of simplex polytopes (triangle, tetrahedron and so on), the count of dimensions is not so strictly limited, it can rise almost to infinity, up to  $d = C$ .

But we consider only hyper-cubic tessellations, not simplex polytopes, since all known generalized Kelvin's problem's candidate solutions, that are optimal packed tessellations, as we have shown, could be produced from hyper-cubic grids by linear shifts, conserving most of their properties, including the parity.

So the estimations above (with minor corrections) can be applied to the bee honeycomb, Kelvin and Weaire-Phelan structures as well as to 4-dimensional Satori structure.

Now we can calculate the sizes (in meters) for the hyper-cubic universe of any dimension count.

For instance, for  $d = 6$  with HCU domains:

$$L = N \times l = 2^{\frac{470}{6} - 70} \text{m} = 2^8 \text{m} = 256\text{m}. \quad (1.15)$$

$d = 5$  gives

$$L = N \times l = 2^{\frac{470}{5} - 70} \text{m} = 2^{24} \text{m} = 16000\text{km}. \quad (1.16)$$

6-dimensional universe with Planck-sized domains will be

$$L = N \times l = 2^{\frac{600}{6} - 113} \text{m} = 2^{-13} \text{m} \approx 0.1\text{mm}, \quad (1.17)$$

while 5-dimensional universe's size

$$L = N \times l = 2^{\frac{600}{5} - 113} \text{m} = 2^7 \text{m} = 128\text{km}. \quad (1.18)$$

### 1.3 Clifford flat torus

The distribution or alternation of domains is presumably determined by minimizing the energy of their neighboring contact with each other.

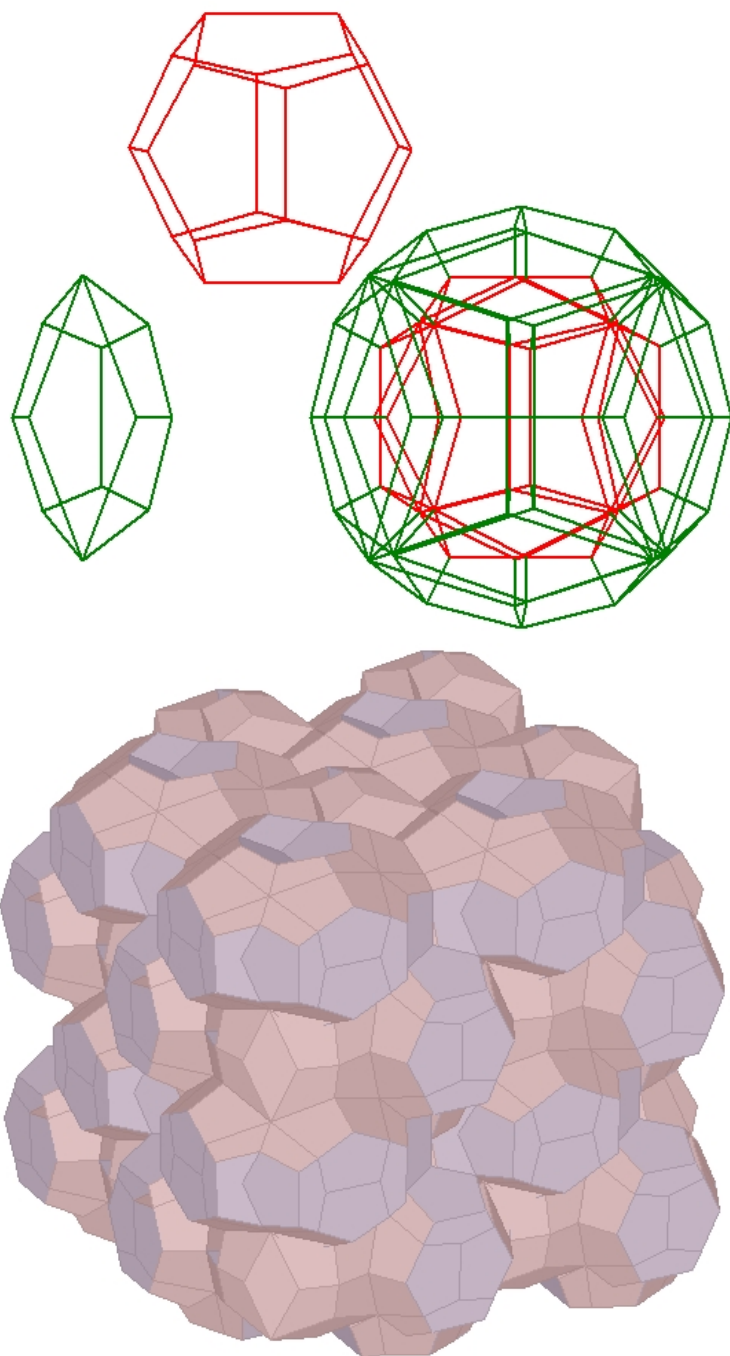
Therefore, we mainly consider tessellations that are solutions or candidates for solutions to the Kelvin's problem of optimal packing [3].

To work with a four-dimensional space, or with spaces of higher dimensions, as well as to get rid of a pre-selected dimension count, we proposed an approach to measure the economy of filling [4], which is independent of the dimension count and is based on comparison with the corresponding simple hypercubic lattice.

Thus, we have made possible the generalized formulation of the Kelvin's problem, in which the search for the optimal filling is not limited to three-dimensional space.

Instead, the dimension of space appears along with the solution of the problem, as a characteristic of space, in which this solution can be nested.

The four-dimensional structure that we found and named 'Satori', is a candidate solution for the generalized Kelvin's problem. Like the three-dimensional candidate solution of Weaire and Phelan (which offers a bit less economy), the Satori structure is chiral, and it offers CPT symmetry.



Applying the principle of energy minimization to the Satori structure with anti-structural defects, we found out that the favorable topology for the model is the four-dimensional Clifford torus with a period of one translation unit.

The result is 'almost' three-dimensional space, having one additional compactified dimension, the radius of which is emergently fixed. Only in this case it

is possible to have defects whose energy is zero, which corresponds to massless particles like photons and neutrinos.

In the absence of compactification or when compactification occurs not in one but in two or more periods, such defects would be massive and the space as a whole would decay by strengthening compactification up to a minimum of one period.

Since the three-dimensional torus is not flat but curved, the same compactification in more than one dimension is likely energetically prohibited due to the curvature energy.

We consider the gluon chain termination with quarks as another way to reduce energy instead of looping the chain.

Considering the structure of Satori in the topology of such a torus, we find that it turns out to be **oriented** along a compactified dimension: all four three-dimensional layers that form the centers of cells or domains are different.

Thus, if we consider these layers as phases of the oscillation of a three-dimensional structure, this oscillation will have the appearance of directional rotation, in which four different phases are ordered in turn, and the two possible directions of sequencing are different.

In this case, the movement of individual domains occurs in such a way that each domain can either rotate in place or move along the remaining three dimensions. However, there is no difference between the two cases due to the fact that the domains are indistinguishable from each other and it is impossible to say which domain is spinning in place and which one is moving. The foregoing relates to the Satori structure with a compactified dimension in the absence of defects. In the case of defects existing in it, a difference in the electric charge appears, and such a defect can either move or spin or alternate one both way of moving. A domain cannot remain in place, since at different phases the same place is occupied by domains of different signs.

Thus, when passing from layer to layer, the defect undergoes bifurcation. An exception is when the defect moves along the model with the highest possible speed. In this case, there are no rotational transitions. This behavior of defects allows us to identify it with the motion of particles, for which, with approaching the speed of light, increased half-life is observed, which is usually associated with a slowdown in own time. In our model, the own time of a particle turns out to be a phenomenon associated with branching during the movement of the corresponding defect in a vacuum undergoing directed oscillations: the amount of own time is determined by the fraction of branching at which the choice is not determined.

## References

1. E.G. Dmitrieff: Experience in modeling properties of fundamental particles using binary codes, in: N.S. Mankoč Borštnik, H.B.F. Nielsen, D. Lukman: Proceedings to the 19th Workshop 'What Comes Beyond the Standard Models', Bled, 11. - 19. July 2016.
2. E.G. Dmitrieff: On triple-periodic electrical charge distribution as a model of physical vacuum and fundamental particles, in: N.S. Mankoč Borštnik, H.B.F. Nielsen, D. Luk-

man: Proceedings to the 21th Workshop 'What Comes Beyond the Standard Models', Bled, 23. - 29. June 2018

3. D. Weaire et al., The Kelvin Problem, Taylor & Francis, 1996.

4. E.G.Dmitrieff: Tessellation approach

in modeling properties of physical vacuum and fundamental particles, in: N.S. Mankoč Borštnik, H.B.F. Nielsen, D. Lukman: Proceedings to the 22nd Workshop 'What Comes Beyond the Standard Models', Bled, July 6-14, 2019



## 2 Neutrino Masses and Mixing Within a SU(3) Family Symmetry Model with Five Sterile Neutrinos

A. Hernandez-Galeana \*

Departamento de Física, ESFM - Instituto Politécnico Nacional.  
U. P. "Adolfo López Mateos". C. P. 07738, Ciudad de México, México

**Abstract.** Within a broken SU(3) local family symmetry, we study neutrino masses and mixing in a framework with five sterile neutrinos.

In this BSM, ordinary heavy fermions, top and bottom quarks and tau lepton, become massive at tree level from **Dirac See-saw** mechanisms implemented by the introduction of a new set of SU(2)<sub>L</sub> weak singlet vector-like fermions, U, D, E, N, with N a sterile neutrino. Right handed neutrinos are introduced to cancel anomalies.

We provide a parameter space region where this framework can account for the neutrino masses ( $m_1 = 0.00584795$ ,  $m_2 = 0.0104888$ ,  $m_3 = 0.051461$ ,  $m_4 = 1.21534$ ,  $m_5 = 2604.12$ ,  $m_6 = 2643.36$ ,  $m_7 = 9.97002 \times 10^6$ ,  $m_8 = 1.00658 \times 10^7$ ) eV, the squared neutrino mass differences  $m_2^2 - m_1^2 = 7.58162 \times 10^{-5}$  eV<sup>2</sup>,  $m_3^2 - m_2^2 = 2.53822 \times 10^{-3}$  eV<sup>2</sup>, and  $m_4^2 - m_1^2 = 1.47441$  eV<sup>2</sup>. We also report the corresponding ( $U_{PMNS}$ )<sub>4×8</sub> lepton mixing matrix.

**Povzetek.** Avtor pojasnjuje obstoj družin v modelu, v katerem doda grupam standardnega modela grupo SU(3). V prispevku obravnava mase nevtrinov s petimi sterilnimi nevtrini.

Avtor doda običajnim kvarkom in leptonom še dva kvarka (U, D) in dva leptona (E, N), vsi so šibki vektorski singleti SU(2)<sub>L</sub>. Maso kvarkov b in t in leptona tau določi Diracov "mehanizem **see-saw**" že na drevesnem nivoju. N je sterilni nevtrino. Anomalije odpravi tako, da uvede še desnoročne nevtrine.

V izbranem območju parametrov modela izračuna nevtrinske mase ( $m_1 = 0.00584795$ ,  $m_2 = 0.0104888$ ,  $m_3 = 0.051461$ ,  $m_4 = 1.21534$ ,  $m_5 = 2604.12$ ,  $m_6 = 2643.36$ ,  $m_7 = 9.97002 \times 10^6$ ,  $m_8 = 1.00658 \times 10^7$ ) eV) in kvadrate masnih razlik ( $m_2^2 - m_1^2 = 7.58162 \times 10^{-5}$  eV<sup>2</sup>,  $m_3^2 - m_2^2 = 2.53822 \times 10^{-3}$  eV<sup>2</sup> in  $m_4^2 - m_1^2 = 1.47441$  eV<sup>2</sup>). Navede tudi pripadajočo leptonsko mešalno matriko ( $U_{PMNS}$ )<sub>4×8</sub>.

Keywords: Quark and lepton masses and mixing, Flavor symmetry,  $\Delta F = 2$  Processes.

Pacs: 14.60.Pq, 12.15.Ff, 12.60.-i

### 2.1 Introduction

The origin of the hierarchy of fermion masses and mixing continue being one of the most important open problems in particle physics. In this report we address

\* E-mail: ahernandez@ipn.mx

the problem of generating neutrino masses and mixing within the framework of a broken  $SU(3)$  gauged family symmetry model [1,2].

This framework introduce a hierarchical mass generation mechanism in which light fermions become massive from radiative corrections, mediated by the massive gauge bosons associated to the  $SU(3)$  family symmetry that is spontaneously broken, while the masses of the top and bottom quarks as well as for the tau lepton, are generated at tree level from "Dirac See-saw" mechanisms implemented by the introduction of a new set of  $SU(2)_L$  weak singlets  $U, D, E$  and  $N$  vector-like fermions, with  $N$  a neutral lepton. In addition this BSM introduce three right handed neutrinos in order to cancel anomalies. Therefore, we have a scenario with five "Standard Model"(SM) singlet "sterile neutrinos" and three active L-handed neutrinos, that is a 3+5 scenario.

Previous theories addressing the problem of quark and lepton masses and mixing with spontaneously broken  $SU(3)$  gauge symmetry of generations include the ones with chiral  $SU(3)$  family symmetry [3]- [6], as well as other  $SU(3)$  family symmetry proposals [7]- [10]

Neutrinos are one of the most exciting areas of research. Cosmology and Short Baseline Oscillation experiments hint the possible existence of light sterile neutrinos. For recent studies of neutrino masses, including sterile neutrinos, see for instance [11]- [14]

## 2.2 $SU(3)$ family symmetry model

The model is based on the gauge symmetry

$$G \equiv SU(3) \otimes SU(3)_C \otimes SU(2)_L \otimes U(1)_Y \quad (2.1)$$

where  $SU(3)$  is a completely vector-like and universal gauged family symmetry. That is, the corresponding gauge bosons couple equally to Left and Right Handed ordinary Quarks and Leptons, with  $g_H, g_s, g$  and  $g'$  the corresponding coupling constants. The content of fermions assumes the standard model quarks and leptons:

$$\Psi_q^o = (3, 3, 2, \frac{1}{3})_L \quad , \quad \Psi_l^o = (3, 1, 2, -1)_L \quad (2.2)$$

$$\Psi_u^o = (3, 3, 1, \frac{4}{3})_R \quad , \quad \Psi_d^o = (3, 3, 1, -\frac{2}{3})_R \quad , \quad \Psi_e^o = (3, 1, 1, -2)_R \quad (2.3)$$

where the last entry is the hypercharge  $Y$ , with the electric charge defined by  $Q = T_{3L} + \frac{1}{2}Y$ .

The model includes two types of extra fermions: Right Handed Neutrinos:  $\Psi_{\nu_R}^o = (3, 1, 1, 0)_R$ , introduced to cancel anomalies [7], and a new family of  $SU(2)_L$  weak singlet vector-like fermions: Vector like quarks  $U_L^o, U_R^o = (1, 3, 1, \frac{4}{3})$  and  $D_L^o, D_R^o = (1, 3, 1, -\frac{2}{3})$ , Vector Like electrons:  $E_L^o, E_R^o = (1, 1, 1, -2)$ , and New Sterile Neutrinos:  $N_L^o, N_R^o = (1, 1, 1, 0)$ .

The particle content and gauge symmetry assignments are summarized in Table 2.1. Notice that all SU(3) non-singlet fields transform as the fundamental representation under the SU(3) symmetry.

	SU(3)	SU(3) <sub>c</sub>	SU(2) <sub>L</sub>	U(1) <sub>Y</sub>
$\psi_q^0$	3	3	2	$\frac{1}{3}$
$\psi_{uR}^0$	3	3	1	$\frac{4}{3}$
$\psi_{dR}^0$	3	3	1	$-\frac{2}{3}$
$\psi_l^0$	3	1	2	-1
$\psi_{eR}^0$	3	1	1	-2
$\psi_{\nu R}^0$	3	1	1	0
$U_{L,R}^0$	1	3	1	$\frac{4}{3}$
$D_{L,R}^0$	1	3	1	$-\frac{2}{3}$
$E_{L,R}^0$	1	1	1	-2
$N_{L,R}^0$	1	1	1	0
$\Phi^u$	3	1	2	-1
$\Phi^d$	3	1	2	+1
$\eta_1, \eta_2$	3	1	1	0

Table 2.1: Particle content and charges under the gauge symmetry

### 2.3 SU(3) family symmetry breaking

SU(3) family symmetry is broken spontaneously by heavy SM singlet scalars  $\eta_1 = (3, 1, 1, 0)$  and  $\eta_2 = (3, 1, 1, 0)$  in the fundamental representation of SU(3), with the "Vacuum Expectation Values" (VEV's):

$$\langle \eta_1 \rangle^T = (\Lambda_1, 0, 0) \quad , \quad \langle \eta_2 \rangle^T = (0, \Lambda_2, 0) . \quad (2.4)$$

It is worth to mention that these two scalars in the fundamental representation is the minimal set of scalars to break down completely the SU(3) family symmetry.

The interaction of the SU(3) gauge bosons to the SM massless fermions is

$$i\mathcal{L}_{\text{int}, \text{SU}(3)} = g_H (f_1^0, f_2^0, f_3^0) \gamma_\mu \begin{pmatrix} \frac{Z_1^\mu}{2} + \frac{Z_2^\mu}{2\sqrt{3}} & \frac{Y_1^{+\mu}}{\sqrt{2}} & \frac{Y_2^{+\mu}}{\sqrt{2}} \\ \frac{Y_1^{-\mu}}{\sqrt{2}} & -\frac{Z_2^\mu}{\sqrt{3}} & \frac{Y_3^{+\mu}}{\sqrt{2}} \\ \frac{Y_2^{-\mu}}{\sqrt{2}} & \frac{Y_3^{-\mu}}{\sqrt{2}} & -\frac{Z_1^\mu}{2} + \frac{Z_2^\mu}{2\sqrt{3}} \end{pmatrix} \begin{pmatrix} f_1^0 \\ f_2^0 \\ f_3^0 \end{pmatrix} \quad (2.5)$$

where  $g_H$  is the SU(3) coupling constant,  $Z_1, Z_2$  and  $Y_j^\pm = \frac{Y_j^1 \mp iY_j^2}{\sqrt{2}}$ ,  $j = 1, 2, 3$  are the eight gauge bosons.

Thus, the contribution to the horizontal gauge boson masses from the VEV's of Eq.(2.4) read

- $\langle \eta_1 \rangle$ :  $\frac{g_H^2 \Lambda_1^2}{2} (Y_1^+ Y_1^- + Y_2^+ Y_2^-) + \frac{g_H^2 \Lambda_1^2}{4} (Z_1^2 + \frac{Z_2^2}{3} + 2Z_1 \frac{Z_2}{\sqrt{3}})$
- $\langle \eta_2 \rangle$ :  $\frac{g_H^2 \Lambda_2^2}{2} (Y_1^+ Y_1^- + Y_3^+ Y_3^-) + g_H^2 \Lambda_2^2 \frac{Z_2^2}{3}$

The ‘‘Spontaneous Symmetry Breaking’’ (SSB) of SU(3) occurs in two stages

$$\text{SU}(3) \times G_{\text{SM}} \xrightarrow{\langle \eta_2 \rangle} \text{SU}(2) \times G_{\text{SM}} \xrightarrow{\langle \eta_1 \rangle} G_{\text{SM}} \quad (2.6)$$

**FCNC ?**

Notice that the hierarchy of scales  $\Lambda_2 > \Lambda_1$  yield an ‘‘approximate SU(2) global symmetry’’ in the spectrum of SU(2) gauge boson masses of order  $g_H \Lambda_1$ .

Therefore, neglecting tiny contributions from electroweak symmetry breaking, the gauge boson masses read

$$(M_1^2 + M_2^2) Y_1^+ Y_1^- + M_1^2 Y_2^+ Y_2^- + M_2^2 Y_3^+ Y_3^- + \frac{1}{2} M_1^2 Z_1^2 + \frac{1}{2} \frac{M_1^2 + 4M_2^2}{3} Z_2^2 + \frac{1}{2} (M_1^2) \frac{2}{\sqrt{3}} Z_1 Z_2 \quad (2.7)$$

$$M_1^2 = \frac{g_H^2 \Lambda_1^2}{2}, \quad M_2^2 = \frac{g_H^2 \Lambda_2^2}{2} \quad (2.8)$$

	Z <sub>1</sub>	Z <sub>2</sub>
Z <sub>1</sub>	M <sub>1</sub> <sup>2</sup>	$\frac{M_1^2}{\sqrt{3}}$
Z <sub>2</sub>	$\frac{M_1^2}{\sqrt{3}}$	$\frac{M_1^2 + 4M_2^2}{3}$

Table 2.2: Z<sub>1</sub> – Z<sub>2</sub> mixing mass matrix

Diagonalization of the Z<sub>1</sub> – Z<sub>2</sub> squared mass matrix yield the eigenvalues

$$M_-^2 = \frac{2}{3} \left( M_1^2 + M_2^2 - \sqrt{(M_2^2 - M_1^2)^2 + M_1^2 M_2^2} \right) \quad (2.9)$$

$$M_+^2 = \frac{2}{3} \left( M_1^2 + M_2^2 + \sqrt{(M_2^2 - M_1^2)^2 + M_1^2 M_2^2} \right) \quad (2.10)$$

and finally

$$(M_1^2 + M_2^2) Y_1^+ Y_1^- + M_1^2 Y_2^+ Y_2^- + M_2^2 Y_3^+ Y_3^- + M_-^2 \frac{Z_-^2}{2} + M_+^2 \frac{Z_+^2}{2}, \quad (2.11)$$

where

$$\begin{pmatrix} Z_1 \\ Z_2 \end{pmatrix} = \begin{pmatrix} \cos \phi & \sin \phi \\ -\sin \phi & \cos \phi \end{pmatrix} \begin{pmatrix} Z_- \\ Z_+ \end{pmatrix} \quad (2.12)$$

$$\cos \phi \sin \phi = \frac{\sqrt{3}}{4} \frac{M_1^2}{\sqrt{M_1^4 + M_2^2(M_2^2 - M_1^2)}} \quad (2.13)$$

## 2.4 Electroweak symmetry breaking

The ‘‘Electroweak Symmetry Breaking’’ (EWSB) is achieved by the Higgs fields  $\Phi_i^u$  and  $\Phi_i^d$ , which transform simultaneously as triplets under SU(3) and as Higgs doublets with hypercharges  $-1$  and  $+1$  under the SM, respectively, explicitly:

$$\Phi^u = \begin{pmatrix} \begin{pmatrix} \phi^o \\ \phi^- \end{pmatrix}_1^u \\ \begin{pmatrix} \phi^o \\ \phi^- \end{pmatrix}_2^u \\ \begin{pmatrix} \phi^o \\ \phi^- \end{pmatrix}_3^u \end{pmatrix}, \quad \Phi^d = \begin{pmatrix} \begin{pmatrix} \phi^+ \\ \phi^o \end{pmatrix}_1^d \\ \begin{pmatrix} \phi^+ \\ \phi^o \end{pmatrix}_2^d \\ \begin{pmatrix} \phi^+ \\ \phi^o \end{pmatrix}_3^d \end{pmatrix}$$

with the VEV’s

$$\langle \Phi^u \rangle = \begin{pmatrix} \frac{1}{\sqrt{2}} \begin{pmatrix} v_{u1} \\ 0 \end{pmatrix} \\ \frac{1}{\sqrt{2}} \begin{pmatrix} v_{u2} \\ 0 \end{pmatrix} \\ \frac{1}{\sqrt{2}} \begin{pmatrix} v_{u3} \\ 0 \end{pmatrix} \end{pmatrix}, \quad \langle \Phi^d \rangle = \begin{pmatrix} \frac{1}{\sqrt{2}} \begin{pmatrix} 0 \\ v_{d1} \end{pmatrix} \\ \frac{1}{\sqrt{2}} \begin{pmatrix} 0 \\ v_{d2} \end{pmatrix} \\ \frac{1}{\sqrt{2}} \begin{pmatrix} 0 \\ v_{d3} \end{pmatrix} \end{pmatrix}$$

The contributions from  $\langle \Phi^u \rangle$  and  $\langle \Phi^d \rangle$  generate the  $W$  and  $Z_0$  SM gauge boson masses

$$\frac{g^2}{4} (v_u^2 + v_d^2) W^+ W^- + \frac{(g^2 + g'^2)}{8} (v_u^2 + v_d^2) Z_0^2 \quad (2.14)$$

+ tiny contribution to the SU(3) gauge boson masses and mixing with  $Z_0$ ,

$v_u^2 = v_{1u}^2 + v_{2u}^2 + v_{3u}^2$ ,  $v_d^2 = v_{1d}^2 + v_{2d}^2 + v_{3d}^2$ . So, if  $M_W \equiv \frac{1}{2}g v$ , we may write  $v = \sqrt{v_u^2 + v_d^2} \approx 246$  GeV.

## 2.5 Fermion masses

### 2.5.1 Dirac See-saw mechanisms

The gauge symmetry  $G \equiv SU(3) \times G_{SM}$ , the fermion content, and the transformation of the scalar fields, all together, avoid Yukawa couplings between SM fermions. The allowed Yukawa couplings involve terms between the SM fermions and the corresponding vector-like fermions U, D, E and N:

The scalars and fermion content allow the gauge invariant Yukawa couplings for quarks and charged leptons

$$H_u \overline{\psi}_q^\circ \Phi^u U_R^\circ + h_{\eta_1}^u \overline{\psi}_{uR}^\circ \eta_1 U_L^\circ + h_{\eta_2}^u \overline{\psi}_{uR}^\circ \eta_2 U_L^\circ + M_U \overline{U}_L^\circ U_R^\circ + \text{h.c}$$

$$H_d \overline{\psi}_q^\circ \Phi^d D_R^\circ + h_{\eta_1}^d \overline{\psi}_{dR}^\circ \eta_1 D_L^\circ + h_{\eta_2}^d \overline{\psi}_{dR}^\circ \eta_2 D_L^\circ + M_D \overline{D}_L^\circ D_R^\circ + \text{h.c}$$

$$H_e \overline{\psi}_l^\circ \Phi^d E_R^\circ + h_{\eta_1}^e \overline{\psi}_{eR}^\circ \eta_1 E_L^\circ + h_{\eta_2}^e \overline{\psi}_{eR}^\circ \eta_2 E_L^\circ + M_E \overline{E}_L^\circ E_R^\circ + \text{h.c}$$

$M_U, M_D, M_E$  are free mass parameters and  $H_u, H_d, H_e, h_{\eta_1}^f, h_{\eta_2}^f, f = u, d, e$  are coupling constants. When the involved scalar fields acquire VEV's, we get for charged leptons in the gauge basis  $\psi_{L,R}^\circ = (e^\circ, \mu^\circ, \tau^\circ, E^\circ)_{L,R}$ , the mass terms  $\overline{\psi}_L^\circ \mathcal{M}^\circ \psi_R^\circ + \text{h.c}$ , where

$$\mathcal{M}^\circ = \begin{pmatrix} 0 & 0 & 0 & H_e v_{d1} \\ 0 & 0 & 0 & H_e v_{d2} \\ 0 & 0 & 0 & H_e v_{d3} \\ h_1^e \Lambda_1 & h_2^e \Lambda_2 & 0 & M_E \end{pmatrix} \quad (2.15)$$

*It is worth to notice that completed analogous tree level mass matrices are obtained for u and d quarks*

$\mathcal{M}^\circ$  is diagonalized by applying a biunitary transformation  $\psi_{L,R}^\circ = V_{L,R}^\circ \chi_{L,R}$ .

$$V_L^{\circ T} \mathcal{M}^\circ V_R^\circ = \text{Diag}(0, 0, -\lambda_3, \lambda_4) \quad (2.16)$$

$$V_L^{\circ T} \mathcal{M}^\circ \mathcal{M}^{\circ T} V_L^\circ = V_R^{\circ T} \mathcal{M}^{\circ T} \mathcal{M}^\circ V_R^\circ = \text{Diag}(0, 0, \lambda_3^2, \lambda_4^2), \quad (2.17)$$

where  $\lambda_3$  and  $\lambda_4$  are the nonzero eigenvalues,  $\lambda_4$  being the fourth heavy fermion mass, and  $\lambda_3$  of the order of the top, bottom and tau mass for u, d and e fermions, respectively. We see from Eqs.(2.16,2.17) that from tree level there exist two massless eigenvalues associated to the light fermions:

## 2.6 Neutrino masses

Now we describe the procedure to generate neutrino masses

### 2.6.1 Tree level Dirac neutrino masses

With the fields of particles introduced in the model, we may write the Dirac type gauge invariant Yukawa couplings

$$h_D \bar{\Psi}_l^o \Phi^u N_R^o + h_1 \bar{\Psi}_\nu^o \eta_1 N_L^o + h_2 \bar{\Psi}_\nu^o \eta_2 N_L^o + h_3 \bar{\Psi}_\nu^o \eta_3 N_L^o + M_D \bar{N}_L^o N_R^o + h.c. \quad (2.18)$$

$h_D$ ,  $h_1$ ,  $h_2$  and  $h_3$  are Yukawa couplings, and  $M_D$  a Dirac type, invariant neutrino mass for the sterile neutrinos  $N_{L,R}^o$ . After electroweak symmetry breaking, we obtain in the interaction basis  $\Psi_{\nu L,R}^{oT} = (\nu_e^o, \nu_\mu^o, \nu_\tau^o, N^o)_{L,R}$ , the mass terms

$$h_D [v_1 \bar{\nu}_{eL}^o + v_2 \bar{\nu}_{\mu L}^o + v_3 \bar{\nu}_{\tau L}^o] N_R^o + [h_1 \Lambda_1 \bar{\nu}_{eR}^o + h_2 \Lambda_2 \bar{\nu}_{\mu R}^o + h_3 \Lambda_3 \bar{\nu}_{\tau R}^o] N_L^o + M_D \bar{N}_L^o N_R^o + h.c. \quad (2.19)$$

### 2.6.2 Tree level Majorana masses:

Since  $N_{L,R}^o$ , Table 1, are sterile neutrinos, we may also write left and right handed Majorana type couplings

$$h_L \bar{\Psi}_l^o \Phi^u (N_L^o)^c + m_L \bar{N}_L^o (N_L^o)^c + h.c. \quad (2.20)$$

and

$$h_{1R} \bar{\Psi}_\nu^o \eta_1 (N_R^o)^c + h_{2R} \bar{\Psi}_\nu^o \eta_2 (N_R^o)^c + h_{3R} \bar{\Psi}_\nu^o \eta_3 (N_R^o)^c + m_R \bar{N}_R^o (N_R^o)^c + h.c., \quad (2.21)$$

respectively. After spontaneous symmetry breaking, we also get the left handed and right handed Majorana mass terms

$$h_L [v_1 \bar{\nu}_{eL}^o + v_2 \bar{\nu}_{\mu L}^o + v_3 \bar{\nu}_{\tau L}^o] (N_L^o)^c + m_L \bar{N}_L^o (N_L^o)^c + h.c., \quad (2.22)$$

$$+ [h_{1R} \Lambda_1 \bar{\nu}_{eR}^o + h_{2R} \Lambda_2 \bar{\nu}_{\mu R}^o + h_{3R} \Lambda_3 \bar{\nu}_{\tau R}^o] (N_R^o)^c + m_R \bar{N}_R^o (N_R^o)^c + h.c. \quad (2.23)$$

Thus, in the basis  $\Psi_\nu^{oT} = (\nu_{eL}^o, \nu_{\mu L}^o, \nu_{\tau L}^o, N_L^o, (\nu_{eR}^o)^c, (\nu_{\mu R}^o)^c, (\nu_{\tau R}^o)^c, (N_R^o)^c)$ , the Generic  $8 \times 8$  tree level Majorana mass matrix for neutrinos  $\mathcal{M}_\nu^o$ , from Table 2.3,  $\bar{\Psi}_\nu^o \mathcal{M}_\nu^o (\Psi_\nu^o)^c$ , read

	$(\nu_{eL}^o)^c$	$(\nu_{\mu L}^o)^c$	$(\nu_{\tau L}^o)^c$	$(N_L^o)^c$	$\nu_{eR}^o$	$\nu_{\mu R}^o$	$\nu_{\tau R}^o$	$N_R^o$
$\overline{\nu_{eL}^o}$	0	0	0	$h_L v_1$	0	0	0	$h_D v_1$
$\overline{\nu_{\mu L}^o}$	0	0	0	$h_L v_2$	0	0	0	$h_D v_2$
$\overline{\nu_{\tau L}^o}$	0	0	0	$h_L v_3$	0	0	0	$h_D v_3$
$\overline{N_L^o}$	$h_L v_1$	$h_L v_2$	$h_L v_3$	$m_L$	$h_1 \Lambda_1$	$h_2 \Lambda_2$	0	$M_D$
$(\overline{\nu_{eR}^o})^c$	0	0	0	$h_1 \Lambda_1$	0	0	0	$h_{1R} \Lambda_1$
$(\overline{\nu_{\mu R}^o})^c$	0	0	0	$h_2 \Lambda_2$	0	0	0	$h_{2R} \Lambda_2$
$(\overline{\nu_{\tau R}^o})^c$	0	0	0	0	0	0	0	0
$(\overline{N_R^o})^c$	$h_D v_1$	$h_D v_2$	$h_D v_3$	$M_D$	$h_{1R} \Lambda_1$	$h_{2R} \Lambda_2$	0	$m_R$

Table 2.3: Tree Level Majorana masses

$$\mathcal{M}_\nu^o = \begin{pmatrix} 0 & 0 & 0 & \alpha_1 & 0 & 0 & 0 & a_1 \\ 0 & 0 & 0 & \alpha_2 & 0 & 0 & 0 & a_2 \\ 0 & 0 & 0 & \alpha_3 & 0 & 0 & 0 & a_3 \\ \alpha_1 & \alpha_2 & \alpha_3 & m_L & b_1 & b_2 & 0 & m_D \\ 0 & 0 & 0 & b_1 & 0 & 0 & 0 & \beta_1 \\ 0 & 0 & 0 & b_2 & 0 & 0 & 0 & \beta_2 \\ 0 & 0 & 0 & 0 & 0 & 0 & 0 & 0 \\ a_1 & a_2 & a_3 & m_D & \beta_1 & \beta_2 & 0 & m_R \end{pmatrix} \quad (2.24)$$

Diagonalization of  $\mathcal{M}_\nu^{(o)}$ , Eq.(2.24), yields four zero eigenvalues:

$$\mathcal{U}_\nu^{oT} \mathcal{M}_\nu^o \mathcal{U}_\nu^o = \text{Diagonal}(0, 0, 0, 0, m_5^o, m_6^o, m_7^o, m_8^o) \quad (2.25)$$

## 2.7 One loop neutrino masses:

### 2.7.1 One loop Dirac Neutrino masses

After the breakdown of the electroweak symmetry, neutrinos may get tiny Dirac mass terms from the generic one loop diagram in Fig. 1, The internal fermion line in this diagram represent the tree level see-saw mechanisms, Eqs.(2.18-2.23). The vertices read from the SU(3) family symmetry interaction Lagrangian

$$i\mathcal{L}_{\text{int}} = \frac{g_H}{2} (\bar{\nu}_e^o \gamma_\mu \nu_e^o - \bar{\nu}_\tau^o \gamma_\mu \nu_\tau^o) Z_1^\mu + \frac{g_H}{2\sqrt{3}} (\bar{\nu}_e^o \gamma_\mu \nu_e^o - 2\bar{\nu}_\mu^o \gamma_\mu \nu_\mu^o + \bar{\nu}_\tau^o \gamma_\mu \nu_\tau^o) Z_2^\mu \\ + \frac{g_H}{\sqrt{2}} (\bar{\nu}_e^o \gamma_\mu \nu_\mu^o Y_1^+ + \bar{\nu}_e^o \gamma_\mu \nu_\tau^o Y_2^+ + \bar{\nu}_\mu^o \gamma_\mu \nu_\tau^o Y_3^+ + \text{h.c.}) \quad (2.26)$$

The contribution from these diagrams may be written as

$$c_Y \frac{\alpha_H}{\pi} m_\nu(M_Y)_{ij} \quad , \quad \alpha_H = \frac{g_H^2}{4\pi} \quad , \quad (2.27)$$

$$m_\nu(M_Y)_{ij} \equiv \sum_{k=5,6,7,8} m_k^o \mathcal{U}_{\nu ik}^o \mathcal{U}_{\nu jk}^o f(M_Y, m_k^o) \quad , \quad (2.28)$$

$$f(M_Y, m_k^o) = \frac{M_Y^2}{M_Y^2 - m_k^{o2}} \ln \frac{M_Y^2}{m_k^{o2}} \approx \ln \frac{M_Y^2}{m_k^{o2}} \quad , \quad M_Y^2 \gg m_k^{o2} \text{ valid for neutrinos.}$$

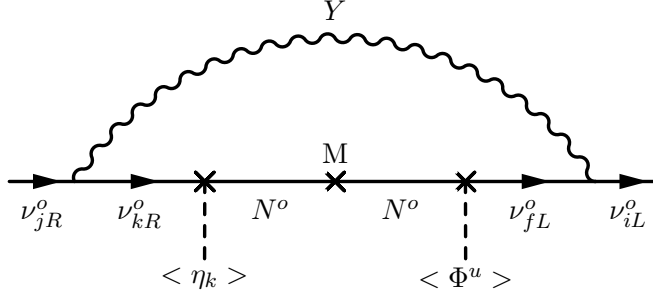


Fig. 2.1: Generic one loop diagram contribution to the Dirac mass term  $m_{ij} \bar{\nu}_{iL}^o \nu_{jR}^o$ .  $M = M_D, m_L, m_R$

	$\nu_{eR}^o$	$\nu_{\mu R}^o$	$\nu_{\tau R}^o$	$N_R^o$
$\bar{\nu}_{eL}^o$	$D_{\nu 15}$	$D_{\nu 16}$	0	0
$\bar{\nu}_{\mu L}^o$	$D_{\nu 25}$	$D_{\nu 26}$	0	0
$\bar{\nu}_{\tau L}^o$	$D_{\nu 35}$	$D_{\nu 36}$	$D_{\nu 37}$	0
$\bar{N}_L^o$	0	0	0	0

Table 2.4: One loop Dirac mass terms  $\frac{\alpha_H}{\pi} D_{\nu ij} \bar{\nu}_{iL}^o \nu_{jR}^o$

### 2.7.2 One loop L-handed and R-handed Majorana masses

Neutrinos also obtain one loop corrections to L-handed and R-handed Majorana masses from the diagrams of Fig. 2 and Fig. 3, respectively. A similar procedure as for Dirac Neutrino masses, leads to the one loop Majorana mass terms

Thus, in the  $\Psi_\nu^o$  basis, we may write the one loop contribution for neutrinos as

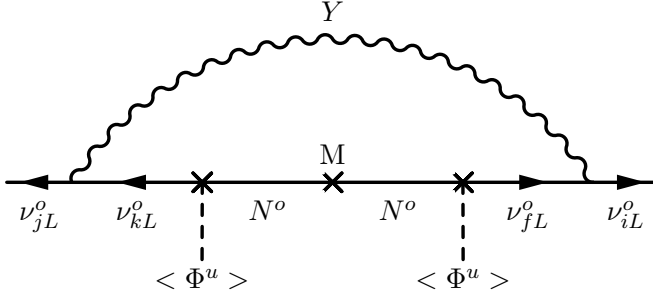


Fig. 2.2: Generic one loop diagram contribution to the L-handed Majorana mass term  $m_{ij} \bar{\nu}_{iL}^o (\nu_{jL}^o)^T$ .  $M = M_D, m_L, m_R$

	$\nu_{eL}^o$	$\nu_{\mu L}^o$	$\nu_{\tau L}^o$	$N_L^o$
$\nu_{eL}^o$	$L_{\nu 11}$	$L_{\nu 12}$	$L_{\nu 13}$	0
$\nu_{\mu L}^o$	$L_{\nu 12}$	$L_{\nu 22}$	$L_{\nu 23}$	0
$\nu_{\tau L}^o$	$L_{\nu 13}$	$L_{\nu 23}$	$L_{\nu 33}$	0
$N_L^o$	0	0	0	0

Table 2.5: One loop L-handed Majorana mass terms  $\frac{\alpha_H}{\pi} L_{\nu ij} \bar{\nu}_{iL}^o (\nu_{jL}^o)^T$

	$\nu_{eR}^o$	$\nu_{\mu R}^o$	$\nu_{\tau R}^o$	$N_R^o$
$\nu_{eR}^o$	$R_{\nu 55}$	$R_{\nu 56}$	0	0
$\nu_{\mu R}^o$	$R_{\nu 56}$	$R_{\nu 66}$	0	0
$\nu_{\tau R}^o$	0	0	0	0
$N_R^o$	0	0	0	0

Table 2.6: One loop R-handed Majorana mass terms  $\frac{\alpha_H}{\pi} R_{\nu ij} \bar{\nu}_{iR}^o (\nu_{jR}^o)^T$

$$\mathcal{M}_{1\nu}^o = \begin{pmatrix} L_{\nu 11} & L_{\nu 12} & L_{\nu 13} & 0 & D_{\nu 15} & D_{\nu 16} & 0 & 0 \\ L_{\nu 12} & L_{\nu 22} & L_{\nu 23} & 0 & D_{\nu 25} & D_{\nu 26} & 0 & 0 \\ L_{\nu 13} & L_{\nu 23} & L_{\nu 33} & 0 & D_{\nu 35} & D_{\nu 36} & D_{\nu 37} & 0 \\ 0 & 0 & 0 & 0 & 0 & 0 & 0 & 0 \\ D_{\nu 15} & D_{\nu 25} & D_{\nu 35} & 0 & R_{\nu 55} & R_{\nu 56} & 0 & 0 \\ D_{\nu 16} & D_{\nu 26} & D_{\nu 36} & 0 & R_{\nu 56} & R_{\nu 66} & 0 & 0 \\ 0 & 0 & D_{\nu 37} & 0 & 0 & 0 & 0 & 0 \\ 0 & 0 & 0 & 0 & 0 & 0 & 0 & 0 \end{pmatrix} \frac{\alpha_H}{\pi}, \quad (2.29)$$

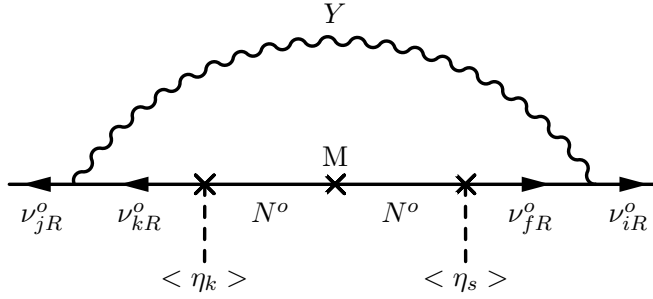


Fig. 2.3: Generic one loop diagram contribution to the R-handed Majorana mass term  $m_{ij} \bar{\nu}_{iR}^o (\nu_{jR}^o)^T$ .  $M = M_D, m_L, m_R$

where, after using the relationships coming from the zero entries of  $\mathcal{M}_\nu^o$ , eq.(2.24);

$$\mathcal{M}_\nu^o = \mathcal{U}_\nu^o \text{Diagonal}(0, 0, 0, 0, m_5^o, m_6^o, m_7^o, m_8^o) \mathcal{U}_\nu^{oT}, \quad (2.30)$$

and in the limit  $M_Y^2 \gg m_k^o{}^2$ , we may write:

$$L_{\nu ij} = \frac{1}{3} F_{ij}, \quad i, j = 1, 2, 3$$

$$D_{\nu 15} = \frac{1}{3} F_{15} + \frac{1}{2} F_{26}, \quad D_{\nu 16} = -\frac{1}{6} F_{16},$$

$$D_{\nu 25} = -\frac{1}{6} F_{25}, \quad D_{\nu 26} = \frac{1}{3} F_{26} + \frac{1}{2} F_{15},$$

$$D_{\nu 35} = -\frac{1}{6} F_{35}, \quad D_{\nu 36} = -\frac{1}{6} F_{36}, \quad D_{\nu 37} = \frac{1}{2} (F_{15} + F_{26})$$

$$R_{\nu 55} = \frac{1}{3} F_{55}, \quad R_{\nu 56} = \frac{1}{3} F_{56}, \quad R_{\nu 66} = \frac{1}{3} F_{66}$$

where

$$F_{ij} = \mathcal{U}_{\nu i5}^o \mathcal{U}_{\nu j5}^o \ln \frac{m_8^o{}^2}{m_5^o{}^2} + \mathcal{U}_{\nu i6}^o \mathcal{U}_{\nu j6}^o \ln \frac{m_8^o{}^2}{m_6^o{}^2} + \mathcal{U}_{\nu i7}^o \mathcal{U}_{\nu j7}^o \ln \frac{m_8^o{}^2}{m_7^o{}^2} \quad (2.31)$$

### 2.7.3 Neutrino mass matrix up to one loop

Finally, we obtain the Majorana mass matrix for neutrinos up to one loop

$$\mathcal{M}_\nu = \mathcal{U}_\nu^{oT} \mathcal{M}_{1\nu}^o \mathcal{U}_\nu^o + \text{Diag}(0, 0, 0, 0, m_5^o, m_6^o, m_7^o, m_8^o), \quad (2.32)$$

### 2.7.4 $(V_{CKM})_{4 \times 4}$ and $(V_{PMNS})_{4 \times 8}$ mixing matrices

Within this scenario, the transformation from massless to physical mass fermion eigenfields for quarks and charged leptons is

$$\psi_L^o = V_L^o V_L^{(1)} \Psi_L \quad \text{and} \quad \psi_R^o = V_R^o V_R^{(1)} \Psi_R,$$

and for neutrinos  $\Psi_\nu^o = \mathcal{U}_\nu^o \mathcal{U}_\nu^1 \Psi_\nu$ ;

$$\mathcal{U}_\nu^{1T} \mathcal{M}_\nu \mathcal{U}_\nu^1 = \text{Diagonal}(\lambda_1, \lambda_2, \lambda_3, \lambda_4, \lambda_5, \lambda_6, \lambda_7, \lambda_8) \quad (2.33)$$

Recall now that vector like fermions, Table 1, are  $SU(2)_L$  weak singlets, and hence, they do not couple to  $W$  boson in the interaction basis. So, the coupling of L-handed up and down quarks;  $f_{uL}^{oT} = (u^o, c^o, t^o)_L$  and  $f_{dL}^{oT} = (d^o, s^o, b^o)_L$ , to the  $W$  charged gauge boson is

$$\begin{aligned} & \frac{g}{\sqrt{2}} \bar{f}_{uL}^o \gamma_\mu f_{dL}^o W^{+\mu} \\ &= \frac{g}{\sqrt{2}} \bar{\Psi}_{uL} [(V_{uL}^o V_{uL}^{(1)})_{3 \times 4}]^T (V_{dL}^o V_{dL}^{(1)})_{3 \times 4} \gamma_\mu \Psi_{dL} W^{+\mu}, \end{aligned} \quad (2.34)$$

with  $g$  the  $SU(2)_L$  gauge coupling. Hence, the non-unitary  $V_{CKM}$  of dimension  $4 \times 4$  is identified as

$$(V_{CKM})_{4 \times 4} = [(V_{uL}^o V_{uL}^{(1)})_{3 \times 4}]^T (V_{dL}^o V_{dL}^{(1)})_{3 \times 4} \quad (2.35)$$

$$[V_{uL}^o V_{uL}^{(1)}]_{3 \times 4} = (V_{uL}^o)_{3 \times 4} (V_{uL}^{(1)})_{4 \times 4}, \quad [V_{dL}^o V_{dL}^{(1)}]_{3 \times 4} = (V_{dL}^o)_{3 \times 4} (V_{dL}^{(1)})_{4 \times 4}$$

Similar analysis of the coupling between active L-handed neutrinos and L-handed charged leptons to  $W$  boson, leads to the lepton mixing matrix

$$(U_{PMNS})_{4 \times 8} = [(V_{eL}^o V_{eL}^{(1)})_{3 \times 4}]^T (\mathcal{U}_\nu^o \mathcal{U}_\nu^1)_{3 \times 8} \quad (2.36)$$

$$[V_{eL}^o V_{eL}^{(1)}]_{3 \times 4} = (V_{eL}^o)_{3 \times 4} (V_{eL}^{(1)})_{4 \times 4}, \quad (\mathcal{U}_\nu^o \mathcal{U}_\nu^1)_{3 \times 8} = (\mathcal{U}_\nu^o)_{3 \times 8} (\mathcal{U}_\nu^1)_{8 \times 8}$$

## 2.8 Numerical results for Neutrino masses and mixing in a 3+5 scenario

We report here numerical results for lepton masses and mixing, at the  $M_Z$  scale [15]

The input values for the horizontal boson masses, Eq.(8), and the coupling constant of the  $SU(3)$  family symmetry are:

$$M_1 = 5.3 \times 10^3 \text{ TeV} \quad , \quad M_2 = 3.3 \times 10^5 \text{ TeV} \quad , \quad \frac{\alpha_H}{\pi} = 0.05, \quad (2.37)$$

$$\Lambda_1 = 3352.7 \text{ TeV}, \Lambda_2 = 10^3 \Lambda_1, g_H = 2.23561$$

Horizontal gauge bosons from the SU(3) family symmetry introduce flavor changing couplings, and in particular mediate  $\Delta F = 2$  processes at tree level. The above high scales and heavy boson masses provide the proper suppression of  $K^0 - \bar{K}^0$  and  $D^0 - \bar{D}^0$  meson mixing from the tree level exchange diagrams mediated by the SU(2) horizontal gauge bosons  $Z_1, Y_2^\pm$ .

### 2.8.1 Charged leptons:

Tree level:

$$\mathcal{M}_e^0 = \begin{pmatrix} 0 & 0 & 0 & 2670.25 \\ 0 & 0 & 0 & 11902.6 \\ 0 & 0 & 0 & 16264.7 \\ 1.21882 \times 10^{10} & -2.32202 \times 10^9 & 0 & 6.07835 \times 10^{10} \end{pmatrix} \text{ MeV},$$

up to one loop corrections:

$$\mathcal{M}_e = \begin{pmatrix} 0 & -19.9797 & -83.226 & -16.9884 \\ 0.6408 & 71.9782 & 293.027 & 59.814 \\ -0.8544 & 168.853 & -1712.54 & 480.432 \\ -2.74 \times 10^{-7} & 0.000054 & 0.000755 & 6.20 \times 10^{10} \end{pmatrix} \text{ MeV}$$

the charged lepton masses

$$(m_e, m_\mu, m_\tau, M_E) = (0.486031, 102.717, 1746.17, 6.20 \times 10^{10}) \text{ MeV}$$

Mixing matrix:

$$V_{eL} = V_{eL}^0 V_{eL}^{(1)}:$$

$$\begin{pmatrix} 0.986458 & 0.0744614 & -0.146138 & 4.30921 \times 10^{-8} \\ 0.00276675 & -0.898433 & -0.439101 & 1.93334 \times 10^{-7} \\ -0.163991 & 0.43275 & -0.886473 & 2.62497 \times 10^{-7} \\ 0 & 5.68933 \times 10^{-8} & 3.23887 \times 10^{-7} & 1 \end{pmatrix}$$

## 2.8.2 Neutrino masses and Lepton ( $\mathbf{U}_{PMNS}$ ) $_{4 \times 8}$ mixing:

Tree level  $\mathcal{M}_\nu^0$ , eq.(2.24): in eV

$$\begin{pmatrix} 0 & 0 & 0 & 30.9559 & 0 & 0 & 0 & 13.2472 \\ 0 & 0 & 0 & 434.898 & 0 & 0 & 0 & 62.502 \\ 0 & 0 & 0 & 1980.48 & 0 & 0 & 0 & 76.9286 \\ 30.9559 & 434.898 & 1980.48 & 40 & 790642. & 114364 & 0 & 4000 \\ 0 & 0 & 0 & 790642. & 0 & 0 & 0 & 9.88602 \times 10^6 \\ 0 & 0 & 0 & 114364. & 0 & 0 & 0 & 1.40868 \times 10^6 \\ 0 & 0 & 0 & 0 & 0 & 0 & 0 & 0 \\ 13.2472 & 62.502 & 76.9286 & 4000. & 9.88602 \times 10^6 & 1.40868 \times 10^6 & 0 & 100000 \end{pmatrix}$$

$\mathcal{M}_{1\nu}^0$ , eq.(2.29): in eV

$$\begin{pmatrix} -0.000216363 & -0.00311126 & -0.0142886 & 0 & -0.240713 & 0.00592337 & 0 & 0 \\ -0.00311126 & -0.04474 & -0.2054720 & -0.0510705 & -0.1576590 & 0 & 0 & 0 \\ -0.0142886 & -0.205472 & -0.943645 & 0 & -0.278496 & 0.367409 & -0.239023 & 0 \\ 0 & 0 & 0 & 0 & 0 & 0 & 0 & 0 \\ -0.240713 & -0.0510705 & -0.278496 & 0 & -4136.09 & -588.853 & 0 & 0 \\ 0.00592337 & -0.157659 & 0.367409 & 0 & -588.853 & -84.537 & 0 & 0 \\ 0 & 0 & -0.239023 & 0 & 0 & 0 & 0 & 0. \\ 0 & 0 & 0 & 0 & 0 & 0 & 0 & 0 \end{pmatrix}$$

$\mathcal{M}_\nu$ , eq.(2.32): in eV

$$\begin{pmatrix} 4.89118 \times 10^{-7} & 0.00534394 & 0.0268319 & -0.0271814 & 0.0229136 & 0.0226125 & 0.161679 & 0.160874 \\ 0.00534394 & -0.00830416 & 0.0484769 & -0.0371462 & -0.0211906 & -0.0209894 & -0.0521349 & -0.0518753 \\ 0.0268319 & 0.0484769 & -0.629274 & 0.62907 & -0.00373038 & -0.00353603 & -0.209602 & -0.208558 \\ -0.0271814 & -0.0371462 & 0.62907 & -0.530945 & -0.221868 & -0.220375 & 0.228698 & 0.22756 \\ 0.0229136 & -0.0211906 & -0.00373038 & -0.221868 & -2604.12 & -0.253956 & -0.940082 & -0.935401 \\ 0.0226125 & -0.0209894 & -0.00353603 & -0.220375 & -0.253956 & 2643.36 & 0.748489 & 0.744762 \\ 0.161679 & -0.0521349 & -0.209602 & 0.228698 & -0.940082 & 0.748489 & -9.97002 \times 10^6 & 2109.94 \\ 0.160874 & -0.0518753 & -0.208558 & 0.22756 & -0.935401 & 0.744762 & -2109.94 & 1.00658 \times 10^7 \end{pmatrix}$$

**Neutrino masses:**

$$(m_1 = 0.00584795, m_2 = 0.0104888, m_3 = 0.051461, m_4 = 1.21534, \\ m_5 = 2604.12, m_6 = 2643.36, m_7 = 9.97002 \times 10^6, m_8 = 1.00658 \times 10^7) \text{ eV}$$

**Squared neutrino mass differences:**

$$m_2^2 - m_1^2 = 7.58162 \times 10^{-5} \text{ eV}^2$$

$$m_3^2 - m_2^2 = 2.53822 \times 10^{-3} \text{ eV}^2$$

$$m_4^2 - m_1^2 = 1.47441 \text{ eV}^2$$

**Neutrino mixing:**  $U_\nu = U_\nu^0 U_\nu^1$ 

$$\left( \begin{array}{cccc} -0.817815 & -0.573736 & -0.0309853 & -0.0302746 \\ 0.398121 & -0.525222 & -0.73405 & 0.0115492 \\ 0.00987364 & 0.0271079 & 0.142716 & -0.645085 \\ 0.0000115219 & 5.86044 \times 10^{-6} & -0.0000891429 & -0.0000792766 \\ 0.0139007 & -0.0158414 & -0.00290156 & -0.106192 \\ -0.0975645 & 0.111201 & 0.0203878 & 0.74528 \\ -0.40357 & 0.617751 & -0.662886 & -0.126871 \\ -9.34653 \times 10^{-7} & -4.8869 \times 10^{-7} & 7.12916 \times 10^{-6} & 6.29816 \times 10^{-6} \\ & 0.00805693 & -0.00800614 & 1.12646 \times 10^{-6} & -1.08644 \times 10^{-6} \\ & 0.115983 & -0.115003 & 6.87784 \times 10^{-6} & -6.81358 \times 10^{-6} \\ & 0.532465 & -0.528342 & 0.0000166682 & -0.0000164536 \\ & -0.702146 & -0.707553 & -0.0565233 & -0.0562542 \\ & -0.0644483 & 0.0634117 & 0.701853 & -0.698211 \\ & 0.450162 & -0.446888 & 0.100018 & -0.0994993 \\ & 0.0000488735 & 0.0000477752 & 0 & 0 \\ & 0.0561715 & 0.056604 & -0.702997 & -0.706708 \end{array} \right)$$

**( $U_{\text{PMNS}}$ ) $_{4 \times 8}$  lepton mixing matrix :**

$$\left( \begin{array}{cccc} -0.807257 & -0.571865 & -0.0560008 & 0.0759557 \\ -0.414308 & 0.440887 & 0.718949 & -0.291791 \\ -0.0640545 & 0.29044 & 0.200336 & 0.571204 \\ 4.43209 \times 10^{-8} & -1.19151 \times 10^{-7} & -1.05789 \times 10^{-7} & -1.68405 \times 10^{-7} \\ & -0.0790509 & 0.0784275 & -1.6032 \times 10^{-6} & 1.60766 \times 10^{-6} \\ & 0.126822 & -0.125914 & 1.11777 \times 10^{-6} & -1.07963 \times 10^{-6} \\ & -0.524122 & 0.520029 & -0.0000179606 & 0.0000177362 \\ & 1.62541 \times 10^{-7} & -1.61267 \times 10^{-7} & 0 & 0 \end{array} \right)$$

## 2.9 Conclusions

We have reported an updated numerical analysis for neutrino masses and mixing in a 3+5 scenario, within a local SU(3) Family symmetry model, which combines tree level "Dirac See-saw" mechanisms and radiative corrections to implement a successful hierarchical spectrum, for charged fermion masses and mixing.

In section 2.8 we report the fit of parameters, which accommodate the neutrino masses ( $m_1 = 0.00584795$ ,  $m_2 = 0.0104888$ ,  $m_3 = 0.051461$ ,  $m_4 = 1.21534$ ,  $m_5 = 2604.12$ ,  $m_6 = 2643.36$ ,  $m_7 = 9.97002 \times 10^6$ ,  $m_8 = 1.00658 \times 10^7$ ) eV, the squared neutrino mass differences  $m_2^2 - m_1^2 = 7.58162 \times 10^{-5}$  eV<sup>2</sup>,  $m_3^2 - m_2^2 = 2.53822 \times 10^{-3}$  eV<sup>2</sup>, and  $m_4^2 - m_1^2 = 1.47441$  eV<sup>2</sup> as well as the  $(U_{PMNS})_{4 \times 8}$  lepton mixing matrix. Notice that the majority of the entries in  $(U_{PMNS})_{3 \times 3}$  submatrix are within the reported limits in [11]- [14].

## 2.10 Acknowledgements

It is my pleasure to thank the organizers N.S. Mankoc-Borstnik, H.B. Nielsen, M. Y. Khlopov, and all participants for this year stimulating Virtual Bled Workshop 2020. This work was partially supported by the "Instituto Politécnico Nacional", Grant from COFAA.

## References

1. A. Hernandez-Galeana, Rev. Mex. Fis. **Vol. 50(5)**, (2004) 522. hep-ph/0406315.
2. A. Hernandez-Galeana, Bled Workshops in Physics, (ISSN:1580-4992), **Vol. 17, No. 2**, (2016) Pag. 36; arXiv:1612.07388[hep-ph]; **Vol. 16, No. 2**, (2015) Pag. 47; arXiv:1602.08212[hep-ph]; **Vol. 15, No. 2**, (2014) Pag. 93; arXiv:1412.6708[hep-ph]; **Vol. 14, No. 2**, (2013) Pag. 82; arXiv:1312.3403[hep-ph]; **Vol. 13, No. 2**, (2012) Pag. 28; arXiv:1212.4571[hep-ph]; **Vol. 12, No. 2**, (2011) Pag. 41; arXiv:1111.7286[hep-ph]; **Vol. 11, No. 2**, (2010) Pag. 60; arXiv:1012.0224[hep-ph]; Bled Workshops in Physics, **Vol. 10, No. 2**, (2009) Pag. 67; arXiv:0912.4532[hep-ph];
3. Z. Berezhiani and M. Yu.Khlopov: Theory of broken gauge symmetry of families, Sov.J.Nucl.Phys. **51**, 739 (1990).
4. Z. Berezhiani and M. Yu.Khlopov: Physical and astrophysical consequences of family symmetry breaking, Sov.J.Nucl.Phys. **51**, 935 (1990).
5. J.L. Chkareuli, C.D. Froggatt, and H.B. Nielsen, Nucl. Phys. B **626**, 307 (2002).
6. Z.G. Berezhiani: The weak mixing angles in gauge models with horizontal symmetry: A new approach to quark and lepton masses, Phys. Lett. B **129**, 99 (1983).
7. T. Yanagida, Phys. Rev. D **20**, 2986 (1979).
8. T. Appelquist, Y. Bai and M. Piai: SU(3) Family Gauge Symmetry and the Axion, Phys. Rev. D **75**, 073005 (2007).
9. T. Appelquist, Y. Bai and M. Piai: Neutrinos and SU(3) family gauge symmetry, Phys. Rev. D **74**, 076001 (2006).
10. T. Appelquist, Y. Bai and M. Piai: Quark mass ratios and mixing angles from SU(3) family gauge symmetry, Phys. Lett. B **637**, 245 (2006).
11. G.H. Collin, C.A. Argüelles, J.M. Conrad, and M.H. Shaevitz, Phys. Rev. Lett. **117**, 221801 (2016).

12. M.C. Gonzalez-Garcia, Michele Maltoni, Jordi Salvado, and Thomas Schwetz, arXiv:1209.3023[hep-ph].
13. Ivan Esteban, M.C. Gonzalez-Garcia, Alvaro Hernandez-Cabezudo, Michele Maltoni, and Thomas Schwetz, arXiv:1811.05487[hep-ph].
14. Suman Bharti, Ushak Rahaman, and S. Uma Sankar, arXiv:2001.08676[hep-ph].
15. Zhi-zhong Xing, He Zhang and Shun Zhou, Phys. Rev. D **86**, 013013 (2012).



### 3 Dark Matter Macroscopic Pearls, 3.55 keV X-Ray Line, How Big ?

H.B. Nielsen <sup>\*1</sup> and C.D. Froggatt<sup>2</sup>

<sup>1</sup> Niels Bohr Institutet

<sup>2</sup>Glasgow University

**Abstract.** We study the 3.55 keV X-ray suspected to arise from dark matter in our model of dark matter consisting of a bubble of a new phase of the vacuum, the surface tension of which keeps ordinary matter under high pressure inside the bubble. We consider two versions of the model:

- Old large pearls model :We worked for a long time on a pearl picture with pearl / bubbles of cm-size adjusted so that the impacts of them on earth could be identified with events of the mysterious type that happened in Tunguska in 1908. We fit both the very frequency, the 3.55 keV, and the overall intensity of the X-ray line coming from the center of the Milky Way and from galaxy clusters with one parameter in the model in which this radiation comes from collisions of pearls.
- New small pearl model: Our latest idea is to let the pearls be smaller than atoms but bigger than nuclei so as to manage to fit the 3.5 keV X-rays coming from the Tycho supernova remnant in which Jeltama and Profumo observed this line. Further we also crudely fit the DAMA-LIBRA observation with the small pearls, and even see a possibility for including the electron-recoil-excess seen by the Xenon1T experiment as being due to de-excitation via electron emission of our pearls. The important point of even our small size pearl model is that the cross section of our “macroscopic” pearls is so large that the pearls interact several times in the shielding but, due to their much larger mass than the typical nuclei, are **not stopped by only a few interactions**. Nevertheless only a minute fraction of the relatively strongly interacting pearls reach the 1400 m down to the DAMA experiment, but due to the higher cross section we can fit the data anyway.

**Povzetek.** Avtorja domnevata, da njun model za temno snov pojasni izvor spektralne črte pri 3.55 keV v rentgenskem območju spektra naše galaksije. Temna snov je po njuno posledica nove faze vakuumu, ki jo tvorijo mehurčki običajne snovi pri visokem tlaku, ki ga vzdržuje površinska napetost. Obravnavata dve različici modela:

- Stari model velikih biserov: Avtorja sta dolgo razvijala model vakuumu z “biseri” (ali mehurčki) centimetrskih velikosti, ki so povzročili eksplozijo v Tunguski leta 1908. Da ima rentgensko sevanje, ki nastaja pri trkih takih “biserov” v centru galaksije in v jatah galaksij, frekvenco 3.55 keV in izmerjeno jakost, morata v modelu prilagoditi samo en parameter.

---

\* Giving talk

- Novi model majhnih biserov: Če pa predpostavita da so "biseri" novega vakuuma manjši od atomov in večji od jeder, njun model dobro opiše spektralno črto pri 3.5 keV, ki prihaja od ostanka Tychove supernove in sta jo opazila Jeltema in Profumo. Njuni zelo masivni "biseri" dosežejo kljub močni interakciji z običajno snovjo v manjšem številu experiment DAMA-LIBRA, ki je 1400 m pod površjem zemlje in se celo večkrat sipljejo na merilcu ne da bi se ustavili. V grobem opišejo meritve DAMA-LIBRA. Elektroni, ki jih "biseri" sevajo, pa morda pojasnijo presežek elektronov, ki ga izmeri Xenon1T.

### 3.1 Introduction

The main purpose of the present article is to put forward the latest developments of our long speculated idea that the so far mysterious dark matter found via its gravitational forces, instead of consisting of particle of atomic masses or an Axion-like condensate, could consist of our proposed type of macroscopic objects with a mass much bigger than that of genuine atoms.

We started our speculations already years ago by supposing cm-size pearls make up the dark matter, but they will be developed in the section 3.8 below into the idea that these pearls could indeed be much smaller and of geometrical size even smallish compared to atoms, although the mass should still be appreciably larger than that of atoms.

#### **We shall stress small macroscopic pearls.**

Even such a dramatic change in our old model into a version with much smaller pearls would not be observed via the gravitational effects provided just that the density of mass per unit volume is kept the same. It is also this fact that really only the mass density matters for the gravitational effects, that makes it possible that these effects cannot distinguish our types of heavy or relatively lighter pearls from the more usual assumption of only atomic weight particles, such as supersymmetric partners of  $Z^0$  or photon say in superstring theory.

However, assuming that indeed the X-ray radiation [1,2] observed by satellites and suspected to come from dark matter does indeed come from dark matter requires more specific models for what the dark matter could be; e.g. it could consist of some new sort of sterile neutrino able to decay although very seldomly into a photon and e.g. an ordinary neutrino. Such a sterile neutrino should then of course have a mass equal to just two times the photon energy number 3.55 keV of the observed X-ray radiation counted in the rest frame of the supposed dark matter in the region observed.

- **Our Old Model:** We develop an alternative version of our model [3–6] in which dark matter consists of cm-size pearls with masses of  $10^8$  kg under the attempt to identify the X-ray radiation seen by satellites [1,2] and supposed to originate from dark matter with the energy per photon 3.55 keV. We shall discuss the possibility that the dark matter pearls be much smaller but still macroscopic. This is our new model with small pearls of a size smaller than atoms but bigger than atomic nuclei.

Actually we assume that our pearls have a skin surrounding them keeping some ordinary matter inside the pearls under such an (appropriate) pressure

that, in the electron system of this ordinary matter inside, there appears an energy gap between filled and empty electron states - called the homolumo gap (to be explained later) - of size close to the energy difference just 3.55 keV of the observed radiation. The idea then is that there can be excitations being (loosely) bound states of an electron in one of the lowest empty states and a hole in one of the at first filled states. These excitons should have an energy close to the observed photon energy in the line. Then one could have that the photons observed astronomically by the satellites are photons from the decay of such excitons in the highly compressed ordinary matter material in our model supposed to exist inside pearls making up the dark matter.

It is a major part of our work [3] to evaluate the rate of such X-ray radiation that will result under the assumption that the main production of the 3.5 keV radiation comes about when two of our dark-matter-pearls collide with each other. We claim it to be a great success that the magnitude of this rate of radiation can be fit together with the energy per photon, the number 3.5 keV. We shall in the present article have in mind really two models, which are essentially inconsistent with each other, In the first model the mass of one pearl is about  $1.4 * 10^8$  kg and in the other model the mass is about  $10^4$  GeV =  $10^{-23}$  kg. The old value of  $1.4 * 10^8$  kg was taken as a fit to the famous Tunguska-event in 1908 taken to be due to the impact of one of our pearls. The small mass proposal of about  $10^{-23}$  kg is rather inspired by an attempt to fit to the DAMA (-LIBRA) experiment (by most people presumably believed to be due to something else other than dark matter). (A presentation of the DAMA results is given in the present Bled Workshop proceedings).

- **Observational Discussion:**

Our small mass  $10^4$  GeV  $\approx 10^{-23}$  kg pearl proposal is filled with ordinary matter with an estimated density of the order of  $10^{14}$  kg/m<sup>3</sup> as we fit the size of the pearl, It is clear that the size of such a small pearl will nevertheless be so big - bigger than an atomic nucleus - that the cross section is likely to be so big that it could not possibly pass through about 1400 m into the earth without interacting. So in this sense our dark matter pearls are not WIMPS since the WI in this acronym stands for **w**eakly interacting. It could still be **dark** in the sense that the interaction with e.g. light *per mass unit* could be small, but not small per pearl.

With such a strong interaction one may worry whether such pearls have any chance of reaching down to give any signal in underground experiments looking for dark matter, because the pearls might be stopped in the shielding above the experimental apparatus; but here the reader should have in mind that a pearl that is heavy compared to atoms or nuclei, when it hits, will not be stopped but just deliver a smaller part of its kinetic energy to the hit particle, so that the latter obtains a speed of the same order as the speed of the incoming pearl.

Of course, if one has a hugely heavy pearl as we estimated of cm-size and with the large mass of  $1.4 * 10^8$  kg, then it will cause a major catastrophe, like the famous one in Tunguska, and a potential underground laboratory would be destroyed rather than making a proper observation.

But with the small size pearl having a mass in the  $10^4$  GeV range the pearl would still interact a lot with the earth in the shielding, but possibly not enough to be fully stopped before reaching say the DAMA-LIBRA laboratory proper. Actually we shall imagine that a very small fraction of the pearls come though to the laboratory, by accident so to say.

If the pearls interact several times passing through the experimental apparatus they will be **disqualified** as dark matter, which is usually assumed to have so small a cross section that they only interact **once** in the detector. Even if a dark matter pearl interacts several times in the shielding - but is not observed to interact because a high mass is not stopped but can continue - it may well be observed essentially as a dark matter event anyway.

Really we would like to propose a picture for the  $10^4$  GeV pearl mass proposal that a major part of the pearls end up getting stopped in the shielding - the earth above the experimental hall underground - but that the pearls with the smallest cross sections come through to the experimental apparatus and is observed there. If the pearls have a much bigger cross section than normal WIMPs they may well produce a non-negligible number of events even if the number reaching through is much lower than the number of WIMPs one would have expected.

In other words for the  $10^4$  GeV mass pearls we shall speculate that compared to the usual WIMP picture the much higher cross section of our pearls than that of the WIMPs can compensate for the lower number of pearls than of WIMPs reaching to the experimental apparatus for two reasons:

- There are fewer pearls than WIMPs if the pearls are as suggested heavier than the WIMPs, because we have to keep the gravitational effects the same to have the same mass density in the universe.
- There are few pearls also because some of the pearls get stopped in the shielding due to the bigger cross section in spite of them being heavy and not so easy to stop.

Now we should also mention that what is truly measured in the DAMA-LIBRA experiment is not so much the full numbers of presumed dark matter particles interacting with the apparatus, but rather the seasonal variation of the number of events. If indeed what they see in DAMA-LIBRA were due to our rather strongly interacting pearls, then there would be a seasonal effect partly due to the pearls coming in one season with higher speed than in another so they would be able to penetrate deeper. If by chance the depth of the laboratory is close to the average stopping place of the pearls, such an effect of different penetration depths in the different seasons might be delicate to estimate, but could make it possible to get a bigger seasonal effect than estimated in a more simple way.

Let us immediately remark, that if indeed such seasonal variation due to relatively small changes with season of the penetration depth of interacting pearls (dark matter particles), then this could mean that the DAMA-LIBRA type of experiment measuring mainly the seasonal effect could be favoured in finding a signal over other experiments not using this technique. This would help solving the main problem or mystery in connection with the DAMA-LIBRA experiment: Why do the other underground experiments looking for

dark matter not see the same amount of it as DAMA-LIBRA ? Now we would answer that DAMA-LIBRA may sit close to the average penetration depth and in one season this penetration depth is a bit deeper and DAMA-LIBRA sees a lot, while in another season the average penetration depth is a bit higher up and one does not see so much. Actually our fit suggests that the average penetration depth is only a small part of the way down the 1400 m but the falling off tail of the distribution which DAMA observes varies exponentially with the variation in average penetration depth and a rather big seasonal effect is indeed expected.

We want to conclude that IMPs (= interacting heavy particles) as our pearls could be denoted rather than the usual WIMP picture is a possibility for what the underground experiment DAMA-LIBRA could have observed.

And our argument about the penetration depth could be used to explain that other experiments did not see the same dark matter.

### 3.1.1 Plan

In the following section 3.2 we present a couple of figures about the dark matter as known already via its gravitational forces, and in the following section we give a couple of figures about impacts of objects like meteors falling on earth with the purpose of comparing the energy delivered with that which dark matter could deliver, if it fell like other objects. Then in section 3.4 we review some of the ideas needed to understand our type of model with pearls consisting of a bubble of a new type of vacuum (this is just our speculation because so far nobody really saw any new vacuum convincingly). In the subsections of this section we present in 3.4.1 our postulated new law of Nature "Multiple Point Principle", which is the main new assumption in our work in as far as, except for this multiple point principle, we only need the Standard Model as the laws of nature. We only make further speculations on the dynamics such as the existence of bound states or in general on results of the too hard to calculate, but by far not excluded possibilities in the Standard Model. In the subsection 3.4.2 we say a few words about the domain walls that will separate such different phases of the vacuum that we speculate exist. In subsection 3.4.3 we mention the effects other than gravitational ones which are probably due to the dark matter. The most important such effect for the present work is the excess X-ray radiation observed as a tiny peak above the best understanding fit to the X-ray spectrum at the photon energy 3.55 keV. Other such likely dark matter effects are an excess of positrons and the associated gamma rays; and then, what we are very keen on, one of the experiments Xenon1T meant to look for dark matter saw a little excess of electrons appearing in the apparatus, at first seemingly not dark matter; but we think it could be our dark matter pearls passing slowly through and delivering electrons with just the energy 3.55 keV.

In section 3.6 we mention that the type of dark matter models most popular in the literature, except for black holes making up the dark matter, need to modify the Standard Model by introducing extra particles corresponding to extra fields. Most popular is to use supersymmetry models in which there has to be included as many

new physics particles as there are particles already. Compared to that one should understand that we only add a new fine-tuning principle the “Multiple Point Principle”, which is an extra assumption about the values of coupling constants that can even be checked and at least are close to work, while the usual modified Standard Model has lots of extra particles not yet found.

Next in section 3.7 we discuss the fitting with our large pearl model, and in section 3.8 we then consider the model with the “small”, meaning little less than atomic size, pearls. Really this “small” size is in fact very large compared to what is considered in more conventional models (such as supersymmetry). In the subsection 3.8.1 we extract the ratio of cross section to mass for the dark matter required from the observation of the 3.55 keV X-rays from the Tycho supernova remnant and compare it to the corresponding ratio for nuclei in subsection 3.8.2. Then in the subsection 3.8.3 we present the fit of the small pearl model, but the fitting is based on the discussion of the DAMA(-LIBRA) experiment that we have first put in the next subsection 3.8.4.

In section 3.9 we resume and conclude the article .

## 3.2 We know something from the gravitational studies

As is well-known the dark matter has mainly and in fact possibly only been seen by its gravitational effects - and it could still be a possibility that there is no dark matter, but instead that something is wrong with our understanding of the gravitational force - but even from only observing it via the gravitational force, one can nevertheless derive some understanding of its distribution and velocity.

In fact one can already estimate that the solar system as a whole moves relative to the local dark matter average velocity with a speed of 232 km/s according to the figure 3.1.

Further the distribution of the dark matter **Motion of Dark Matter, stars etc. Numbers for Crude Estimates**

- **Density of Dark Matter in Solar System Neighborhood:**

$$D = \frac{0.3 \text{ GeV}}{\text{cm}^3} = 5.35 * 10^{-22} \frac{\text{kg}}{\text{m}^3} \quad (3.1)$$

- **Typical Speed (also relative to each other):**

$$v = 200 \text{ km/s} = 2 * 10^5 \text{ m/s} \quad (3.2)$$

- **Rate of Impacts on crossing Area, per m<sup>2</sup>:**

$$\text{Rate} = vD = 1.07 * 10^{-16} \frac{\text{kg}}{\text{m}^2\text{s}} \quad (3.3)$$

These numbers may be crudely estimated by looking at the distributions in figure 3.2, which have been gotten from the ERIS simulation of the dark matter.

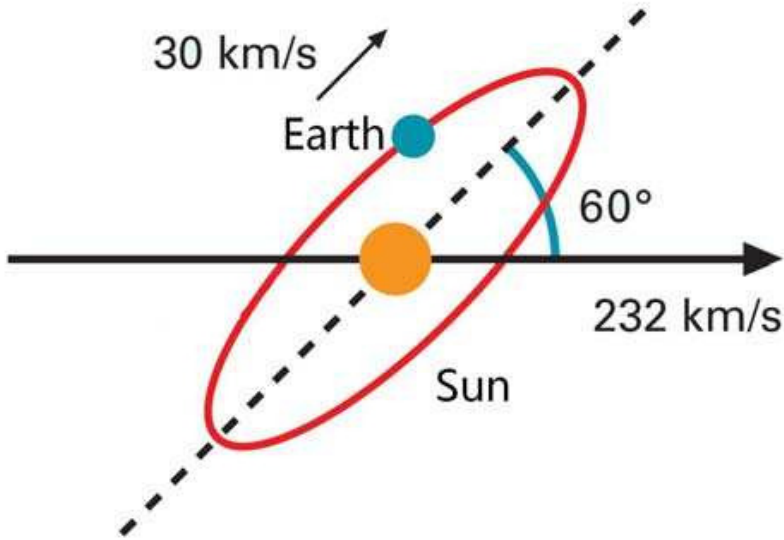


Fig. 3.1: Motion relative to Dark Matter Here is drawn how the solar system moves along relative to the supposed rest system of the bulk of the dark matter. One shall imagine the earth going around the ellipse drawn which in perspective is an approximate circle representing the orbit of the earth. Note how the speed of the earth w.r.t. the dark matter average will vary with the season.

### 3.3 Compare to Rates of Impacts on Earth

For the dark matter we have thus found the rate

$$\text{Rate} = vD = 1.07 * 10^{-16} \frac{\text{kg}}{\text{m}^2\text{s}} \tag{3.4}$$

In Table 3.1 we use this  $vD$  for dark matter in our neighborhood to derive a few estimates of impact rates for dark matter, if dark matter were indeed macroscopic particles with the masses listed in the first column of this table:

**Hitting Rates for some Masses:**

In the first column is given the mass of the dark matter pearl. The second column gives the rate of impacts such a mass would give per  $\text{m}^2$  and in the third column this rate is translated into the time between the impacts on this square meter. The fourth and fifth column similarly give the rates and the time in between impacts for impacts on the Earth in total instead of just on a square meter. Notice that in the row corresponding to the mass of the dark matter particle being  $10^8\text{kg}$  there is - in the last column - about 100 years between the impacts. Now it was approximately 100 years ago when the famous Tunguska event occurred, meaning that if the Tunguska event should be caused by a dark matter pearl, then the mass would be of the order of  $10^8\text{kg}$ .

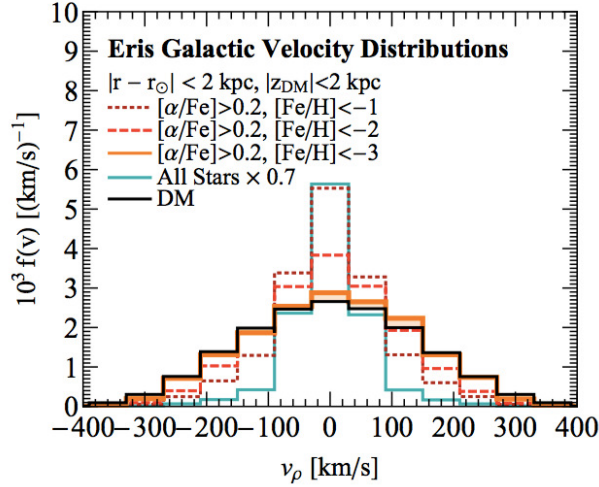


Fig. 3.2: Velocity histogram of different components of the Milky Way, as seen in the ERIS simulation. The black histogram shows the velocity distribution of dark matter. The cyan histogram illustrates the velocity of all stars, and has a much larger central peak than the dark matter distribution. The orange histogram, however, which includes only metal-poor stars, is very similar to the dark matter velocity distribution. (Herzog-Arbeitman et al. [7])

mass	m <sup>2</sup> rate	m <sup>2</sup> time	earth rate	earth time
10 <sup>-16</sup> kg = 5 * 10 <sup>10</sup> GeV	1s <sup>-1</sup>	1 s	5 * 10 <sup>16</sup> s <sup>-1</sup>	2 * 10 <sup>-15</sup> s
10 <sup>-8</sup> kg = 10μg	10 <sup>-8</sup> s <sup>-1</sup>	10 <sup>8</sup> s = 3y.	5 * 10 <sup>8</sup> s <sup>-1</sup>	2 * 10 <sup>-9</sup> s
1 kg	10 <sup>-16</sup> s <sup>-1</sup>	10 <sup>16</sup> s	5s <sup>-1</sup>	0.2s
10 <sup>8</sup> kg = 10 <sup>5</sup> ton	10 <sup>-24</sup> s <sup>-1</sup>	10 <sup>24</sup> s	5 * 10 <sup>-10</sup> s <sup>-1</sup>	2 * 10 <sup>9</sup> s ~ 100y

Table 3.1: A few rates for hypothetical dark matter pearls

Next we now give a similar table for meteor impacts as observed, impacts a priori expected to be made from “ordinary matter” (i.e. atoms). Here it is meant that the impacts are counted for the whole Earth:

#### Compare Impacts of Ordinary Matter

10<sup>-2</sup> kg : 10<sup>5</sup> per year

1 kg : 10<sup>4</sup> per year.

10<sup>8</sup> kg : 10<sup>-3</sup> per year.

You may consider the numbers in this table 3.1 as extracted from the figure 3.3.

Since a year has  $3.16 \times 10^7$  s this corresponds to a mass density  $D_{\text{meteor}}$  times the velocity  $v_{\text{meteor}}$  being of the order

$$v_{\text{meteor}} D_{\text{meteor}} \sim \frac{10^4 \text{ kg/year/eartharea}}{3.16 \times 10^7 \text{ s/year}} \tag{3.5}$$

$$= \frac{3 \times 10^{-3} \text{ kg/eartharea/s}}{0.5 \times 10^{15} \text{ m}^2/\text{eartharea}} \tag{3.6}$$

$$= 2 \times 10^{-18} \text{ kgs}^{-1} \text{ m}^{-2}; \tag{3.7}$$

formally a **factor 50 smaller** than the dark matter. Rather than the mass of the impact object you might use its size and then we get the graph in figure 3.3:

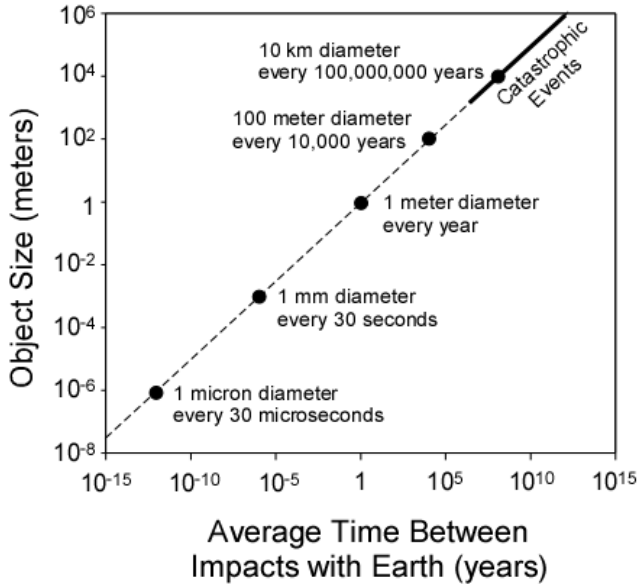


Fig. 3.3: Size of Impact goes as square root of “time in between”

From this figure 3.3 we can read off an approximate dependence of the size of the impacts on earth and their frequency. Approximately the inverse frequency being the “time between” goes as the square of the size of the impacting object. So a formula easy to remember is:

$$\text{“impact size” in m} = \sqrt{\text{av. “time between” in years}} \tag{3.8}$$

on earth.

On the figure 3.4 we see the relation between energy release by the impact and again the frequency measured in impacts per year.

**Would Macroscopic Dark Matter Dominate Meteors?**

- Taking very roughly the graph as having the slope -1 in the logarithmic plot we may read off that the energy of impacts per year is of the order of magnitude of  $10^{13}$ J/y to  $10^{14}$ J/y.

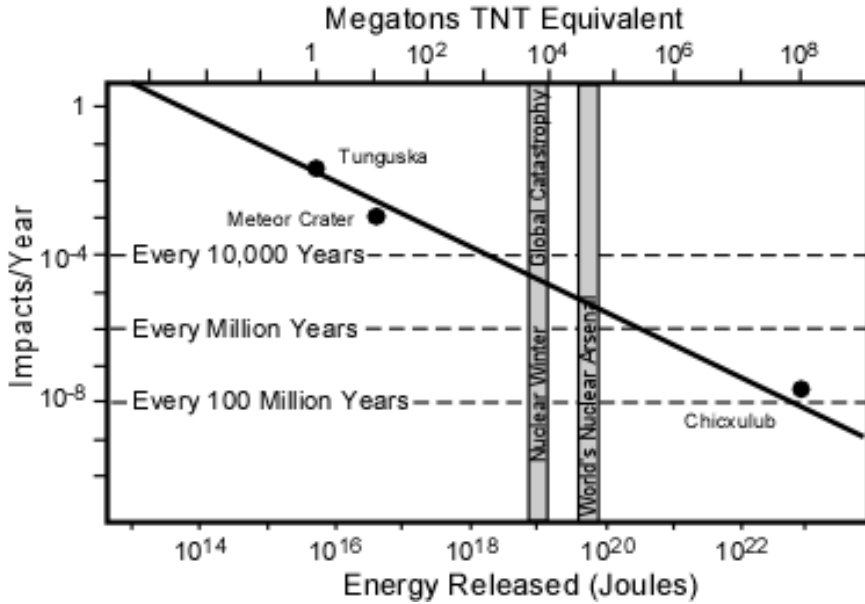


Fig. 3.4: Relation between energy released and impacts per year

- To compare with that the kinetic energy in the column of dark matter hitting the earth per year is for non-relativistic dark matter particles of the order of

$$\text{“dark matter power on earth”} = \quad (3.9)$$

$$= \frac{1}{2} * (300 \text{ km/s})^3 * 0.3 \text{ GeV/cm}^3 * \pi * (6.38 * 10^6 \text{ m})^2 \quad (3.10)$$

$$= \frac{1}{2} (3 * 10^5 \text{ m/s})^3 * 0.3 * 1.78 * 10^{-21} \text{ kg/m}^3 * \pi * (6.38 * 10^6 \text{ m})^2 \quad (3.11)$$

$$= 1.27 * 10^{16} \text{ J/y} \quad (3.12)$$

(using 1 year = 31556952 s)

So it looks that unless some of the kinetic energy of the dark matter hitting the earth is lost from showing up as observable impacts, there is too much energy in the dark matter to match the impacts as observed.

In our old work [6] we took it that because of the smallness of even cm-sized pearls they penetrate so deeply into the earth that it is realistic that an appreciable part possibly 19/20 of the energy is penetrating so deep into the earth, that it does not appear as observed energy on the surface of the earth. Since we could well find it consistent that our big pearl (=cm-size) would go thousands of km into the earth, it would indeed be hard to get all the energy out so quickly as to be identified with the energy of the impact.

### 3.4 Requisites for Our Model(s)

Before going on to fit our type of model and discussing how well such pearl models for the dark matter matches much of our knowledge about the dark matter, as it actually will, we shall put forward a few prerequisites needed for understanding the speculations making up at least one concrete example of a macroscopic pearl model of the dark matter.

As a motivation for just our concrete picture for how the pearls could come about let us stress: **Our picture of dark matter pearls can come about in the pure Standard Model, i.e. without any new physics in the sense of new basic particles.** We shall rather only speculate about new particles which are bound states of the already known particles, and thus do not require any modification of the Standard Model. We have e.g. no supersymmetric partners, because we do not have supersymmetry at least not in the relevant region of energy for our model.

Gia Dvali showed that the existence of several vacua is inconsistent unless they are degenerate in the article "Safety of Minkowski Vacuum" [8].

#### 3.4.1 Multiple Point (Criticality) Principle

The point in our work, which comes closest to assuming new physics, is the principle that the coupling constants of the true model for physics - for our purpose here the Standard Model - are by a "new Law of Nature" tuned in to just arrange that there are a series different phases of the vacuum - different vacua we could say - which all have the same energy density (= cosmological constant) [9–12]. We call this principle of such fine-tuning of the coupling constants the **Multiple Point (Criticality) Principle (MPP)** [9–12]. There has been given various arguments for it [8–12], and we can claim that using it we have even made correct **predictions**, e.g. the number of families, prior to the LEP measurement of the number of light neutrino species. We fitted fine structure constants in a rather complicated model called ANTIGUT and the fitting parameter was indeed the number of families. We **predicted** that to be 3. Later we obtained a mass prediction [13] for the Higgs of  $m_{\text{Higgs}} = 135 \pm 10 \text{ GeV}$  **before the Higgs was found.**

For our pearl-models of the dark matter it is important that Nature should have this fine-tuning at least to an appreciable accuracy making the inside and the outside vacua for our pearls of equal energy density. This is because otherwise almost certainly one of the phases would spread out and it would be very hard to get pearls that are stable. Actually even with the degenerate vacua we have in our model the need for getting the pearls filled by ordinary matter under high pressure to withstand the pressure coming from the tension of the surrounding skin or domain wall. Guesses as to the order of magnitude for what the energy density difference should be, if not tuned to be small, would be so high that our model would become unlikely. Though, if e.g. the energy density difference was only of the order corresponding to the observed order of magnitude for the vacuum energy in the universe it would contribute so little over one of our pearls that it would not disturb our calculations taking the difference to be zero.

### 3.4.2 Domain walls in general

There is also a discussion of walls in another article [14] in these proceedings.

We ourselves like to point out, that once we have the “Multiple Point Principle” we have in principle the possibility that some even large regions in space could be filled by one phase while another region could be filled by another phase of the vacuum. Had we had a spontaneously broken discrete symmetry it would induce a case of “Multiple point principle” in as far as two or more phases related by the broken symmetry would of course have for symmetry reasons the same energy density. It is however, not such a case of a spontaneously broken discrete symmetry, which *we* imagine in our model. We rather speculate that two a priori different, and not connected to each other by symmetry, vacuum phases are to be used. Having the spontaneously broken discrete symmetry is also phenomenologically badly working, in as far it would typically lead to random vacua coming to dominate in various regions outside the horizons of each other. Such outside each others horizon different dominating vacua would cause domain walls extending over longer distances than the horizon and in turn make up huge amounts of domain walls in cosmology. Unless the wall tension was extremely small such horizon scale walls would get to dominate under all circumstances in the long run; and that would spoil our cosmological models.

So we must hope, and we actually do expect, that the domain walls due to the asymmetry between their sides - i.e. due to the fact that the different vacuum phases are not connected by symmetry - will contract a bit more towards diminishing one vacuum than the other one. Thus at an early stage in the history of the universe one of the vacua only survives in **small** bubbles compared to the universe size. It is such small surviving bubbles that should be the dark matter. Actually even the small bubbles only survive because at a stage they get stopped from contracting by having collected so many nucleons inside that they can provide a sufficient pressure to stop the contraction.

For our cm-size pearls we had an estimate that the contraction of the pearls to the stability point where they just have the size given by their content of nucleons, counter acting the pressure, would end about the time in cosmology, when the big bang nuclear synthesis is about to start and temperature is of MeV size. It is very needed for our model that the pearls have become so compact and effectively disconnected from the rest of the plasma before the big bang nuclear synthesis properly begins, because otherwise our model would modify this big bang nuclear synthesis, and it would be an unconvincing refitting even if we managed to fit the abundances of the various light isotopes resulting from the big bang nuclear synthesis.

Nevertheless one should of course investigate astronomically if some of the big voids observed in the matter distribution should actually be a result of domain walls. If one had, for some accidental or other reason, an astronomical size region with the same vacuum as inside our pearls, formally an enormously large dark matter pearl, then we would expect there to be the same matter density inside this huge pearl as on the average in the universe. But now there would be no way to have true dark matter in the region, because the whole region is already formally dark matter. Pearls inside it of the present phase vacuum would repel rather than

attract nucleons and would thus totally collapse. Therefore in such regions one would in practice lack the dark matter and have it replaced by a higher density of ordinary matter. The latter would, however, have electrons staying relativistic longer than dark matter would have stayed relativistic. Thus these regions would presumably develop their inhomogeneities later than the regions where the present vacuum dominates. This could then be likely to delay the development of stars and galaxies in such formal huge dark matter bubbles of astronomical size. Such regions might appear as voids?

### 3.4.3 Non-gravitational Dark Matter Observations

We believe it is true to say that all non-gravitational signs from dark matter are somewhat doubtful. Nevertheless our main aim in this article to look especially for whether our model can get support from the observations of one of the presumed non-gravitational observations of dark matter, the 3.55 keV X-ray radiation in outer space, mainly seen [1,2] from our Milky Way Center or from big clusters of galaxies.

**The 3.55 keV X-rays** We have already mentioned this for us so important X-ray observation in a line of frequency 3.55 keV, which seems not to be explained by the atomic ion transitions expected in the plasmas from which the X-rays come. But it is only a tiny little deviation from the main fit of the X-ray spectrum and e.g. an unexpectedly high abundance of potassium in the plasmas could make a line in the region of the 3.55 keV be increased so much as to replace the tiny suspected dark matter line.

Using the expectations from the gravitational knowledge about the distribution of the dark matter, fits have been made to the 3.55 keV radiation expected both under the assumption that the emission from a region depends linearly on the density  $D$  of dark matter and under the assumption, that the amount of 3.55 keV line radiation is proportional to the square of the dark matter density  $D^2$ . It is the latter dependence that should come out of our model, because we postulate that the 3.55 keV radiation arises when our pearls **collide**. Both types of fits are not hopeless, and even the rather well fitting analysis by Cline and Frey [15], which we use in our work, has at least one severe discrepancy: one of the measurements in the outskirts of the Perseus Cluster delivers about 1000 times more 3.55 keV radiation experimentally than one should expect by extrapolating the fits to the other observations.

In our use of the analysis of Cline and Frey, we simply had to delete this observation to obtain a meaningful average for the overall scale of the radiation which is then what we ourselves sought to fit.

We should investigate, if we could understand this deviating measurement in the Perseus Cluster as due to our pearls getting energy for 3.55 keV radiation in a different way than from the collisions. In fact we have similar problem with the Tycho supernova remnant in which the square of the density  $D^2$  over the supernova remnant region is very tiny in comparison to galaxy clusters and the Milky Way Center extensive volumes. The supernova remnant region, even taking

into account the closeness of the Tycho supernova remnant, is so small that it would not be expected that Jeltema and Profumo should have seen the 3.55 X-ray line from the dark matter there. But in fact Jeltema and Profumo [24] **have seen 3.55 keV radiation from the supernova remnant.**

Our suggestion is that the cosmic rays or X-rays in the Tycho supernova region can excite the pearls, which then whatever the excitation energy - collision or cosmic ray excitation - will emit an appreciable part of the energy as 3.55 keV radiation.

One could of course hope - and we hope to find out - that there are some similar cosmic rays or X-rays reaching the outskirts of the Perseus Galaxy Cluster.

Of course, if the cosmic ray or X-ray activity is about the same in two neighboring regions in say the Perseus Cluster, then the ratio of the X-ray or cosmic ray feeded radiation relative to the one feeded by the collisions will go in the ratio  $\frac{D}{D^2} = D^{-1}$ . This is because the rate from cosmic ray feeding goes as  $D * \text{“density of cosmic rays”}$ , while the collision rate goes as  $D^2$ . In the outskirts of the cluster the density of dark matter  $D$  presumably goes down, and thus the cosmic ray feeded radiation becomes relatively more important.

**Positrons and Other Gamma-rays** Also positrons above some 10 GeV in energy have shown an excess suggested to be due to dark matter together, as one could imagine, with gamma-rays not in a line but in a broader spectrum. In this connection there is a little problem:

Using usual types of model for dark matter identified with some type of particle simply decaying into among other things the positron to make the excess, it is very hard to avoid that associated with this positron emission one does not also get some gamma-rays. Now, however, the fitting does not go well and it seems that experimentally there are not so many gamma-rays as is almost unavoidably needed for matching the positron excess!

This little tension with an elementary particle dark matter interpretation could provide support for our type of model, because at the collision and strong heating up of the uniting pearls a large amount of electrons will be emitted and can easily create electric fields that in a rather low acceleration way can accelerate e.g. positrons. Thus one can get positrons which are not produced at high speed almost abruptly, but which are “slowly” accelerated. The latter gives much less electromagnetic radiation and thus our model has the potential of making positrons with much fewer gamma rays connected with them. This would agree better with the too few observed gamma-rays.

**Xenon1T Electron Recoil Excess** Yet another effect, which we shall count as a non-gravitational effect of dark matter, but which is not obviously dark matter at all: the Xenon1T electron recoil excess.

Apart from the DAMA/LIBRA and the DAMA experiment all other experiments seem to find only negative results, when looking for the dark matter in direct searches. There was, however, found one unexpected result [16] although at first not seemingly related to dark matter:

The experiment Xenon1T investigated what they call electron recoil in their Xenon experiment. In the Xenon experiment one has a big tank of liquid xenon with some gaseous xenon above it and photomultipliers looking for the scintillation of this xenon, the philosophy being that a dark matter WIMP e.g. hits a nucleus inside the xenon and the recoil of this creates a scintillation signal S1 and also an electron, which is then driven up the xenon tank by an electric field and at the end by a further electric field made to give a signal at the top S2. By the relative size of the signals S1 and S2 one may classify the events - which are taken to be almost coinciding pairs of these signals S1 and S2 - as being nucleus recoil or electron recoil. One expects to find the dark matter in the nucleus recoils, since a dark matter particle is not expected to make an electron have sufficient energy to make an observable electron recoil event.

But now by carefully estimating the expected background, the Xenon1T experimenters found an **excess of electron recoil events**.

Ideas proposed for explaining it include axions from the sun or neutrinos having bigger magnetic moments or perhaps less interestingly that there could be more tritium than expected in the xenon.

But here with our model of relatively stronger interacting particles able to radiate the line 3.55 keV when excited we have a possible explanation:

Going through the earth above the detector and the rest of the shielding, the pearls or particles get excited so as to emit 3.55 keV X-ray just as they would do in the Tycho supernova remnant, where they also get excited by matter or cosmic rays. But then the particles passing through the deep underground Xenon1T experiment are already excited and prepared for emitting the 3.55 keV radiation. Now they could possibly simply do that in the xenon tank or they might dispose of the energy by a sort of Auger effect by rather sending out an electron with an extra energy of 3.55 keV. Such an electron with an energy of a few keV could be detected and taken for an electron recoil event in the Xenon1T experiment.

It is remarkable that the signal of these excess electron recoil events appears as having just an energy of the recoiling electron very close to the value 3.55 keV. Indeed the most important bins for the excess are the bins between 2 and 3 keV and the bin between 3 and 4 keV.

So we would claim that there is in our model no need for extra solar axions or a neutrino magnetic moment, nor tritium.

But we claim it to be 3.55 keV radiating dark matter one sees in the xenon experiment!

**The Dark Ages, 21 cm line** As a possible place to look for information about dark matter - especially of the pearl type say - is the influence it could have had in the "Dark ages" before the stars lit up the universe, a time that may be investigated through the study of the H1 radio line of 21 cm wavelength. Recent studies [17, 18] were pointed out to us by Astri Kleppe.

**Supernova Introductory Burst** As an interesting possibility for studying our dark matter pearls astronomically, we should also mention our older work, in

which we claim [19] that our dark matter pearls can not only help the supernovae to explode more, which is what is called for, but also to explain a neutrino burst appearing some hours before the genuine explosion, as appears to have been observed by the neutrino experiment LSD [20].

### 3.5 Status of Searches

Before going on to describe our models for dark matter being pearls of a new phase of vacuum, let us shortly review the status of the searches for dark matter in underground experiments. The plot in figure 3.5 shows the excluded regions in the cross section versus mass plane for dark matter particles in the usual WIMP-theory: It is important to notice for our work below that inside the region excluded

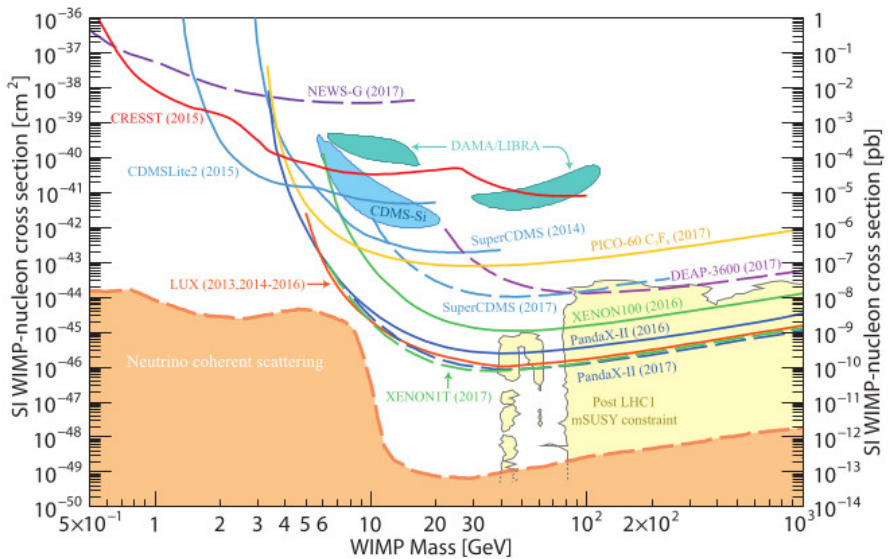


**Figure 27.1:** WIMP cross sections (normalized to a single nucleon) for spin-independent coupling versus mass. The DAMA/LIBRA [72], and CDMS-Si enclosed areas are regions of interest from possible signal events. References to the experimental results are given in the text. For context, the black contour shows a scan of the parameter space of 4 typical SUSY models, CMSSM, NUHM1, NUHM2, pMSSM10 [73], which integrates constraints set by ATLAS Run 1.

Fig. 3.5: Areas of the cross section versus mass of WIMP dark matter particles above the curves are excluded. So one sees that regions favoured by DAMA and CDMS-Si are seemingly in disagreement (although not in a theory independent way). See reference [21].

by several experiments there is a spot in which the DAMA-LIBRA experiment - in fact by 9 standard deviations - claim to have **found** the dark matter (or at least something with very similar properties) by their special technology of looking for

seasonal variations, that should appear because the speed of the Earth relative to the average velocity of the dark matter varies with season (see figure 3.1 above).

### 3.6 Dark Matter with only the Standard Model (except MPP)

Contrary to everybody else, except for the people who take primordial black holes for dark matter, we want to propose a dark matter model **inside the Standard Model**, only with a certain assumption about the coupling constants in the Standard Model, that there are several vacua fine-tuned to have the same energy density. So we have very little “new physics”:

- We assume a law of nature - of a somewhat unusual kind - the “Multiple Point Principle” saying: there are **several** different **vacuum phases**, and they all have the **same energy density** (or we can include that they have  $\sim 0$  energy density.)
- Apart then from mentioning an attempt mainly with Yasutaka Takanishi to explain the baryon excess, we shall use **only the Standard Model**, even for dark matter!

### 3.7 Our Fit

We performed a detailed fit with the model [3] in which we first of all looked for the absolute scale of the intensity of our model of dark matter pearls or balls emitting the X-ray line with photon energies of 3.55 keV in the rest system as apparently observed by satellites etc.

#### 3.7.1 The Intensity

The intensity we take in our model to be emitted by pearls, that have collided with one another - a rather infrequent event - but when they finally collide it is assumed, that the very strong skin surrounding the pearls can contract and thereby deliver energy, which can be used for the radiation in the 3.5 keV line or for other frequencies. There is in our model so to speak an active “energy production from the contraction”. But this we can in fact estimate, if we have the parameters of the model. Of course the fact that we need collisions of a pair of pearls to get the radiation in the 3.5 keV line means, that the intensity resulting in a given region of the space becomes proportional to the **square** of the density  $\rho_D$  of dark matter in that region. A fit to a model of this kind- which would also be applicable for a model in which the dark matter particles annihilate with each other - was performed using the astronomical - mainly satellite - data by Cline and Frey [15]. For the purpose of our model we can interpret it that they measure an intensity proportional parameter, which basically is in our language  $\frac{N\sigma}{M^2}$ , where M is the mass of the typical / average pearl,  $\sigma$  the cross section for one such pearl hitting another one, and N the number of 3.5 keV photons emitted when such a collision actually happens. From the results of Cline and Frey we find the number

$$\left(\frac{N\sigma}{M^2}\right)_{\text{exp}} = (1.0 \pm 0.2) * 10^{23} \text{ cm}^2/\text{kg}^2 \quad (3.13)$$

or rather we extract this number from their table:

Name Units	$N < \sigma_{CFV} > * \left( \frac{10 \text{ GeV}}{M} \right)^2$ $10^{-22} \text{ cm}^3 \text{ s}^{-1}$	$v$ km/s	boost	$\left( \frac{N < \sigma_{CFV} >}{v * \text{boost}} \right) * \left( \frac{10 \text{ GeV}}{M} \right)^2$ $10^{-27} \text{ cm}^2$	Remark
Clusters [1]	$480 \pm 250$	975	30	$0.016 \pm 0.008$	
Perseus [1]	1400 - 3400	1280	30	0.037 - 0.09	
Perseus [2]	$(1 - 2) * 10^5$	1280	30	2.7 - 5.3	ignored
Perseus [23]	2600 - 4100	1280	30	0.07 - 0.11	
CCO [1]	1200 - 2000	926	30	0.04 - 0.07	
M31 [2]	10 - 30(NFW)	116	10	0.0086 - 0.026	
	30 -50 (Burkert)			0.026 -0.043	
MW [22]	0.1 -0.7 (NFW)	118	5	0.00017 - 0,0012	ignored
	50 -550 (Burkert)			0.084 - 0.93	in average
Average				$0.032 \pm 0.006$	

Table 3.2: This table is based on the table 1 in reference [15].

It should be noticed though that something is not fitting well in the case of the Perseus Cluster in as far as one measurement in the outskirts of this galaxy cluster turns out to give a factor 1000 more radiation in the 3.5 keV line than the one that would have fitted with the proportionality to the squared density estimated from gravitational considerations. In our averaging we left this observation out totally, since it would have led to a very bad fitting for the other observations. But without this badly fitting observation we get the average (3.13).

### 3.7.2 The Frequency

The very frequency or the photon energy 3.5 keV, we sought to fit with the “homolumo gap” in the ordinary material under high pressure - comparable to that in white dwarf stars - inside our dark matter pearls. Such a “homolumo gap” is a very general feature for materials containing a degenerate Fermi sea of fermions, say electrons, and in addition has some structure -like a glass or almost all materials - consisting in that the material in detail adjusts so as to partly lower the energy density of the Fermi-sea. It is obvious that the energy of the Fermi sea is lower the lower in energy the filled fermion states, whereas lowering the energy of the empty states does not lower the total energy. The adjustment to a ground state of the material will therefore (almost) unavoidably lead to a lowering of the filled states and thus cause a gap between the filled and the empty states. It is this gap between the filled and the empty single particle states which is called the homolumo-gap. It is namely the gap between **highest occupied molecular orbit** (the chemist expression for single particle fermion state), HOMO and the lowest **unoccupied molecular orbit**, LUMO.

We estimated in [3] the value in energy of this homolumo gap partly just by a dimensional argument and partly by using a Thomas-Fermi approximation.

The formula for our estimate of the homolumo gap, which also turns out to be the expected frequency or photon energy for the line, was

$$E_H = \sqrt{2} \left( \frac{\alpha}{c} \right)^{3/2} E_f. \tag{3.14}$$

Here  $\alpha$  is the fine structure constant considered for the purpose of our dimensional arguments as a velocity (by multiplying it by the velocity of light  $c$ ) and  $E_f$  is the Fermi energy of the electrons in the hard compressed material inside our pearls.

### 3.7.3 The fitting and theoretical speculations

In our model we imagine that there are at least two phases of the vacuum - in addition presumably to several other ones too, but in the work now being reviewed we cared for only two important ones - and that the one in which we do not live, but which is realized inside the dark matter pearls, is distinguished from the present vacuum by there being a (boson) condensate of a speculated bound state of 6 top plus 6 anti-top quarks. In the vacuum phase inside the pearls we would at first have speculated that the expectation value of the Higgs field should go to zero, but that would give us an estimate of the tension of the skin separating interior and the exterior of the pearls, which would not give an acceptable fit. Indeed assuming that the usual Higgs spontaneous breakdown of the weak gauge symmetry in the vacuum inside the pearl is absent would suggest an order of magnitude of the tension in the skin of the pearls of the order of  $(100 \text{ GeV})^3$ , but the fitting we made gives an appreciably smaller tension.

Name	$\frac{\xi * 10 \text{MeV}}{\Delta V}$	$\ln \frac{\xi * 10 \text{MeV}}{\Delta V}$	Uncertainty	
Frequency "3.5keV"	5.0	1.61	100%	
Intensity $\frac{N\sigma}{M^2}$	3.8	1.3	90%	
$S^{1/3}$ theory 1)	0.28	-1.3	40%	
$S^{1/3}$ theory 2)	1	0	40%	
Combined theory $\xi, \Delta V$	0.18	-1.7	100%	
Ratio $\frac{t_{\text{spread}}}{t_{\text{radiation}}}=1$	2.4	0.88	80%	l.b.

Table 3.3: Table of four theoretical predictions of the parameter  $\frac{\xi * 10 \text{MeV}}{\Delta V}$  on which the quantities happen to mainly depend. The first column denotes the quantities for which we can provide a theoretical or experimental value to be expected for our fit to that quantity. The next column gives what these expected values need the parameter combination  $\frac{\xi * 10 \text{MeV}}{\Delta V}$  to be. The third column is the natural logarithm of that required value for the ratio  $\frac{\xi * 10 \text{MeV}}{\Delta V}$ , i.e.  $\ln \frac{\xi * 10 \text{MeV}}{\Delta V}$ . The fourth column contains crudely estimated uncertainties of the parameter thus fitted counted in this natural logarithm. In the last column we just marked the ratio  $\frac{t_{\text{spread}}}{t_{\text{radiation}}}$  with l.b. to stress that it is only a lower bound and shall not be considered a great agreement for our theory.

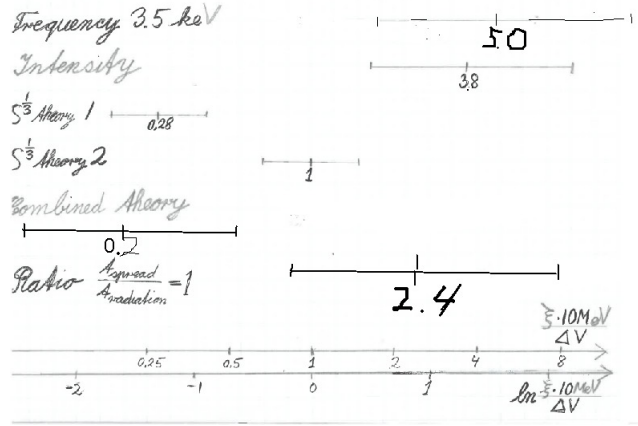


Fig. 3.6: The values of the ratio  $\frac{\xi * 10 \text{ MeV}}{\Delta V}$  as needed for four constraints. There are two experimental constraints from the frequency and intensity of the 3.5 keV radiation respectively and two theoretical constraints in two versions corresponding to taking theory 1 or theory 2 for the tension. We make the simplifying assumption that all energy from the surface contraction in a collision gets emitted as 3.5 keV X-rays. The sixth line "Ratio  $\frac{t_{\text{spread}}}{t_{\text{radiation}}} = 1$ " represents the lower bound ensuring that all the energy actually goes into 3.5 keV radiation.

The essential parameter we used in our fit was defined as

$$\frac{\xi * 10 \text{ MeV}}{\Delta V} = \frac{10 \text{ MeV} * R / R_{\text{crit}}}{\text{"potential difference for nucleon in the two vacua"}}. \quad (3.15)$$

In order to reduce the number of parameters in our earlier paper [6] we assumed that the pearls just had such a size that they were on the borderline to collapse and we call the radius of such barely stable pearls  $R_{\text{crit}}$ . We now denote the actual radius of the (typical) pearl by just  $R$  and define the parameter  $\xi = \frac{R}{R_{\text{crit}}}$ . The parameter  $\Delta V$  is the binding energy of a nucleon relative to when it is in the vacuum phase in the interior of the pearls. One should imagine that nucleons are attracted by the pearls by having a lower potential by the amount  $\Delta V$  inside the pearl. If the pearl gets too small and the pressure from the skin thus too high it will pay energetically for the nucleons inside the pearl to escape and the pearl thus collapses; this is what happens when the radius is smaller than the critical radius  $R_{\text{crit}}$ . The 10 MeV was just a conventional number, we put in to make the parameter dimensionless.

It turned out from our calculations that the combined parameter ratio  $\frac{\xi * 10 \text{ MeV}}{\Delta V}$  is the main one to fit, because the interesting measurable and theoretically interesting quantities mainly depend on it.

We thus used it to make fits especially to the experimentally predictable quantities, the intensity of the 3.5 keV radiation scale and the very frequency 3.5 keV. The fitted values of the combined parameter  $\frac{\xi * 10 \text{ MeV}}{\Delta V}$  for these quantities are

presented in Table 3.3 together with those expected for a tension of  $(100 \text{ GeV})^3$  as obtained from the Higgs field consideration above (theory 1) - even a somewhat smaller value for the tension is speculated about and called theory 2 - and for a theoretical expectation. These predictions are also plotted in Figure 3.6.

We see that the theoretical expectations for the tension  $S$  tend to fit with too small values of our parameter combination  $\frac{\xi \cdot 10 \text{ MeV}}{\Delta V}$  and so does our theoretical estimate of the  $\xi$  deviation from criticality combined with the expected value for  $\Delta V$  represented in the table and the figure below as “combined theory”. The last line in the table and the figure represents a parameter value below which it is expected that more and more energy is lost to higher frequency radiation than the 3.5 keV one. This is because the pearl in the collision gets heated up and then the heat spreads out so quickly that only a very little part goes into the line observed as the 3.5 keV line. The point is indeed that we expect the temperature from the contraction of the surface to be much higher than 3.5 keV, but then this heat spreads out of course gradually on a second time scale to the whole pearl. Under this spreading out there is a spreading border at the place to which the heating has reached at any moment. Near that border the temperature is about 3.5 keV and the 3.5 keV radiation is produced and because the pearl material is supposed to be transparent to the 3.5 keV and lower frequency radiation, it is radiated out to outer space. But if the heat reaches all through the pearl the outer surface of the pearl gets appreciably hotter than 3.5 keV; then most radiation comes with higher frequency and is correspondingly lost for radiation in the observed 3.5 keV line. The “time ratio  $\frac{t_{\text{spread}}}{t_{\text{radiation}}} = 1$ ” represents the fitting to the value 2.4 of our parameter  $\frac{\xi \cdot 10 \text{ MeV}}{\Delta V}$  at which the heat just reaches to the border of the pearl. That is to say for smaller parameter values there is a significant loss in energy to higher frequencies, while for larger values of our parameter we expect that a major part of the energy from the contractions manages to be emitted as the line.

### 3.8 Latest Idea: Smaller Pearls giving also DAMA observation and Tycho Supernova Remnant Observation of 3.5 keV

After the Bled conference we have looked at the idea that we could ignore the connection to the Tunguska event, which was at first so terribly important for our studies and instead seek a combined fitting of not only as just presented the 3.5 keV radiation from the clusters of galaxies and the center of our Milky Way, but also an observation, that would at first look like spoiling the hypothesis that the 3.55 keV line comes from dark matter. In fact this observation was considered by the authors of [24] to be a clear sign that the 3.5 keV line must after all be an effect of some ordinary ions - such as an unexpectedly high abundance of potassium (K) - but not a signal from dark matter. This observation is the observation by Jeltema and Profumo that the 3.5 keV line is indeed also emitted from the Tycho supernova remnant! In almost all usual dark matter models as elementary particles this appearance from the supernova remnant with very little dark matter compared to ordinary matter is rather absurd. It can only come about if the dark matter can somehow absorb the energy present in the remnant region and convert it into the 3.5 keV line.

We are now working on fitting the requirement to get the sufficient 3.5 keV radiation from the supernova remnant and it certainly points towards smaller values for the tension than even the fit above.

In fact we have a crude fit to both the observation by Jeltema et al. and the DAMA and DAMA LIBRA observations, but now with both the cubic root of the tension  $S^{1/3}$  and the potential difference for a nucleon passing through the skin of the pearl  $\Delta V$  being of the order of 1 or 2 MeV only.

In this picture the pearls are less than atomic size and thus much more like dark matter models with WIMPs. But, especially to cope with the amount of interaction needed for the Tycho supernova remnant observation, they have to interact so strongly that they will interact several times on the way down through the earth to the DAMA-LIBRA observatory. So they should not be called weakly interacting, i.e the W in WIMP should be left out. Because they are, however, still very heavy, say  $10^3$  GeV or even heavier, compared to usual WIMP speculations, they are difficult to stop even when they hit matter in the shielding. So they can pass on and penetrate into the apparatus even if they have been somewhat hitting on the way down. Assuming that they as macroscopic objects - they are still pearls although now smaller - have somewhat different cross sections, some pearls may come through. Then even if only a small part comes through the shielding they could cause a number of events, as the observations suggest anyway in experiments like DAMA-LIBRA. Actually such a survival is only expected for some exceptional ones among the dark matter particles, which could easily lead to an enhanced dependence on the season and thus be especially suitable to be detected by DAMA-LIBRA relative to other experiments, that just observe the events independent of their season variation.

### 3.8.1 $\frac{\sigma}{M}$ from Tycho Observation

The mysterious 3.55 keV line has been seen, corrected to zero Doppler shift, not only from various galaxy clusters and the Milky Way Center, but also from the remnant of the supernova described by Tycho Brahe after its appearance in 1572. This at first seems to be in contradiction to the hypothesis that the X-rays should come from dark matter at all.

The authors Jeltema et al. [24] take it that this Tycho supernova remnant observation means that the 3.55 keV line radiation cannot come from dark matter because basically there would not be dark matter in sufficient amounts in the supernova remnant. It would then have to be an ordinary transition line in excited ions, which must have been underestimated in the theoretical calculation of the other radiation from the supernova remnant say. Actually some underestimate of the abundance of potassium K could deliver a line in the region.

But we basically take the point of view, that dark matter consists of some (type of) particles which have the possibility of being excited, and then when excited to send out especially X-rays in the 3.55 keV line. So we have the option of having the activity in the supernova remnant excite the dark matter particles there and thus make them radiate with their characteristic frequency 3.55 keV. (In the galactic clusters etc. we have a model of exciting them by collisions causing

skin contraction and thus extra energy being set free. But the emission is again the characteristic line 3.55 keV.)

But of course the absolute imperative for such a model for creating the 3.55 keV line radiation in the supernova remnant is that the dark matter particles (whatever they may be) have sufficiently big cross sections to at least pick up enough energy for the emission of the observed 3.55 keV line radiation.

**How we got the need for  $\frac{\sigma}{M} \geq 6 * 10^{-7} \text{m}^2/\text{kg}$**

**What observed:** Jeltema and Profumo claim [24] that they have observed an X-ray spectral peak - fitted with difficulty, but nonetheless fitted to be there - with an intensity of  $2.2 * 10^{-5}$  photons per  $\text{cm}^2$  per s. Thus in each  $\text{cm}^2$  of the sphere around Tycho passing through the earth, there passes  $2.2 * 10^{-5}$  photons per s per  $\text{cm}^2$  (or is it  $2.2 * 10^{-6}$ ? as there is a discrepancy with the figure in [24], and if the figure is right).

The distance to Tycho (SN1572) is about 9000 light-years. In fact, according to Wikipedia:

“The distance to the supernova remnant has been estimated to between 2 and 5 kpc (approx. 6,500 and 16,300 light-years), with recent studies suggesting a narrower range of 2.5 and 3 kpc (approx. 8,000 and 9,800 light-years).”

Taking 1 light-year =  $10^{16}$  m, the area of the sphere around Tycho going through the earth is

$$\text{sphere area} = 4\pi * (9000\text{ly} * 10^{16}\text{m/ly})^2 \quad (3.16)$$

$$= 10^{41}\text{m}^2 \quad (3.17)$$

So the number of 3.55 keV photons passing through this surface will be

$$\# \text{ of photons} = (2.2 \pm 0.3) * 10^{-5} \text{cm}^{-2} \text{s}^{-1} * 10^{41} * 10^4 \text{cm}^2 \quad (3.18)$$

$$= 2 * 10^{40} \text{s}^{-1} \quad (3.19)$$

$$\sim \text{“an energy rate”} : 3.5\text{keV} * 2 * 10^{40} \text{s}^{-1} \quad (3.20)$$

$$= 10^{32} \text{erg/s.} \quad (3.21)$$

**Rate of Energy Ploughing up** The total energy in the remnant region will still in first approximation be equal to the energy ejected from the supernova, if we assume that the energy escaping as light going so far away that we no more can count it as belonging to the remnant is small compared to the part remaining in the remnant region. A major part of this energy is presumably in the form of fast moving particles or even X-rays, so that order of magnitudewise we may count it as cosmic rays moving with the speed of light relative to the dark matter pearls, which of course have a much lower velocity of the order of the escape velocity from the Galaxy.

All over the remnant region we assume that the density of dark matter is very similar to that in the neighborhood of our solar system

$$D_{\text{sun}} = \frac{0.3 \text{ GeV}}{\text{cm}^3}, \quad (3.22)$$

so that the number of pearls we have in every  $\text{cm}^3$  is  $\frac{0.3 \text{ GeV}}{M}$ . In each second each of these pearls pick up the cosmic rays or whatever material in the remnant in a volume  $\sigma * v \approx \sigma * c$  where  $\sigma$  is the cross section for a pearl and  $v$  is the average relative velocity of the pearl and the remnant matter or radiation. That is to say, that during a second the fraction of the volume getting ploughed through is

$$\text{“Fraction ploughed through”} = \frac{D_{\text{sun}}}{M} * \sigma * v. \quad (3.23)$$

So if one observes a 3.55 keV line with an intensity  $I = 2.2 * 10^{-5}$  photons per s per  $\text{cm}^2$  we need the total energy rate (power) at a distance  $d = 9 * 10^{19}$  m to be

$$W = I * 4\pi * d^2 * 3.55 \text{ keV} * 2.2 * 10^{-5} \text{ cm}^{-2} \text{ s}^{-1} = 10^{32} \frac{\text{erg}}{\text{s}}. \quad (3.24)$$

Then we must have

$$W = E_{\text{remnant}} * v D_{\text{sun}} * \frac{\sigma}{M}, \quad (3.25)$$

or

$$\frac{\sigma}{M} \Big|_{\text{Tycho}} = \frac{W}{E_{\text{remnant}} * D_{\text{sun}} v} \quad (3.26)$$

$$= \frac{10^{32} \text{ erg/s}}{10^{51} \text{ erg} * 0.3 \text{ GeV/cm}^3 * 3 * 10^{10} \text{ cm/s}} \quad (3.27)$$

$$= 0.56 * 10^{-2} \text{ cm}^2/\text{kg} \quad (3.28)$$

$$= 10^{-29} \text{ cm}^2/\text{GeV} \quad (3.29)$$

$$= \frac{1}{(3.4 \text{ GeV})^3} \quad (3.30)$$

### 3.8.2 Comparing to Nuclear $\sigma/M$ Ratio

The material inside our pearls is highly compressed and taken to be mainly carbon (with atomic number  $A = 12$ ). Then using a crude formula  $1.2A^{1/3} \text{ fm}$  for the radius of a nucleus and  $\pi(1.2A^{1/3})^2 \text{ fm}^2$  for the cross section for some smaller particle scattering on the nucleus, we get for nucleus scattering:

$$\frac{\sigma}{M} \Big|_{\text{nuclear}} = \frac{\pi * 1.2^2 \text{ fm}^2 * A^{2/3}}{A * 0.94 \text{ GeV}} \quad (3.31)$$

$$= \frac{123 \text{ GeV}^{-3}}{\sqrt[3]{12}} \quad (3.32)$$

$$= \frac{1}{(0.265 \text{ GeV})^3}. \quad (3.33)$$

Combining these numbers for the ratio  $\frac{\sigma}{M}$  needed for the dark matter in the supernova remnant (3.30) with the one for a suitable nucleus (3.31) we see that the needed lower bound is

$$\frac{\frac{\sigma}{M} \Big|_{\text{Tycho}}}{\frac{\sigma}{M} \Big|_{\text{nuclear}}} = \frac{(0.26 \text{ GeV})^3}{(3.4 \text{ GeV})^3} \quad (3.34)$$

$$= 0.076^3 = 4.5 * 10^{-4}. \quad (3.35)$$

This means that about 1/2000 of the accessible energy would indeed become 3.5 keV photons, if the cross section for the pearls in Tycho was actually equal to the nuclear cross section. Actually such an efficiency of  $4.5 * 10^{-4}$  is not at all unlikely. So we could claim that, having in mind that the orders of magnitude could have run out to wildly different values, the rather close agreement could be taken to mean that indeed the true  $\frac{\sigma}{M}$  for the dark matter pearls being excited is indeed equal to the nuclear one (3.31). If indeed the pearls were so small that there was no significant shadowing by one nucleus of another of the nuclei in the pearls, then the cross section to mass ratio would just be the nuclear one. So an order of magnitude agreement with the actual cross section to mass ratio being the nuclear value should be taken almost as successful agreement.

Let us say this in other words:

If we assume that the tension  $S$  and the parameter  $\frac{\xi_{fs}}{\Delta V}$  have such values that **formally** the cross section to mass ratio  $\frac{\sigma}{M}$  would be smaller than the corresponding nuclear ratio (3.31), the actual cross section to mass ratio would only be approximately equal to the nuclear ratio. (Here  $\xi_{fs}$  is the radius scaling factor for fixed tension  $S$ , see section 3.8.3). For so thin pearls a cosmic ray say could with high probability pass through the pearl without hitting any nuclei inside. For such parameters one would obtain for the cross section to mass ratio just the nuclear value, see Figure 3.7. But anyway of course there would be an appreciable loss of energy that would not go to the 3.5 keV radiation, even compared to the amount of 3.5 keV radiation having been corrected with the time ratio for the fact that the emission into 3.5 keV radiation only takes place in a short period of time  $t_{spread}$ . Let us say that it is only the fraction  $1/l$  of the energy available in the period when the surface of the pearl is still cold that really comes out as this radiation.

Having in mind instead of the collision events the events in the Tycho supernova remnant this time ratio correction is not present, because the single cosmic ray exciting the pearl is supposed not to heat it up so much that the problem of the pearl being hot comes up. So for the Tycho supernova remnant the emission of the 3.5 keV radiation should be calculated without this time ratio correction. But it should still for “general” inefficiency be reduced by the factor  $l$ .

For pedagogical reasons we could imagine, that we could estimate the efficiency  $1/l$  sufficiently accurately that we could say: Fantastic that we just get the radiation as observed by Jeltema et al. from the Tycho Supernova remnant equal to this  $l$  divided into the rate expected if all the energy went to 3.5 keV radiation and the cross section to mass ratio was just the nuclear physics one (3.31). In this optimistic thinking we would have an empirically based suggestion saying that the size of the pearls are actually so small that the cross section to mass ratio becomes equal to the nuclear ratio. But for this to happen it would have to be that the formally calculated ratio should be *larger* than or equal to this nuclear ratio. This in turn will put an upper limit on the tension  $S$  depending somewhat on our parameter  $\frac{\xi_{fs}}{\Delta V}$ , since the cross section to mass ratio is a decreasing function of the tension  $S$  and then of course also as a function of the third root of this tension  $S^{1/3}$  which we mainly use in our text and figures. The upper limit following from this consideration based on claiming the nearness of the ratio actually estimated from

Jeltema et al. to the nuclear ratio is shown on Figure 3.9 below as the line labeled "nuclear".

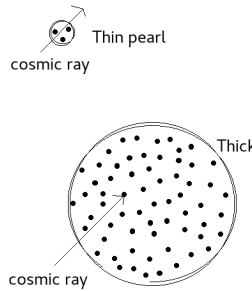


Fig. 3.7: This figure illustrates that for the density inside a pearl being very high a cosmic ray particle hitting the pearl will sooner or later in the interior hit a nucleus, while for a very little pearl with the same density the thickness of the pearl is insufficient for all cosmic ray particles to hit a nucleus and the cross section will be less than the geometrical one  $\sigma = \pi R^2$ . The ratio  $\frac{\sigma}{M}$  is then rather equal to the nuclear value (3.31).

**Resume of Comparison with Nuclear Ratio  $\frac{\sigma}{M}$**  But let us stress again that, if the loss of energy by the inefficiency of making 3.5 keV radiation from all the energy available could be estimated to be a factor of the order of  $l = 2000$ , then we could claim the very value of the Jeltema et al. observation strength as a victory for the picture.

### 3.8.3 Combined Fitting, Small Pearl Model

**Formulas for the Critical Case, Pearls Just about to Collapse** First let us give a list of the interesting quantities in terms of the cubic root of the tension of the surface  $S^{1/3}$  and the energy difference for the nucleon on passing the domain wall  $\Delta V$  in the case of a critical sized pearl. By this we mean the case in which a further parameter has been avoided by adjusting it so that the tension provides a pressure on the material inside the pearl making it just on the border to collapse by spitting out nucleons. In other words providing enough pressure to just barely compensate the potential difference  $\Delta V$  per nucleon. So now we should note the various parameters in this borderline/critical situation (see reference [3] for details

on the notation):

$$\text{Pearl radius } R_{\text{crit}} = \frac{3\pi^2 S}{2(\Delta V)^4} \quad (3.36)$$

$$\text{Fermi momentum } p_{f \text{ crit}} = 2\Delta V \quad (3.37)$$

$$\text{Energy release by collision } E_{S \text{ crit}} = S(\sim 4\pi)R_{\text{crit}}^2 \quad (3.38)$$

$$= \pi^5 * 9S^3 / (\Delta V)^8 \quad (3.39)$$

$$\text{Collision cross section } \sigma_{\text{crit}} = \pi * (2R_{\text{crit}})^2 = 6 * \pi^3 S^2 / (\Delta V)^8 \quad (3.40)$$

$$t_{\text{spread crit}} = \frac{\rho c_p}{4k} * R_{\text{crit}}^2 \quad (3.41)$$

$$= \frac{\alpha 55 R^2 T}{24 c^3} |_{\text{crit}} \quad (3.42)$$

$$t_{\text{radiation crit}} = \frac{E_S}{4\pi R^2 \sigma_{ST} (3.5 \text{keV})^4} \quad (3.43)$$

$$= \frac{60S}{\pi^2 (3.55 \text{keV})^4}; \quad (3.44)$$

$$\frac{\sigma_{\text{crit}}}{M_{\text{crit}}} = \frac{6 * \pi^3 S^2 / (\Delta V)^8}{m_N * \frac{24\pi^5 S^3}{(\Delta V)^9}} \quad (3.45)$$

$$= \frac{\Delta V}{4\pi^2 S m_N} \quad (3.46)$$

$$\frac{E_{S \text{ crit}}}{M_{\text{crit}}} = \frac{S(\sim 4\pi) \left( \frac{3\pi^2 S}{(\Delta V)^4} \right)^2}{m_N \frac{24\pi^5 S^3}{(\Delta V)^9}} \quad (3.47)$$

$$= \sim \frac{\Delta V}{2m_N} \quad (3.48)$$

$$\frac{N_{\text{crit}}}{M_{\text{crit}}} = \frac{E_{S \text{ crit}}}{M_{\text{crit}} * 3.55 \text{KeV}} \sim \frac{\Delta V}{2m_N * 3.55 \text{KeV}} \quad (3.49)$$

$$\frac{N\sigma}{M^2} \Big|_{\text{all } E_S \rightarrow 3.5 \text{keV}; \text{ crit}} = \frac{N_{\text{crit}} * \sigma_{\text{crit}}}{M_{\text{crit}} * M_{\text{crit}}} \quad (3.50)$$

$$= \frac{(\Delta V)^2}{8\pi^2 S m_N^2 * 3.55 \text{keV}} \quad (3.51)$$

$$\frac{t_{\text{spread}}}{t_{\text{radiation}}} * \frac{N\sigma}{M^2} \Big|_{\text{all } E_S \rightarrow 3.5 \text{keV}} \propto (\Delta V)^{-5} (3.5 \text{keV})^3 \quad (3.52)$$

$$\text{frequency} = E_H = 137^{-3/2} \sqrt{2} p_f = 137^{-3/2} \sqrt{2} 2\Delta V \quad (3.53)$$

$$\sqrt[3]{\frac{9\pi M_{\text{crit}}}{8m_N}} = (R p_f) |_{\text{crit}} \quad (3.54)$$

$$\frac{M_{\text{crit}}}{m_N} = \frac{24\pi^5 S^3}{(\Delta V)^9}. \quad (3.55)$$

**With Radius Scale up Parameter  $\xi_{fS}$**  The critical case is not realistic except very crudely. The pearls would collapse by the tiniest deformation during the contraction in the early universe situation. We must expect that there must be an appreciable safety margin in the sense, that the number of nucleons inside the

contracting pearl for the pearl not to collapse immediately must be so large, that the final radius, when the fluctuations from the contraction have died out will be say  $R = \xi_{fS} * R_{crit}$  with  $\xi_{fS} \approx 5$ . We estimated in earlier articles this expected ratio of the average radius to the critical or borderline one to be  $\sqrt{4\pi} * 24/9 \approx 5$ .

The dependence of some of the important quantities with this  $\xi_{fS}$  goes as follows. Here we also include the dependence on  $\Delta V$  and on  $S$ :

$$\text{Pearl radius } R = \xi_{fS} R_{crit} = \xi_{fS} \frac{S * 24\pi^2}{(2\Delta V)^4} \quad (3.56)$$

$$\text{Cubic root of tension } S^{1/3} = S^{1/3}(\text{fixed}) \quad (3.57)$$

$$\text{Fermi momentum } p_f = \xi_{fS}^{-1/4} 2\Delta V \quad (3.58)$$

$$\text{Energy release by collision } E_S = \pi^5 * 9S^3 \xi_{fS}^2 / (\Delta V)^8 \quad (3.59)$$

$$\text{Collision cross section } \sigma = 6\pi^3 \xi_{fS}^2 S^2 / (\Delta V)^8 \quad (3.60)$$

$$t_{spread} = \frac{\alpha 55 R^2 T}{24c^3} \quad (3.61)$$

$$\text{(where } T \approx 0.3\Delta V) \quad (3.62)$$

$$= 1.10\Delta V * S^2 \left( \frac{\xi_{fS}^{1/4}}{\Delta V} \right)^8 \quad (3.63)$$

$$t_{radiation} = \frac{60S}{\pi^2 (3.55\text{keV})^4} = \frac{6.08S}{(3.55\text{keV})^4}; \quad (3.64)$$

$$\frac{t_{spread}}{t_{radiation}} = \frac{1.10\Delta V * S^2 \left( \frac{\xi_{fS}^{1/4}}{\Delta V} \right)^8}{\frac{6.08S}{(3.55\text{keV})^4}} \quad (3.65)$$

$$= 0.18 * (3.55\text{keV})^4 * S \left( \frac{\xi_{fS}^{1/4}}{\Delta V} \right)^8 \Delta V \quad (3.66)$$

$$\frac{\sigma}{M} = \frac{6 * \pi^3 S^2 \left( \frac{\xi_{fS}^{1/4}}{\Delta V} \right)^8}{m_N * 24\pi^5 S^3 \left( \frac{\xi_{fS}^{1/4}}{\Delta V} \right)^9} = \frac{1}{4\pi^2 S m_N * \frac{\xi_{fS}^{1/4}}{\Delta V}} \quad (3.67)$$

$$\frac{E_S}{M} = \frac{S(\sim 4\pi)R_{crit}^2}{m_N 24\pi^5 S^3 \left( \frac{\xi_{fS}^{1/4}}{\Delta V} \right)^9} \sim \frac{1}{2m_N * \frac{\xi_{fS}^{1/4}}{\Delta V}} \quad (3.68)$$

$$\frac{N}{M} = \frac{E_S}{M * 3.55\text{keV}} \sim \frac{1}{2m_N * \frac{\xi_{fS}^{1/4}}{\Delta V} * 3.55\text{keV}} \quad (3.69)$$

$$\left. \frac{N\sigma}{M^2} \right|_{\text{all } E_S \rightarrow 3.5\text{keV}} = \frac{N}{M} * \frac{\sigma}{M} = \frac{1}{8\pi^2 S m_N^2 * \left( \frac{\xi_{fS}^{1/4}}{\Delta V} \right)^2 * 3.55\text{keV}} \quad (3.70)$$

$$\frac{t_{\text{spread}}}{t_{\text{radiation}}} * \frac{N\sigma}{M^2} \Big|_{\text{all } E_S \rightarrow 3.5\text{keV}} = 0.18 * (3.55\text{keV})^4 S \left( \frac{\xi_{fS}^{1/4}}{\Delta V} \right)^8 \Delta V * \quad (3.71)$$

$$* \frac{1}{8\pi^2 S m_N^2 * \left( \frac{\xi_{fS}^{1/4}}{\Delta V} \right)^2} 3.55\text{keV} \quad (3.72)$$

$$= 1.15 * 10^{-13} \text{GeV} \Delta V * \left( \frac{\xi_{fS}^{1/4}}{\Delta V} \right)^6 \quad (3.73)$$

$$\text{frequency} = E_H = 137^{-3/2} \sqrt{2} p_f = \xi_{fS}^{-1/4} \frac{2\sqrt{2}}{137^{3/2}} \Delta V \quad (3.74)$$

$$\frac{M}{m_N} = \frac{8}{9\pi} (R p_f)^3 \quad (3.75)$$

$$= 24\pi^5 \left( \frac{S^{1/3} \xi_{fS}^{1/4}}{\Delta V} \right)^9 \quad (3.76)$$

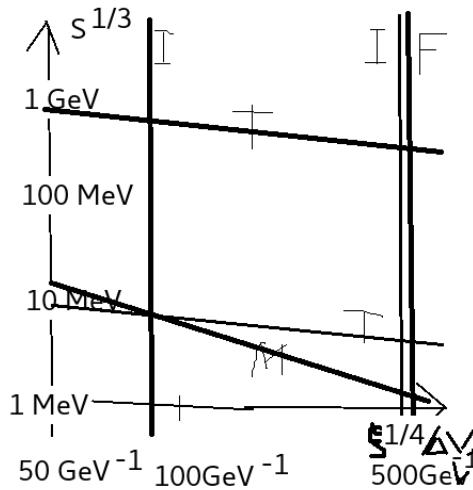


Fig. 3.8: This figure illustrates the fitting of our two parameters  $S^{1/3}$  along the ordinate,  $\frac{\xi_{fS}}{\Delta V}$  along the abscissa, while our third parameter  $l$  is just illustrated by shifting the two fitting restriction lines from  $l = 1$ , thickest line to slightly thinner lines for  $l = 82^2$ . The lines are marked by: I for the fitting to the intensity from galactic clusters etc, T for the Tycho observation, F for the frequency, and M for the DAMA mass restriction. It is only the restriction lines for I and T that move when  $l$  is shifted to be less than unity. Even our  $l = 82^2$  does not completely fit, but the reader can extrapolate by eye to see that even a bit larger  $l$  somewhere around  $l = 800^2$  would give a crude fit around  $S^{1/3} = 1\text{MeV}$  and  $\frac{\xi_{fS}^{1/4}}{\Delta V} = 1000 \text{ GeV}^{-1} = 1 \text{ MeV}^{-1}$ . But this points to a surprisingly large value of  $l$ .

**Fitting with also inefficiency, Only 1/l goes to 3.5 keV** We have to take into account that even though there is the possibility energy-wise for producing 3.5 keV X-rays of a certain amount only say 1/l of the a priori expected amount is actually produced and emitted. So to get a fit for a given experimental observation, we will have to take the calculated value with the initially chosen parameters  $S^{1/3}$ ,  $\Delta V$ , and  $\xi_{fs}$  for emission of an amount of 3.5 keV radiation to be corrected to actually deliver a larger amount by a factor l. In order to get a larger amount of 3.5 keV line emission we shall take a smaller cubic root of tension  $S^{1/3}$  and a bigger value of the combined parameter  $\frac{\xi_{fs}^{1/4}}{\Delta V}$ . This means, that corresponding to a combination of a couple of values ( $S^{1/3}$ ,  $\frac{\xi_{fs}^{1/4}}{\Delta V}$ ) we get a track, a half line, of possibilities by switching on the further parameter l (which is larger than or equal to unity). Here we had in mind a double logarithmic plot, otherwise the half curve would not be a half line.

The final step in our small pearl fitting assumes that one can estimate the mass of the pearls by looking at how many events are observed by the DAMA-LIBRA experiment. We do this by using the fact that the flux of pearls must of course be bigger the smaller in mass the pearls, so as to agree with the density of dark matter as needed from the gravitational effects. However, since our pearls interact rather strongly on their way through the shielding, this estimate has to be severely corrected to get the mass needed at the end.

The fitting procedure is illustrated in Figure 3.8.

For the sake of fitting in such a way to the DAMA-LIBRA observations we take the “observed mass”  $M_{obs} = 10^3$  GeV to  $10^4$  GeV. But it is rather uncertain, because the pearls are strongly interacting and only reach through the shielding earth because of their very high masses ( $\sim 10^3$  GeV) compared to usual WIMP expectations so that they do not get stopped even when hitting a nucleus, but rather continue slightly slower. Nevertheless we imagine the majority of the pearls to get stopped before reaching the instrument, so that only about 1 in  $10^{12}$  come through and thus a  $10^{12}$  times smaller mass is needed than the mass  $M' = 1.56 * 10^{14}$  GeV, which corresponds to getting the observed number of event match with number of pearls hitting the region at all. The value  $10^{-12}$  of the suppression of the number of pearls coming through was estimated by comparing our expected  $\frac{\sigma}{M}$  from the supernova remnant measurement with the observations of such a ratio in the DAMA-fitting by the experimentalists.

The Figure 3.9 illustrating the final fit is complicated by there being an inconsistency in the Jeltema and Profumo paper by the number in their figure for the rate of 3.55 keV radiation observed deviating by a factor 10 from the number in the text. But ignoring one of these two versions of the figure, we may give here the meaning of the lines on the figure:

The value of the frequency of the radiation, i.e. the very number 3.55 keV happens to depend only on our combined parameter and it fits it to the value  $\frac{\xi_{fs}^{1/4}}{\Delta V} = 0.5 \text{ MeV}^{-1}$ . If we ignore an extra very weak dependence on the  $\Delta V$  and put say  $\Delta V = 20 \text{ MeV}$  then also the intensity of the 3.55 keV line radiation mainly depends on our combined variable and requires a fitted value of  $\frac{\xi_{fs}^{1/4}}{\Delta V} = 0.086 \text{ MeV}^{-1}$ . So the fitting of the intensity of the various clusters of galaxies

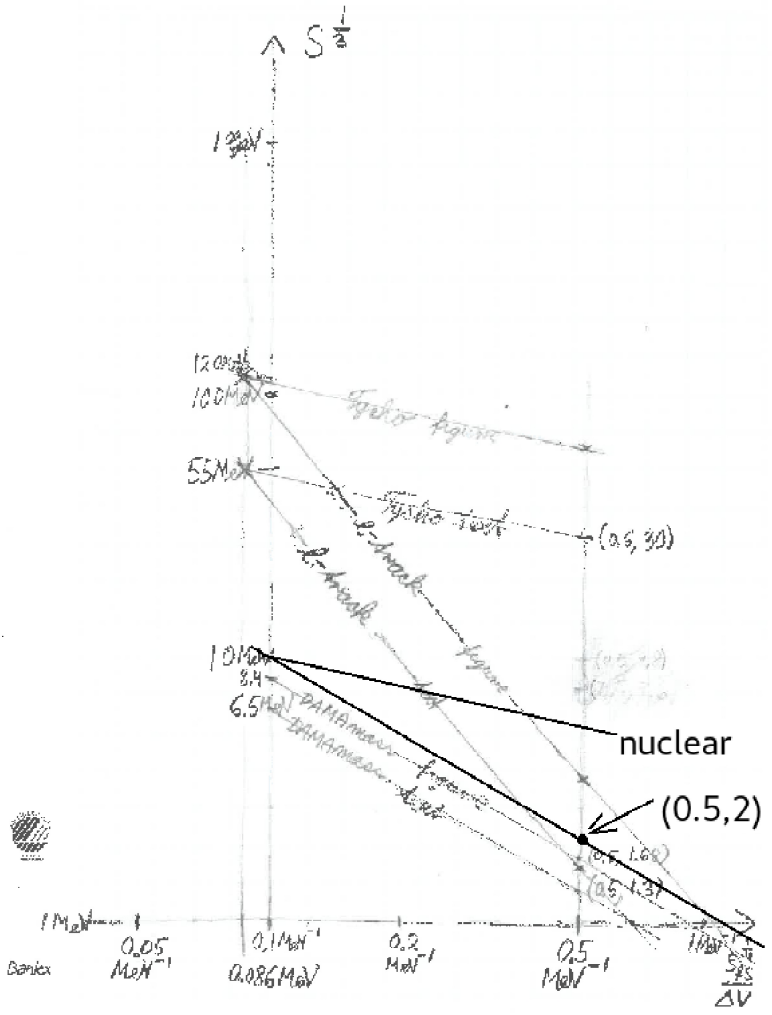


Fig. 3.9: This is the same as the foregoing figure but with a line added corresponding to the  $\frac{\sigma}{M}$  being as for nuclei, thus called "nuclear". It represents with our assumptions an upper limit for  $S^{1/3}$  as a function of the other variable. In fact the piece of the "l-track" below this line represents the factor in  $l$  called  $l_{\text{penetration}}$  represents the correction to the geometrical cross section to mass ratio due to the say cosmic ray just penetrating the pearl instead of interacting.

etc. requires the vertical line of our plot 3.9 to the left at  $0.086 \text{ MeV}^{-1}$ . The lines crossing the figure and denoted "Tycho figure" and "Tycho text" are the spaces for the allowed parameter combinations for the  $l$  fixed to unity to fit the intensity of radiation from the supernova remnant when the intensity is taken from the figure

and text respectively of the Jeltema et al. paper. The important point here is where these two lines cross the vertical line at  $0.086 \text{ MeV}^{-1}$  which is the requirement of the intensity measurement. From the crossing point on the figure is then drawn a half line representing the pairs  $(\frac{\xi_{fs}}{\Delta V}^{1/4}, S^{1/3})$  which by varying the l-parameter give the possible allowed values fitting both the intensity of the galactic clusters etc and the Tycho supernova remnant. These half lines go down from the upper left to the lower right. Similarly we have actually two (because of the slight inconsistency in the Jeltema article) half lines on which one, using the l-parameter in combination, can fit the mass required by the DAMA-LIBRA experiment and our considerations for the number of events in DAMA-LIBRA and again the intensity of the 3.55 keV radiation from the galactic clusters etc.

Now the success of the fitting can be taken to be that for a given - the right one - interpretation of the Jeltema article data (text or figure right) the two lines, one corresponding to the variation of l called "l-track" and the other called "DAMA-mass", cross each other just on the vertical line corresponding to the frequency 3.55 keV.

For instance the "text" three lines cross in a really very small triangle meaning the fit is very good! The middle of this very small triangle is the point with  $(\frac{\xi_{fs}}{\Delta V}^{1/4}, S^{1/3}) = (0.6 \text{ MeV}^{-1}, 1.6 \text{ MeV})$ . This is a very small value we would think for the tension  $S^{1/3}$  and a surprisingly big value for our combined parameter. But translated to energy scale the two parameters are both surprisingly small being an MeV in order of magnitude.

We note that the fitted values of the parameters at the center of the triangle lie below the very heavy line which represents the nuclear value for the ratio of cross section to mass. This is in apparent conflict with our hypothesis above claiming that the Tycho supernova observation was consistent with the coincidence of the cross section to mass ratio for the pearls being equal to the nuclear value.

**More Coincidences** Really the accuracy of our estimates is so crude that we have e.g. the point we find for fitting  $(\frac{\xi_{fs}}{\Delta V}^{1/4}, S^{1/3}) = (0.5 \text{ MeV}^{-1}, 2 \text{ MeV})$  could be considered lying on the line marked "nuclear", which would mean that the true cross section to mass ratio of the pearls would be equal to that of carbon nuclei.

But by a little by eye improvement, we could make this story even a bit better:

In fact if we take it that it is remarkable and in fact true that the mass of the pearls coincide with the lower limit at which the macroscopic calculation stops working and the density of electrons spreads out in a bigger cloud than the pearl as marked by just the skin, then the situation should be that the density of electrons is actually somewhat lowered compared to the calculation we used.

Crudely correcting for that would mean, that since the predicted line frequency - that should end up 3.55 keV - would fall by the density being lowered, we would have to correct it a bit back by claiming that the fitting value of the  $\frac{\xi_{fs}}{\Delta V}^{1/4}$  parameter should be a bit smaller than the value  $0.5 \text{ MeV}^{-1}$  which we used without such improvement.

Because the crossing lines in the figure go skewly down from left to right, such a diminishing of the fitting value of the abscissa would mean that the fitting

$S^{1/3}$  would tend to rise. In fact this would then make it even easier to claim that we just have the nuclear sigma to mass ratio.

Indeed we would then be able to claim that we have the following coincidences:

- The  $\frac{\sigma}{M}$  ratio for the pearls would be just the nuclear one.
- The mass of the pearls would (as the dominant value) just be the lower bound for the macroscopic picture to work, i.e. the electron would just not expand outside significantly.
- Then of course as before it is a coincidence that one gets a fit at all, although our number of parameters was only one below the number of fitted quantities.

So we would claim a somewhat more remarkable fit!

### 3.8.4 DAMA-LIBRA Mass Extraction

The major speculation and idea behind the small pearl study, in addition to the inclusion of the Jeltema and Profumo observation of 3.55 keV X-ray radiation from the Tycho supernova remnant, is the inclusion of an attempt to fit and explain the controversial DAMA-LIBRA experiment [25]. In contrast to other underground searches for dark matter, DAMA-LIBRA *did* find the dark matter by the technique of seasonal variation.

According to the above crude coincidence discussed in subsections 3.8.2 and 3.8.2 the cross section to mass ratio  $\frac{\sigma}{M}$  for our pearls needed to fit reasonably the Tycho supernova remnant observation agrees - we wanted to say as a "coincidence" (but that is only very optimistically true) - with the same ratio for e.g. carbon nuclei.

Indeed we found (3.31)

$$\frac{\sigma}{M} \Big|_{\text{nuclear}} = \frac{1}{(0.26 \text{ GeV})^3} \quad (3.77)$$

$$= 1.25 * 10^{-3} \text{ m}^2/\text{kg} \quad (3.78)$$

while the DAMA-LIBRA experiment presented two allowed regions for WIMP observation in the mass of the particle versus cross section plane:

$$(M, \sigma) = (18 \text{ GeV}, 2 * 10^{-4} \text{ pb}) = (3.2 * 10^{-26} \text{ kg}, 2 * 10^{-44} \text{ m}^2) \quad (3.79)$$

and

$$(M, \sigma) = (180 \text{ GeV}, 10^{-4} \text{ pb}) = (3.2 * 10^{-26} \text{ kg}, 10^{-44} \text{ m}^2), \quad (3.80)$$

giving respectively

$$\frac{\sigma}{M} = \frac{2 * 10^{-4} \text{ pb}}{18 \text{ GeV}} \quad (3.81)$$

$$= 6.24 * 10^{-19} \text{ m}^2/\text{kg} \quad (3.82)$$

and

$$\frac{\sigma}{M} = \frac{10^{-4} \text{ pb}}{180 \text{ GeV}} \quad (3.83)$$

$$= 3.1 * 10^{-20} \text{ m}^2/\text{kg}. \quad (3.84)$$

It means that the ratio  $\frac{\sigma}{M}$  fitted to WIMPs by DAMA is about a factor  $10^{12}$  (or even  $10^{13}$ ) lower than the number which our fit using the Jeltema and Profumo 3.55 keV observation points to, namely  $6 * 10^{-7} \text{ m}^2/\text{kg}$  (if we use the “figure-value”  $6 * 10^{-8} \text{ m}^2/\text{kg}$  we could get  $10^{11}$  only). If we take it that really the  $\frac{\sigma}{M}$  ratio for our pearls is equal to the nuclear value, then the deviation from the observed ratio in DAMA-LIBRA is even larger, by about a factor 2000 bigger.

As we shall see in the next subsection 3.8.4 we estimate that the number of particles / events observed requires that the mass be at most  $1.56 * 10^{14} \text{ GeV}$ , since otherwise with the known density  $D_{\text{sol}} \approx 0.3 \text{ GeV}/\text{cm}^3$  there could not be enough particles so as to fit the observed ones.

The main idea now is that we assume that, due to some filtering and breaking of the particles that come in with our speculated rather high cross section and thus cannot avoid interacting with the shielding amounts of earth, removes effectively all but one particle in  $10^{12}$ . This number was just taking from the comparison of the assumed cross section and the seemingly measured one being  $10^{12}$  as we just discussed. To cope with this suppression of the number of particles we need an increase in the number coming in by the factor  $10^{12}$  and thus to reduce the mass to fit our model relative to the  $1.56 * 10^{14} \text{ GeV}$  to the mass estimate:

$$\text{“Mass estimate from DAMA”} \approx 1.56 * 10^{14} \text{ GeV}/10^{12} \quad (3.85)$$

$$= 160 \text{ GeV}. \quad (3.86)$$

Had we used the supposed more correct value by taking the factor  $10^{12}$  bigger by a factor 2000, the pearl mass estimate would be reduced by a further factor 2000. But we could not tolerate that in our model because there would then not even be one nucleon in the pearls and the macroscopic estimates of e.g. the homolumo gap leading to the frequency 3.55 keV would not appear. Our pearls must not just be ordinary atoms surrounded by a skin, they must be **many** atoms surrounded by the skin. There should at least be so many  $Z$  charges on protons in the pearl that a potential of the order of magnitude of  $\Delta V$  can be achieved. Using the well-known formula for the ground state of the electron binding energy for a hydrogen like atom  $ZRy \approx Z * 13 \text{ eV}$ , we need to get  $Z \approx 10^5$  at least, just to reach even the surprisingly small  $\Delta V$  coming out of our fit to the small pearls. So we cannot keep the model unless we let the mass  $M$  of the pearls be at least  $10^5 \text{ GeV}$ . This is a factor 100 or 1000 times bigger mass than the estimates used on the figure called respectively “DAMAmass figure” and “DAMAmass text”. Thus the line representing the DAMAmass on the figure should be lifted by the logarithm of the ninth root of 100 compared to “DAMAmass figure” or by the logarithm of the ninth root of 1000 compared to the line marked “DAMAmass text”. In both cases the line as needed by the requirement of making sense of our macroscopic estimates passes the vertical line for  $\frac{\xi_{fs}^{1/4}}{\Delta V} = 0.1 \text{ MeV}^{-1}$  at  $S^{1/3} = 14 \text{ MeV}$ . Including the possibility for varying  $l$  leads to the allowed line which then passes through  $(0.1 \text{ MeV}^{-1}, 14 \text{ MeV})$  and is parallel to the other “DAMAmass”-lines drawn. It fits actually even better than the previous fits and both the “text” and the “figure” lines concerning the Tycho supernova measurement.

**How Many Particle Hit the DAMA Experiment?** In this subsection we shall now estimate the promised approximate absolutely lowest needed number of dark matter particles coming in and thereby the upper bound on the mass of these particles as follows:

The modulated part of the signal is found by DAMA/LIBRA to be of the order 0.01 cpd/kg/keV in the region of energy of the signal in the range 1keV to 6 keV where any modulation if found at all. Taking this as averaged over the range of 5 keV it means that one in total saw at least 0.05 cpd/kg even modulated and thus dark matter related events meaning for the whole apparatus about  $250 \text{ kg} * 0.05 \text{ cpd/kg} = 12.5 \text{ cpd}$ . Since the apparatus has an area of the order of  $1/4 \text{ m}^2$  - it consists of 25 essentially  $10 \times 10 \times \dots$  blocks - this means an absolutely needed flux - whatever the theory - of  $50 \text{ cpd/m}^2$ . Here cpd means counts per day, and should be compared to what we trust about the dark matter: We have in our region a mass density  $0.3 \text{ GeV/cm}^3 = 3 * 10^5 \text{ GeV/m}^3$  and a velocity of the order  $300 \text{ km/s}$  meaning  $300 \text{ km/s} * 86400 \text{ s/day} = 26 * 10^6 \text{ km/day} = 2.6 * 10^{10} \text{ m/day}$ . So  $1/4 \text{ m}^2$  tracks per day a volume  $1/4 * 2.6 * 10^{10} \text{ m}^3 = 6.5 * 10^9 \text{ m}^3$  containing a mass of  $6.5 * 10^9 \text{ m}^3 * 3 * 10^5 \text{ GeV/m}^3 = 19.5 * 10^{14} \text{ GeV} = 2.0 * 10^{15} \text{ GeV}$ . This  $2.0 * 10^{15} \text{ GeV}$  mass is to be shared on 12.5 counts, since there have been seen 12.5 cpd. Thus the particles must at least have masses less than or equal to  $2.0 * 10^{15} \text{ GeV} / 12.5 = 1.56 * 10^{14} \text{ GeV}$ . There is the possibility that with the strongly interacting pearls in our small mass model the modulation part relative to the total number of interactions with the apparatus gets appreciably enhanced. In fact the depth into which the pearls penetrate must be strongly dependent on the impact velocity, since it takes more collisions to stop a fast pearl than a slow one (compared to Earth velocity). Since presumably the DAMA-LIBRA experiment is working with the few pearls coming especially deep down the number of them could be very strongly velocity dependent. It is in fact possible that these modulation part particles are almost the only dark matter particles, although this would usually be a bit strange if it were so. Such enhancement of the modulation could explain the long standing mystery, why DAMA-LIBRA sees the dark matter while the other experiments - not using the modulation technique - do not see anything.

Now we estimated that to just get that there were as many particles at all passing the DAMA/LIBRA detector, even if being WIMPs, as the number of observed events would require a mass of the order  $M = 1.56 * 10^{14} \text{ GeV}$ . We have now to say that we need the mass  $M$  to be  $10^{12}$  times smaller than this number, so that we can get  $10^{12}$  times more particles to begin with. That means we need a mass of the order

$$M = 10^{-12} * 1.6 * 10^{14} \text{ GeV} \quad (3.87)$$

$$= 1.6 * 10^2 \text{ GeV}. \quad (3.88)$$

We then even need that the particles that come through essentially almost all interact in the apparatus, but that may not be so impossible in our model with rather strongly interacting particles. You would rather have to consider how many of them may become disqualified by interacting several times.

Because of a printing mistake in the Jeltema et al. paper one can choose not to believe their published rate for the number of 3.55 keV photons they observe,

but instead use the value in their figure. This then gives a factor 10 times lower observation rate, and thus with the figure used instead of the number in the article, we could claim that they find rather  $\frac{\sigma}{M} = 6 * 10^{-8} \text{m}^2/\text{kg}$ . In this case the shielding caused factor would not be  $10^{12}$  as above but rather only  $10^{11}$  and our estimate of the mass  $M$  would then go up to  $1.6 * 10^3 \text{ GeV}$ .

In the following subsection 3.8.5 we redo this estimate in a slightly different way using some rather simple formulas:

### 3.8.5 Simple Formulas on Underground Searches for Dark Matter

Usually people assume that dark matter consists of weakly interacting particles, so called WIMPs (= weakly interacting massive particles). But if the particles could be heavy, they could also be so strongly interacting that the particles would interact several times on the way down through the earth shielding the experiments looking for dark matter underground. However they do not need to be sufficiently strongly interacting that it would make them visible on the sky. Such particles would not deserve the name WIMP but rather only IMP.

Since all we know from the gravitational effect of the dark matter is the mass density  $D$ , the quantity that crudely measures the degree of visibility of the dark matter would be the amount of absorption or of any kind of observable effect, say some cross section  $\sigma$  per unit volume in outer space. For fixed  $D$  that quantity would be proportional to the ratio  $\frac{\sigma}{M}$ , i.e. to the amount of cross section per unit mass.

We shall in this section, taking just this ratio  $\frac{\sigma}{M}$ , look for what one crudely measures in experiments looking for WIMPs or IMPs impacting on earth.

Calling the mass of the average nucleus or whatever is taken to be the most important constituent of the earth hitting the dark matter particles  $M_{\text{nucleon}}$ , we may crudely estimate that the number of collisions it takes for a dark matter particle to be effectively stopped in passing through the shielding is

$$\text{“ Number hit for stop ”} \approx \frac{M}{M_{\text{nucleus}}}. \quad (3.89)$$

The argument for this estimate is the following:

During its passage through the shielding - the layer of earth above the detector - the dark matter particle / pearl of mass  $M$  hits earth particles of mass  $M_{\text{nucleus}}$ , which then obtain a speed of the order of magnitude of the speed  $v$  of the dark matter particle itself. Thereby the hit particles achieve a kinetic energy of the order of  $M_{\text{nucleus}}v^2/2$  which is  $\frac{M_{\text{nucleus}}}{M}$  times the kinetic energy of the dark matter pearl itself  $Mv^2/2$ . Thus to bring the kinetic energy of this pearl down to about zero it is needed of the order of the inverse of the fraction  $\frac{M_{\text{nucleus}}}{M}$  such hits. But that is just what (3.89) says.

**Estimation of Number of Hits Needed** As we shall see in a moment we shall avoid the pearl making too many hits when passing the counting sensitive region of the experiment. The reasons are:

- If one sees more than one hit in the experiment, one counts it as a background interaction and does not include it in the usual searches for WIMPs.
- Below we shall give an estimate of the number of hits to be seen in the experimental sensitive region. If there are many interactions/hits in this region there will not be so many counts of something happening as the estimation below. They will so to speak be used up on multiple hits instead.

We estimate now an effective thickness of the experimentally sensitive region in say the DAMA-LIBRA experiment to be of the order of  $l_{\text{sensitive}} = \frac{1}{2} m$ . Then we argue that the stopping length  $l_{\text{stop}}$  divided by "Number hit for stop"  $\approx \frac{M}{M_{\text{nucleus}}}$ , should be larger than or of order of magnitude of  $\frac{1}{2} m$ . I.e.

$$\frac{l_{\text{stop}} M_{\text{nucleus}}}{M} \geq l_{\text{sensitive}} \approx \frac{1}{2} m. \quad (3.90)$$

**Penetration in Terms of  $\frac{\sigma}{M}$**  If one thinks of WIMPs the very number of observed dark matter particles or pearls in an underground experiment is proportional (crudely at least) to the ratio  $\frac{\sigma}{M}$  of cross section to mass. This is because, taking the density of dark matter  $D$  in the astronomical neighborhood and the typical velocity  $v$  as given, the flux of dark matter particles passing by becomes inversely proportional to the mass  $M$  and the interaction rate must of course always be proportional to the cross section  $\sigma$  for hitting.

Therefore really the ratio  $\frac{\sigma}{M}$  estimated by an underground experiment is basically an estimate of the intensity of hits in the sensitive part of the apparatus. Assuming dark matter consists of WIMPs this number is basically measured by the underground experiments, essentially just by counting events.

Now, however, if the pearls interact several times on their way down through the shielding then the effect of such full or partial stopping of the particles can of course drastically change the result of measuring the ratio  $\frac{\sigma}{M}$  as if they were WIMPs.

Almost by dimensional arguments we could write down the stopping length

$$l_{\text{stop}} = \frac{M}{\sigma \rho_{\text{shield}}}. \quad (3.91)$$

In fact supposing that the shielding material is mass-wise dominated by the one particle - presumably a nucleus - of mass  $M_{\text{nucleus}}$  the (mass) density is given as

$$\rho_{\text{shield}} = \text{"number density"} * M_{\text{nucleus}}. \quad (3.92)$$

and the distribution of the pearl's first hit on this material is given as

$$\propto \exp(-l_{\text{hit}} x) \text{ (where } x \text{ is depth into shielding)} \quad (3.93)$$

where

$$l_{\text{hit}} = \frac{1}{\text{"number density"} * \sigma} \quad (3.94)$$

$$= \frac{M_{\text{nucleus}}}{\rho_{\text{shield}} * \sigma}, \quad (3.95)$$

we obtain

$$l_{\text{stop}} = \frac{M}{M_{\text{nucleus}}} * l_{\text{hit}} \quad (3.96)$$

$$= \frac{M}{\sigma \rho_{\text{shield}}}. \quad (3.97)$$

For simplicity we shall at first assume that the suppression of the rate of the part of the dark matter coming through the shielding is proportional to  $\exp(-x/l_{\text{stop}})$  where  $x$  is the depth, meaning the penetration depth into the earth, even in the case of multiple scattering. This simplification is of course not mathematically true and we shall return to it later. However proceeding with our simplifying assumption we find that the cross section to mass ratio  $\frac{\sigma}{M}|_{\text{WIMP}}$  to be effectively found as if we had WIMPs will be

$$\frac{\sigma}{M}|_{\text{as WIMP}} = \frac{\sigma}{M} * \exp(-x/l_{\text{stop}}). \quad (3.98)$$

Using (3.96) we write this in the form

$$\frac{\sigma}{M}|_{\text{as WIMP}} = \frac{\sigma}{M} * \exp\left(-\frac{x \rho_{\text{shield}} \sigma}{M}\right), \quad (3.99)$$

which we can consider as a transcendental equation from which to determine the true  $\frac{\sigma}{M}$  for the dark matter pearls from the experimentally observed “as if WIMP” value  $\frac{\sigma}{M}|_{\text{as WIMP}}$ , which can be identified with the DAMA-LIBRA fitted value. There is in this equation for a small value of the  $\frac{\sigma}{M}|_{\text{as WIMP}}$  the WIMP-solution, but there are **two** solutions. The second solution is a strong coupling solution. To solve the equation in this strong coupling case we of course have to put in the value of the depth  $x$  under earth of the experiment. It is given as 3400 mwe (= meters water equivalent), which means we can put  $x = 3400$  m and then  $\rho_{\text{shield}} = 1000 \text{ kg/m}^3$ . In principle we have to correct for the fact that the dark matter particles will typically move in a skew direction and the true value of  $x$  will be somewhat larger than the minimal distance from the earth’s surface to the experiment. Since we anyway calculate very crudely and since in the strongly interacting case the shortest way down will come to give the dominant contribution, we here simply take  $x = 3400$  m and  $\rho_{\text{shield}} = 1000 \text{ kg/m}^3$ . Then we obtain

$$(\rho_{\text{shield}})_{\text{for DAMA}} = 3400 \text{ m} * 1000 \text{ kg/m}^3 \quad (3.100)$$

$$= 3.4 * 10^6 \text{ kg/m}^2 \quad (3.101)$$

For illustration let us remark that e.g. for what we called “nuclear” cross section to mass ratio  $1.25 * 10^{-3} \text{ m}^2/\text{kg}$ , see equation (3.78), the exponent would become  $-3.4 * 10^6 \text{ kg/m}^2 * 1.25 * 10^{-3} \text{ m}^2/\text{kg} = -4.3 * 10^3$ .

The cross section to mass ratio for WIMPs seemingly observed in the DAMA-LIBRA controversial underground experiment may be taken from the two allowed regions in the mass of particle versus cross section plane as presented by the experimentalists:

$$(M, \sigma) = (18 \text{ GeV}, 2 * 10^{-4} \text{ pb}) = (3.2 * 10^{-26} \text{ kg}, 2 * 10^{-44} \text{ m}^2) \quad (3.102)$$

and

$$(M, \sigma) = (180 \text{ GeV}, 10^{-4} \text{ pb}) = (3.2 * 10^{-26} \text{ kg}, 10^{-44} \text{ m}^2), \quad (3.103)$$

giving respectively

$$\frac{\sigma}{M} \Big|_{\text{as WIMP}} = \frac{2 * 10^{-4} \text{ pb}}{18 \text{ GeV}} = \frac{2 * 10^{-44} \text{ m}^2}{3.2 * 10^{-26} \text{ kg}} \quad (3.104)$$

$$= 6.24 * 10^{-19} \text{ m}^2/\text{kg} \quad (3.105)$$

and

$$\frac{\sigma}{M} \Big|_{\text{as WIMP}} = \frac{10^{-4} \text{ pb}}{180 \text{ GeV}} = \frac{10^{-44} \text{ m}^2}{3.2 * 10^{-25} \text{ kg}} \quad (3.106)$$

$$= 3.1 * 10^{-20} \text{ m}^2/\text{kg} \quad (3.107)$$

Solving the transcendental equation (3.99) iteratively we first find that

$$x\rho_{\text{shield}} * \frac{\sigma}{M} \approx \ln \left( \frac{\sigma}{M} * \frac{M}{\sigma} \Big|_{\text{as WIMP}} \right). \quad (3.108)$$

Taken at first the logarithm to be of order unity we shall test as first iteration  $\frac{\sigma}{M} = (x\rho_{\text{shield}})^{-1} = (3.4 * 10^6 \text{ kg/m}^2)^{-1} = 2.94 * 10^{-7} \text{ m}^2/\text{kg}$ . But inserting that value into the logarithm gives the value  $\ln(\frac{2.94 * 10^{-7} \text{ m}^2/\text{kg}}{10^{-20} \text{ m}^2/\text{kg}}) = \ln(3 * 10^{13}) = 31$ . So the next iteration gives

$$\frac{\sigma}{M} \Big|_{2. \text{ sol.}} \approx 2.94 * 10^{-7} \text{ m}^2/\text{kg} * 31 \quad (3.109)$$

$$= 9.1 * 10^{-6} \text{ m}^2/\text{kg}. \quad (3.110)$$

Crudely we can consider this number  $9.1 * 10^{-6} \text{ m}^2/\text{kg}$  as the DAMA measured value for the cross section to mass ratio provided the second - i.e. the strong interaction solution - is taken.

This value is then to be compared to the value we need for the Jeltema and Profumo Tycho supernova observation:

$$\frac{\sigma}{M} \Big|_{\text{Tycho}} = 5.6 * 10^{-7} \text{ m}^2/\text{kg} \text{ (for text)}. \quad (3.111)$$

The “measured” value is only 15 times larger than the one required for the Tycho supernova remnant observation. Had we used the “figure” reading of the paper instead of the “text” value, we would have got the 10 times smaller value

$$\frac{\sigma}{M} \Big|_{\text{Tycho}} = 5.6 * 10^{-8} \text{ m}^2/\text{kg} \text{ (for figure)}. \quad (3.112)$$

But remember now we speculated that these numbers from the Tycho observation are only lower limits and that we suggested the  $\frac{\sigma}{M}$  ratio should be a factor  $l = 2000$  times bigger than the Tycho measurement. Such a factor as that would bring the deviation from the “measured ratio” to the opposite side. So we should really conclude that the agreement of the DAMA estimation of the ratio and that from Tycho is very good.

**Number of Hits during Stopping** The number 31 which we got for the value of the logarithm in the solving of the transcendental equation above is actually equal to the depth  $x$  measured in stopping lengths  $l_{\text{stop}}$ . And so we would conclude that

$$31 * \rho_{\text{shield}} l_{\text{stop}} = (3400 \text{ mwe}) * \rho_{\text{water}} = 3.4 * 10^6 \text{ kg/m}^2, \quad (3.113)$$

giving

$$\rho_{\text{shield}} l_{\text{stop}} = \frac{3.4 * 10^6 \text{ kg/m}^2}{31} = 1.1 * 10^5 \text{ kg/m}^2. \quad (3.114)$$

Now in order to avoid getting more than one hit in the sensitive thickness of the apparatus taken to be  $1/2$  m, we have the inequality:

$$l_{\text{hit}} \geq \frac{1}{2} \text{ m}. \quad (3.115)$$

So taking the density in this sensitive apparatus to be say  $\rho_{\text{apparatus}} = 3000 \text{ kg/m}^3$ , we have

$$\frac{\rho_{\text{apparatus}} l_{\text{hit}}}{\rho_{\text{water}} l_{\text{stop}}} \geq \frac{(31 * 3000 \text{ kg/m}^3) * \frac{1}{2} \text{ m}}{3400 \text{ m} * 1000 \text{ kg/m}^3} \quad (3.116)$$

$$= 1.37 * 10^{-2} = \frac{1}{73}. \quad (3.117)$$

This means that there is at most 73 times as much weight in the pearl compared to the important nucleus weight in the shield. If say the important or average nucleus in the shield is silicon with mass 28 GeV, then the pearl's mass is of the order of  $73 * 28 \text{ GeV} = 2000 \text{ GeV}$ .

Now in order to have a proper macroscopic electron cloud in the pearl that can give the macroscopically estimated homolumo gap, we need that the pearl nuclear charge  $Z$  (i.e. the number of protons) is at least large enough that an atom of this atomic number can provide  $\Delta V$  order of magnitude binding energies. Taking the binding energy to be of the order of  $Z$  Rydberg, it means we need  $Z \geq \frac{\Delta V}{1 \text{ Rydberg}}$ , so that for say  $\Delta V = 1 \text{ MeV}$  we would need  $Z \geq 10^4$ . This would be a problem for our model if we took the above estimate of 2000 GeV too accurately. But this limit is so close that we shall of course rather take it that now we know the bound must be very close and we shall take the mass to be  $M \approx 2000$  to  $10000 \text{ GeV}$  - see Figure 3.10.

**An Interesting Coincidence** Let us note, that we have got almost coincidence between the mass  $10^4 \text{ GeV}$  needed for our macroscopic approximation to be valid and the value obtained above. In other words we can say that the mass needed for keeping a sufficiently high electron density such that e.g. our homolumo-gap calculation is still valid and the mass estimated from DAMA-LIBRA, say 2000 GeV, are essentially the same, which is a funny coincidence!

Actually if we begin to fit with a mass a bit smaller than  $10^4 \text{ GeV}$ , there will be a correction to the formula for the homolumo gap size and thus for our prediction

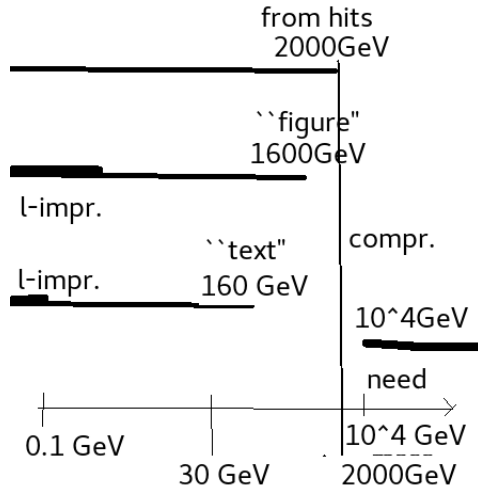


Fig. 3.10: How we get the mass suggested by DAMA-LIBRA for our model as a “compromise” (denoted by “compr.” on the figure) to be  $\sim 2000$  GeV. Formally, using the “simple formulas”, we have an upper bound of 2000 GeV and similar crude upper bounds using the number of events in DAMA-Libra. Using the “figure” or the “text” values in the Jeltema and Profumo paper give upper limits for the pearl mass of 1600 GeV or 160 GeV respectively. But if one corrects for the energy lost from going to the 3.5 keV line, as indicated by “l-impr.” in the figure, the  $\frac{\sigma}{M}$  for the pearls is increased by a factor of the order 2000 and we get the upper limits indicated with a thick line of about 1 GeV or 0.1 GeV. So formally we have an inconsistency of our requirement but, considering that we only have order of magnitude bounds which should approximately be equalities, we have a good compromise value.

of the very frequency 3.55 keV. So the true prediction of this frequency would be a bit lower, if such corrections for the bigger extension of the electron cloud than the size of the skin is corrected for.

This actually means that the true homolumo gap has a maximum very near to the values we here use to fit with. This may be of some significance for really getting a peak in the X-ray spectrum (at 3.55 keV), since a priori pearls of a bit different size will give different frequencies for the radiation and thus smear out the peak relative to what would appear, if all the pearls have exactly the same size. It may only go with the fourth root that there is such a dependence but still it is a smearing out.

Suppose it happens that the dominant size of the pearls is just around a point where the approximation of the electron cloud keeping inside the skin of the pearls stops being valid. Then there will be a correction that for making the pearl smaller counteracts the increase in frequency that the smaller pearl should cause. The result is a maximum in the frequency spectrum of the X-ray radiation. This means an improvement in the sharpness of the line is predicted.

If we somehow argue that just such a maximum is favoured it would mean we could consider this coincidence as a success.

### 3.8.6 Xenon1T Electron Recoil Excess

An observation that may fit very well into our version of the pearl model for dark matter with the less than atomic size pearls is the Xenon1T Electron Recoil Excess [16]. This effect of electrons seemingly appearing with energy close to just 3.5 keV - note the coincidence we want to stress with the 3.5 keV X-ray line photon energy - would independent of the details the dark matter model be very indicative, since we already have a strong suggestion that dark matter tends to emit light with the 3.5 keV frequency.

Apart from the DAMA/LIBRA and DAMA experiment the other direct search experiments seem to find only negative results when looking for the dark matter. There was, however, found one unexpected result [16] although at first not seemingly due to dark matter:

The experiment Xenon1T investigated what they call electron recoil in their Xenon experiment. In the Xenon experiment one has a big tank of liquid Xenon with some gaseous Xenon above it and photomultipliers looking for the scintillation of this xenon. The philosophy behind the experiment that a dark matter WIMP e.g. hits a nucleus inside the xenon and the recoil of this creates a scintillation signal S1 and also an electron which is then driven up the xenon tank by an electric field and at the end by a further electric field made to give a signal at the top S2. By the relative size of the signals S1 and S2 one may classify the events - which are taken to be almost coinciding pairs of these signals S1 and S2 - as being nucleus recoil or electron recoil. One expects to find the dark matter in the nucleus recoils, since a dark matter particle is not expected to make an electron with sufficient energy to make an observable electron recoil event.

But now carefully estimating the background expected the Xenon1T experimenters found an excess of electron recoil events.

Proposed ideas for explaining it include axions from the sun or neutrinos having bigger magnetic moments or perhaps less interestingly that there could be more tritium than expected in the xenon.

But here our model of relatively stronger interacting particles able to radiate the line 3.55 keV when excited provides a possible explanation:

Going through the earth and the rest of the shielding the pearls or particles get excited so as to emit 3.55 keV X-ray just as they would do it in the Tycho supernova remnant, where they also get excited by matter or cosmic rays. But then the particles passing through the deep underground Xenon1T experiment are already excited and prepared for sending out the 3.55 keV radiation. Now they could possibly simply do that in the xenon tank or they might dispose of the energy by a sort of Auger effect by rather sending out an electron with an extra energy of 3.55 keV. Such an electron with an energy of a few keV could be detected and taken for an electron recoil event in the Xenon1T experiment.

It is remarkable that the signal of these excess electron recoil events appears to have just an energy of the recoiling electron very close to the value 3.55 keV.

Indeed the most important bins for the excess are the bins between 2 and 3 keV and the bin between 3 and 4 keV.

So we would claim that there is in our model no need for extra solar axions or neutrino magnetic moment, nor tritium. But we claim it to be 3.55 keV radiating dark matter one sees in the xenon experiment!

### 3.9 Conclusion

We have put up two slightly different models for dark matter being actually pearls which have a new phase or type of vacuum inside, which by our "Multiple Point Principle" is supposed to have the same energy density as the present vacuum. The two models only differ by taking the parameters different, especially the tension of the surface separating the inside with its vacuum from the outside with the present vacuum.

The two models are thus given as roughly:

- Big pearls, adjusted to the Tunguska event being due to one falling down onto the earth:  
The cubic root  $S^{1/3}$  of the tension is several GeV, the size of the pearls is cm-size.
- Small pearls:  
The cubic root of the tension  $S^{1/3}$  is of the order of 1 MeV, the size of the pearls a bit bigger than atomic nuclei.

Our main result was that we could fit both very frequency 3.5 keV of the X-ray radiation suspected to come from dark matter and the intensity as fitted by Cline and Frey to a series of observations of this line from various galaxy clusters with essentially one parameter, which we wrote as  $\frac{\xi * 10 \text{ MeV}}{\Delta V}$ . So two observed quantities by one parameter. Both observations concern the still doubtful 3.5 keV X-ray radiation.

We can essentially keep this parameter whether we take the pearls big with a big surface tension or small with a small surface tension.

Taking the model with the small pearls, on which we have far from finished everything, we hope that we can further:

- Make the DAMA-LIBRA controversial observation of dark matter by the seasonal variation technique compatible with the model.
- Fit the a priori very strange observation by Jeltema and Profumo of 3.5 keV radiation coming from the Tycho supernova remnant in the picture with the 3.5 keV radiation coming from dark matter. (Something they take themselves as the sign that this 3.5 keV line is not coming from dark matter but from some ion such as potassium).
- We have for our model a very promising coincidence of the electron excess energy from the Xenon1T experiment with the number 3.5 keV. The point is that the our pearls - in the small size model - come through the apparatus of the Xenon1T experiment and are excited with some extra electrons or simply have some excitons in them - excited during the passage through the shielding

- which then deliver just the 3.5 keV energy to an electron in the Xenon1T experiment. And that is then giving an excess of such events with just an excited electron which was the ununderstood effect seen by Xenon1T.

### 3.9.1 The fitting of the Small Pearl Version

We basically make predictions from the small pearl version with the following parameters:

- The surface tension represented by its cubic root:  $\xi^{1/3}$ ,
- Essentially the potential difference  $\Delta V$  for a nucleon inside versus outside the pearl, represented by the combination  $\frac{\xi_{fs}^{1/4}}{\Delta V}$  (where  $\xi_{fs}$  is the ratio of the radius of the pearl to the "critical" radius at which the nucleons would be just about to be spit out. Presumably even coming in under the fourth root this ratio  $\xi_{fs}$  is not of much significance and probably is  $\sim 5$ ).
- An efficiency parameter  $l$  for getting 3.55 KeV radiation compared to what our estimates at first suggest. One gets really  $1/l$  times the energy available in the time during which the pearl is sufficiently cold for radiating appreciably in the 3.55 keV line.

With these parameters we fit 1) the intensities of the Cline-Frey fit, 2) the Supernova remnant intensity, 3) the very frequency 3.55 keV and 4) a crude mass extracted from the observations of DAMA-LIBRA in the way it is interpreted by us, namely with somewhat strongly interacting pearls, only coming through by means of their high mass. So we fit 4 data point with 3 parameters. This is still formally a success, but now we claim that in addition and crudely consistent with the fit we have that the actual cross section to mass ratio for our small pearls coincides with the cross section to mass ratio for e.g. carbon nuclei. This corresponds to the fact that our pearls are so small that cosmic rays in the supernova remnant say passing though the pearls only interact when they hit a nucleus but otherwise can escape through without touching the pearl. The pearls are so to speak so thinly filled that the cosmic rays "see" the single nuclei in the sack making up the pearl.

Further it is a coincidence, although not obviously reasonable to understand physically, that the size of the pearls is just such that the electron cloud begins to emerge significantly outside the skin surrounding the pearl. This means that the homolumo gap providing the very frequency 3.55 keV for the radiation has a maximum at just this fitted situation. Thus the 3.55 keV line will be especially sharp compared to the possibility that this coincidence was not realized.

If we even counted this last coincidence as understandable as say a stable point more likely than a general point, then we could claim we rather fitted 4 data points with 3 parameters and 2 constraints, meaning really only with  $3-2 = 1$  parameter.

### 3.9.2 Parameters $S^{1/3}$ and $\Delta V$ Small and Outlook

The parameter values we obtained with our “Small Pearls Version” were

$$S^{1/3} = 3 \text{ MeV} \quad (3.118)$$

$$\frac{\xi_{fS}^{1/4}}{\Delta V} = 0.5 \text{ MeV}^{-1}, \quad (3.119)$$

which with

$$\xi_{fS} \approx 2^{4/9} * \sqrt{4\pi} \approx 5 \quad (3.120)$$

gives

$$\Delta V \approx 1.34 \text{ MeV}. \quad (3.121)$$

Both these values for the parameters in the notation in which they have dimension of energy are - one would say embarrassingly - small compared to the dimensional argument expectations, if one speculated that Higgs physics and top-quark physics were involved. That would namely instead give e.g.  $S^{1/3} \sim 100 \text{ GeV}$ . This means that Higgs and/or top-quark physics is not at all a promising possible explanation behind the vacuum-phases. We rather need physics of an energy order of magnitude even under or at least in the very low energy scale end of strong interaction physics, or it should be rather a kind of atomic physics involved.

We have ideas under development taking as a starting point the work by Kryjevski Kaplan and Schaefer [26], who calculated the phase diagram for nuclear matter under various high nuclear densities and considered the so called CFL phase. This stands for color flavour locking phase meaning that the  $SU(3)_c$  color group is broken spontaneously in a direction locked with that of the flavour  $SU(3)_f$  group. It is remarkable that these authors find a triple point as a function of the light quark masses coinciding with the experimental quark masses. This is, however, not quite what we would need to have a case of MPP degenerate vacuum-phases. Because of the high baryon density used in the study of Kryjevski Kaplan and Schaefer [26] their phases are namely not vacua.

Nevertheless we are working on arguing that their phase diagram might be extrapolated down to zero baryon density and thus tell us about vacuum phases. In that case an energy scale for the phase transition physics of the order of the strong interaction scale  $\Lambda_{\text{QCD}} \approx 300 \text{ MeV}$  could be understandable. Even reaching down to a few MeV is at least closer than if one should begin with the Higgs-mass scale.

Such surprisingly low tension domain walls also bring the chances for them to really be acceptable astronomically much closer. The problem with domain walls coming to dominate energetically the whole cosmology and thus being phenomenologically unacceptable is of course weakened the lower the tension and thereby from Lorentz invariance also the energy per unit wall-area is.

## References

1. E. Bulbul, M. Markevitch, A. Foster et al., *ApJ*. **789**, 13 (2014) [arXiv:1402.2301] al.,

2. A. Boyarsky, O. Ruchayskiy, D. Iakubovskiy and J. Franse, *Phys. Rev. Lett.* **113**, 251301 (2014) [arXiv:1402.4119]
3. Colin D. Froggatt, Holger B. Nielsen “The 3.5 keV line from non-perturbative Standard Model dark matter balls” arXiv:2003.05018
4. C. D. Froggatt and H. B. Nielsen, *Phys. Rev. Lett.* **95** 231301 (2005) [arXiv:astro-ph/0508513]
5. C.D. Froggatt and H.B. Nielsen, Proceedings of Conference C05-07-19.3 [arXiv:astro-ph/0512454]
6. C. D. Froggatt and H. B. Nielsen, *Int. J. Mod. Phys. A* **30** no.13, 1550066 (2015) [arXiv:1403.7177]
7. J. Herzog-Arbeitman, M. Lisanti, P. Madau and L.Necib, *Phys. Rev. Lett.* **120** 041102 (2018) [arXiv:1704.04499]
8. Gia Dvali, “Safety of the Minkowski Vacuum”, arXiv:1107.0956
9. D. L. Bennett, C. D. Froggatt and H. B. Nielsen, NBI-HE-94-44, GUTPA-94-09-3, Presented at Conference: C94-07-20 (ICHEP 1994), p.0557-560.
10. D. L. Bennett, C. D. Froggatt and H. B. Nielsen, NBI-95-15, GUTPA-95-04-1, Presented at Conference: C94-09-13 (Adriatic Meeting 1994), p.0255-279 [arXiv:hep-ph/9504294].
11. D. L. Bennett and H. B. Nielsen, *Int. J. Mod. Phys. A* **9** 5155 (1994).
12. D. L. Bennett, C. D. Froggatt and H. B. Nielsen, NBI-HE-95-07, Presented at Conference: C94-08-30 (Wendisch-Rietz) p.394-412
13. C. D. Froggatt and H. B. Nielsen, *Phys. Lett.* **B368** 96 (1996) [arXiv:hep-ph/9511371].
14. Alexander A. Kirillov, Boris S. Murygin, “Domain walls and strings formation in the early Universe”, see this Volume, p. 128, arXiv:2011.07041v1 [hep-th]
15. J. M. Cline and A. R. Frey, *Phys. Rev.* **D90** 123537 (2014) [arXiv:1410.7766]
16. Xenon-collaboration “Observation of Excess Electronic Recoil Events in XENON1T” arXiv:2006.09721v2 (2020)
17. J. Bowman et al, *Nature* **555** 67 (2018). 1
18. R. Barkana, *Nature* **555** 71 (2018).
19. C. D. Froggatt and H. B. Nielsen, *Mod. Phys. Lett.* **A30** no.36, 1550195 (2015) [arXiv:1503.01089].
20. M. Aglietta et al., *Europhys. Lett.* **3** 1315 (1987).
21. M. Tanabashi et al (Particle Data Group), *Phys. Rev.* **D98** 030001 (2018)
22. A. Boyarsky, J. Franse, D. Iakubovskiy and O. Ruchayskiy, *Phys. Rev. Lett.* **115**, 161301 (2015) [arXiv:1408.2503]
23. O. Urban, N. Werner, S. W. Allen, A. Simionescu, J. S. Kaastra and L. E. Strigari, *MNRAS* **451**, 2447 (2015) [arXiv:1411.0050]
24. T. Jeltema and S. Profumo, *MNRAS* **450**, 2143 (2015) [arXiv:1408.1699]
25. R. Bernabei; et al. (2013). “Final model independent result of DAMA/LIBRA–phase1”. *European Physical Journal C.* **73** (12): 2648. arXiv:1308.5109.  
and contribution in the present volume, and earlier volumes: Workshop 2020 on “Beyond the Standard Models” organized by Norma Mankoc Borstnik, D. Lukman, M. Khlopov and H.B. Nielsen.  
R. Bernabei, DAMA/LIBRA, LNGS scientific committee meeting, 26–27 March 2018, <https://agenda.infn.it/conferenceDisplay.py?confId=15474>, 2018
26. Andrei Kryjevski, David B. Kaplan, Thomas Schaefer “New phases in CFL quark matter” arXiv:hep-ph/0404290v1



## **Scientific Debuts**

All contributions are arranged alphabetically with respect to the authors' names.





## 4 Problems of the Correspondence Principle for the Recombination Cross Section in Dark Plasma

K. Belotsky <sup>\*</sup>, E. Esipova <sup>\*\*</sup>, D. Kalashnikov <sup>\*\*\*</sup> and A. Letunov <sup>†</sup>

National Research Nuclear University MEPhI, 115409 Moscow, Russia

**Abstract.** We raise the issues concerning correspondence principle in description of a recombination of oppositely charged particles. These issues have come from cosmological dark matter (DM) problem investigations. Particles possessing Coulomb-like interaction are considered. Such Coulomb-like interaction between DM particles is assumed though the problem seems to be more general. Analysis showed that usage of different semiclassical approaches leads to the apparent discrepancy between numbers of recombination acts. We attempted to find some conditions under which classical cross-section (which relates to multiple soft photon process) reduces to quantum one, which is obtained in semi-classical approximation (Kramers' formula). We just draw attention to this and provide some (not decisive) arguments.

**Povzetek.** Avtorji opozorijo na probleme, ki se pojavijo pri uporabi korespondenčnega načela za opis rekombinacije delcev z nasprotnimi naboji. Na te probleme so naleteli pri raziskavah sipanja delcev temne snovi, ki interagirajo s Coulombovi podobnimi interakcijami. Ugotavljajo pa, da se te vrste problemov pojavijo tudi pri drugih interakcijah. Analize so namreč pokazale, da različni semiklasični približki ne napovedo enakega števila rekombinacij. Iščejo pogoje, pri katerih se klasični sipalni preseki za procese, pri katerih se izseva večje število mehkih fotonov, ujemajo s kvantnimi računi v semiklasičnem približku (Kramersova formula).

Keywords: correspondence principle, dark matter, dark plasma, collision theory, semiclassical approach

### 4.1 Introduction

Investigation of dark matter (DM) is one of the most important problems in cosmology and particle physics. Many experiments are being carried out to detect DM particles and explore its properties [1–5]. A part of the models considers self-interacting DM including Coulomb-like interaction [6–13]. Within the framework of such models, several disadvantages of the standard  $\Lambda$ CDM scenario can be

<sup>\*</sup> E-mail: k-belotsky@yandex.ru

<sup>\*\*</sup> E-mail: esipovaea@gmail.com

<sup>\*\*\*</sup> E-mail: impermast@gmail.com

<sup>†</sup> E-mail: letunovandrey11@yandex.ru

avoided. These are cuspy density profile of the halo, number of small halos and similar other.

Models with Coulomb-like interaction lead to the differences in cosmological evolution. Dark charged particles can form a bound state. If they are a particle and an antiparticle, they annihilate, what significantly reduces their density. If they are not particle and antiparticle but have opposite "dark" charges (they can be called in this case "dark electron" and "dark proton"), binding processes (recombination) lead to a decrease of free dark charged particles. This significantly changes dynamics of dark matter during the formation of structures in the Universe [8, 14] and thermodynamical evolution which we considered previously [15]. Thus, accounting for recombination is an essential part of such models.

Theory of atomic kinetics is deeply studied section of plasma physics [16, 17]. Density evolution of specific particle's sort is routinely calculated. These methods were applied to the study of dark matter [18]. However, the authors of the present work are deeply convinced that the question of choosing the correct expression for the cross-section of atomic processes in cosmological structures is not clear enough. For example in the famous paper [19] devoted to density of monopoles in the Universe the authors used the classical approach for the recombination calculations.

Rate of recombination depends on its cross-section. The Kramers formula (4.1) is typical of kinetic plasma calculations. Its semiclassical expression describes a single-photon recombination for a hydrogen-like atom [20]

$$\sigma_q(n) = \frac{32\pi}{3\sqrt{3}} \alpha^3 a_0^2 \frac{\hbar\omega_0^2}{E\omega n^3}, \quad (4.1)$$

where  $\hbar\omega_0$  is the energy of ground state,  $n$  is the principle number of a bound state,  $\omega$  is the frequency of emitted photon,  $\alpha$  is the fine-structure constant and  $a_0$  is the Bohr radius.

The approximate summing (coming up to integration) of (4.1) leads to the following expression

$$\sigma_q = \frac{32\pi}{3\sqrt{3}} \alpha r_0^2 Z^2 \left(\frac{c}{v}\right)^2 \ln \frac{Zc\alpha}{v}, \quad (4.2)$$

where  $Z$  is a charge of ion,  $r_0 = \frac{e^2}{m_e c^2} \sim \alpha$  is the classical electron radius and  $v$  is initial velocity.

An another formula for the recombination cross-section was derived by Yelutin [21]

$$\sigma_{cl} = \pi (4\pi)^{\frac{2}{5}} r_0^2 Z^{\frac{8}{5}} \left(\frac{c}{v}\right)^{\frac{14}{5}}. \quad (4.3)$$

The expression (4.3) was obtained in terms of the classical mechanics. A single electron is considered as moving from infinity losing its energy due to dipole radiation. When electron's energy becomes zero it comes to bound state.

Expressions (4.2) and (4.3) have different conditions of applicability. Formula (4.2) is valid when

$$Ze^2 \gg \hbar v. \quad (4.4)$$

That is  $v \ll \alpha$  in natural unites ( $\hbar = c = 1$ ) and  $Z = 1$ . It is a common condition for semiclassical approximation in scattering theory [22].

For the classical cross-section we have

$$Z^4 \left(\frac{c}{v}\right)^2 \gg \alpha^{-5}, \quad (4.5)$$

i.e.  $v \ll \alpha^{5/2}$  in natural unites with  $Z = 1$ .

However, if electron's speed satisfies (4.5), one will point out dramatic discrepancies. Firstly, the cross-sections have different initial speed dependencies. Secondly, the expression for the classical cross section is several orders of magnitude larger than the quantum. Finally, expressions have different orders of fine-structure constant.

Derivation of an accurate quantum expression for the many-photon recombination is sophisticated problem. The semiclassical consideration of a stimulated bremsstrahlung is presented in [23]. This paper shows that every partial cross-section depends on its own photon frequency. Establishing a relation between the number of photons and their energies is very complex issue. Well-known description of quantum single-photon processes is presented in [24]. Although, cross-sections of considered reactions have an analytical form, its derivation is quite cumbersome. The bremsstrahlung cross-section is expressed in terms of the complex hyper-geometric series. Additional photons make establishing correspondence between quantum expression and (4.3) almost impossible.

To sum it up, the investigation of dark matter led us to the problem on scattering theory. How to obtain an expression for recombination cross-section when low energy electron emits infinitely many photons? Unfortunately, classical monographs devoted to atomic physics do not contain the solution [25,26].

Here we list some considerations on this topic which do not give solution of the issue. One of the argument, bases on an action, is taken from our previous work [14]. We just want to collect together something existing for thought just to attract attention to this issue.

## 4.2 Correspondence between classical expression and Kramers formula

Now we want to find the situation when two expressions would coincide. In order to do this we have to guess energy loss of an electron. One can notice that if  $\omega$  in the denominator of the formula (4.1) will be changed to  $E$  it can coincide with (4.3). It will be shown below.

We are considering the electron moving from infinity losint it's energy. Just before the last this iteration(the photon emission) it is possible to use Kramers formula for one-photon recombination. In order to achive the coincidence we will establish the following relation

$$E^2 = \tilde{E} \hbar \tilde{\omega} \quad (4.6)$$

where  $\tilde{E}$  is the total energy of the electron before coming to the bound state and  $\tilde{\omega}$  is the last emitted photon.

Also the following relations express energy coversion

$$\tilde{E} = \hbar\tilde{\omega} - \frac{\hbar\omega_0}{n^2} \quad (4.7)$$

$$\tilde{E} = E - \Delta E \quad (4.8)$$

where  $\Delta E$  is the total energy loss of the electron before last emitting of a photon.

After substitution of (4.7) and (4.8) in (4.6) one will obtain the quadratic equation for  $\Delta E$ . The solution for  $\Delta E$  has the following form

$$\Delta E = E + \frac{\hbar\omega_0}{2n^2} \pm \frac{1}{2} \sqrt{4E^2 + \left(\frac{\hbar\omega_0}{n^2}\right)^2} \quad (4.9)$$

It is necessary to choose the sign  $-$  to satisfy the energy conservation law.

The next step is summation over new partial cross sections

$$\tilde{\sigma}_q(n) = \frac{32\pi}{3\sqrt{3}} \alpha^3 a_0^2 \frac{\hbar\omega_0^2}{E^2 n^3}$$

starting with number  $k$  that we assume bigger than unit to be in the framework of semiclassical limit.

$$\tilde{\sigma}_q = \sum_{n=k}^{\infty} \tilde{\sigma}_q(n) = \frac{16\pi Z^4}{3\sqrt{3}} \frac{\alpha^3 r_0^2}{k^2} \left(\frac{c}{v}\right)^4 \quad (4.10)$$

After comparsion of (4.3) and (4.10) it is easy to obtain the result for  $k$

$$k = \alpha^{\frac{3}{2}} \left(\frac{c}{v}\right)^{\frac{3}{5}} Z^{\frac{6}{5}} \quad (4.11)$$

Assume  $k \gg 1$  and we will obtain

$$Z^4 \left(\frac{c}{v}\right)^2 \gg \alpha^{-5} \quad (4.12)$$

This condition reproduce (4.5). Thus, this approach let one point out the connection between two expression: Kramers single-photon cross-section can be integrated into the process of bremsstrahlung.

To clarify the physical situation we will give the following reasoning. Slow electron moving from infinity loses it's energy because of bremsstrahlung. In order to understand the correspondence between classical expression (4.3) and Kramers formula (4.2) it is necessary to do some manipulations. Firstly, one can notice that when electron initial speed satisfies (4.5), energy of a single emitted photon have to be relatively large. Electron's energy must be spent on coming to bound state (it has negative energy). Secondly, we rightly assume that if electron overcomes a great distance is not influenced by any other external factors, it will emit many photons. Finally, we establish total energy loss of electron before coming to bound state. Summing all new partial cross sections and comrasion of obtained formula and (4.3) lets one reproduce original condition (4.5).

### 4.3 Estimation of action

Evaluating of an electron's action also leads to (4.5). We will consider an electron moving in the external Coulomb-like field. In order to simplify the calculation charge of ion  $Z$  is put equal to unit

$$S = \int_{t_1}^{t_2} \left( \frac{mv^2}{2} + \frac{e^2}{r} \right) dt \quad (4.13)$$

where  $S$  is the action of the electron.

In the region of interest kinetic energy is proportional to potential

$$\frac{mv^2}{2} \sim \frac{e^2}{r} \quad (4.14)$$

This immediately implies  $v \sim \sqrt{\frac{2e^2}{mr}}$ .

$$S \sim \int_{r_1}^{r_2} 2 \frac{e^2 dr}{rv} \sim \sqrt{me^2} (\sqrt{r_2} - \sqrt{r_1}) \quad (4.15)$$

Here  $r_1$  corresponds to radius of coming to bound state and  $r_2$  is the same value with adding the distance, which electron needs to cover for losing most of it's initial energy (see [14]). Eventually, if one **requires**  $S \ll \hbar$  and obtains

$$\frac{v}{c} \ll \alpha^{\frac{5}{2}}. \quad (4.16)$$

Obviously, this condition is in agreement with (4.5).

### 4.4 Conclusion

Calculations originally connected with an estimation of dark matter particles in the Universe generated problem on collision theory. Dark matter is considered as self-interacting according to the law of Coulomb. It immediately implies that darkly charged particles will recombine intensively. Rate of recombination is proportional to the cross-section of its process. Dark matter is considered to have very low energy, what is naturally realised in the Universe (CMB has temperature 3 K, non-relativistic DM should have much lower temperature), what possibly accounts for applicability of classical approximation in a recombination process description.

This should be understood in the sense of scattering theory. Characteristic speed of particle is lower than atomic speed. This condition is expressed by (4.4). In contrast to the Born approximation, semiclassics is applicable here. The problem of the correct expression for the recombination cross-section was discovered. On the one hand, Kramers formula [20] is widely used in atomic kinetics. On the other hand, classical expression [21] describing the electron capture does not correlate with Kramers cross-section. Of course, this discrepancy is connected with the fact that these sections relate to different reactions. Expression describes a

single-photon recombination. Formula (4.3) relates to the process with emitting of infinitely many photons. An attempt to link these two approaches reproduced initial applicability condition (4.5) for (4.3). Moreover, the estimation of the electron's action also leads to the same inequality (4.16).

In order to completely solve this problem, it is necessary to obtain expressions for cross-section of infinitely many photon recombination. This is a rather ambitious task, but without this the question remains open.

## Acknowledgements

The work of K.B. was supported by the Ministry of Science and Higher Education of the Russian Federation by project No 0723-2020-0040 "Fundamental problems of cosmic rays and dark matter". E.E. is also supported by fund Basis, project № 18-1-5-89-1.

Also, we would like to thank A.Barabanov, M.Faifman, V.Lensky, S.Rubin, M.Skorokhvatov for interest to this work and discussions.

## References

1. R Bernabei, P Belli, F Cappella, R Cerulli, CJ Dai, A d'Angelo, HL He, A Incicchitti, HH Kuang, JM Ma, et al. First results from dama/libra and the combined results with dama/nai. *The European Physical Journal C*, 56(3):333–355, 2008.
2. CDMS II Collaboration et al. Dark matter search results from the cdms ii experiment. *Science*, 327(5973):1619–1621, 2010.
3. Elena Aprile, KL Giboni, P Majewski, K Ni, M Yamashita, R Gaitskell, P Sorensen, Luiz DeViveiros, L Baudis, A Bernstein, et al. The xenon dark matter search experiment. *New Astronomy Reviews*, 49(2-6):289–295, 2005.
4. Ko Abe et al. The xmass experiment. In *J. Phys. Conf. Ser.*, volume 120, 2008.
5. The XENON collaboration et al. Projected wimp sensitivity of the xenonn dark matter experiment, 2020.
6. Petraki, Kalliopi, Pearce, Lauren, and Kusenko, Alexander. Self-interacting asymmetric dark matter coupled to a light massive dark photon. *Journal of Cosmology and Astroparticle Physics*, 2014(07):039, 2014.
7. Francis-Yan Cyr-Racine and Kris Sigurdson. Cosmology of atomic dark matter. *Physical Review D*, 87(10):103515, 2013.
8. Benedict Von Harling and Kalliopi Petraki. Bound-state formation for thermal relic dark matter and unitarity. *Journal of Cosmology and Astroparticle Physics*, 2014(12):033, 2014.
9. K.M. Belotsky, M. Yu. Khlopov, and K.I. Shibaev. Composite dark matter and its charged constituents. *arXiv preprint astro-ph/0604518*, 2006.
10. Daniel Feldman, Zuowei Liu, Pran Nath, and Gregory Peim. Multicomponent dark matter in supersymmetric hidden sector extensions. *Physical Review D*, 81(9), May 2010.
11. Sean Tulin and Hai-Bo Yu. Dark matter self-interactions and small scale structure. *Physics Reports*, 730:1–57, Feb 2018.
12. Ayuki Kamada, Manoj Kaplinghat, Andrew B. Pace, and Hai-Bo Yu. Self-interacting dark matter can explain diverse galactic rotation curves. *Physical Review Letters*, 119(11), Sep 2017.

13. Yuji Kajiyama, Hiroshi Okada, and Takashi Toma. Multicomponent dark matter particles in a two-loop neutrino model. *Physical Review D*, 88(1), Jul 2013.
14. K.M. Belotsky, E.A. Esipova, and A.A. Kirillov. On the classical description of the recombination of dark matter particles with a coulomb-like interaction. *Physics Letters B*, 761:81–86, Oct 2016.
15. K M Belotsky, E A Esipova, and A A Kirillov. On the temperature evolution of multicomponent dark matter with coulomb-like interaction. *Journal of Physics: Conference Series*, 675(1):012017, feb 2016.
16. LA Vajnshtejn. I.i. sobelman, e.a. ukov, excitation of atoms and spectral lines broadening, 253p. *The Science*, 1979.
17. D. R. Bates. *Atomic and molecular processes*, volume 13. Elsevier, 2012.
18. D. E. Kaplan, G. Z. Krnjaic, K. R. Rehermann, and C. M. Wells. Atomic dark matter. *Journal of Cosmology and Astroparticle Physics*, 2010(05):021, 2010.
19. Ya. B. Zeldovich and M. Yu. Khlopov. On the concentration of relic magnetic monopoles in the universe. *Physics Letters B*, 79(3):239–241, 1978.
20. HA Kramers. London, edinburgh, dublin philos. mag. *J. Sci*, 46:836–71, 1923.
21. P.V. Yelutin. Classical cross-section for recombination. *theoretical and mathematical physics*, 34(2):180–184, 1978.
22. L. D. Landau and E. M. Lifshitz. *Quantum mechanics: non-relativistic theory*, volume 3. Elsevier, 2013.
23. I. Ya. BERSON. Semiclassical approximation for stimulated bremsstrahlung. *Zhurnal Eksperimental'noi i Teoreticheskoi Fiziki*, 80:1727–1736, 1981.
24. V. B. Berestetskii, E. M. Lifshitz, and L. P. Pitaevskii. *Quantum Electrodynamics: Volume 4*, volume 4. Butterworth-Heinemann, 1982.
25. I. I. Sobelman. *Introduction to the Theory of Atomic Spectra: International Series of Monographs in Natural Philosophy*, volume 40. Elsevier, 2016.
26. H Bethe and E Salpeter. Quantum mechanics of atoms with one and two electrons [russian translation]. *Pizmatgiz, Moscow I*, 960, 1960.



## 5 Neutrino Cooling Effect of Primordial Hot Areas in Dependence on its Size

K.M. Belotsky <sup>\*1</sup>, M.M. El Kasmi <sup>\*\*1,2</sup> and S.G. Rubin <sup>\*\*\* 1,3</sup>

<sup>1</sup> National Research Nuclear University MEPhI, Kashirskoe Shosse 31, Moscow 115409, Russia

<sup>2</sup> Physics Department, Faculty of Science, Sohag University, Sohag Center, Sohag 82524, Egypt

<sup>3</sup> N. I. Lobachevsky Institute of Mathematics and Mechanics, Kazan Federal University, Kremlevskaya Street 18, Kazan 420008, Russia

**Abstract.** We consider the temperature dynamics of hypothetical primordial hot areas in the Universe. Such areas can be produced by the primordial density inhomogeneities and can survive to the modern era, in particular due to primordial black hole (PBH) cluster of size  $R \gtrsim 1$  pc and more. Here we concentrate on the neutrino cooling effect which is realized due to reactions of weak  $p \leftrightarrow n$  transitions and  $e^\pm$  annihilation. The given neutrino cooling mechanism is found to work in a wide range of parameters. For those parameters typical for PBH cluster considered, the cooling mechanism is quite valuable for the temperatures  $T \gtrsim 3$  MeV.

**Povzetek.** Avtorji obravnavajo temperaturne spremembe v domnevnih prvotnih vročih območjih v vesolju. Takšna območja lahko nastanejo zaradi prvotnih nehomogenosti gostote in lahko preživijo do danes, če so kopice prvotnih črnih lukenj velikosti  $R \gtrsim 1$  parsek. Obravnavajo predvsem ohlajanje vesolja z nevtrini, ki se sproščajo pri šibkih prehodih  $p \leftrightarrow n$  in z anihilacijo  $e^\pm$ . Ugotovijo, da je območje parametrov, ki omogočijo ohlajanje z nevtrini, zelo široko. Za parametre, ki ustrezajo obravnavanim kopicam črnih lukenj, je ta mehanizem hlajenja ustrezen za temperature  $T \gtrsim 3$  MeV.

Keywords: Primordial hot areas, primordial black holes, cosmic neutrinos

### 5.1 Introduction

There are some observations [1] indicating the existence of local heated areas in the early Universe. Hypothetical nature of local heated areas was discussed earlier [2–4]. Such areas can appear due to large primordial density fluctuations and can be related to the clusters of Primordial Black Holes (PBHs) [1, 5, 6].

We assume that the baryonic matter has been captured by the gravitational forces of these regions at the early Universe. They would remain hot for a long

\* E-mail: k-belotsky@yandex.ru

\*\* E-mail: m.elkasemy@science.sohag.edu.eg

\*\*\* E-mail: sgrubin@mephi.ru

time. At the same time, many processes can heat or cool the matter inside them during their formation after it. Short list of them is the neutrino cooling [6], nuclear reactions, radiation of the hot plasma and stars formed inside the region [8], gravitational dynamics of the system, shock waves, diffusion of matter, variation of the vacuum state while the region is born [9], energy transfer from collapsing walls [10–13], accretion, the Hawking evaporation. The last mechanisms are relevant in the case of PBHs origin of the regions [5, 14–16]. In this proceedings, we continue our consideration of neutrino cooling of such regions. It could be the most important reason for the temperature evolution within initial temperature range  $keV < T < 10 \text{ MeV}$ .

In this research, we follow the initial conditions taken from [5, 6], where the mass of trapped matter is in wide range  $10^4 - 10^8 M_\odot$ . The main initial parameters are as follows: the size of the region is about  $R \sim 1 \text{ pc}$ , its mass  $10^4 M_\odot$ , initial temperature is in the interval  $T_0 \sim 1 \text{ keV} \div 10 \text{ MeV}$ . This temperature of such regions could be reached in several ways. The region can start to be formed at higher temperature and finish to do it having cooled down to  $T_0$ . Also, the region could be heated up during formation, e.g., in the framework of model with collapsing domain walls [7].

Without specific assumptions, we show that effect of neutrino cooling is wide spread phenomena valid in wide range of parameters. The range of initial parameters is under consideration.

Neutrino cooling effect can be suppressed at high temperatures and large sizes when the area becomes opaque to the neutrinos.

Neutrinos are produced due to reactions of  $p \leftrightarrow n$  transition and  $e^+e^-$  annihilation. The characteristic time for photons to escape **the area** is bigger than the modern Universe age, this indicates that the size of cluster is big enough not to lose photons.

In the given proceedings we study the impact of the size of the **region** on the neutrino cooling effect.

Mechanism of neutrino cooling rates for the main reactions of the neutrino production is considered in Section 2. The impact of the diffusive character of particle propagation inside the cluster is briefly discussed in Section 3.

## 5.2 Cooling Rates

Let us consider the reactions of the neutrino production:

$$e^- + p \rightarrow n + \nu_e, \quad (5.1)$$

$$e^+ + n \rightarrow p + \bar{\nu}_e, \quad (5.2)$$

$$e^+ + e^- \rightarrow \nu_{e,\mu,\tau} + \bar{\nu}_{e,\mu,\tau}, \quad (5.3)$$

$$n \rightarrow p + e^- + \bar{\nu}_e. \quad (5.4)$$

The produced neutrinos leave the heated area if it is not very big. The energy inside the volume is decreased that leads to the temperature decreasing. The rates

per unit volume,  $\gamma_i \equiv \Gamma_i/V$ , for reactions listed above are respectively

$$\gamma_{ep} = n_{e^-} n_p \sigma_{ep} v, \quad \gamma_{en} = n_{e^+} n_n \sigma_{en} v, \quad (5.5)$$

$$\gamma_{ee} = n_{e^-} n_{e^+} \sigma_{ee} v, \quad \gamma_n = \frac{n_n}{\tau_n}. \quad (5.6)$$

Here  $n_i$  is the concentration of the respective species,  $\sigma_{ij}$  is the cross section (see e.g. [6]) of interacting particles  $i$  and  $j$  and  $\tau_n \approx 1000$  s is the neutron lifetime. We consider the relativistic plasma so that the relative velocity  $v \simeq 1$ .

The backward reactions for Eqs.(5.1)–(5.4) are suppressed if neutrinos freely escape the cluster. We consider all densities to be independent of the space coordinate inside the region. The number densities are roughly described by the following formulas, see [6],

$$n_{e^-} = n_{e^+} + \Delta n_e, \quad n_{e^+} = n_e^{\text{eq}}(T) \exp\left(-\frac{m_e}{T}\right), \quad (5.7)$$

$$n_B \equiv n_p + n_n = g_B \eta n_\gamma(T_0), \quad \Delta n_e \equiv n_{e^-} - n_{e^+} = n_p. \quad (5.8)$$

which are slightly corrected for better adjustment to the non-relativistic limit. Here  $\eta = n_B/n_\gamma \approx 0.6 \cdot 10^{-9}$  is the baryon to photon ratio in the modern Universe,  $g_B \sim 1$  is the correction factor of that relation due to entropy re-distribution,  $n_\gamma(T) = \frac{2\zeta(3)}{\pi^2} T^3$  and  $n_e^{\text{eq}}(T) = \frac{3\zeta(3)}{2\pi^2} T^3$  are the equilibrium photon and relativistic electron number densities respectively.

Note that  $n_\gamma(T_0)$  defines baryon density which is supposed to be unchanged starting from initial temperature  $T_0$  contrary to that of  $e^\pm$  and  $\gamma$ . Number of  $e^\pm$  (along with  $\gamma$ ) changes due to  $e - \nu$ -conversion processes (reactions Eqs.(5.1) – (5.4)). The temperature of the system decreases due to neutrino escape. Number densities of the electrons and photons fall down with temperature as  $\sim T^3$ .

### 5.3 Escaping Time

The escape time of neutrinos from the region of the size  $R$  with temperature  $T$  can be calculated as:

$$t_{\text{esc}} \sim \frac{R^2}{D} \sim R^2 \cdot n_e \sigma_\nu \quad (5.9)$$

in diffusion approximation. Here the diffusion coefficient is  $D = \frac{\lambda_\nu v}{3}$  [17], velocity  $v = 1$ , the neutrino mean free path is  $\lambda_\nu = 1/n_e \sigma_\nu$  and  $e - \nu$  interaction cross section was roughly taken as  $\sigma_\nu \sim G_F^2 \cdot T^2$ . The electron number density  $n_e \sim n_{e^-} + n_{e^+} \sim n_{e^+}$  is given by Eq.(5.7) which is  $\sim T^3$  at  $T > m_e$ .

One can conclude from inequality

$$t_{\text{esc}} \sim R^2 G_F^2 T^5 < t_U \quad (5.10)$$

that the neutrino cooling effect is significant up to the present time  $t_U$  for the region of the size

$$R < 35 \cdot (T/\text{MeV})^{-5/2} \text{ pc}. \quad (5.11)$$

Here conditions  $T \gtrsim m_e$  and  $n_e \sim T^3$  are assumed.

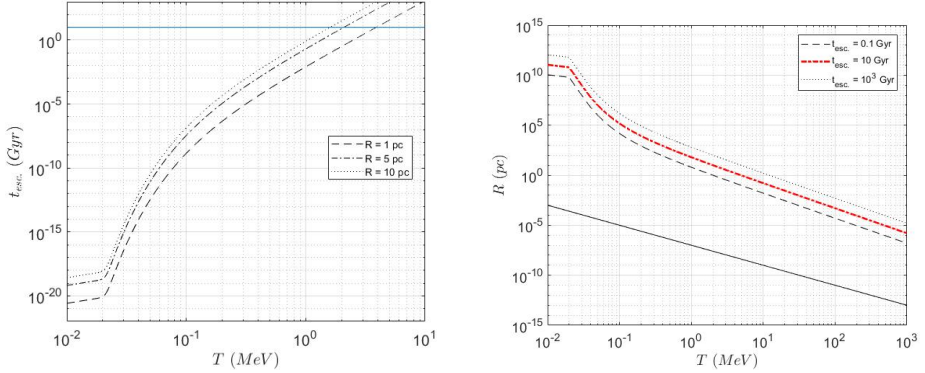


Fig. 5.1: Left: The relation between escaping time of neutrino and temperature of the area and the blue line is the modern age of the Universe. (Behaviour of the curves at  $t_{\text{esc}} \sim 10^{-20}$  Gyr reflects the fact that  $n_e$  becomes  $\sim \Delta n_e$ , i.e. constant.) Right: The relation between size and temperature of the area. Neutrino cooling effect plays a prominent role below the thick red dot-dashed curve. The black solid line corresponds to the dependence of the Universe horizon from its temperature ( $R = 10^{-7}(\text{MeV}/T)^2$  pc).

Neutrino cooling effect due to reactions of weak  $p \leftrightarrow n$  transitions and  $e^\pm$  annihilation are represented in Figure 5.1 where the escaping time of neutrinos in dependence on temperature is shown. As seen, at the temperature  $T \lesssim 3$  MeV the escaping time for the most of considered cluster sizes is less than the modern Universe age, thus neutrino cooling works. Note, that at  $T \ll m_e$  the curves start to fall until the number density of electrons becomes  $n_e \sim \Delta n_e$ .

Dependence  $R(T)$  is shown in Figure 5.1, right panel, which follows from Figure 5.1, left panel. The region above the red line relates to the case when neutrino cooling is suppressed (neutrinos do not run away from the region during the Universe age). Black line shows the horizon size of the Universe in dependence on the matter temperature. One can see, horizon size is much smaller than the maximal size of region at the same temperature when neutrino cooling effect is, shown by the red line. Therefore, the neutrino cooling effect holds under usual conditions, and can be suppressed in extreme cases.

The region can start its formation at very high temperature so that it could be cooled to the considered temperature during its detachment from Hubble flow and virialization. Also, the region could be heated up additionally during its formation, e.g. due to wall collapsing [7]. During detachment and virialization, the region could expand to some extent and hence, cool down.

## 5.4 Conclusions

In earlier work [6], we have shown that due to neutrino emission (at a fixed size) the primordial hot areas are cooling down to the temperature value  $\sim 0.01 \div 0.1$

MeV. Here we just investigated the neutrino cooling mechanism of the heated region and dependence on its size. Considering the result of equation (5.9) for escaping time, we can find the size-changing more effectively with temperature. At the temperature  $T > 3$  MeV, the diffusive character of particle propagation makes the time of escaping or time of cooling more than the modern Universe age. This result is obtained at the definite initial region parameters (size and temperature, relevant for PBH cluster model [5]) that could be slightly varied. It illustrates general property for such possible primordial inhomogeneities.

It is seen that neutrino cooling effect should take place for a wide reasonable size/temperature range of parameter. Extreme heating up of the area while it has being formed could change situation.

There are a variety of mechanisms that can be responsible for the area heating. Additional heating during their creation is also possible. As was mentioned in the Introduction, the area could be heated by the collapsing walls - the scalar field kinks. The fermion reflection on kinks was studied in [7]. It was shown that the reflection weakly depends on the fermion mass. Therefore the kinks could prevent the neutrinos from escaping. More detailed analysis is necessary to clarify this effect.

## Acknowledgements

The work of K.B. was supported by the Ministry of Science and Higher Education of the Russian Federation by project No 0723-2020-0040 "Fundamental problems of cosmic rays and dark matter" and of S.R. by the project "Fundamental properties of elementary particles and cosmology" No 0723-2020-0041. The work of S.R. is performed according to the Russian Government Program of Competitive Growth of Kazan Federal University and RFBR grant 19-02-00930.

## References

1. A. Kashlinsky, Y. Ali-Haïmoud, S. Clesse, J. Garcia-Bellido, L. Wyrzykowski, A. Achúcarro, L. Amendola, J. Annis, A. Arbey and R. G. Arendt, *et al.*: Electromagnetic probes of primordial black holes as dark matter, *Bull. Am. Astron. Soc.*, **51**, 51 (2019).
2. V. K. Dubrovich and S. I. Glazyrin: Cosmological dinosaurs, [arXiv:1208.3999 [astro-ph.CO]] (2012).
3. S. Kumar, E. Dimastrogiovanni, G. D. Starkman, C. Copi and B. Lynn: CMB Spectral Distortions from Cooling Macroscopic Dark Matter, *Phys. Rev. D* **99**, no.2, 023521 (2019).
4. A. Kogut, M. H. Abitbol, J. Chluba, J. Delabrouille, D. Fixsen, J. C. Hill, S. P. Patil and A. Rotti: CMB Spectral Distortions: Status and Prospects, [arXiv:1907.13195 [astro-ph.CO]], (2019).
5. K. Belotsky, V. Dokuchaev, Y. Eroshenko, E. Esipova, M. Khlopov, L. Khromykh, A. Kirillov, V. Nikulin, ; S. Rubin, I. Svadkovsky: Clusters of Primordial Black Holes, *Eur. Phys. J. C.* **79**, 1-20 (2019).
6. K. Belotsky, M. E. Kasmi and S. Rubin: Neutrino Cooling of Primordial Hot Regions, *Symmetry* **12**, 1442 (2020).
7. A. A. Kurakin and S. G. Rubin, [arXiv:2011.01757 [physics.gen-ph]].

8. A. Dolgov, K. Postnov: Electromagnetic radiation accompanying gravitational waves from black hole binaries, *J. Cosmol. Astropart. Phys.* **2017**, 18 (2017).
9. K. M. Belotsky, Y. A. Golikova and S. G. Rubin: Local heating of matter in the early universe owing to the interaction of the Higgs field with a scalar field, *Phys. Atom. Nucl.* **80**, 718-720 (2017).
10. V. Berezhin, V. Kuzmin, I. Tkachev: Thin-wall vacuum domain evolution, *Phys. Lett. B* **120**, 91–96 (1983).
11. M. Y. Khlopov, R. V. Konoplich, S. G. Rubin and A. S. Sakharov: Formation of black holes in first order phase transitions, arXiv:hep-ph/9807343 [hep-ph], (1998).
12. S. G. Rubin, M. Y. Khlopov and A. S. Sakharov: Primordial black holes from nonequilibrium second order phase transition, *Grav. Cosmol.* **6**, 51-58 (2000).
13. H. Deng, A. Vilenkin and M. Yamada: CMB spectral distortions from black holes formed by vacuum bubbles, *JCAP* **07**, 059 (2018).
14. A. Dolgov, J. Silk: Baryon isocurvature fluctuations at small scales and baryonic dark matter, *Phys. Rev. D* **47**, 4244-4255 (1993).
15. A. Dolgov: Massive and supermassive black holes in the contemporary and early Universe and problems in cosmology and astrophysics, *Phys.-Uspekhi*, **61**, 115–132 (2018).
16. J. García-Bellido: Primordial Black Holes, *PoS EDSU2018*, 042 (2018).
17. E. M. Lifshitz, L. P. Pitaevskii: *Physical Kinetics. Course of Theoretical Physics*, Butterworth-Heinemann, Oxford, 2006.



## 6 Consideration of a Loop Decay of Dark Matter Particle into Electron-Positron from Point of View of Possible FSR Suppression

K. M. Belotsky \* and A.Kh. Kamaletdinov \*\*

National Research Nuclear University MEPhI (Moscow Engineering Physics Institute),  
115409, Kashirskoe shosse 31, Moscow, Russia

**Abstract.** Cosmic positron anomaly is still not explained. Explanation with dark matter (DM) decay or annihilation is one of the main attempts to do it. But they suffer with shortcoming as overproduction of induced gamma-radiation which contradict to cosmic gamma-background. Final state radiation (FSR) in such processes is supposed under standard conditions (by default) to have the basic contribution in it. Our group elaborates possibility to evade this problem in different ways. Here we continue one of them connected with possibility of suppression of FSR due to specifics of Lagrangian describing DM particle decay. Loop through two new spinors and scalar is considered. Effect of FSR suppression is found to be existing but at the very low level in the considered case.

**Povzetek.** Avtorja iščeta model, ki bi pojasnil presežek pozitronov v kozmičnih žarkih. Poskusi, da bi presežek pozitronov razložili z razpadi ali anihilacijami temne snovi, se niso obnesli, ker se pri tem sprosti preveč žarkov gamma. Avtorja in njuna skupina iščejo poti, ki bi razložile presežek pozitronov, izsevani žarki gamma pa bi bili v skladu z meritvami. Lagrangeovi gostoti za temno snov sta dodala sklopitev z dvema novima fermionoma in enim skalarnim poljem, vendar nov model količino izsevanih žarkov gama le neznatno zniža.

Keywords: dark matter, positron anomaly, cosmic rays, final state radiation, loop decay

### 6.1 Introduction

The problem of Dark Matter (DM) is one of the main long-term problems of fundamental physics. Many direct and indirect searches for DM particles are undertaken. Cosmic rays (CR) relate to the indirect one and the revealed cosmic positron anomaly (PA) [1–5] can be supposed to be a possible indication of DM.

But attempts to explain the positron anomaly with DM face a problem of agreement with data on cosmic gamma-rays (see, e.g., our works [6–8] and other

---

\* E-mail: k-belotsky@yandex.ru

\*\* E-mail: kamaletdinov.a.h@yandex.ru

[9–13]) and CMB [14] and some other for specific DM model case. Constraint following from CMB can be more easily avoided (see, e.g., the references in [15–17]) than that from data on cosmic gamma-ray background [19]. This constraint seems to be the least model dependent. When high energy positrons and electrons  $e^\pm$  are produced from DM decay or annihilation, it will be accompanied by final state radiation (FSR) and they will scatter on medium photons. Both processes give us gamma of high energy.

The most popular alternative approach to the solution of the problem of PA origin is associated with nearby pulsars. But it also strongly constrained (if not excluded) by data on gamma-radiation [20–22]. So the question of PA origin is still open.

We consider possibility of PA explanation with the help of DM and elaborate two approaches for it: one is connected with space distribution of DM in Galaxy ('Dark disk' model) [6–9, 23, 24], other one is connected with possible physics of DM interaction leading to annihilation or decay which can give suppressed FSR [15–17]. The latter was attempted to be considered by other recently [25]. Here we make one more step in this investigation. We study one more decay mode of DM particle which contains a loop from spinor and scalar particle of dark sector. The process is drawn below. The obtained answer is that the effect is negligible in the considered case, though it exists in principle, i.e. relative probability of FSR photon production can be changed.

Below we present theoretical initial settings for interaction/decay physics of DM particles and basic calculations, then conclude.

## 6.2 DM decay model considered and calculation details

Let us consider two processes of DM particle ( $X$ ) decay:  $X \rightarrow e^+e^-$  and the same with FSR  $X \rightarrow e^+e^-\gamma$ . The goal of the task is to minimize the ratio:

$$\frac{\Gamma(X \rightarrow e^+e^-\gamma)}{\Gamma(X \rightarrow e^+e^-)} = \min, \quad (6.1)$$

where  $\Gamma(X \rightarrow e^+e^-(\gamma))$  are the respective decay widths.

In order to be able to see the photon suppression at different energies, we study the energy distribution of the photon emission probability in the decays of DM particles (6.2).

$$\frac{\partial \text{Br}(e^+e^-\gamma)}{\partial \omega} \equiv \frac{\partial}{\partial \omega} \left( \frac{\Gamma(X \rightarrow e^+e^-\gamma)}{\Gamma(X \rightarrow e^+e^-)} \right), \quad (6.2)$$

where  $\omega$  is the energy of the final state photon.

As was shown earlier [15], the simplest interaction vertices such as (6.3, 6.4) do not lead to a significant suppression of the photon yield in a such decays. These are

$$\mathcal{L}_{\text{scalar}} = X\bar{\psi}(a + b\gamma^5)\psi, \quad \mathcal{L}_{\text{vector}} = \bar{\psi}\gamma^\mu(a + b\gamma^5)X_\mu\psi, \quad (6.3)$$

$$\mathcal{L}_C = X\bar{\psi}^C(a + b\gamma^5)\psi, \quad \mathcal{L} = \bar{\psi}\gamma^\mu\left(a + \frac{b(\gamma^\nu\partial_\nu)}{m}\right)X_\mu\psi. \quad (6.4)$$

Also shown that complication of process kinematics does not give an effect [17, 18].

Here we consider one of the options for complicating the DM-SM interactions. On the base of previous works we suppose that it is worth to consider other type of the processes. Loop diagrams of DM decays into  $e^+$ ,  $e^-$  particles can be worth to be studied. We consider here the interaction Lagrangian of the form (6.5):

$$\mathcal{L}_\Delta = X\bar{\theta}(a + i b\gamma^5)\theta + \eta \bar{\theta}(c + i d\gamma^5)\Psi + \eta^* \bar{\Psi}(c + i d\gamma^5)\theta, \quad (6.5)$$

where  $\theta$  is considered as the fermionic neutral DM component, and  $X, \eta$  – as the scalar DM particles. In this work, to simplify the calculations, the mass of the  $\eta$  particles is assumed to be very large so that the photon emission by the  $\eta$  propagator can be neglected. The leading order of the process  $X \rightarrow e^+ e^-$  in such case describes by triangle-loop diagram shown in figure 6.1.

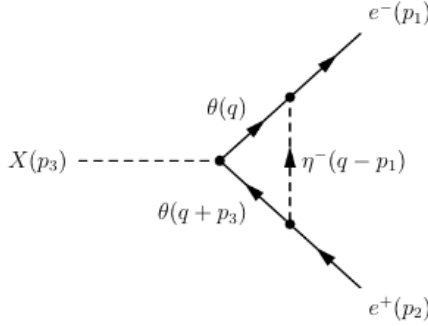


Fig. 6.1: Feynman diagram of two body decay process.

We evaluate the corresponding matrix element (6.6) here through the form-factors  $F_1$  and  $F_2$  using the Passarino-Veltman (PV) reduction procedure, described in [26, 27]. In order to perform calculations with PV-functions the PackageX [29] tool for Wolfram Mathematica was used. Matrix element is

$$i \mathcal{M} = i \bar{u}(p_1) \left( F_1(\sqrt{s}) - i F_2(\sqrt{s}) \gamma^5 \right) v(p_2), \quad (6.6)$$

$$\begin{aligned} F_1(\sqrt{s}) &= a(c^2 - d^2) \left( B(\sqrt{s}) + (m_2^2 + m_1 m_3) C_0(p_1, p_2) \right) + \\ &+ 2bcd \left( B(\sqrt{s}) + (m_2^2 - m_1 m_3) C_0(p_1, p_2) \right), \\ F_2(\sqrt{s}) &= b(c^2 - d^2) \left( B(\sqrt{s}) + (m_2^2 - m_1 m_3) C_0(p_1, p_2) \right) - \\ &- 2acd \left( B(\sqrt{s}) + (m_2^2 + m_1 m_3) C_0(p_1, p_2) \right). \end{aligned} \quad (6.7)$$

We use here and further notation  $B(\sqrt{s}) \equiv B_0(\sqrt{s}; m_1, m_3)$ ,  $C_i(p_1, p_2) \equiv C_i(p_1, p_2; m_1, m_2, m_3)$ . In this case, the squared amplitude of the two-body decay averaged over the final state polarizations takes the form:

$$\frac{1}{4} \sum_{\lambda} \mathcal{M} \mathcal{M}^* = \frac{m_X^2}{2} \left( F_1(\sqrt{s})^2 + F_2(\sqrt{s})^2 \right), \quad (6.8)$$

After the same calculations carried out for the three-body decay process ( $X \rightarrow e^+ e^- \gamma$ ) (see figure 6.2) and looking at their ratio one can obtain the expression for final-state photon yield energy distribution (6.2):

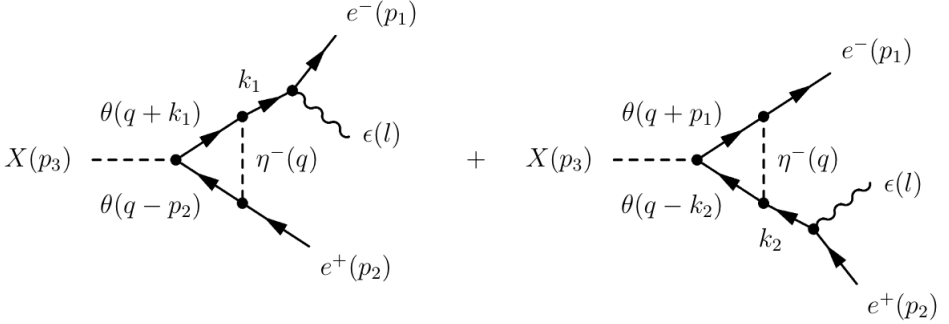


Fig. 6.2: Feynman diagrams of three body decay process.

$$\frac{1}{4} \sum_{\lambda} \mathcal{M} \mathcal{M}^* = \frac{(c^2 + d^2)^2}{4} (A_{11} - A_{12} - A_{21} + A_{22}), \quad (6.9)$$

$$A_{ii} = a^2 \frac{|X_i^+|^2 + 2m_1^2(l \cdot p_i)^2(p_1 \cdot p_2)|Y_i|^2}{(p_i + l)^4} + b^2 \frac{|X_i^-|^2 + 2m_1^2(l \cdot p_i)^2(p_1 \cdot p_2)|K_i|^2}{(p_i + l)^4}, \quad (6.10)$$

$$A_{ij} = 2m_1^2(p_1 \cdot p_2)(l \cdot p_1)(l \cdot p_2) \frac{a^2 Y_i Y_j^* - 4a^2 C_i C_j^* + b^2 K_i K_j^*}{(p_i + l)^2(p_j + l)^2} - (p_1 \cdot (p_2 + l)) (p_2 \cdot (p_1 + l)) \frac{a^2 X_i^+ X_j^{+*} + b^2 X_i^- X_j^{-*}}{(p_i + l)^2(p_j + l)^2} \quad (6.11)$$

where  $K_1 = C_0(k_1, p_2)$ ,  $K_2 = C_0(p_1, k_2)$ ,  $C_1 = C_1(k_1, p_2)$ ,  $C_2 = C_1(p_1, k_2)$ ,

$$\begin{aligned} X_1^{\pm} &= 2(l \cdot p_1)C_1 + B(\sqrt{s}) + K_1(m_2^2 \pm m_1^2), \\ X_2^{\pm} &= 2(l \cdot p_2)C_2 + B(\sqrt{s}) + K_2(m_2^2 \pm m_1^2), \\ Y_1 &= 2C_1 + K_1 \quad Y_2 = 2C_2 + K_2. \end{aligned} \quad (6.12)$$

The study of the influence of model parameters variation on the photon emission showed that the suppression turns out to be insignificant in order to explain satisfactorily the high energy cosmic positron spectrum not contradicting to gamma-ray background.

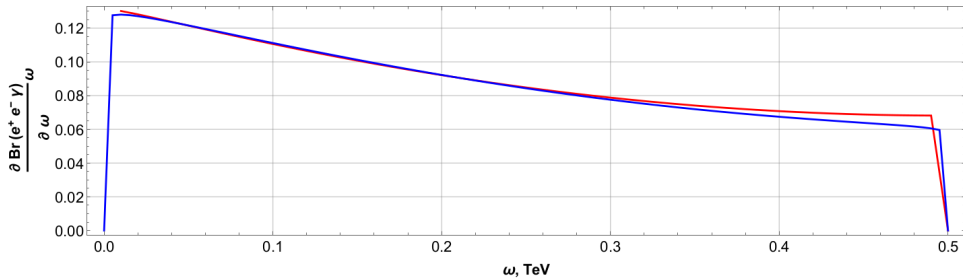


Fig. 6.3: The comparison of the photon yields in the case of simplest scalar vertice (6.3) (blue) and the loop vertice (red)

### 6.3 Conclusion

In this paper we continue our studying possibility to suppress FSR (gamma emission) in DM explanation of cosmic positron anomaly. Here we consider specific DM-lepton interaction Lagrangian which allows decaying DM particle to  $e^\pm$  through the loop of intermediate particles of dark sector. We obtained relative probability of FSR production (branching ratio of the respective mode) in dependence of final photon energy analytically up to the level of the squared matrix element. It is important for understanding whether or not possible FSR suppression looking at dependence on model parameters at high photon energies (most critical) and prospectiveness of possible complication of the model. Now it is obtained that the considered variant of the loop decay is not able to facilitate solution PA origin with DM, though shows (maybe, opens new) principal opportunity of FSR yield changing.

### Acknowledgements

The work was supported by the Ministry of Science and Higher Education of the Russian Federation by project No 0723-2020-0040 “Fundamental problems of cosmic rays and dark matter”. Also, we would like to thank M.Solovyov for the help in providing by references.

### References

1. O. Adriani et al. (PAMELA Collab.): Observation of an anomalous positron abundance in the cosmic radiation, *Nature* **458**, 607–609 (2009).
2. M. Aguilar et al. (AMS Collab.), *Phys. Rev. Lett.* **110**, 141102 (2013).
3. L. Accardo et al. (AMS Collab.), *Phys. Rev. Lett.* **113**, 121101 (2014).
4. M. Ackermann et al. (Fermi LAT Collaboration): Measurement of Separate Cosmic-Ray Electron and Positron Spectra with the Fermi Large Area Telescope, *Phys. Rev. Lett.* **108**, 011103 (2012).
5. S. Abdollahi et al. (Fermi-LAT Collaboration): Search for Cosmic-Ray Electron and Positron Anisotropies with Seven Years of Fermi Large Area Telescope Data, *Phys. Rev. Lett.* **118**, 091103 (2017).

6. K. Belotsky, R. Budaev, A. Kirillov, M. Laletin: Fermi-LAT kills dark matter interpretations of AMS-02 data. Or not?, *JCAP*, **01**, 021 (2017).
7. V. V. Alekseev, K. M. Belotsky, Yu. V. Bogomolov, R. I. Budaev et al.: On a possible solution to gamma-ray overabundance arising in dark matter explanation of cosmic antiparticle excess, *Journal of Physics: Conference Series*, **675**, 012026 (2016).
8. V. V. Alekseev, K. M. Belotsky, Yu. V. Bogomolov, R. I. Budaev et al.: High-energy cosmic antiparticle excess vs. isotropic gamma-ray background problem in decaying dark matter Universe, *Journal of Physics: Conference Series*, **675**, 012023 (2016).
9. M. Laletin: A no-go theorem for the dark matter interpretation of the positron anomaly, *Frascati Phys.Ser.* **63**, 7-12 (2016).
10. M. Ackermann et al. (Fermi-LAT Collaboration): Dark matter constraints from observations of 25 Milky Way satellite galaxies with the Fermi Large Area Telescope, *Phys. Rev. D* **89**, 042001 (2014).
11. M. Cirelli, E. Moulin, P. Panci, P. D. Serpico, A. Viana: Gamma ray constraints on decaying dark matter, *Phys. Rev. D* **86**, 083506 (2012).
12. Sh. Andoa, K. Ishiwatab: Constraints on decaying dark matter from the extragalactic gamma-ray background, *Journal of Cosmology and Astroparticle Physics*, **2015**, (2015).
13. W. Liu, Xiao-Jun Bi, Su-Jie Lin, Peng-Fei Yin: Constraints on dark matter annihilation and decay from the isotropic gamma-ray background, *Chinese Physics C*, **41**, 4 (2017)
14. P. A. Ade, N. Aghanim, M. Arnaud, M. Ashdown, J. Aumont, C. Baccigalupi et al.: Planck 2015 results-xiii. Cosmological parameters, *Astronomy Astrophysics* **594**, A13 (2016).
15. K.M. Belotsky, E.A. Esipova, A.Kh. Kamaletdinov, E.S. Shlepkina, M.L. Solovyov: Indirect effects of dark matter, *Int. J. Mod. Phys. D*, **28**, 1941011 (2019).
16. K.M. Belotsky, A. Kh. Kamaletdinov, E. S. Shlepkina, M. L. Solovyov: Cosmic Gamma Ray Constraints on the Indirect Effects of Dark Mater, *Particles* **3**(2), 336–344 (2020).
17. K. Belotsky, A. Kamaletdinov, M. Laletin, M. Solovyov: The DAMPE excess and gamma-ray constraints, *Physics of the Dark Universe* **26**, 100333 (2019).
18. M. L. Solovyov, K. M. Belotsky, A. H. Kamaletdinov, E. A. Esipova: Studying the possibility of FSR suppression in DM decay in dependence of the mass of intermediate particle and vertex, *Journal of Physics: Conference Series*, **1390**, 012096 (2018).
19. M. Ackermann, M. Ajello, A. Albert, W.B. Atwood, L. Baldini, J. Ballet, G. Barbiellini, D. Bastieri, K. Bechtol, R. Bellazzini, et al: The spectrum of isotropic diffuse gamma-ray emission between 100 MeV and 820 GeV, *Astrophys. J.* **799**, 86 (2015).
20. A. U. Abeysekara, A. Albert, R. Alfaro, C. Alvarez, J. D. Alvarez, R. Arceo et al.: Extended gamma-ray sources around pulsars constrain the origin of the positron flux at Earth, *Science* **358**, 911–914 (2017).
21. S.-Q. Xi, R.-Y. Liu, Z.-Q. Huang, K. Fang, H. Yan and X.-Y. Wang, GeV observations of the extended pulsar wind nebulae challenge the pulsar interpretations of the cosmic-ray positron excess, *Astrophys. J.* **878**, 2(104) (2019).
22. M. Linares, M. Kachelriess: Cosmic ray positrons from compact binary millisecond pulsars, *arXiv e-prints*, arXiv:2010.02844, (2020).
23. K. M. Belotsky, A. A. Kirillov, M. L. Solovyov: Development of dark disk model of positron anomaly origin, *Int. J. Mod. Phys. D* **26**, 06(1841010) (2016).
24. K. M. Belotsky, R. I. Budaev, A. A. Kirillov, M. L. Solovyov: Gamma-rays from possible disk component of dark matter, *Journal of Physics: Conference Series*, **798**, 1(012084) (2017).
25. J. Buchner, E. Carquin, M. A. Díaz, G. A. Gómez-Vargas, B. Panes, N. Viaux: Probing the anomalous positron fraction origin with fully leptonic decaying gravitino dark matter candidates, *arXiv e-prints*, arXiv:2011.09344, (2020).

26. R. Ellis, Z. Kunszt, K. Melnikov, G. Zanderighi: One-loop calculations in quantum field theory: from Feynman diagrams to unitarity cuts, *Phys. Rept.* **518**, 141–250 (2012).
27. A. Denner, S. Dittmaier: Reduction schemes for one-loop tensor integrals, *Nucl. Phys. B.* **734**, 62–115 (2006).
28. G. Devaraj, R. G. Stuart: Reduction of one loop tensor form-factors to scalar integrals: A General scheme, *Nucl. Phys. B.* **519**, 483–513 (1998).
29. H.H Patel: Package-X 2.0: A Mathematica package for the analytic calculation of one-loop integrals, *Comput. Phys. Commun.* **218**, 66–70 (2017).



## 7 Theoretical Indication of a Possible Asymmetry in Gamma-Radiation Between Andromeda Halo Hemispheres Due to Compton Scattering on Electrons From Their Hypothetical Sources in the Halo

K.M. Belotsky \*, E.S. Shlepkina \*\* and M.L. Soloviev \*\*\*

National Research Nuclear University MEPhI (Moscow Engineering Physics Institute),  
115409, Kashirskoe shosse 31, Moscow, Russia

**Abstract.** Dark matter (DM) can give observable effects decaying or annihilating with production of electrons or /and photons. Such probability was widely researched for our Galaxy. Here we consider one aspect of similar effect for Andromeda galaxy. We explicitly estimate the energy of the photon of the medium experiencing Inverse Compton (IC) scattering off electron in halo. These photons can be registered by different experiments. Dark matter annihilation or decay could be the source of high energy electrons in halo, though the source could be of other origins too (e.g. running neutron stars). Because of specifics in space orientation of Andromeda galaxy disk (a little inclined to the line of sight), the difference in energies could arise for the photons from two hemispheres of Andromeda halo. It is obtained that such asymmetry can be at the level of several 10%.

**Povzetek.** Temno snov merilci zaznajo pri različnih procesih, denimo, pri razpadu ali anihilaciji delcev temne snovi, pri cemer se rodijo elektroni in/ali fotoni. Za našo Galaksijo so te procese obravnavali številni avtorji. V tem prispevku obravnavajo avtorji podobne pojave v sosednji galaksiji, v Andromedi. Iz meritev ocenijo energijo fotona, ki se preko inverznega Comptonovega pojava sipa na elektronih v haloju. Izmerjeni visokoenergijski elektroni v haloju galaksije se lahko rodijo pri anihilaciji ali razpadu delcev temne snovi, lahko pa nastanejo tudi v drugih procesih (povzročijo jih, denimo, gibanja nevtronskih zvezd). Ker Andromedin disk ni pravokoten na smer našega opazovanja, avtorji ocenjujejo, da se izmerjene energije fotonov, ki prihajajo iz dveh različnih koncev Andromedinega haloja, lahko raxlikujejo za nekaj 10%.

Keywords: dark matter, gamma-rays, inverse Compton scattering, observational asymmetry effects, Gamma-400

### 7.1 Introduction

Dark matter (DM) can be the source of high energy electrons and photons due to its annihilation or decay. There are many works elaborating possible observational

\* E-mail: k-belotsky@yandex.ru

\*\* E-mail: shlepkinaes@gmail.com

\*\*\* E-mail: max07s@mail.ru

effects from it in cosmic rays (CR) in our Galaxy. Here we consider issue of possible observational effect from Andromeda galaxy.

If the source of high energy electrons or positrons in halo exist, the process of Inverse Compton (IC) scattering can happen for photons of the medium – of star light first of all. It is known that the angle distribution of final photon is anisotropic in this scattering process with respect to momentum of incident photon in the initial electron rest frame. This effect should remain in arbitrary reference frame, and will depend on momenta of electron and photon to be scattered. Since star disk of Andromeda galaxy is little inclined with respect to the line of sight, there will be different predominant scattering angle in ‘upper’ and ‘lower’ hemispheres of Andromeda halo.

There should be two effects: in energy and in flux. Here we consider effect in energy only. There should be effect in flux also, which consists in the difference of the values of the photon flux.

We evaluate a net effect for two fixed points upper and below galaxy disk, what allows doing further predictions of possible effects. We will consider the effects of the Andromeda geometry and the line of sight as well as make calculation of the energy spectrum in our future works. It can wash out effect in part, nonetheless it may remain in to some degree, so a geometry modulation of energetic spectrum can be expected. Considered simple case shows how it works. It gives that three energy intervals exist where effect is different: at very low final photon energy the ratio  $R$  of energies from upper and lower hemispheres is about unity, at higher energy upto  $m^2/\omega \sim 1$  TeV  $R \approx 0.6$ , where  $m$  is the electron mass,  $\omega$  is the initial photon energy, and at even higher energy  $R \rightarrow 1$ . Effect should be observed for any photon energy, here we focus on maximum value of final photon energy, though formula obtained is universal.

Besides effect in the flux, asymmetry in prompt photons radiation from decay/annihilation process (FSR) [22], comparison with observation sensitivity and background, comparison with other calculation methods [13, 16, 17, 20] are to be taken into account in future.

Andromeda is a rare galaxy which has been recently observed in gamma by Fermi-LAT satellite experiment [1, 4]. Ground experiments (like HAWC [2], HESS [18], MAGIC [8], LHAASO [6], VERITAS [14]) do not have so high angle resolution (though it depends on energy and they allowed observing several galaxies) and can register only very high energy photons. Effect we are talking about may manifest at any energy including intermediate and low energy ranges. In connection with it, forthcoming satellite gamma-ray telescope project Gamma-400 [15] with especially high angle resolution is of special importance for similar research. There was attempt to connect possible excess in  $\gamma$ -rays from Andromeda halo with DM [19]. We suggest general feature of asymmetry related with DM or other sources in halo.

## 7.2 IC photon energy

We assume that there can be sources of high energy electrons or/and positrons in the halo of Andromeda galaxy. Such assumption is based on the attempts to

explain positron anomaly [3,5,7] in CR with the help of DM annihilation or decay in our Galaxy. These attempts inevitably involve an effect in gamma-radiation, which was investigated, in particular by our group [9–12]. Production of high energy  $e^\pm$ , firstly, is accompanied by FSR, and, secondly, gives energetic photons as a result of IC scattering of these  $e^\pm$  on photons of the medium. To have IC effect at high energy, photons of star light should be taken since they are most energetic from widespread radiations within galaxy.

Also one can note that if dark matter annihilation is indeed the origin of the excess of positrons, then we deal with continuously distributed in space high-energy  $e^\pm$  sources, so we can take arbitrary point to consider effect.

Let us consider one arbitrary act of electron (or positron, what does not matter in the framework of QED) and photon scattering.

The scheme of the process is shown in the Fig. 7.1a and 7.2.  $k$  and  $k'$  are the initial and final photon 4-momenta,  $\omega$  and  $\omega'$  are their energies,  $\theta$  and  $\theta'$  are the angles between initial momentum of electron and initial and final ones of photons respectively,  $\chi$  is the angle between initial and final momenta of the photon. Index 'lab' relates to the same values in the initial electron rest frame.

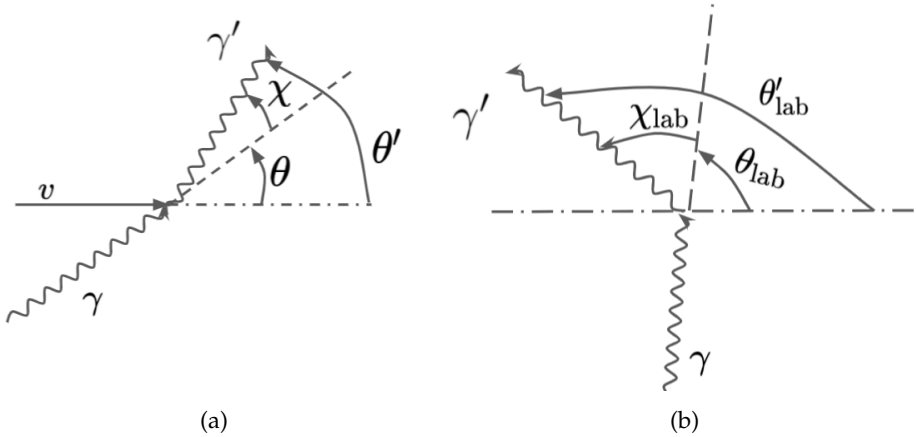


Fig. 7.1: The scheme for scattering process in upper and lower Andromeda hemispheres with the chosen points. Observer is on the right.

Let us take Compton formula (one can refer to any textbook, e.g. [21]) for final photon energy in the 'lab' reference frame

$$\omega'_{lab} = \frac{\omega_{lab}}{1 + \frac{\omega_{lab}}{m}(1 - \cos \chi_{lab})}, \tag{7.1}$$

where  $m$  is the electron mass,  $\chi_{lab}$  is the photon scattering angle as shown in the Fig. 7.1b We can easily express  $\omega_{lab}$  from the respective photon energy in the real reference frame ( $\omega$ ) through the Lorentz's transformation:

$$\omega_{lab} = \gamma \omega (1 - v \cos \theta), \tag{7.2}$$

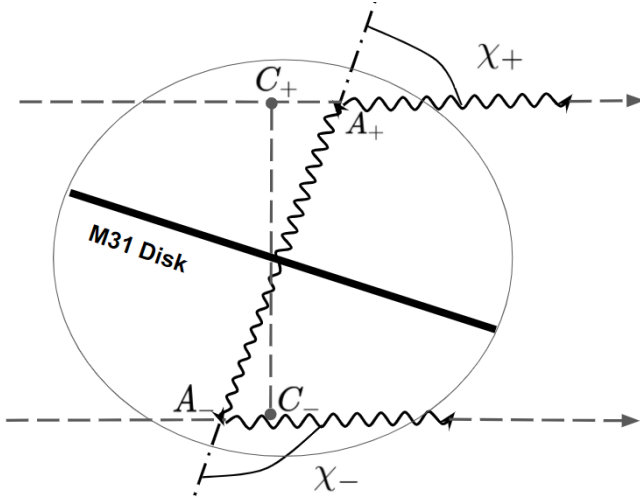


Fig. 7.2: The scheme for scattering process in upper and lower Andromeda hemispheres with the chosen points. Observer is on the right.

and the same transformation takes place for final photon in the 'lab' frame

$$\omega'_{\text{lab}} = \gamma \omega'(1 - v \cos \theta') = \gamma \omega'(1 - v \cos(\theta + \chi)). \quad (7.3)$$

We applied relation between angles  $\theta' = \theta + \chi$  which is seen from the Fig. 7.1. Here and thereafter we use that the absolute value of photon momentum is equal to its energy  $\omega_{(\text{lab})}^{(r)}$ . Everywhere  $v$  and  $\gamma$  mean velocity and  $\gamma$ -factor of initial electron.

One needs to connect  $\cos \chi$  with  $\cos \chi_{\text{lab}}$ . It can be done through scalar product of initial and final photon momenta written out in different reference frames and using Lorentz transformations for photon energy:

$$(kk') = \omega \omega'(1 - \cos \chi) = \omega_{\text{lab}} \omega'_{\text{lab}}(1 - \cos \chi_{\text{lab}}). \quad (7.4)$$

From where

$$1 - \cos \chi_{\text{lab}} = \frac{\omega_{\text{lab}} \omega'_{\text{lab}}}{\omega \omega'}(1 - \cos \chi), \quad (7.5)$$

where from Eq. 7.2 and Eq. 7.3 one gets

$$\frac{\omega_{\text{lab}} \omega'_{\text{lab}}}{\omega \omega'} = \frac{1}{\gamma^2(1 - v \cos \theta)(1 - v \cos(\theta + \chi))}. \quad (7.6)$$

Substituting in Eq. 7.1 one obtains

$$\begin{aligned} \omega'_{\text{lab}} &= \frac{\gamma \omega(1 - v \cos \theta)}{1 + \frac{\gamma \omega(1 - \cos \theta)}{m}} \frac{1 - \cos \chi}{\gamma^2(1 - v \cos \theta)(1 - v \cos(\theta + \chi))} = \\ &= \frac{\gamma \omega(1 - v \cos \theta)}{1 + \frac{\omega}{\gamma m} \frac{1 - \cos \chi}{1 - v \cos(\theta + \chi)}}. \end{aligned} \quad (7.7)$$

From Eq. 7.3 one has

$$\omega' = \frac{\omega'_{\text{lab}}}{\gamma(1 - v \cos(\theta + \chi))}, \quad (7.8)$$

and, finally, taking into account Eq. 7.7 one gets

$$\omega' = \frac{\omega(1 - v \cos \theta)}{1 - v \cos(\theta + \chi) + \frac{\omega}{\gamma m}(1 - \cos \chi)}, \quad (7.9)$$

where  $\frac{\omega}{m} \equiv \gamma_{\text{cr}}^{-1} \sim (2 \div 4) \cdot 10^{-6}$ .

One can see from Eq. 7.9 that there are different situations that can be easily analyzed. Let the velocity be  $v \approx 0$ . Then the small third term in denominator  $\omega/m(1 - \cos \chi)$  will give a tiny anisotropy between hemispheres (what is not important for us). The energy ratio between upper and lower hemispheres

$$R \equiv \omega'_+ / \omega'_- \quad (7.10)$$

will be a little bigger than unity for the chosen two points  $A_+$  and  $A_-$  in Fig. 7.2, where  $\omega'_\pm$  are the final photon energies from upper and lower hemispheres respectively. Scattering angles in upper and lower hemispheres of Andromeda  $\chi_\pm$  are introduced in the Fig. 7.2. When  $v \sim 1$ , third term in denominator of Eq. 7.9 (which is proportional to  $\omega/m$ ) is negligible and  $\omega'$  comes to maximum at  $\cos(\theta + \chi) = 1$ . So  $\theta = -\chi$ , what corresponds to the case when initial electron goes in direction to the observer<sup>1</sup>. It corresponds to narrow sharp maximum in photon energy which is of bigger interest. Next, if  $v \rightarrow 1$  so  $1 - v$  becomes smaller than  $\omega/\gamma m$ , i.e. when  $\gamma \gg \gamma_{\text{cr}}$ , the third term in denominator starts to dominate again and in this limit denominator and numerator are canceled.

Finally, we obtain for maximal final photon energy in the real reference frame

$$\omega'_{\text{max}} = \frac{\omega(1 - v \cos \chi)}{1 - v + \frac{\omega}{\gamma m}(1 - \cos \chi)} = \frac{(1 + v)\gamma^2 \omega(1 - v \cos \chi)}{1 + (1 + v)\gamma \frac{\omega}{m}(-\cos \chi)} \sim \begin{cases} \frac{1}{1 + \frac{\omega}{m}(1 - \cos \chi)} \approx 1 & v = 0 \\ 1 - \cos \chi & 1 \ll \gamma \ll \gamma_{\text{cr}} \\ \frac{1 - \cos \chi}{1 - \cos \chi} = 1 & \gamma \gg \gamma_{\text{cr}}. \end{cases} \quad (7.11)$$

So, there exists wide electron energy interval,  $1 \ll \gamma \ll \gamma_{\text{cr}}$  (what corresponds to initial electron energy  $m \ll E \ll \text{TeV}$  for  $\omega \sim 1 \text{ eV}$ ), where the effect takes place

$$R = \frac{1 - \cos \chi_+}{1 - \cos \chi_-} \approx 0.6 \quad (7.12)$$

for the chosen two points  $A_+$  and  $A_-$  in the Fig. 7.2.

The ratio  $R$  for maximal photon energy as dependent on  $\gamma$ -factor followed from the Eq. 7.11 is illustrated in Fig. 7.3.

<sup>1</sup> One notes that consideration of other configuration of momenta (angles) in the Fig. 7.1 can lead to the relation  $\theta' = \theta - \chi$ . But it does not change conclusion that  $\cos(\theta') = \cos(\theta - \chi) = 1$  and that in the given angle system frame initial electron travels in direction to the observer.

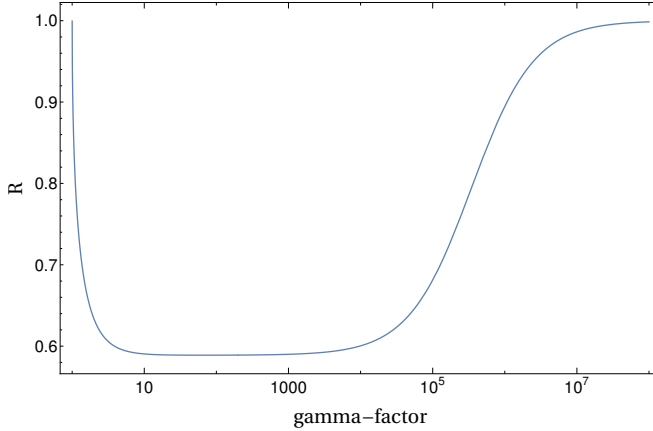


Fig. 7.3: Dependence of  $R$  showing asymmetry effect for maximal observed photon energy  $\omega'_{\max}$  between upper and lower hemispheres of Andromeda galaxy from  $\gamma$ -factor of initial electron. Figure relates to the chosen two points  $A_+$  and  $A_-$  of Fig. 7.2

#### *Comments on line of sight integration*

We have shown explicit effect for two fixed points above and below galaxy disk. Certainly, one should take into account the effects caused by our line of sight and distributed photon and electron sources, what could wash out difference between hemispheres. Nonetheless effect should remain in some degree since situation for upper line of sight and lower one is not symmetric (see Fig.7.2) because of dependence of Compton scattering from initial relative angle between momenta of the scattered electron and photon. As was seen from Eq. 7.11, when initial photon and electron move towards each other ( $\theta > 90^\circ$  in Fig. 7.2) final photon (maximal) energy  $\omega'$  is bigger in wide its value range than when they move co-directionally ( $\theta < 90^\circ$ ).

Line of sight Integration can be done taking into account a flux and under extra assumption about  $e^\pm$  source distribution. Qualitatively, two factors will make difference between upper and lower lines of sight: it is density of  $e^\pm$  sources and density of medium photons. Density of the sources is expected to decrease from distance to the galaxy center, concentration of photons - from distance to the stars in disc. For example, one can consider two nearest to the galactic center points  $C_+$  and  $C_-$  in Fig. 7.2 of two opposite lines of sight. Source densities in them is expected to be equal and maximal over all given lines of sight. But in point  $C_+$  the closest part of galaxy disc will shine co-directionally, while for  $C_-$  will do towards. Similarly one can consider other parts of lines of sight and there will be effects of different signs, though their full compensation is hardly expected.

### 7.3 Conclusion

We considered possible effect of asymmetry of gamma radiation from another galaxy connected with its geometric orientation with respect to line of sight. Here we considered an effect in energy between two hemispheres of galaxy related to IC scattering of medium photons on high energy  $e^\pm$  from their hypothetical source in galaxy halo. There also will be an effect in flux. The effect can be achievable for existing or future experiments since it may not seem to be vanishing, it can be at the level 10 (several tens) percents.

Our future work will concern the flux, sensitivity and data on cosmic gamma-background, and include the prompt (FSR) photons appearing under the assumption that  $e^\pm$  has DM decay/annihilation origin.

### Acknowledgements

The work was supported by the Ministry of Science and Higher Education of the Russian Federation by project No 0723-2020-0040 "Fundamental problems of cosmic rays and dark matter". Also we would like to thank A.Egorov, M.Khlopov, M.Laletin and S.Rubin for interest to the work and useful discussions and also D.Fargion for providing relevant references.

### References

1. A. A. Abdo, M. Ackermann, M. Ajello, A. Allafort, W. Atwood, L. Baldini, J. Ballet, G. Barbiellini, D. Bastieri, K. Bechtol, et al. Fermi large area telescope observations of local group galaxies: detection of m 31 and search for m 33. *Astronomy & Astrophysics*, 523:L2, 2010.
2. A. Abeyssekara, R. Alfaro, C. Alvarez, J. Álvarez, R. Arceo, J. Arteaga-Velázquez, H. Solares, A. Barber, B. Baughman, N. Bautista-Elivar, et al. The hawc gamma-ray observatory: Observations of cosmic rays. *preprint arXiv:1310.0072*, 2013.
3. L. Accardo et al. High statistics measurement of the positron fraction in primary cosmic rays of 0.5–500 gev with the alpha magnetic spectrometer on the international space station. *Phys. Rev. Lett.*, 113:121101, 2014.
4. M. Ackermann, M. Ajello, A. Albert, L. Baldini, J. Ballet, G. Barbiellini, D. Bastieri, R. Bellazzini, E. Bissaldi, E. Bloom, et al. Observations of m31 and m33 with the fermi large area telescope: a galactic center excess in andromeda? *The Astrophysical Journal*, 836(2):208, 2017.
5. O. Adriani et al. An anomalous positron abundance in cosmic rays with energies 1.5-100 GeV. *Nature*, 458:607–609, 2009.
6. F. Aharonian, V. Alekseenko, Q. An, L. Bai, Y. Bao, D. Bastieri, X. Bi, H. Cai, Z. Cao, Z. Cao, et al. Prospects for a multi-teV gamma-ray sky survey with the lhaaso water cherenkov detector array. *Chinese Physics C*, 44(6):065001, 2020.
7. M. Ajello et al. Fermi-LAT Observations of High-Energy Gamma-Ray Emission toward the Galactic Center. *The Astrophysical Journal*, 819:44, 2016.
8. D. Bastieri, R. Bavikadi, C. Bigongiari, E. Bisesi, P. Boinee, A. De Angelis, B. De Lotto, A. Forti, T. Lenisa, F. Longo, et al. The magic experiment and its first results. In *Frontiers of Fundamental Physics*, pages 291–296. Springer, 2006.

9. K. Belotsky, R. Budaev, A. Kirillov, and M. Laletin. Fermi-lat kills dark matter interpretations of ams-02 data. or not? *Journal of Cosmology and Astroparticle Physics*, 2017(01):021, 2017.
10. K. Belotsky, A. Kamaletdinov, M. Laletin, and M. Solovyov. The dampe excess and gamma-ray constraints. *Physics of the Dark Universe*, 26:100333, 2019.
11. K. Belotsky, A. Kamaletdinov, M. Solovyov, E. Esipova, and E. Shlepkina. Indirect effects of dark matter. *Int. J. Mod. Phys. D*, 28:1941011, 2019.
12. K. M. Belotsky, A. K. Kamaletdinov, E. S. Shlepkina, and M. L. Solovyov. Cosmic gamma ray constraints on the indirect effects of dark matter. *Particles*, 3(2):336–344, 2020.
13. M. Cirelli and P. Panci. Inverse compton constraints on the dark matter  $e^\pm$  excesses. *Nuclear Physics B*, 821(1-2):399–416, 2009.
14. V. Collaboration, T. WEEKES, V. ACCIARI, T. ARLEN, T. AUNE, M. BEILICKE, W. BENBOW, D. BOLTUCH, S. BRADBURY, J. BUCKLEY, et al. Veritas: Status summary 2009. *International Journal of Modern Physics D*, 19(06):1003–1012, 2010.
15. A. E. Egorov, N. P. Topchiev, A. M. Galper, O. D. Dalkarov, A. A. Leonov, S. I. Suchkov, and Y. T. Yurkin. Dark matter searches by the planned gamma-ray telescope gamma-400. *arXiv preprint arXiv:2005.09032*, 2020.
16. D. Fargion, R. V. Konoplich, and A. Salis. Inverse compton scattering on laser beam and monochromatic isotropic radiation. *Zeitschrift für Physik C Particles and Fields*, 74(3):571–576, 1997.
17. D. Fargion and A. Salis. Inverse compton scattering off black body radiation in high energy physics and gamma (mev–tev) astrophysics. *Physics-Uspokhi*, 41(8):823, 1998.
18. C. Hoischen, A. Blazer, E. Bissaldi, M. Füßling, T. Garrigoux, D. Gottschall, M. Holler, A. Mitchell, P. O’Brien, R. Parsons, et al. Grb observations with hess ii. *preprint arXiv:1708.01088*, 2017.
19. C. Karwin, S. Murgia, I. Moskalenko, S. Fillingham, A.-K. Burns, and M. Fieg. Dark matter interpretation of the fermi-lat observations toward the outer halo of m31. *preprint arXiv:2010.08563*, 2020.
20. I. V. Moskalenko and A. W. Strong. Anisotropic inverse compton scattering in the galaxy. *The Astrophysical Journal*, 528(1):357, 2000.
21. M. Peskin. *An introduction to quantum field theory*. CRC press, 2018.
22. M. Solovyov. Gamma-radiation from annihilating dark matter with the disk component, 2017. In russian.



## 8 Numerical Simulation of Dark Atom Interaction With Nuclei

T.E. Bikbaev<sup>1</sup>, M.Yu. Khlopov<sup>1,2,3</sup> \* and A.G. Mayorov<sup>1</sup>

<sup>1</sup> National Research Nuclear University MEPhI (Moscow Engineering Physics Institute), 115409 Moscow, Russia

<sup>2</sup> Institute of Physics, Southern Federal University, Stachki 194 Rostov on Don 344090, Russia

<sup>3</sup> Université de Paris, CNRS, Astroparticule et Cosmologie, F-75013 Paris, France

**Abstract.** The old and still not solved problem of dark atom solution for the puzzles of direct dark matter searches is related with rigorous proof of the existence of a low energy bound state in the dark atom interaction with nuclei. Such proof must involve a self-consistent account of the nuclear attraction and Coulomb repulsion in such interaction. In the lack of usual small parameters of atomic physics like smallness of electromagnetic coupling of the electronic shell or smallness of the size of nucleus as compared with the radius of the Bohr orbit the rigorous study of this problem inevitably implies numerical simulation of dark atom interaction with nuclei. Our approach to such simulations of OHe – nucleus interaction involves multi-step approximation to the realistic picture by continuous addition to the initially classical picture of three point-like body problem essential quantum mechanical features.

**Povzetek.** Avtorji obravnavajo atome temne snovi kot rešitev ugank direktnega iskanja temne snovi v povezavi z rigoroznim dokazom obstoja nizko energijskega vezanega stanja interakcije temnega atoma z jedrom. Dokaz mora vključevati usklajen opis jedrskega privlaka in Coulombskega odboja v teh interakcijah. V obravnavanem problemu, za razliko od običajnih atomov, ne vemo vnaprej, kateri parametri so majhni, zato se moramo zateči k numerični rešitvi problema. Pristop avtorjev k simulaciji interakcij OHe –jedro poteka tako, da klasičnemu modelu treh točkastih teles postopoma dodajajo kvantne popravke.

Keywords: Physics beyond the standard model; stable charged particles; composite dark matter; dark atoms; nuclear interactions; Coulomb interaction; OHe

PACS: 02.60.-x; 02.70.-c; 12.60.-i; 36.10.-k; 98.80.-k

### 8.1 Introduction

According to the modern cosmology, dark matter is non-baryonic and is associated with physics that has not yet been sufficiently studied and, in fact, unknown to us. If it consists of particles, then they are predicted beyond the Standard Model. To

\* E-mail: khlopov@apc.univ-paris.fr

be considered as candidates for dark matter these particles must satisfy a set of conditions: they must be stable, must explain the measured dark matter density, and decouple from plasma and radiation, at least before the beginning of the matter dominated stage [1,2]. The easiest way to satisfy the above conditions is to assume the existence of neutral, elementary Weakly Interacting Massive Particles (WIMP). However, the results of the WIMP searches are contradictory and the existing uncertainty in the choice of “dark” particles has given rise to many different models suggesting various objects for the role of dark matter candidates [3–6]. In these models, new particles should possess some new fundamental symmetry and the corresponding conserved charge in order to protect their stability [5,7,8].

An important problem for scenarios of hypothetical, stable, electrically charged particles is their absence in the matter around us. If they exist, they should be present in the ordinary matter in the form of anomalous isotopes (with an anomalous  $Z/A$  ratio). The main difficulty for these scenarios is the suppression of the abundance of positively charged particles bound with electrons, which behave like anomalous isotopes of hydrogen or helium. Serious experimental restrictions on such isotopes, especially on anomalous hydrogen, very severely limit the possibility of stable positively charged particles [9].

This problem is also unsolvable if the model predicts stable particles with charge  $-1$ . Such particles bind with primordial helium in  $+1$  charged ions, which recombine with electrons in atoms of anomalous hydrogen [10].

In this connection, stable negatively charged particles can only have charge  $-2$  – we will denote them by  $O^{--}$  or in the general case even charge  $-2n$ , where  $n$  is any natural number.

In the present paper, we consider a scenario of composite dark matter, in which hypothetical stable  $O^{--}$  particles avoid experimental discovery, because they form neutral atom-like states  $OHe$  with primordial helium, called “dark” atoms [11]. Since all these models also predict the corresponding  $+2$  charged antiparticles, the cosmological scenario should provide a mechanism for their suppression, which, naturally, can take place in the charge-asymmetric case corresponding to an excess of  $-2$  charged particles  $O^{--}$  [4]<sup>1</sup>. Then their positively charged antiparticles can effectively annihilate in the early universe. There are various models in which such stable  $-2$  charged particles are predicted [12–14].

## 8.2 “Dark” atoms $OHe$

“Dark” atom is the bound system of  $O^{--}$  particle and  ${}^4He$  nucleus. In the approximation of our current numerical model,  $\alpha$ -particle is point-like and moves along the Bohr radius. Then the binding energy of  $OHe$  for a point charge of  ${}^4He$  is given by:

$$I_0 = \frac{Z_{O^{--}}^2 Z_{He}^2 \alpha^2 m_{He}}{2} \approx 1.6 \text{ MeV}, \quad (8.1)$$

where  $\alpha$  – is a fine structure constant,  $Z_{O^{--}}$  and  $Z_{He}$  – electric charges of  $O^{--}$  particle and nuclei  $He$  respectively,  $m_{He}$  – is the  $\alpha$ -particle mass.

<sup>1</sup> Electric charge of this excess is compensated by the corresponding excess of positively charged baryons so that the electroneutrality of the Universe is preserved

The Bohr radius of He rotation in “dark” OHe atoms is equal to [15]:

$$R_b = \frac{\hbar c}{Z_{O^{--}} Z_{He} m_{He} \alpha} \approx 2 \cdot 10^{-13} \text{ cm} \quad (8.2)$$

In all models of O-helium,  $O^{--}$  behaves like a lepton or as a specific cluster of heavy quarks of new families with suppressed hadron interaction [16]. Therefore, the strong interaction of OHe with matter is determined by the nuclear interaction of He. The mass  $O^{--}$ ,  $m_{O^{--}}$ , is the only free parameter of new physics. The experimental search at the LHC for stable doubly charged particles gives a lower limit for their mass about 1TeV [17].

The neutral primordial nuclear-interacting objects, that is, “dark” OHe atoms, dominate in the modern density of nonrelativistic matter and play the role of a non-trivial form of strongly interacting dark matter. The active influence of this type of dark matter on nuclear transformations requires special research and development of the nuclear physics of O-helium. This is especially important for a quantitative assessment of the role of “dark” atoms in primordial cosmological nucleosynthesis and in the evolution of stars [15].

The importance of the O-helium hypothesis is that it can explain the conflicting results of a direct search for dark matter, due to the specifics of the interaction of “dark” atoms with the matter of underground detectors [18]. Namely, positive results on the detection of dark matter particles in experiments such as DAMA / NaI and DAMA / LIBRA, which seem to contradict all other experiments, for example, with XENON100, LUX, CDMS, which give a negative result.

One of the main problems with the “dark” OHe atoms is that their constituents can interact too strongly with ordinary matter. This is because O-helium, although neutral, initially has an unshielded nuclear attraction to the nuclei of matter. Which can lead to the destruction of the bound OHe system and the formation of anomalous isotopes. In turn, there are very strong experimental limitations on the concentration of these isotopes in the terrestrial soil and sea water [9]. To avoid this problem, it is assumed that the effective potential of OHe-nucleus interaction will have a barrier preventing the merging of He and/or  $O^{--}$  with nucleus. Under these conditions, “dark” atoms interaction with matter doesn’t lead to anomalous isotopes overproduction, which is the key point for the O-helium hypothesis.

In this work, a description of the performed numerical simulation of the interaction of “dark” O-helium atoms with the nuclei of baryonic matter is given with the aim to explore the conditions for the existence of their low-energy bound state, which can explain positive results of DAMA/NaI and DAMA/LIBRA experiments. Within the framework of the proposed approach to such modeling, in order to reveal the essence of the processes of nuclear interaction of OHe with nuclei of baryonic matter, the approach is based on the classical model, where the effects of quantum physics are gradually introduced.

### 8.3 Numerical modeling of the interaction of OHe with the nucleus of baryonic matter.

#### 8.3.1 Modeling OHe.

To model the "dark" atom of O-helium (the OHe system) was considered, consisting of two point-like, bound particles: the He nucleus and the  $O^{--}$  particle. A spherical coordinate system was introduced, at the center of which the particle  $O^{--}$  is meant, and around it along the surface of the sphere, the radius of which is equal to the radius of the atom OHe  $R_b$  (see formula (2)) the He nucleus moves stochastically, with a constant Bohr velocity  $V_\alpha$ . The speed  $V_\alpha$  is:

$$V_\alpha = \frac{\hbar c^2}{m_{He} R_b} \approx 3 \cdot 10^4 \frac{\text{cm}}{\text{s}} \tag{8.3}$$

The initial task in modeling the interaction of OHe with nuclei was to construct a numerical model of O-helium, which would allow to describe the motion of an  $\alpha$ -particle around  $O^{--}$ . It should be used in the main numerical model, in which the motion and interaction of OHe with the nuclei will be simulated.

Let us consider how the OHe system was modeled (see Figure 8.1).

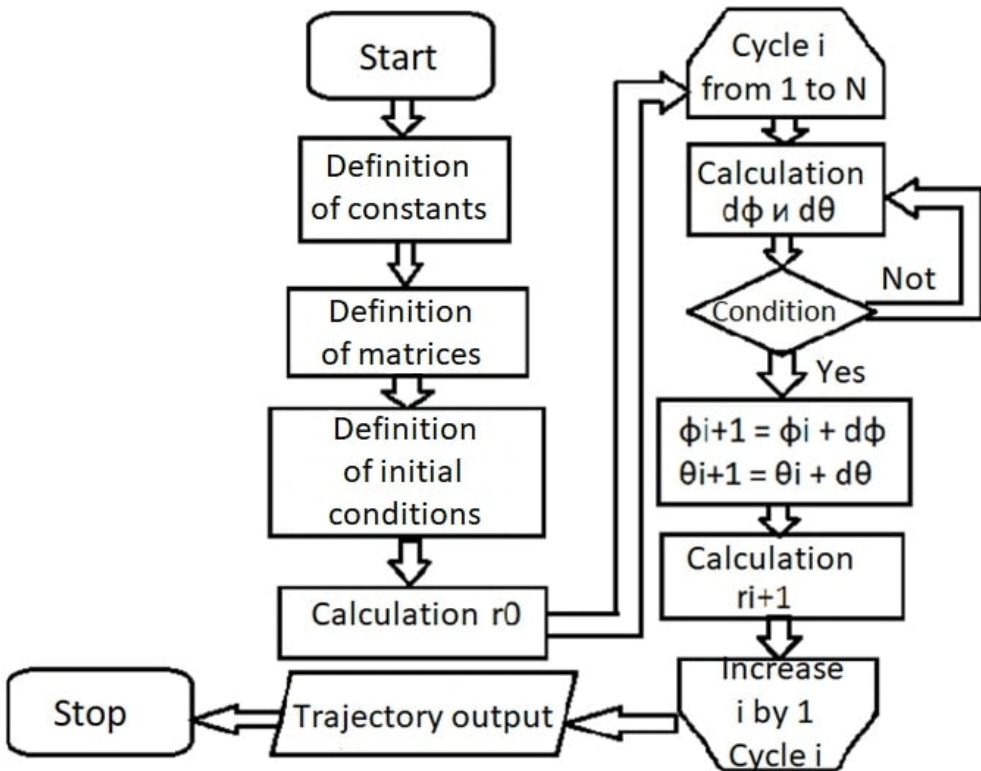


Fig. 8.1: Block diagram of the OHe system simulation

An  $\alpha$ -particle in the bound OHe system has only two independent degrees of freedom, which are taken as the polar and azimuthal angles. Its Cartesian coordinates are expressed through the projections  $R_b$ , that is, the components of the radius vector at each moment of time, in order to use them to construct the trajectory of the  $\alpha$ -particle. In Figure 1, the defined matrices mean all the quantities necessary to describe the motion of the  $\alpha$ -particle, that is, its polar  $\theta$  and azimuthal  $\phi$  angles, as well as the change in these angles ( $d\theta$  and  $d\phi$ ) and components of the radius vector  $r$ .

$\phi_0$  and  $\theta_0$  in Figure 1 are the initial values of the angles through which the initial components of the radius vector of the  $\alpha$ -particle  $r_0$  are calculated.

Changes in the polar  $d\theta$  and azimuthal  $d\phi$  angles are defined as follows:

$$d\theta = \left( \frac{V_\alpha dt}{R_b} \right) (2\text{rand} - 1) \quad (8.4)$$

$$d\phi = \frac{\sqrt{\left( \frac{V_\alpha dt}{R_b} \right)^2 - (d\theta)^2}}{\cos(\theta)} (2\text{rand} - 1) \quad (8.5)$$

where  $\text{rand}$  is a random variable with a uniform distribution over the range from 0 to 1.

The condition in Figure 8.1 means the following inequality:

$$(d\theta)^2 + (\cos \theta d\phi)^2 \leq \left( \frac{V_\alpha dt}{R_b} \right)^2 \quad (8.6)$$

The physical meaning of this condition is that the square of the distance traveled by an  $\alpha$ -particle in time  $dt$  over the surface of a sphere of radius  $R_b$  with a constant velocity  $V_\alpha$  cannot be less than the sum of the squares of the distances covered for that the same time over the surface of a sphere of the same radius with the same velocity in the polar and azimuthal directions.

In general, from Figure 8.1 it is clear that in each iteration, changes in the azimuthal and polar angles are determined, which are added to their old values ( $\phi_i$  and  $\theta_i$ ) and using the new angles obtained ( $\phi_{i+1}$  and  $\theta_{i+1}$ ) the following components of the radius vector of the  $\alpha$ -particle  $r_{i+1}$  are calculated.

As a result, according to the obtained data, written in the matrix containing the values of the components of the radius vector of the  $\alpha$ -particle at each moment of time  $r$ , the program builds its trajectory along the surface of a sphere of the Bohr radius  $R_b$  (Figure 8.2). Figure 8.2 shows a sphere of radius  $R_b$ , on the surface of which the red dots mark the location of the  $\alpha$ -particle between times  $dt$ . Filling the sphere with dots depends on the number of loop iterations, that is, if there are too many of them, the sphere will be densely filled with dots.

### 8.3.2 The coordinate system of the OHe–nucleus system.

Before we start modeling the OHe system and the nucleus of baryonic matter, taking into account all the forces acting between particles, that is, modeling the

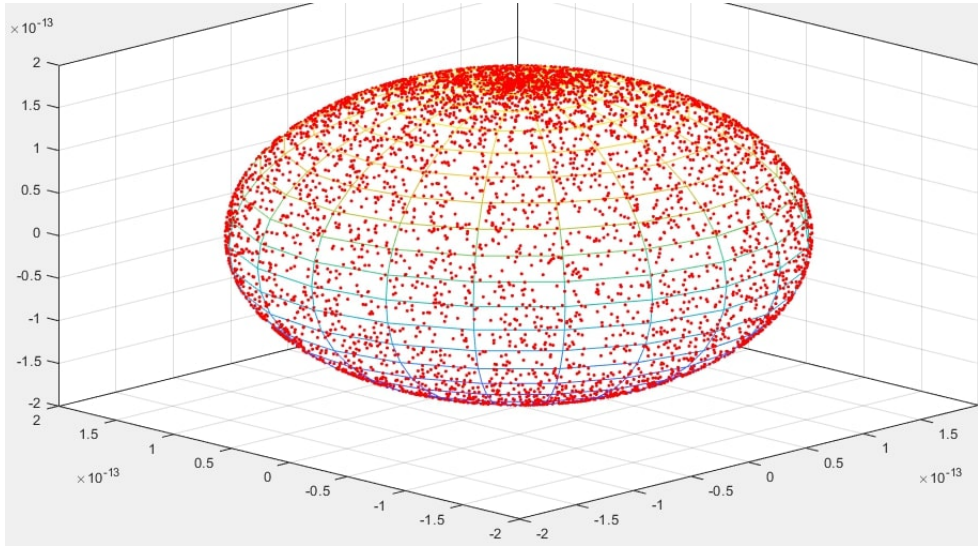


Fig. 8.2: The density of the distribution of the coordinates of the  $\alpha$ -particle on the surface of the sphere of the Bohr radius  $R_b$

interaction of three bodies, let us consider the coordinate system for the OHe-nucleus system.

The system OHe-nucleus consists of three charged, pointlike (in this work) particles, in which a linked system of two other particles moves to one particle “fixed” at the center of coordinates. The particle at the origin is target nucleus of the baryonic matter, and the moving particles mean the  $\alpha$ -particle and the  $O^{--}$ . In this case, the  $\alpha$ -particle rotates along the Bohr radius  $R_b$  around the particle  $O^{--}$ .

In order to describe the trajectories of motion of the  $\alpha$ -particle and the  $O^{--}$  consider a spherical coordinate system with a point target nucleus  $A$  at the origin of the coordinate system. It introduces the radius vector (see Figure 8.3) of the  $O^{--}$   $\vec{r}$  and the radius vector of the  $\alpha$ -particle  $\vec{r}_\alpha$ . Wherein:

$$\vec{r}_\alpha = \vec{r} + \vec{R}_b \tag{8.7}$$

Accordingly, for the radius vector of the  $\alpha$ -particle and the  $O^{--}$  azimuthal ( $\phi_\alpha$  and  $\phi_{O^{--}}$ ) and polar ( $\theta_\alpha$  and  $\theta_{O^{--}}$ ) angles. Figure 3 also shows the particle velocity vector  $O^{--}$ ,  $\vec{V}$ , the angle between  $\vec{V}$  and the horizontal line,  $\alpha$ , and the initial coordinates of the particle  $O^{--}$   $[X_0, Y_0, Z_0]$ . Before proceeding to the description of modeling the OHe system and the nucleus of baryonic matter, taking into account interactions between particles, it should be said that it is possible to construct the effective potential between O-helium and the nucleus of baryonic matter (see Figure 8.4). This potential includes electromagnetic and nuclear interactions. And the task of modeling is precisely to introduce these interactions in order to reproduce the effects of this potential numerically.

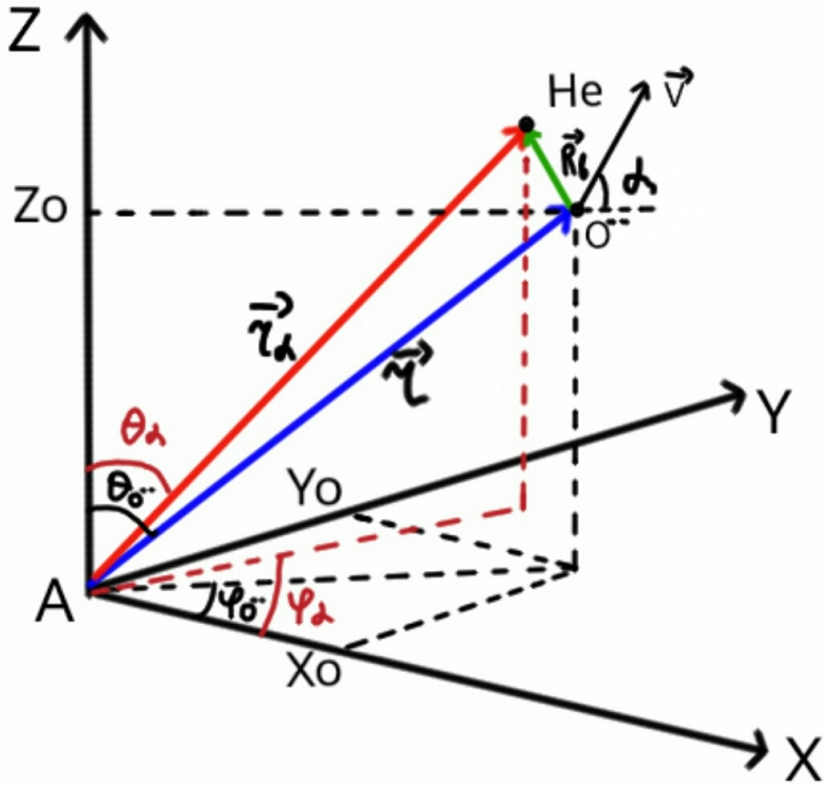


Fig. 8.3: Coordinate system OHe–core.

### 8.3.3 Coulomb interaction in the OHe –nucleus system

At this stage of modeling, a system of three point systems interacting with each other through the Coulomb forces of charged particles is considered, with the above choice of the coordinate system.

A Coulomb interaction acts between the  $\alpha$ -particle and the target nucleus in the considered coordinate system, which is determined by the force:

$$\vec{F}_{Z\alpha}^e = \vec{F}_{Z\alpha}^e(\vec{r}_\alpha) = \frac{ZZ_\alpha e^2 \vec{r}_\alpha}{r_\alpha^3}, \quad (8.8)$$

where  $Z$  is the charge of nucleus. Coulomb interaction between the  $O^{--}$  particle and the target nucleus, which is determined by the force:

$$\vec{F}_{ZO}^e = \vec{F}_{ZO}^e(\vec{r}) = \frac{ZZ_O e^2 \vec{r}}{r^3}. \quad (8.9)$$

The task of this stage was to simulate the interaction, by means of Coulomb forces (8.8) and (8.9), in the coordinate system OHe –nucleus, where the motion of the He

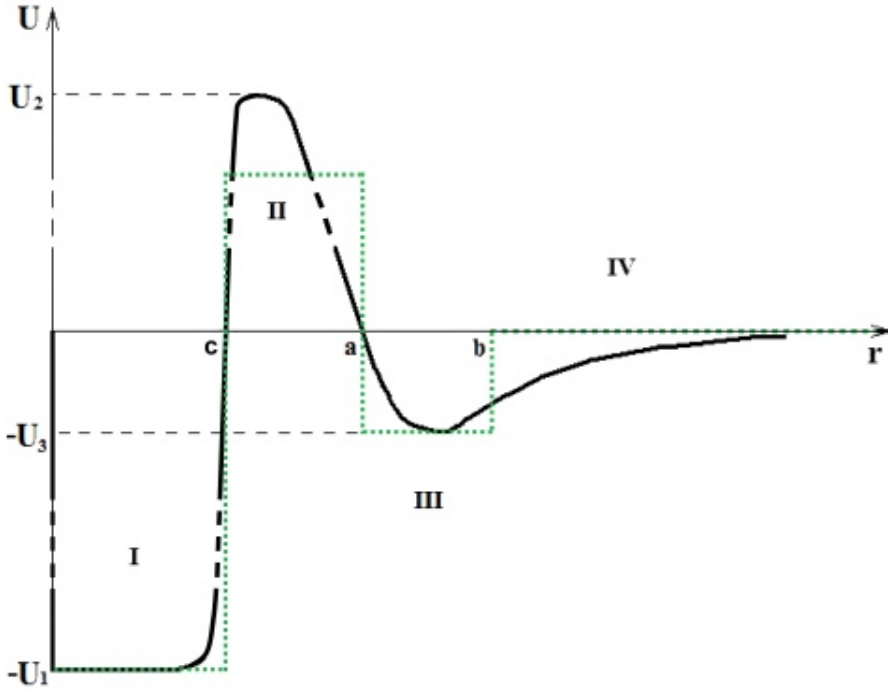


Fig. 8.4: Effective potential between OHe and the nucleus of baryonic matter [15]

nucleus in the bound state OHe is described according to the algorithm presented in the previous section.

The simulation was carried out as follows (see Figure 8.5).

We use the following initial conditions: the initial coordinates of  $O^{--}$   $[x_0, y_0, z_0]$  (or  $r_0$ ) and the initial components of its velocity  $[V_{x_0}, V_{y_0}, V_{z_0}]$  (or  $V_0$ ). Then the initial values of all previously determined values are calculated.

Before condition 1, the algorithm determines the  $i$ -th value of the increment of the momentum of  $\alpha$ -particle  $dP_{\alpha_i}$ :

$$d\vec{P}_{\alpha_i} = \vec{F}_{\alpha_i}^e dt \tag{8.10}$$

It corresponds to the termination of the program when the excess of  $dT$  kinetic energy transferred to He exceeds the ionization potential of O –helium  $I_0$ , which results in the destruction of the bound O –helium system:

$$dT < I_0 \approx 1.6\text{MeV} \tag{8.11}$$

$$dT = \frac{dP_{\alpha_i}^2}{2m_{\alpha}} \tag{8.12}$$

Condition 2 is described by formula (6) in the previous section. As you can see from Figure 8.6, at each loop, the program calculates the total force acting on the OHe system:

$$\vec{F}_{\text{sum}} = \vec{F}_{ZO}^e + \vec{F}_{\alpha}^e \tag{8.13}$$

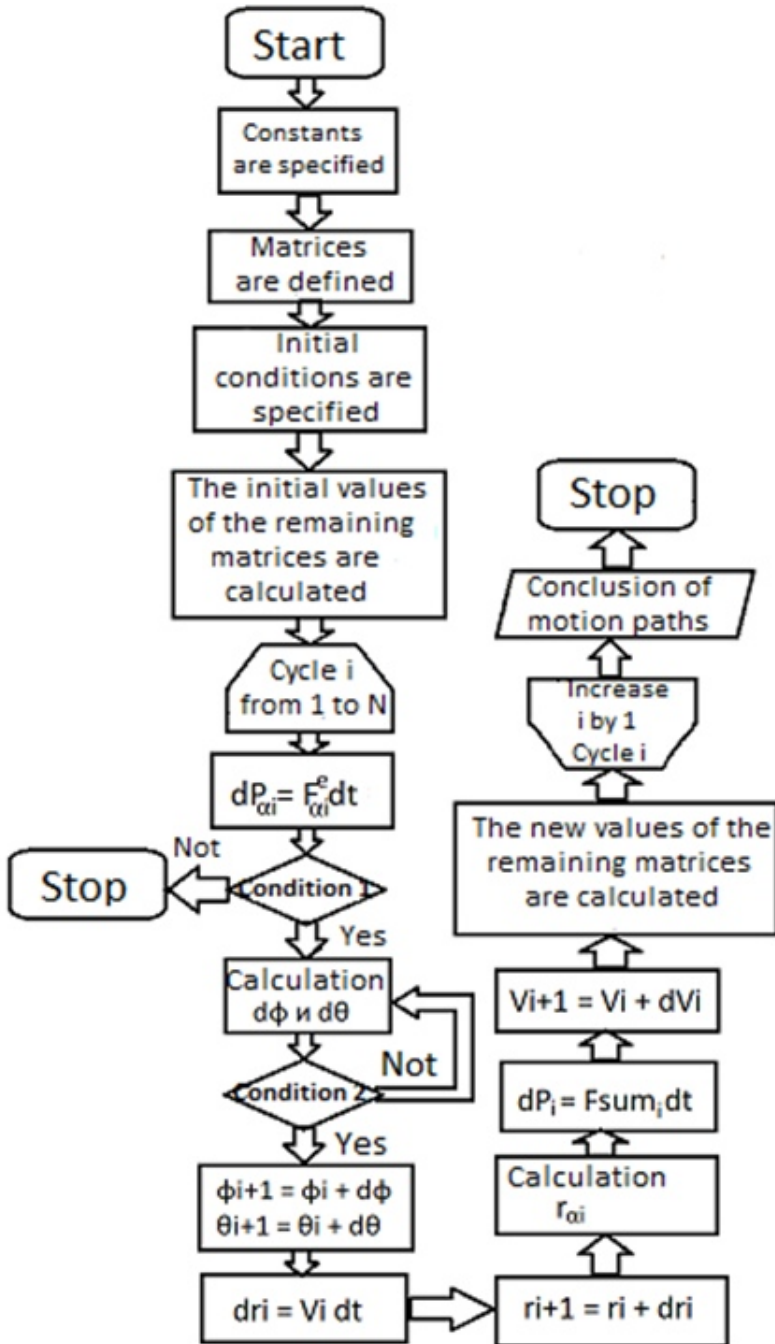


Fig. 8.5: Block diagram for modeling the Coulomb interaction in the OHe –nucleus system

With its help, the increment of the momentum  $dP$  of OHe system is calculated, which is, in the aggregate, the increment of the momentum of  $O^{--}$ .

$$d\vec{P} = \vec{F}_{sum} dt \tag{8.14}$$

Using the momentum increment  $d\vec{P}$ , the  $O^{--}$  velocity increment  $d\vec{V}$  is calculated for the subsequent finding of the new velocity used in the next iteration:

$$d\vec{V} = \frac{d\vec{P}}{m_{O^{--}} + m_{\alpha}} \quad (8.15)$$

The result of the algorithm is the reconstructed trajectories of  $\alpha$ -particle and  $O^{--}$ . One example is shown in Figure 6, where the blue circle shows the location of the target nucleus, the red asterisk and the purple square are the initial locations of the  $\alpha$ -particle and the  $O^{--}$  particle, respectively, yellow dots and the green dashed line show the trajectories of the  $\alpha$ -particles and particles  $O^{--}$  respectively. In the figure under consideration, one can observe the deviation of the trajectory  $O^{--}$  from the initial direction, which is associated with the Coulomb interaction between the He nucleus and the target nucleus. This happens because He is closer to the origin and is repelled from the target nucleus more strongly than the  $O^{--}$  particle is attracted to it.

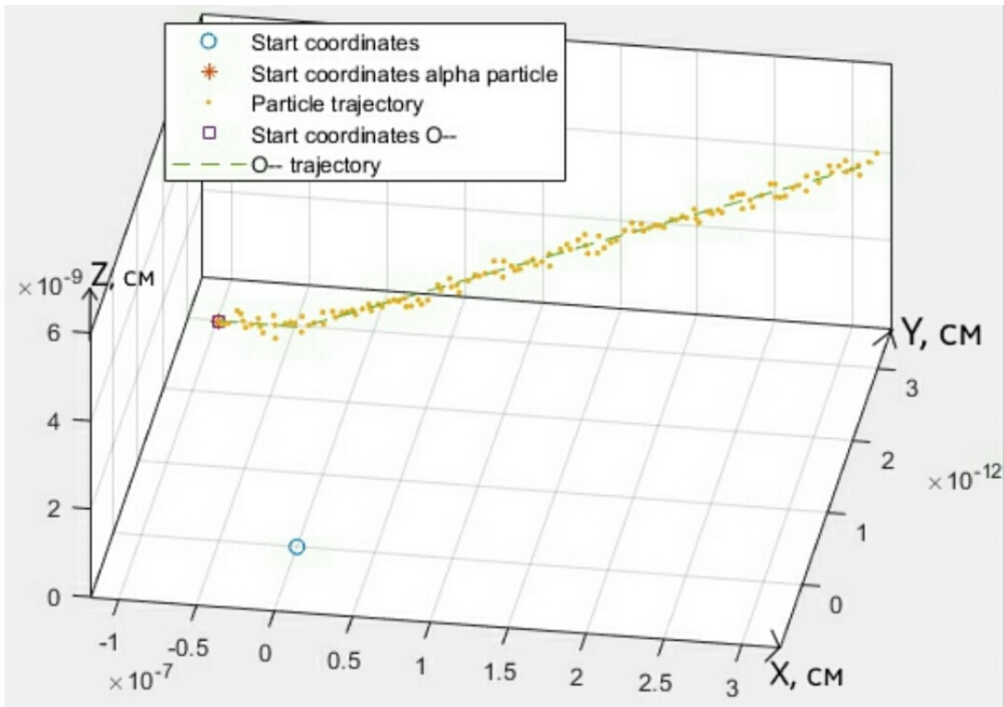


Fig. 8.6:  $\alpha$ -particle and particle  $O^{--}$  trajectories

### 8.3.4 Nuclear interaction in the OHe $^{-}$ -nucleus system

At this stage, the program was supplemented with a nuclear interaction of the Saxon-Woods type, between the He nucleus and the target nucleus, determined

by the force  $\vec{F}_\alpha^N$ :

$$\vec{F}_\alpha^N = -\frac{U_0}{a} \exp\left(\frac{r_\alpha - R_Z}{a}\right) \frac{\vec{r}_\alpha}{\left(1 + \exp\left(\frac{r_\alpha - R_Z}{a}\right)\right)^2}, \quad (8.16)$$

where  $R_Z$  is the radius of the target nucleus,  $U_0$  is the depth of the potential well,  $a$  is a constant parameter.

In this case, the total force acting on the system OHe,  $\vec{F}_{\text{Sum}}$ , is now calculated as follows:

$$\vec{F}_{\text{Sum}} = \vec{F}_{ZO}^e + \vec{F}_\alpha, \quad (8.17)$$

where  $\vec{F}_\alpha$  is the total force acting on the  $\alpha$ -particle:

$$\vec{F}_\alpha = \vec{F}_\alpha^e + \vec{F}_\alpha^N \quad (8.18)$$

Simulation is performed according to the algorithm described in the previous paragraph, where  $d\vec{P}_\alpha$ , the increment of the  $\alpha$ -particle momentum, is now calculated as follows:

$$d\vec{P}_\alpha = \vec{F}_\alpha dt \quad (8.19)$$

Based on the data obtained, the program builds the trajectories of the  $\alpha$ -particle and the  $O^{--}$ . In Figure 7, which shows the result of the program, the blue circle shows the location of the target nucleus, yellow dots and the green dashed line show the trajectories of the  $\alpha$ -particle and the  $O^{--}$  particle in the XY plane, respectively.

Figure 7 shows the effect of adding a nuclear force of interaction between the target nucleus and the  $\alpha$ -particle. Which consists in the fact that at small distances between particles, nuclear force can compensate for the effect of electromagnetic interaction. As a result, some beats are observed in the trajectory  $O^{--}$ .

## 8.4 Conclusions

The advantage of the OHe composite dark matter model is that it includes only one parameter of the "new" physics – the  $O^{--}$  mass. Atoms OHe – these neutral primary nuclear-interacting objects, provide the modern density of the dark matter and play the role of a non-trivial form of strongly interacting "dark" matter. Also, the OHe hypothesis can explain the conflicting results of a direct search for "dark" matter, due to the specifics of the interaction of O –helium with the substance of underground detectors. However, the correct quantum consideration of this model turns out to be rather difficult.

The OHe hypothesis cannot work if no repulsive interaction occurs at some distance between OHe and the nucleus, and the solution of this problem is vital for the further existence of the OHe dark atom model [10].

Nuclear forces fall off exponentially, but they can be quite strong when the OHe system comes close to the outer target nucleus. These are insignificant and insufficient distances for considering the He nucleus as a point object. In this case, the perturbation theory can no longer be applied and it becomes rather

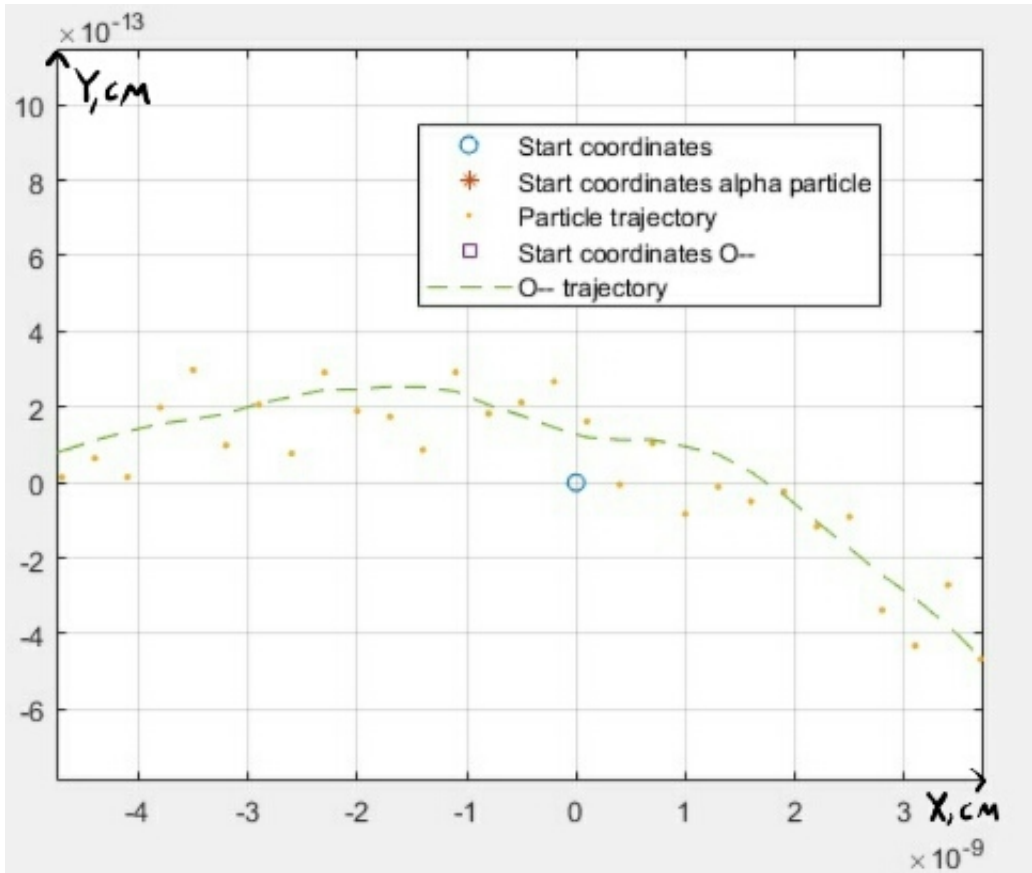


Fig. 8.7: The trajectory of  $\alpha$ -particle and the  $O^{-}$  in the XY plane

problematic to solve the Schrödinger equation. Therefore, the purpose of this work was to numerically simulate the interaction of the OHe atom of "dark" matter with the nuclei of baryonic matter in order to reveal the conditions for the existence of their low-energy bound state and to calculate their effective interaction potential by a numerical method.

At the current stage, the our model describes a system of three point, interacting with each other through the Coulomb and nuclear forces, charged particles. The results of the work of the numerical model are the trajectories of motion of point particles entering the OHe atom of dark matter, taking into account the electromagnetic and nuclear interactions between  $O^{-}$ -helium and the target nucleus of baryonic matter, in the coordinate system  $OHe^{-}$ -nucleus.

However, the process of numerical simulation has not yet been fully completed and in the future it is planned to improve it by introducing finite sizes of nuclei, by taking into account the distribution of the density of nucleons and the density of protons, and introducing the quantum-mechanical effect of tunneling He nucleus into the nucleus of baryonic matter.

## Acknowledgements

The work by MK has been supported by the grant of the Russian Science Foundation (Project No-18-12-00213). The work by AM has been supported by the grant of the Russian Science Foundation, RSF 19-72-10161.

## References

1. M.Yu. Khlopov in *Cosmion-94*, Eds. M.Yu.Khlopov et al. (Editions frontieres, 1996) P. 67; M. Y. Khlopov in hep-ph/0612250, p 51.
2. M.Y.Khlopov, *Bled Workshops in Physics* 8, 114 (2007); in arXiv:0711.4681, p. 114; M. Y. Khlopov and N. S. MankocBorstnik, *ibid*, p. 195.
3. G. Bertone, D. Hooper, J. Silk: Particle dark matter: evidence, candidates and constraints, *Physics Reports* **405**, 279 – 390 (2005)
4. M. Khlopov: Fundamental particle structure in the cosmological dark matter, *International Journal of Modern Physics A*. **28**, 1330042 (2013)
5. M. Y. Khlopov: Dark matter reflection of particle symmetry, *Modern Physics Letters A*. **32**, 1740001 (2017)
6. P. Scott: *Searches for Particle Dark Matter: An Introduction*, (2011)
7. M. Fabbrichesi, E. Gabrielli, G. Lanfranchi: *The Dark Photon*, (2020)
8. M. Khlopov: Cosmoparticle physics of dark matter, *EPJ Web of Conferences* **222**, 01006 (2019)
9. J. R. Cudell, M. Y. Khlopov, Q. Wallemacq: The nuclear physics of OHe, *Bled Workshops Physics* **13**, 10 –27 (2012)
10. M. Yu. Khlopov: 10 years of dark atoms of composite dark matter, *Bled Workshops Physics* **16**, 71 –77 (2015)
11. M. Y. Khlopov: *Conspiracy of BSM physics and cosmology*, (2019)
12. K. M. Belotsky, M. Y. Khlopov, K. I. Shibaev: *Composite Dark Matter and its Charged Constituents*, (2006)
13. M. Y. Khlopov, C. A. Stephan, D. Fargion: Dark matter with invisible light from heavy double charged leptons of almost-commutative geometry?, *Classical and Quantum Gravity* **23**, 7305 –7354 (2006)
14. M. Y. Khlopov, C. Kouvaris: Strong interactive massive particles from a strong coupled theory, *Physical Review D* **77**, (2008)
15. M. Yu. Khlopov, A. G. Mayorov, E. Yu. Soldatov: The dark atoms of dark matter, *Prespace. J.* **1**, 1403 –1417 (2010)
16. M. Y. Khlopov: Composite dark matter from 4th generation, *JETP Letters* **83**, 1 –4 (2006)
17. V. Beylin, M. Khlopov, V. Kuksa, N. Volchanskiy: New physics of strong interaction and Dark Universe, *Universe* **6**, 196 (2020)
18. R. Bernabei: Dark matter investigation by dama at gran sasso, *International Journal of Modern Physics A* **28**, 1330022 (2013)
19. W. M. Seif, H. Mansour: Systematics of nucleon density distributions and neutron skin of nuclei, *Int. J. Mod. Phys.* **E24**, 1550083 (2015)



## 9 Anihelium Flux From Antimatter Globular Cluster

M.Yu. Khlopov<sup>1,2,3</sup>, A.O. Kirichenko<sup>\*2</sup> and A.G. Mayorov<sup>2</sup>

<sup>1</sup> Institute of Physics, Southern Federal University, Stachki 194 Rostov on Don 344090, Russia

<sup>2</sup> National Research Nuclear University MEPhI, (Moscow Engineering Physics Institute), 115409 Moscow, Russia

<sup>3</sup> Université de Paris, CNRS, Astroparticule et Cosmologie, F-75013 Paris, France

**Abstract.** Macroscopic cosmic antimatter objects are predicted in baryon asymmetrical Universe in the models of strongly nonhomogeneous baryosynthesis. We test the hypothesis of the existence of an old globular cluster of anti-stars in the galactic halo by evaluating the flux of helium anti-nuclei in galactic cosmic rays. Due to the symmetry of matter and antimatter we assume that the antimatter cluster evolves in a similar way as a matter cluster. The energy density of antiparticles in galactic cosmic rays from antimatter globular cluster is estimated. We propose a method for the propagation of a flux of antinuclei in a galactic magnetic field from the globular cluster of antistars in the Galaxy.

**Povzetek.** Modeli za krepko nehomogeno sintezo barionov napovedo, da so v vesolju makroskopski objekti antisnovi. Avtorji preverjajo domnevo o obstoju starih krogelnih kopic antizvezd v haloju galaksije. Ocenjujejo gostoto jeder antihelija v galaktičnih kozmičnih žarkih. Ker so interakcije med antidelci poznane, sklepajo da se kopice antizvezd razvijajo podobno kot kopice običajnih zvezd. Odtod dobijo oceno energijske gostote antidelcev v kozmičnih žarkih, ki prihajajo iz kopic zvezd iz antisnovi. Predlagajo metodo za izračun pritoka antidelcev iz kroglastih kopic antizvezd skozi galaktično magnetno polje naše galaksije.

Keywords: Antimatter; cosmic rays; globular clusters of anti-stars; search for antihelium; Baryon asymmetry of the Universe; AMS 02;  
PACS: 98.80.Bp; 98.70.Sa; 97.60.Bw; 98.35.Eg; 21.90.+f;

### 9.1 Introduction

At the end of the 1920s, Paul Dirac predicted the existence of antiparticles — that is new particles, which are opposite in sign of electric, baryonic, lepton and other charges of already known particles [1]. Antimatter is detected in cosmic rays. According to the modern concepts it has three possible nature of origin:

- Primordial antimatter. It could be created in the early Universe as the reflection of nonhomogeneous baryosynthesis [2, 3], evolve in antimatter domains and

\* E-mail: aokirichenko@yandex.ru

now it can exist in the form of macroscopic antimatter objects like globular clusters of antimatter stars [2].

- Secondary antimatter. It is formed as a result of the collision of the nuclear component of cosmic rays with interstellar gas or with a supernova shell [4].
- Antimatter from exotic sources like evaporation of primordial black holes or the decay/annihilation of hypothetical particles of dark matter [2].

According to [5], such object can be present in the Galaxy in the form of a globular cluster of antimatter stars. The prediction [5] assumes similarity in the properties of antimatter and matter globular clusters. Based on this similarity we consider here possibilities to test the hypothesis of antimatter globular cluster in searches for antihelium component of cosmic rays. Our approach is aimed to specify the predictions of this hypothesis with the account of realistic description of the production and propagation of cosmic antihelium fluxes in the Galaxy.

## 9.2 Primordial antimatter

The baryon asymmetry of the Universe is the observed predominance of matter over antimatter in the visible part of the Universe. Explaining the origin of the baryon asymmetry of the Universe is one of the key problems of modern cosmology and physics of elementary particles. A. D. Sakharov [6] and V.A. Kuzmin [7] formulated the necessary conditions for baryosynthesis in the early Universe:

1. Asymmetry between particles and antiparticles as a violation of charge C- and combined CP-symmetry.
2. Violation of the law of conservation of baryon charge.
3. Violation of local thermodynamic equilibrium.

On the other hand, it was shown in [8] - [11] that almost all existing mechanisms of baryosynthesis allow the existence of domains with an excess of antimatter, if baryosynthesis is strongly nonhomogeneous. The size of domains depends on the details of the considered mechanisms and can be both small and reaching the size of a Metagalaxy.

The macroscopic region of antimatter with an excess of antibaryons at the same temperature and density evolves in the same way as ordinary matter of macroscopic size. Experiments on accelerators synthesizing antimatter show that the properties of particles and antiparticles coincide, except of the small effect of CP-violation [12].

An astronomical object smaller than a globular cluster cannot be formed surrounded by matter during cosmological evolution [13]. With smaller sizes, antimatter would annihilate with matter before the Galaxy formation. The larger size of domains is constrained by the observed fluxes of gamma radiation.

Globular clusters of antistars could form during the formation of the Galaxy and remain in its halo by now.

Cosmic ray fluxes of antinuclei are the profound signature of antimatter stars and provide the probe of their existence.

### 9.3 Secondary antimatter

The detected fluxes of cosmic antiparticles are formed as a result of collisions of high-energy nuclear component of cosmic rays with interstellar gas. Study of the processes of antiproton and light antinuclei production at accelerators made it possible to determine the cross section of these processes. The data obtained were used to predict the cross sections for heavier nuclei. This analysis (figure 9.1) shows that detection of  $\overline{\text{He}}^3$ ,  $\overline{\text{He}}^4$  at level of sensitivity of experiment can not explained by secondary antinuclei.

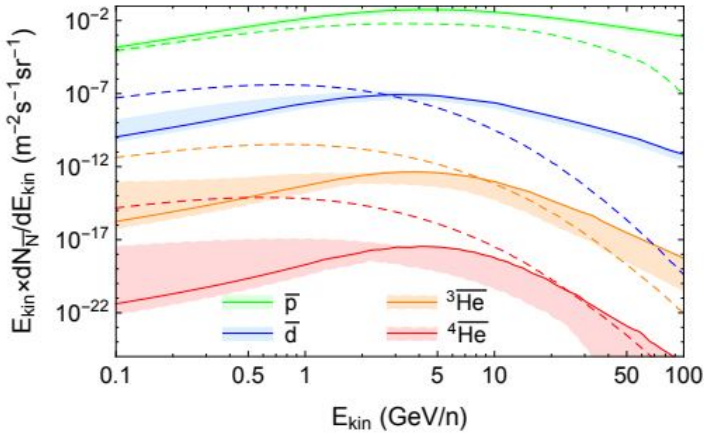


Fig. 9.1: Upper limits for of secondary [14] antihelium, antiproton, antideuteron together with previous results.

### 9.4 Antimatter from exotic sources

Modern cosmology classifies as exotic sources of antimatter annihilation or decay of hypothetical particles of dark matter and evaporation of primordial black holes.

#### 9.4.1 Dark matter

Dark matter makes up  $\sim 85\%$  of all matter in the universe. Its presence is implied in many astrophysical and astrological observations, including gravitational effects and large-scale structure formation. Such effects cannot be explained by the action of baryonic matter. Since dark matter has not yet been observed, if it exists, then it must interact through gravity with baryonic matter and radiation. The decay and annihilation of such particles can lead to the formation of antiparticles [15].

### 9.4.2 Primordial black hole

Primordial black holes are a hypothetical type of black hole formed after the Big Bang. In the early Universe, high densities and inhomogeneous conditions could lead to gravitational collapse in dense regions, forming black holes. Ya. B. Zeldovich and I. D. Novikov in 1966 for the first time suggested the existence of such objects [16]. The theory of their origin was first deeply studied by S. Hawking in 1971 [17].

Hawking showed that, due to quantum effects, black holes radiate like a black body with a temperature inversely proportional to the mass of the black hole. A physical understanding of the process can be obtained by imagining that particle-antiparticle radiation is emitted from beyond the event horizon. According to the modern concept, primordial black holes can also be sources of positrons and antiprotons [18].

## 9.5 Globular clusters in the galactic halo

A globular star cluster is a collection of stars that forms a spherical cluster rotating around the core of the Galaxy. Globular clusters are very closely connected by gravity, which gives them a spherical shape and a relatively high density of stars towards their centers. The name of this category of star clusters comes from the Latin *globulus* - a small sphere.

Globular clusters are located in the galactic halo and contain more stars and are much older than the less dense open clusters found in the galactic disk. Globular clusters are common, with about 150 globular clusters currently known in the Milky Way [19].

Observations of globular clusters show that these stellar formations originate mainly in regions of effective star formation, where the interstellar medium is denser than normal star-forming regions. Currently, none of the known globular clusters show active star formation, they are free of gas and dust, and it is assumed that all the gas and dust were long ago either turned into stars or blown out of the cluster during the initial explosion of star formation. This is consistent with the opinion that globular clusters are the oldest objects in the Galaxy and were among the first clusters of stars [20].

The trajectories of the globular clusters are eccentric and inclined to the plane of the galaxy. Orbiting the "outskirts" of a galaxy, globular clusters take several hundred million years to complete one orbit. Stars can reach a density of 100 to 1000 stars per cubic parsec in the center of a globular cluster. This is different from the density of stars around our Sun, which is estimated at about 0.14 stars per cubic parsec.

Globular clusters are usually made up of stars that have a low proportion of elements other than hydrogen and helium compared to stars like the Sun. The proportion of heavier elements may indicate the age of a star, with older stars usually having lower metallicities [21]- [22].

## 9.6 Discussion about the source function

The paper considers a typical globular cluster, presumably consisting of anti-stars. As an example, we take one of the closest clusters - M4 in the Messier catalog (figure 9.1) (NGC 6121 in the new general catalog (NGC)).

Age, Gy	Distance from the Sun, kpc	Number of stars
12	1.72	$8 \cdot 10^4$

Table 9.1: Parametrs of globular cluster M4 [23]

Then we also assume that globular cluster M4 is a source of  $\overline{\text{He}}^4$  in galactic cosmic rays.

Three possible mechanisms for the injection of antihelium into cosmic rays from the globular cluster M4:

### 1. Stationary outflow of matter from the surface of antistars

If the diapason of propagation of antimatter from the globular cluster crosses the galactic disk, then the stellar wind will enter the disk, and then into the solar system. A stationary outflow of star matter in a cluster is considered for this. Stars are constantly losing part of their mass, so the concentration of particles from the entire globular cluster can be large. These are very low energies, a process of additional acceleration of particles is required to effectively overcome the solar magnetic field, but this effect is suppressed. In this case, we expect an energy  $\sim$  MeV.

### 2. Flares on antistars

It is a known fact that active explosive processes occur on the Sun, accompanied by the acceleration of particles and the appearance of solar cosmic rays. We assume the existence of similar processes on antistars in a globular cluster.

Particles from flares on antistars can receive higher energy ( $\sim$  GeV), forming the antinuclear component of galactic cosmic rays.

### 3. Explosions of antisupernovae in a globular cluster of antistars

Supernova explosions are the result of the evolution of stars, which is accompanied by the release of high energy up to  $\sim 10^{51}$  erg. The shell from the exploded anti-star propagates at high speed. Particles can acquire energy ( $\sim 10^{15}$  eV) as a result of various acceleration mechanisms on the supernova shell, accelerate and inject into cosmic rays. By analogy with the fact that stars are the source of particles in cosmic rays, antistars should be the main source of antiparticles in cosmic rays. Supernovae may be the most likely source of antinuclei in galactic cosmic rays.

## 9.7 Results

### 9.7.1 Supernova explosions

The analysis begins with the most probable mechanism - antiper supernova explosions, because the magnetic fields of the Galaxy prevent the penetration of low-energy antiparticles into the Galactic disk.

But it is also important to note that the frequency of the explosion of such supernovae is low against the background of outbursts of anti-stars and against the background of a constant outflow of stationary matter of anti-stars. The first two cases will be discussed later.

**Calculation of the energy density of antiparticles in cosmic rays** Figure (9.2) shows a graph of the evolution of the population of the M4 cluster [24]. The graph shows the processes occurring in the early stages of the life of the cluster, the results of these processes can be compared with the present time. Let's pay attention to the number of neutron stars on the graph. Their number has not changed over 12 billion years. This means that about 12 billion years ago they could have formed as a result of the explosion of antiper supernovae. This fact can be used to calculate the energy density of antiparticles in cosmic rays.

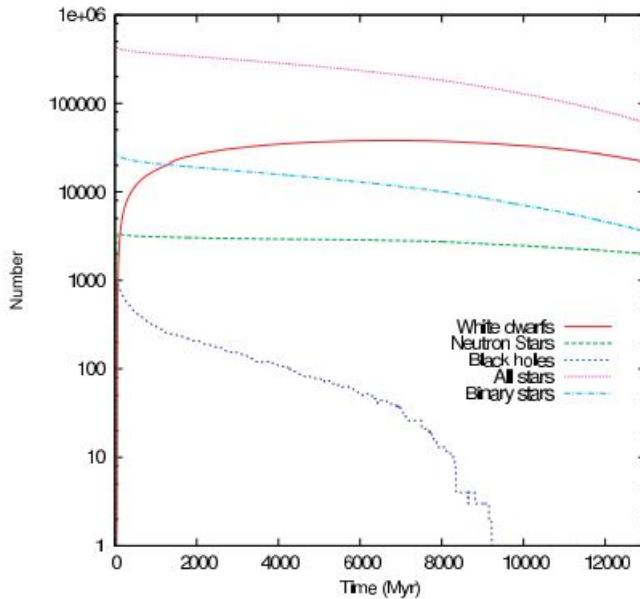


Fig. 9.2: Change in the population of M4 in time

Using the formula for the energy density of cosmic rays of matter

$$\rho_{\text{CR}} = \frac{E_{\text{sn}} \dot{N}_{\text{sn}} t_{\text{ret}}}{V} \quad (9.1)$$

$N_{\text{sn}}$  – number of neutron stars in M4,  $t$ – cluster age,  $\dot{N}_{\text{sn}}$ – average supernova explosion frequency,  $E_{\text{sn}}$  – energy realized from supernova,  $t_{\text{ret}}$ – cosmic ray lifetime,  $V$ - volume of the region of propagation of cosmic rays (to calculate the volume, we considered a model of a cylinder with a height and radius of 30 kpc and 10 kpc, respectively. In order to consider not only the region of the disk, but also the halo of the Galaxy).

We present all the numerical values of these quantities in the form of a table figure (9.2).

$N_{\text{sn}}$	$t, \text{Gy}$	$\dot{N}_{\text{sn}}$	$E_{\text{sn}}, \text{erg}$	$t_{\text{ret}}, \text{myr}$	$V, \text{kpc}^3$
12	1.72	$8 \cdot 10^4$	$10^{51}$	$2 \cdot 10^{-5}$	$3 \cdot 10^3$

Table 9.2: Table of numerical characteristics of quantities for calculating the energy density of antiparticles

the density using formula (1) and the values in the table:

$$\rho_{\overline{\text{CR}}} \sim 10^{-4} \text{eV/cm}^3 \quad (9.2)$$

For comparison, we present the value of the energy density of cosmic rays of matter:

$$\rho \sim 1 \text{eV/cm}^3 \quad (9.3)$$

We also pay attention to the fact that the energy density for secondary antiprotons:

$$\rho_{\overline{\text{p}}} \sim 10^{-5} \text{eV/cm}^3 \quad (9.4)$$

The obtained value does not correspond to the established experimental data for the energy density of antiprotons. But given the fact that particles of cosmic rays pass through the magnetic fields of the Galaxy and lose some of the energy in them, it is necessary to consider in more detail the mechanism of motion of cosmic rays, which will be presented in the following part.

**Particle motion in a Galaxy's magnetic field** In order for us to estimate the real fraction of particles from the initial flux that penetrates into the disk of the Galaxy, it is necessary to simulate the motion of particles in the magnetic field of the Galaxy.

*Simulation of the magnetic field of the galaxy.* Based on the equations according to the data of [25], we have compiled a function program, the input parameters of which are the coordinates in the Galaxy, and the output parameters are the components of the magnetic field in the Cartesian coordinate system.

The components of the magnetic field in a cylindrical coordinate system centered at the Galactic center taken from [25]:

$$B_\phi = -\frac{B_1}{2R/R_0} \frac{z}{(z+z_0)} \left( \sqrt{(R/R_0)^2 + (z/z_0)^2} - z/z_0 \right)$$

$$B_R = \frac{1}{2} B_1 \frac{z_0^2}{(z+z_0)^2} \tanh(R/R_0)$$

$$B_z = \frac{0.1B_1 z_0}{R_0} + \frac{1}{2} B_1 \frac{z_0^2}{(z+z_0)^2} \left( \frac{\tanh(R/R_0)}{R} + \frac{\text{sech}^2(R/R_0)}{R_0} \right)$$

Where  $R_0 = 5$  kpc and  $z_0 = 0.5$ pc are taken as scale lengths, and the  $B_1$  parameter is free in [25] and is determined by calibration, for example, by the magnetic field near the solar system according to the data of [26].

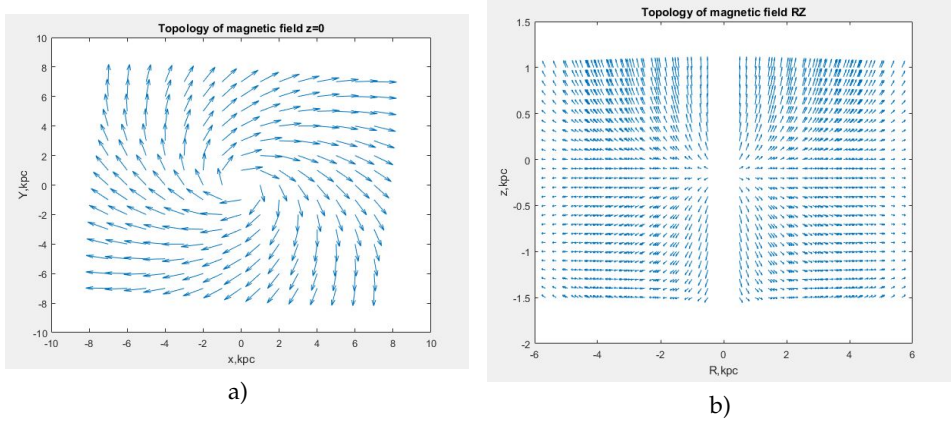


Fig. 9.3: Topology of the magnetic field of the Galaxy in the projection  $Z = 0$  and in the projection  $RZ$

We have constructed the topology of the Magnetic field of the Galaxy in the projection  $RZ$  and in the projection  $Z=0$  ( $R$  and  $z$  are coordinates in a cylindrical coordinate system, a coordinate system centered at the Galactic center).

You can see in figure (9.3a), that the magnetic field lines spiral out from the center of the Galaxy, this corresponds to the concept of the global magnetic field of the Galaxy in the plane of the galactic disk. The figure (9.3b) shows the vertical projection of the magnetic field of the Galaxy at  $y = 0$ , we see that the lines of force diverge in different directions according to the law determined by the equations from ([25]). We have reproduced the magnetic field given in ([25]), and now we will simulate the propagation of particles in this magnetic field and will observe how particles are transported in our Galaxy.

## 9.8 Conclusion

In this work, we considered the typical globular cluster M4, whose observed features can reproduce the expected properties of a globular cluster of anti-stars in

the Galaxy. Based on the symmetry of the properties of matter and antimatter, we discuss the evolution of this GC and the mechanisms of injection of antimatter in CR.

We calculated the energy density of high energy antiparticles ejected by antimatter GC in cosmic rays, and also checked the operation of the program to simulate the propagation of these antiparticles in the magnetic field of the Galaxy.

Further work is aimed at modeling the motion of particles in the magnetic field of the Galaxy, in order to estimate the minimum energy that a particle penetrating into a galactic disk should have. Implementation of our research program will help to obtain predictions of the expected flux of antinuclei as the signature of antimatter stars in our Galaxy.

## Acknowledgements

The research of MK was financially supported by Southern Federal University, 2020 Project № VnGr/2020-03-IF. Research of AM was supported by the Ministry of Science and Higher Education of the Russian Federation under Project "Fundamental problems of cosmic rays and dark matter", No. 0723-2020-0040.

## References

1. P. A. M. Dirac: The quantum theory of the electron, Proc. Roy. Soc. (London) **A117**, 610—624 (1928).
2. M. Y. Khlopov: *Fundamentals of Cosmoparticle Physics* CISP-Springer, Cambridge, UK, 2012.
3. A. D. Dolgov: Matter and antimatter in the universe, Nucl. Phys. Proc. Suppl. **113** 40 (2002).
4. Nicola Tomassetti, Alberto Oliva: Secondary antinuclei from supernova remnants and background for dark matter searches, 35th International Cosmic Ray Conference – ICRC2017, (2017).
5. M.Yu. Khlopov: An antimatter globular cluster in our Galaxy - a probe for the origin of the matter, Gravitation and Cosmology, **4**, 69-72 (1998).
6. A.D. Sakharov: Violation of CP-invariance, C-asymmetry and baryon asymmetry of the Universe, JETP Lett, **5**, 32 (1967).
7. V.A. Kuzmin: CP violation and baryon asymmetry of the universe, JETP Lett, **12**, 228 (1970).
8. V.M. Chechetkin, M.G. Sapozhnikov, M.Yu. Khlopov and Ya.B.Zeldovich: Astrophysical aspects of antiproton interaction with He (Antimatter in the Universe), Phys. Lett. **118B**, 359-362 (1982).
9. V.M. Chechetkin, M.Yu. Khlopov and M.G. Sapozhnikov: Antiproton interactions with light elements as a test of GUT cosmologies., Rivista Nuovo Cimento, **5**, 1-80 (1982).
10. A.D. Dolgov, A.F. Illarionov, N.S. Kardashev, I.D. Novikov, Cosmological model of a baryon island, JETP, **67**, 1517-1524 (1988).
11. M.Yu. Khlopov, S.G. Rubin, A.S. Sakharov: Possible Origin of Antimatter Regions in the Baryon Dominated Universe., Phys.Rev.D **62**, 083505 (2000).
12. M. Charlton, S. Eriksson, G. M. Shore: Fundamental Physics in Antihydrogen Experiments, 97-98 (2020).

13. M.Yu. Khlopov, R.V. Konoplich, R. Mignani, et al.: Evolution and observational signature of diffused antiworld., *Astroparticle Phys.*, **12**, 367-372 (2000).
14. I. Cholis, T. Linden: Anti-Deuterons and Anti-Helium Nuclei from Annihilating Dark Matter FERMILAB-PUB-20-021-A, (2020).
15. V. Trimble Existence and Nature of Dark Matter in the Universe., *Annual Review of Astronomy and Astrophysics.*, **25**, 425-472 (1987).
16. Ya.B. Zeldovich, I.D. Novikov: The Hypothesis of Cores Retarded During Expansion and the Hot Cosmological Model, *Soviet Astronomy*, **10**, 602 (1966).
17. S. Hawking: Gravitational collapsed objects of very low mass. *Mon. Not. Roy. astron. Soc.*, **152**, 75-78 (1971).
18. W. Carroll Bradley, A. Ostlie Dale: *An Introduction to Modern Astrophysics*, Reading, MA: Addison-Wesley Publishing, 1996.
19. <http://gclusters.altervista.org/>
20. M. Paul: *Star Clusters. Encyclopedia of Astronomy and Astrophysics*, 2014.
21. <https://www.astro.keele.ac.uk/workx/globulars/globulars.html>
22. J. S. Kalirai, H. B. Richer: Star clusters as laboratories for stellar and dynamical evolution, Royal society publishing, (2009).
23. D. C. Heggie and M. Giersz: Modelling individual globular clusters, Cambridge University Press Access S246, **3**, 121-130 (2007).
24. D. C. Heggie, M. Giersz: Monte Carlo simulations of star clusters – V. The globular cluster M4, *Monthly Notices of the Royal Astronomical Society* **1**, **388**, 429–443 (2008).
25. C. J. Nixon, T. O. Hands: The origin of the structure of large-scale magnetic fields in disc galaxies *Notices of the Royal Astronomical Society* **3**, **477**, 3539–3551 (2018).
26. M. Opher, F. Alouani Bibi: A strong, highly-tilted interstellar magnetic field near the Solar System, *Nature*, **462**, 1036–1038 (2009).



## 10 Domain Walls and Strings Formation in the Early Universe

A.A. Kirillov \* and B. S. Murygin \*\*

National Research Nuclear University MEPhI  
(Moscow Engineering Physics Institute)

**Abstract.** Soliton formation through classical dynamics of two scalar fields with the potential having a saddle point and one minimum in (2+1)-space-time is discussed. We show that under certain conditions in the early Universe both domain walls and strings can be formed even if scalar fields are inflaton ones.

**Povzetek.** Avtorja obravnavata tvorbo solitonov s klasično dinamiko dveh skalarnih polj s potencialom, ki ima sedlo in en minimum v (2+1)-razsežnem prostoru. Pokazeta, da lahko nastanejo zidovi domen in strune, ob določenih pogojih v zgodnjem Vesolju, tudi v primeru skalarnih polj, ki so inflatonska.

Keywords: solitons, strings, domain walls

PACS: 03.50.-z, 11.27.+d, 98.80.Cq

### 10.1 Introduction

Multi-field inflation models such as the hybrid inflation [8] or the natural inflation [7, 10] may contain potentials of non-trivial forms. If potential has at least one saddle point, the field dynamics in such models may lead to formation of topologically non-trivial structures named solitons [9, 11, 14]. Moreover, under certain conditions, they may produce primordial black holes in the radiation era due to collapse of domain walls [1] or loops of cosmic strings [5] that affects the early Universe [13].

Previously, it was shown solitons may be formed in (1+1) space-time even potential has only one minimum and at least one saddle point [3, 4]. In this paper, we continue study of the possibility in (2+1) space-time.

### 10.2 Model in (2+1) space-time

Let us consider the dynamics of two real scalar fields  $\varphi$  and  $\chi$  with the Lagrangian of the system

$$\mathcal{L} = \frac{1}{2} g^{\mu\nu} (\partial_\mu \varphi \partial_\nu \varphi + \partial_\mu \chi \partial_\nu \chi) - \mathcal{V}(\varphi, \chi), \quad (10.1)$$

\* E-mail: AAKirillov@mephi.ru

\*\* E-mail: MuryginBS@gmail.com

where  $g^{\mu\nu}$  is the Friedman-Robertson-Walker metric tensor with the cosmic scale factor  $a(t)$ . Then, the classical motion equations for  $\varphi$  and  $\chi$  in (2+1) space-time take the form

$$\begin{aligned}\varphi_{tt} - 3H\varphi_t - \varphi_{xx} - \varphi_{yy} &= -\frac{\partial\mathcal{V}}{\partial\varphi}, \\ \chi_{tt} - 3H\chi_t - \chi_{xx} - \chi_{yy} &= -\frac{\partial\mathcal{V}}{\partial\chi}.\end{aligned}\quad (10.2)$$

Here,  $H = \dot{a}/a$  is the Hubble parameter which is  $H_I \sim 10^{13}$  GeV during the inflation and becomes smaller in the radiation era. For equations (10.2), the Hubble parameter plays a role of a friction term, and its time dependence does not affect our conclusions. Thus, we assume it remains constant after the end of the inflation. In addition, the Hubble parameter  $H$  gives a natural scale for all units. Therefore, we express all dimension variables in  $H_I$  units.

To solve the system (10.2), we have to define initial and boundary conditions. We choose the initial conditions in the form

$$\begin{aligned}\varphi(x, y, 0) &= \mathcal{R} \cos \Theta + \varphi_1, & \varphi_t(x, y, 0) &= 0; \\ \chi(x, y, 0) &= \mathcal{R} \sin \Theta + \chi_1, & \chi_t(x, y, 0) &= 0,\end{aligned}\quad (10.3)$$

where

$$\mathcal{R}(r) = \mathcal{R}_0 \cosh^{-1} \frac{r_0}{r}, \quad \Theta = \theta. \quad (10.4)$$

It sets correspondence between the fields space  $(\varphi, \chi)$  and the physical plane  $(x, y)$ . Here, the point  $(\varphi_1, \chi_1)$  corresponds to the center of the initial fields area in the form of the circular disk with the radius  $\mathcal{R}(r)$  and the polar angle  $0 \leq \Theta \leq 2\pi$ ,  $r = \sqrt{x^2 + y^2}$  and  $\theta$  are a distance from the coordinate origin and a polar angle in a physical  $xy$ -plane, respectively, and  $\mathcal{R}_0$  and  $r_0$  are positive parameters.

The boundary conditions are chosen as

$$\begin{aligned}\varphi_x(\pm\infty, y, t) &= 0, & \varphi_y(x, \pm\infty, t) &= 0; \\ \chi_x(\pm\infty, y, t) &= 0, & \chi_y(x, \pm\infty, t) &= 0.\end{aligned}\quad (10.5)$$

We study classical evolution of the scalar fields  $\varphi$  and  $\chi$  with the potential used in [3,4]:

$$\mathcal{V} = d(\varphi^2 + \chi^2) + a \exp[-b(\varphi - \varphi_0)^2 - c(\chi - \chi_0)^2], \quad (10.6)$$

where  $a, b, c, d$  are positive parameters. The parameter  $a$  sets a height of a local maximum,  $b$  and  $c$  set its shape, and  $d$  is responsible for a slope of the potential. The described potential has only one saddle point and one minimum, but could be easily modified to obtain any number of saddle points by adding terms like the last one.

Additionally, we consider the well-known potential ‘‘tilted Mexican hat’’ [10]

$$\mathcal{V} = \lambda \left( \varphi^2 + \chi^2 - \frac{g^2}{2} \right)^2 + \Lambda^4 \left( 1 - \frac{\varphi}{\sqrt{\varphi^2 + \chi^2}} \right), \quad (10.7)$$

where  $\lambda, g, \Lambda$  are positive parameters. The parameter  $g$  sets a position of a circle of degenerate minima in the case of the Mexican hat without a tilt,  $\lambda$  sets a height

of a local maximum at the point  $(\varphi_0, \chi_0) = (0, 0)$  and  $\Lambda$  sets a tilt of the potential. Note, a potential slope makes minima non-degenerate. However, non-degeneracy is not a necessary condition for solitons production.

The energy density of the system is given by

$$\rho = \frac{1}{2} \sum_i ((\partial_i \varphi)^2 + (\partial_i \chi)^2) + \mathcal{V}(\varphi, \chi), \quad (10.8)$$

where partial derivatives are taken over the variables  $\{t, x, y\}$ .

### 10.3 Results

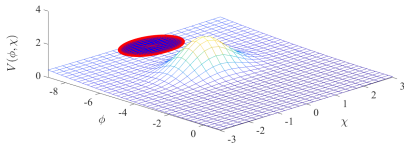
For the potential (10.6), we choose the parameters as follows  $d = 0.005$ ,  $a = 2$ ,  $b = 1$ ,  $c = 1$ ,  $\varphi_0 = -5$ ,  $\chi_0 = 0$  and the parameters of the initial conditions (10.3)  $\mathcal{R}_0 = 1$ ,  $r_0 = 1$ ,  $\varphi_1 = -8$  and  $\chi_1 = 0$  (all dimensional values are taken in  $H_I$  units). The initial fields configuration is separated from the minimum by the peak of the potential, see fig. 10.1a. Note, the potential has the minimum at the point  $(\varphi_{\min}, \chi_{\min}) = (0, 0)$ .

The final state of the fields evolution is presented in fig. 10.1b. Due to the slope of the potential, the fields tend to reach its minimum; however, there are two possible ways to achieve it. Thus, the fields may bypass the peak from both sides. Note, we do not consider the situation when energy of the system is large enough to overcome the peak without bypassing. As a result of our calculations, the configuration reaches the minimum in both possible ways and stops in the equilibrium state.

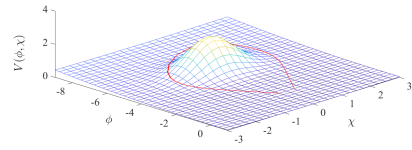
The energy density of the fields configuration determined by (10.8) is presented in fig. 10.2a. It corresponds to well-known type of solitons named domain walls and confirms the results of [4] for the winding number  $N = 1$ . This stable soliton may play a significant role in the early Universe. Closed domain walls with high enough energy could collapse due to surface tension and thus produce primordial black holes [6, 12].

If we fix all parameters except  $\varphi_1$ , the other solitons type is obtained. We choose new value  $\varphi_1 = -5$ , it changes the initial conditions in fields space  $(\varphi, \chi)$ , see fig. 10.1c. One can see, the initial state is now at the top of the peak. The system evolution leads that the fields tend to the potential minimum. Thus, the configuration leaves the peak in all directions. The final state is shown in fig. 10.1d. The energy density of the formed soliton is presented in fig. 10.2b, it corresponds to the formation of the string with the ridge. The last essentially distinguishes this soliton from well-known strings.

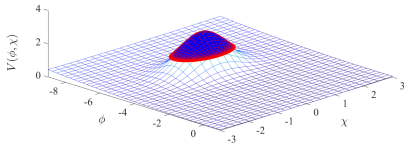
It is interesting to note that changing only one parameter  $\varphi_1$  leads to the other soliton type. Thus, both domain walls and strings could be formed in one model. However, it does not take place for all possible sets of the parameters. Domain wall stability requires the second term of the potential (10.6) corresponding to the local maximum height to be much bigger than the first one corresponding to the slope of the potential. It imposes boundaries on the parameters  $a$  and  $d$  showing whether domain walls may be formed. In the case of strings formation,



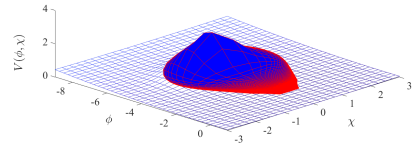
(a) The initial conditions for domain wall production.



(b) The final state showing the domain wall production.

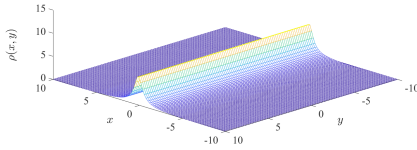


(c) The initial conditions for string production.

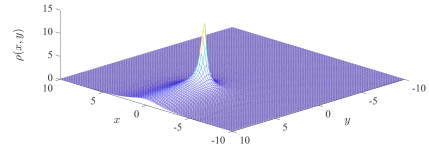


(d) The final state showing the string production.

Fig. 10.1: The initial and final states of the fields configuration with the potential (10.6) are shown.



(a) The energy density of the domain wall.



(b) The energy of the string with the ridge.

Fig. 10.2: The energy densities of the final states are shown.

the parameter  $\mathcal{R}_0$  may be restricted because the big value gives the system too large initial potential energy which may lead to destruction of solitons.

Finally, let us demonstrate solitons formation in the well-known tilted Mexican hat model (10.7) describing the inflation. The possibility of domain walls production in this potential was considered in [4]. Here we focus on the other solitons type. We choose the parameters of the potential as follows  $g = 1$ ,  $\lambda = 0.1$ ,  $\Lambda = 5 \cdot 10^{-13}$  and the parameters of the initial conditions  $\mathcal{R}_0 = 0.9$ ,  $r_0 = 1$ ,  $\varphi_1 = \chi_1 = 0$  (all in  $H_1$  units). It is shown in fig. 10.3a where the initial state of the fields is located on the peak top. Because the tilt is very small, fields configuration shrinks around the peak due to surface tension and stops when potential slope compensates it (see fig. 10.3b). The energy density of the final distribution is presented in fig. 10.4. One can see, it corresponds to the string formation. The ridge is not seen due to the extremely small slope of the potential. If the parameter  $\Lambda$  increases, the ridge appears.

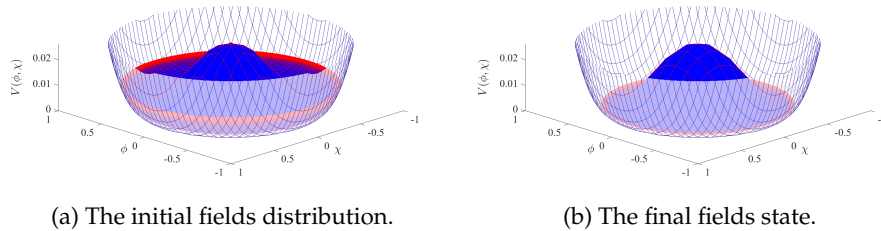


Fig. 10.3: The initial and final states of the fields with the tilted Mexican hat potential (10.7) are shown.

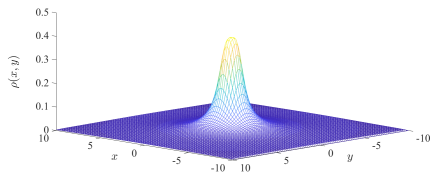


Fig. 10.4: The final energy density distribution corresponding to string for tilted Mexican hat is shown.

## 10.4 Conclusion

The solitons formation in the system of the scalar fields with potentials having a saddle point and one minimum was discussed. It is shown both domain walls and strings may be formed in the same model depending on the initial fields configuration. Note, the initial conditions may affect the solitons production even if the scalar fields are inflaton ones (it takes place if potential has at least one saddle point). In this case, it is important to check whether solitons appear in the model in order to avoid their overproduction in the early Universe, and, consequently, primordial black holes that may contradict observational data [2].

## Acknowledgement

The authors are grateful to K. M. Belotsky, V. A. Gani, and S. G. Rubin for useful discussions. The work was supported by the grant RFBR No 19-02-00930.

## References

1. K. M. Belotsky, V. I. Dokuchaev, Y. N. Eroshenko, E. A. Esipova, M. Y. Khlopov, L. A. Khromykh, A. A. Kirillov, V. V. Nikulin, S. G. Rubin, and I. V. Svadkovsky. Clusters of Primordial Black Holes. *Eur. Phys. J. C*, 79(3):246, Mar. 2019.
2. B. Carr, K. Kohri, Y. Sendouda, and J. Yokoyama. Constraints on Primordial Black Holes.
3. V. A. Gani, A. A. Kirillov, and S. G. Rubin. Transitions between topologically non-trivial configurations. *J. Phys. Conf. Ser.*, 934:012046, Dec. 2017.
4. V. A. Gani, A. A. Kirillov, and S. G. Rubin. Classical transitions with the topological number changing in the early Universe. *J. Cosmol. Astropart. Phys.*, 2018(4):042, Apr. 2018.

5. T. Helfer, J. C. Aurrekoetxea, and E. A. Lim. Cosmic string loop collapse in full general relativity. *Phys. Rev. D*, 99(10):104028, May 2019.
6. M. Y. Khlopov, S. G. Rubin, and A. S. Sakharov. Primordial structure of massive black hole clusters. *Astropart. Phys.*, 23(2):265–277, Mar. 2005.
7. J. E. Kim, H. P. Nilles, and M. Peloso. Completing natural inflation. *J. Cosmol. Astropart. Phys.*, 2005(1):005, Jan. 2005.
8. A. Linde. Hybrid inflation. *Phys. Rev. D*, 49(2):748–754, Jan. 1994.
9. N. Manton and P. Sutcliffe. *Topological Solitons*. Cambridge University Press, Cambridge, 2004.
10. M. Peloso and C. Unal. Trajectories with suppressed tensor-to-scalar ratio in Aligned Natural Inflation. *J. Cosmol. Astropart. Phys.*, 2015(6):040, June 2015.
11. R. Rajaraman. *Solitons and instantons*. North-Holland Publishing Company, Amsterdam, 1989.
12. S. G. Rubin, A. S. Sakharov, and M. Y. Khlopov. The Formation of Primary Galactic Nuclei during Phase Transitions in the Early Universe. *J. Exp. Theor. Phys.*, 92(6):921–929, June 2001.
13. A. Vilenkin, Y. Levin, and A. Gruzinov. Cosmic strings and primordial black holes. *J. Cosmol. Astropart. Phys.*, 2018(11):008, Nov. 2018.
14. A. Vilenkin and E. Shellard. *Cosmic Strings and Other Topological Defects*. Cambridge University Press, Cambridge, 2000.



## 11 The Interaction of Domain Walls with Fermions in the Early Universe

A.A. Kurakin <sup>\*1</sup> and S.G. Rubin <sup>\*\*1,2</sup>

<sup>1</sup> National Research Nuclear University MEPhI (Moscow Engineering Physics Institute),  
<sup>2</sup>N.I. Lobachevsky Institute of Mathematics and Mechanics, Kazan Federal University,  
Kremlevskaya Street 18, 420008 Kazan, Russia

**Abstract.** We consider the scalar field solitons and their interaction with the fermions in the early Universe. The analytical form of the reflection coefficient is obtained. The fermion mass is a function of the distance between the fermion and the soliton (wall). The function was approximated by the Woods-Saxon potential.

**Povzetek.** Avtorja obravnavata solitone skalarnih polj in njihovo interakcijo s fermioni v zgodnjem vesolju. Izpeljeta analitično formulo za koeficient odboja. Masa fermiona je v njenem modelu funkcija razdalje med fermionom in solitonom (steno), za funkcijo razdalje uporabita Woods-Saxonov potencial.

Keywords: domain wall, Dirac equation, PBH, early Universe

### 11.1 Introduction

Primordial black holes (PBHs) have been a source of significant interest for over 50 years. The possibility of the existence of such objects was predicted by Zeldovich and Novikov [14]. Despite the absence of direct evidence of their existence, there is a lot of observational data that can be interpreted in the framework of the hypothesis of the origin of black holes (BH) at the initial stages of the origin of the Universe [3,4,7].

In this paper, we base on the model of PBH formation as a result of the collapse of domain walls [2, 5, 11]. As a result of phase transitions during and after the inflationary stage, closed domain walls are formed. The formed non-spherical wall evolves: when interacting with hot plasma, the kinetic energy of the wall dissipates. As a result, the oscillations of the domain wall decay, the energy is transferred to the surrounding plasma, which leads to its additional heating. Further, the wall spheres and collapses into BH.

The rate of energy transfer from the domain wall to the surrounding plasma depends on the wall thickness, the initial plasma temperature and its density.

\* E-mail: kurakin-1993@mail.ru

\*\* E-mail: sergeirubin@list.ru

The wall thickness is characterized by the parameters of the initial Lagrangian and can vary over a wide range. Plasma temperature and density depend on the moment the walls appear. Moreover, the dynamics of plasma parameters depends on whether it participates in cosmological expansion or is separated from it due to the gravitational well created by closed walls.

In this paper, we consider the fermion interaction with the scalar field solitons (walls).

## 11.2 Model of domain wall

Consider the domain wall model. We describe We describe the wall by a complex scalar field with a Lagrangian:

$$\mathcal{L}_{\text{wall}} = \partial_\mu \phi^\dagger \partial^\mu \phi - \frac{1}{4}(\phi^\dagger \phi - f^2/2)^2 - \Lambda^4(1 - \cos \theta), \quad (11.1)$$

where  $\phi$  - complex scalar field and  $\theta$  is its phase. At the end of inflation, the  $\phi$  field is captured by the potential minimum for which  $|\phi| = f$ . Then we write the complex field in the form:

$$\phi = \frac{f}{\sqrt{2}} e^{i\theta} = \frac{f}{\sqrt{2}} e^{i\chi/f}. \quad (11.2)$$

Substitution of the expression (11.2) into Lagrangian (11.1) gives Lagrangian, that describing the phase of complex scalar field:

$$\mathcal{L}_{\text{wall}} = \frac{1}{2}(\partial_\mu \chi)^2 - \Lambda^4(1 - \cos(\chi/f)). \quad (11.3)$$

The the phase  $\chi$  is determined as follows [10]:

$$\chi(x) = 4f \arctan \left( \exp \left[ \frac{\Lambda^2}{f} x \right] \right) = 4f \arctan \left( \exp \left[ \frac{2x}{d} \right] \right), \quad (11.4)$$

where we introduced the wall thickness parameter  $d$

$$d = \frac{2f}{\Lambda^2}. \quad (11.5)$$

Let us choose the Lagrangian of fermions in the form:

$$\begin{aligned} \mathcal{L}_f &= i\bar{\psi} \gamma^\mu \partial_\mu \psi + g_0(\phi \bar{\psi} \psi + \text{h.c.}) - m\bar{\psi} \psi = \\ &= i\bar{\psi} \gamma^\mu \partial_\mu \psi + \sqrt{2}g_0 f \bar{\psi} \psi \cos(\chi/f) - m\bar{\psi} \psi. \end{aligned} \quad (11.6)$$

where expression (11.2) is used.

The interaction of the fermions with the domain wall is

$$\mathcal{L}_{\text{int}} = m_0 \cos(\chi/f) \bar{\psi} \psi = m_0 \left( 1 - \frac{2}{\cosh^2(2x/d)} \right) \bar{\psi} \psi; \quad m_0 = \sqrt{2}f g_0. \quad (11.7)$$

Then Lagrangian of fermions can be rewritten as

$$\mathcal{L}_f = i\bar{\psi} \gamma^\mu \partial_\mu \psi - m_0 \frac{2}{\cosh^2(2x/d)} \bar{\psi} \psi - m_f \bar{\psi} \psi, \quad (11.8)$$

where  $m_f = m - m_0$  - fermion mass.

### 11.3 Dirac equation

A description of the interaction between fermions and domain wall within the framework of the approach to solving the equation of motion is given in the papers [1, 6, 12]. The result for the interaction of the wall with scalar particles is given in the monograph [13]. In the papers [1, 6, 12] the description of the domain wall is given by the kink solution:  $\phi \sim \tanh x$ . In such model, the asymptotic fermion mass takes different values:  $x \rightarrow \pm\infty$ . This problem does not arise for the Lagrangian (11.8): the fermion mass is the same on both sides of the wall.

The Dirac equation

$$0 = (i\gamma^\mu \partial_\mu - g(x)) \psi, \quad (11.9)$$

holds for fermion Lagrangian (11.8) where function

$$g(x) = \frac{2m_0}{\cosh^2(2x/d)} + m_f \quad (11.10)$$

is effective mass, depending on the coordinate in the coordinate  $x$  perpendicular to the wall. Hereinafter, in asymptotics, we have:  $g(x) \xrightarrow{x \rightarrow \pm\infty} m_f$ .

The fermion wave function is as follows

$$\psi(x) = (u_1(x) \ u_2(x) \ u_3(x) \ u_4(x))^T e^{-iEt + ip_t x_t}. \quad (11.11)$$

Here we put  $p_t = 0$  for simplicity, i.e. the component of the momentum in the plane of the domain wall is zero and the incident wave is perpendicular to the wall. Then the equation takes the form:

$$0 = (E\gamma^0 + i\gamma^3 \partial_x - g(x)) \psi(x). \quad (11.12)$$

Hereafter, we choose the following representation of gamma matrices:

$$\gamma^0 = \begin{pmatrix} 0 & 1 \\ 1 & 0 \end{pmatrix}, \quad \gamma^3 = \begin{pmatrix} 0 & \sigma^3 \\ -\sigma^3 & 0 \end{pmatrix} \quad (11.13)$$

As a result of substitution, we obtain a system of equations for the bispinor components:

$$\begin{aligned} 0 &= E u_3(x) + i u_3'(x) - g(x) u_1(x) \\ 0 &= E u_1(x) - i u_1'(x) - g(x) u_3(x). \end{aligned} \quad (11.14)$$

We obtain a similar system for the components  $u_2, u_4$  if we replace:  $u_1 \rightarrow u_4, u_3 \rightarrow u_2$ .

Let's consider the following linear combinations of bispinor components:

$$\begin{aligned} \phi_+(x) &= u_1(x) + i u_3(x) \\ \phi_-(x) &= u_1(x) - i u_3(x). \end{aligned} \quad (11.15)$$

As a result of such substitution we obtain a system:

$$\begin{aligned} 0 &= iE\phi_-(x) + \phi_+'(x) - g(x)\phi_+(x) \\ 0 &= iE\phi_+(x) + \phi_-'(x) + g(x)\phi_-(x). \end{aligned} \quad (11.16)$$

Excluding the variables, we obtain the equations for the components  $\phi_{\pm}(x)$ :

$$0 = \left( \frac{d^2}{dx^2} \mp g'(x) + E^2 - g^2(x) \right) \phi_{\pm}(x). \quad (11.17)$$

Let us carry out an approximation by a function for which the solution can be obtained in an analytical form. Let us choose the Woods-Saxon potential. The scattering problem for the Woods-Saxon potential is considered in detail in the papers [8,9]: After approximation, the function  $g(x)$  takes the form

$$g(x) = \frac{A\theta(x)}{1 + \exp(a(x - x_0))} + \frac{A\theta(-x)}{1 + \exp(-a(x + x_0))} + m_f, \quad (11.18)$$

where parameters:  $A \rightarrow A = 2.392m_0$ ,  $m_f = m - m_0$ .

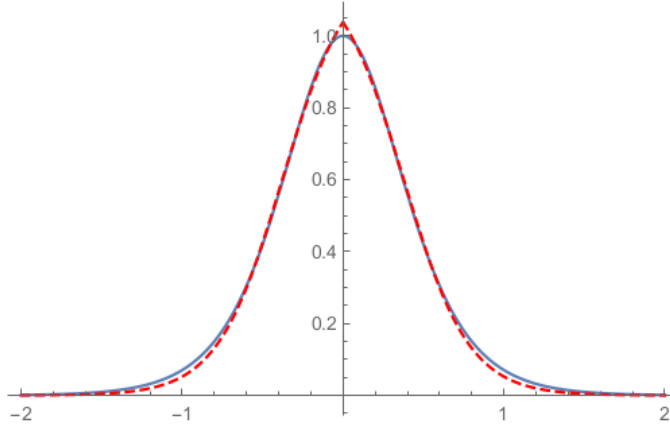


Fig. 11.1: Approximation of the function  $g(x)$ . Blue solid line -  $g(x)$ , red dotted line - Woods-Saxon potential

We solve the equation for two regions:  $x < 0$  and  $x > 0$

Consider the region  $x < 0$ . We will solve the equation for  $\phi_{+}^L(x)$  (the superscript L denotes the region  $x < 0$ ). Let's make a replacement:

$$\xi = -\exp(-a(x + x_0)). \quad (11.19)$$

Then the equation (11.17) takes the form:

$$0 = \left( a^2 \xi \frac{d}{d\xi} \left( \xi \frac{d}{d\xi} \right) - \left( m_f + \frac{A}{1 - \xi} \right)^2 + \frac{aA\xi}{(1 - \xi)^2} + E^2 \right) \phi_{+}^L(\xi). \quad (11.20)$$

The solution of the equation (11.20) is as follows:

$$\begin{aligned} \phi_{+}^L(\xi) = & C_1 \xi^{-\alpha} (1 - \xi)^{-\beta} {}_2F_1(-\alpha - \nu - \beta, -\alpha + \nu - \beta, 1 - 2\alpha; \xi) \\ & + C_2 \xi^{\alpha} (1 - \xi)^{-\beta} {}_2F_1(\alpha - \nu - \beta, \alpha + \nu - \beta, 1 + 2\alpha; \xi). \end{aligned} \quad (11.21)$$

where the parameters  $\alpha$ ,  $\beta$ ,  $\nu$  are defined as

$$\begin{aligned}\alpha &= \frac{1}{a} \sqrt{(m_f + A)^2 - E^2} = \frac{ip}{a} \\ \beta &= -\frac{A}{a} \\ \nu &= \frac{1}{a} \sqrt{m_f^2 - E^2} = \frac{i}{a} \sqrt{E^2 - m_f^2} = \frac{ik}{a}.\end{aligned}\quad (11.22)$$

Let's consider the limit  $x \rightarrow -\infty \Rightarrow \xi \rightarrow -\infty$ . Then, for the function  $\phi_{\pm}^L$  we obtain superposition of two waves: incident and reflected waves:

$$\phi_{\pm}^L \xrightarrow{x \rightarrow -\infty} D_1 e^{ik(x+x_0)} + D_2 e^{-ik(x+x_0)}. \quad (11.23)$$

The coefficients  $D_1$ ,  $D_2$  are determined by the formulas:

$$\begin{aligned}D_1 &= C_1 \frac{\Gamma(1-2\alpha)\Gamma(-2\nu)}{\Gamma(-\alpha-\nu-\beta)\Gamma(1-\alpha-\nu+\beta)} e^{-i\pi\alpha} + \\ &\quad C_2 \frac{\Gamma(1+2\alpha)\Gamma(-2\nu)}{\Gamma(\alpha-\beta-\nu)\Gamma(1+\alpha-\nu+\beta)} e^{i\pi\alpha} \\ D_2 &= C_1 \frac{\Gamma(1-2\alpha)\Gamma(2\nu)}{\Gamma(-\alpha+\nu-\beta)\Gamma(1-\alpha+\nu+\beta)} e^{-i\pi\alpha} + \\ &\quad + C_2 \frac{\Gamma(1+2\alpha)\Gamma(2\nu)}{\Gamma(\alpha-\beta+\nu)\Gamma(1+\alpha-\nu+\beta)} e^{i\pi\alpha},\end{aligned}\quad (11.24)$$

where  $C_1, C_2 = \text{const}$ . The asymptotic for  $\phi_{\pm}^L$  is obtained by substituting solution  $\phi_{\pm}^L$  (11.23) into the first equation of system (11.16). As a result, we obtain:

$$\phi_{\pm}^L(x) \xrightarrow{x \rightarrow -\infty} -\frac{k+im}{E} D_1 e^{ik(x+x_0)} + \frac{k-im}{E} D_2 e^{-ik(x+x_0)}. \quad (11.25)$$

The region  $x > 0$  can be considered in the similar manner to obtain the function  $\phi_{\pm}^R(x)$  to the right of the wall.

In order to find coupling between coefficients  $C_1$  and  $C_2$  we match the solutions at  $x = 0$ :

$$\begin{aligned}\phi_{\pm}^R|_{x=0} &= \phi_{\pm}^L|_{x=0} \\ (\phi_{\pm}^R)'|_{x=0} &= (\phi_{\pm}^L)'|_{x=0}.\end{aligned}\quad (11.26)$$

The normal component of the fermion current density is written as:

$$\begin{aligned}j &= \bar{\psi}(x)\gamma^3\psi(x) = -|u_1(x)|^2 + |u_2(x)|^2 + |u_3(x)|^2 - |u_4(x)|^2 = \\ &= -\phi_{\pm}^* \phi_{\pm} - \phi_{\pm}^* \phi_{\pm}.\end{aligned}\quad (11.27)$$

Substitute the obtained functions. As a result, we obtain The final form of the current

$$j = \frac{k}{E} (|D_1|^2 - |D_2|^2) = j_{\text{inc}} - j_{\text{ref}}, \quad (11.28)$$

is obtained by substitution of the explicit form of functions  $\phi_{\pm}^L$  and  $\phi_{\pm}^R$  into the expressions for the current density. Here  $j_{\text{inc}}$  is the current density of the incident particles,  $j_{\text{ref}}$  - of the reflected ones.

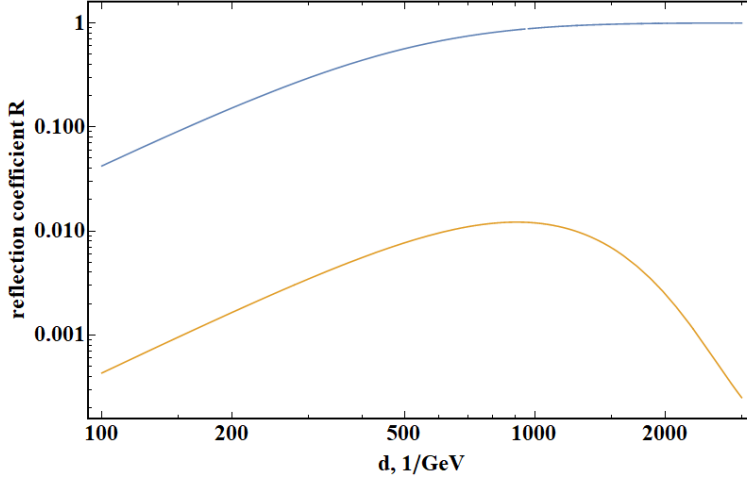


Fig. 11.2: Dependence of the reflection coefficient  $R$  on thickness  $d$ ,  $\text{GeV}^{-1}$ . Blue line -  $m_0 = 10^{-3}$  GeV,  $E - m_f = 1$  MeV; orange line -  $m_0 = 10^{-4}$  GeV,  $E - m_f = 1$  MeV

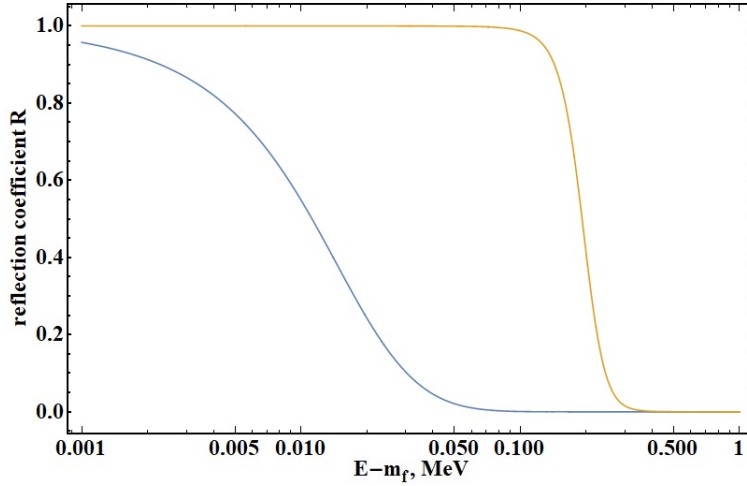


Fig. 11.3: Dependence of the reflection coefficient  $R$  on kinetic energy  $E - m_f$  MeV. Blue line -  $m_0 = 10^{-5}$  GeV,  $d = 10^4$   $\text{GeV}^{-1}$ ; orange line -  $m_0 = 10^{-4}$  GeV,  $d = 10^4$   $\text{GeV}^{-1}$

The reflection and transmission coefficients are determined through the ratio of the current densities as follows

$$R = \frac{j_{\text{ref}}}{j_{\text{inc}}} = \frac{|D_2|^2}{|D_1|^2}. \quad (11.29)$$

The coefficients  $D_1$ ,  $D_2$  are determined by the formulas (11.24). The results of calculating the reflection coefficient for electrons ( $m_f = 0.5$  MeV) are shown in Figure 11.2, 11.3.

## 11.4 Conclusion

The deceleration of the primordial walls due to the interaction with the surrounding media is the important process that could influence the formation of the black holes clusters. In this paper, we have found the reflection probability of the fermions. This is necessary step for studying the cluster heating by the wall fluctuation.

## Acknowledgements

This research was funded by the Ministry of Science and Higher Education of the Russian Federation, Project “Fundamental properties of elementary particles and cosmology” N 0723-2020-0041 and RFBR grant 19-02-00930. The work of S.R. is performed according to the Russian Government Program of Competitive Growth of Kazan Federal University.

## References

1. A. Ayala, J. Jalilian-Marian, L. D. McLerran, and A. P. Vischer. Scattering in the presence of electroweak phase transition bubble walls. *Phys. Rev. D*, 49:5559–5570, 1994.
2. K. M. Belotsky, V. I. Dokuchaev, Y. N. Eroshenko, E. A. Esipova, M. Y. Khlopov, L. A. Khromykh, A. A. Kirillov, V. V. Nikulin, S. G. Rubin, and I. V. Svadkovsky. Clusters of primordial black holes. *Eur. Phys. J. C*, 79(3):246, 2019.
3. B. Carr and F. Kuhnel. Primordial Black Holes as Dark Matter: Recent Developments. 6 2020.
4. S. Clesse and J. García-Bellido. Seven Hints for Primordial Black Hole Dark Matter. *Phys. Dark Univ.*, 22:137–146, 2018.
5. H. Deng, A. Vilenkin, and M. Yamada. CMB spectral distortions from black holes formed by vacuum bubbles. *JCAP*, 07:059, 2018.
6. G. R. Farrar and J. McIntosh, John W. Scattering from a domain wall in a spontaneously broken gauge theory. *Phys. Rev. D*, 51:5889–5904, 1995.
7. A. Kashlinsky et al. Electromagnetic probes of primordial black holes as dark matter. 3 2019.
8. P. Kennedy. The Woods-Saxon potential in the Dirac equation. *J. Phys. A*, 35:689–698, 2002.
9. O. Panella, S. Biondini, and A. Arda. New exact solution of the one dimensional Dirac Equation for the Woods-Saxon potential within the effective mass case. *J. Phys. A*, 43:325302, 2010.
10. R. Rajaraman. *Solitons and instantons. An introduction to solitons and instantons in quantum field theory*. 1 1982.
11. S. G. Rubin, A. S. Sakharov, and M. Y. Khlopov. The Formation of primary galactic nuclei during phase transitions in the early universe. *J. Exp. Theor. Phys.*, 91:921–929, 2001.
12. D. A. Steer and T. Vachaspati. Domain walls and fermion scattering in grand unified models. *Phys. Rev. D*, 73:105021, May 2006.
13. A. Vilenkin and E. S. Shellard. *Cosmic Strings and Other Topological Defects*. Cambridge University Press, 7 2000.
14. Y. B. Zel’dovich and I. Novikov. The hypothesis of cores retarded during expansion and the hot cosmological model. *Soviet Astronomy*, 10:602, 1967.



## 12 Cosmological Accumulation of Conserved Numbers in Kaluza-Klein Theories

V.V. Nikulin \*

National Research Nuclear University MEPHI

**Abstract.** We develop a new mechanism for the accumulation of conserved numbers in the early Universe in Kaluza-Klein-like theories. The relaxation of the primordial extra space perturbations existing in the early Universe leads to the establishment of a symmetric final state and the appearance of Killing vectors. As a result, the initial non-zero value of symmetry associated numbers occurs after the inflation. We show this conceptual idea on a toy model of 2-dimensional apple-like extra space with  $U(1)$  symmetry. This mechanism naturally arises in the Kaluza-Klein theories and can be used to explain the observed cosmological baryon asymmetry.

**Povzetek.** Avtor opiše zgodnje vesolje s teorijo Kaluze in Klaina v večrazsežnem zgodnjem vesolju. Predlaga nov mehanizem, ki poskrbi za akumulacijo števil, ki se ohranijo. Zmanjšanje perturbacij, ki jih povzročijo dodatne dimenzije, vodi v njegovem predlogu do simetričnega končnega stanja in ustreznih Killingovih vektorjev. Posledično se začetna neničelna vrednost števil, povezanih s simetrijo, pojavi po inflaciji. Avtor idejo pojasni na modelu 2-dimenzionalnega dodatnega prostora v obliki jabolka in s simetrijo  $U(1)$ . Njegov mehanizem pojasni opažene kozmološke asimetrije barionov.

Keywords: Kaluza-Klein theory, apple-shaped extra space, baryon asymmetry,  $f(R)$ -gravity, cosmological inflation.

PACS: 04.50.Cd, 04.50.+h, 04.50.-h, 04.50.Kd,  
11.30.Fs, 11.30.Ly, 11.30.-j

### 12.1 Introduction

One of the advantages of using Kaluza–Klein compact extra dimensions is that they can explain the origin of internal symmetry in particle physics. The idea of the approach is that the internal symmetry of the gauge theory is considered as a consequence of the geometric properties of compact extra space, characterized by the presence of Killing vector fields [2].

The stability of the compact extra space is the well-known issue of the Kaluza–Klein theory. The stabilization can usually be achieved by introducing external material fields [5] or by modifying action for gravity [4]. The process of stabilization obviously should take place in a very early Universe at the energy scales

\* E-mail: N-Valer@yandex.ru

$\sim 1/r_0$ , when  $r_0$  is the radius of compact extra space. In our work [13] we show how dramatically the presence of compact extra space can affect the cosmological inflationary process.

In this paper, we investigate the process of relaxation of the extra space metric during the cosmological inflation. As a result of symmetrization, Killing vector fields appears at the end of inflation and its Noether-associated numbers is asymptotically conserved. The initial non-zero value of this conserved numbers is caused by the extra metric perturbations that took place during inflation. This mechanism could be an explanation for the observed cosmological baryon asymmetry.

## 12.2 Theoretical description

Today we do not really understand how a compact extra space can be born in higher-dimensional theories. However, we have no reason to believe that its geometry has any symmetry, as this process is clearly random. As a result of further development, the metric of extra space undergoes relaxation and symmetrization. The deep causes for the inevitable appearance of symmetry in this process is related to the establishment of thermodynamic equilibrium and entropy growth [10].

### 12.2.1 Conserved numbers in Kaluza-Klein theory

We know that according to the Noether theorem symmetries lead to the conservation of associated numbers. In particular, for (extra) spatial symmetries, the conserved numbers can be interpreted as the physical (angular) moments carried by material fields along the corresponding Killing vectors [2, 6].

Spatial symmetry (extra spatial in our case) usually characterized by Killing vector field  $\xi^a(x)$ . It means that Lie derivative of the extra space metric along the Killing vector field  $L_\xi g_{d,mn} = 0$  and the metric stays invariant under the small shifts  $x_m \rightarrow x_m + \xi^m(x)$ . From to the Noether's theorem (see technical details in [2]) we get a conserved current associated with the invariance  $\partial_a J^a = 0$ . This current for any material field  $\chi$  is

$$J^a = \frac{\partial L_m(\chi)}{\partial(\partial_a \chi)} \xi^b \partial_b \chi - \xi^a L_m(\chi), \quad (12.1)$$

where  $L_m$  is a matter Lagrangian. The associated conserved number

$$Q = \int J^0 \sqrt{|g_4|} \sqrt{|g_d|} d^3x d^d y. \quad (12.2)$$

we can interpret as some component of (angular) momentum. Until the extra metric reaches a symmetrical final configuration, this number will not be conserved ( $Q = Q(t)$ ). The number will accumulate over time, until the relaxation processes stop. We need to simulate the extra metric and scalar field evolution to the final stable state in order to calculate the value of the accumulated number.

**12.2.2 Gravitational dynamics of compact space**

Consider as a final result of the stabilization a compact 2–dim apple–like extra space. This configuration is stationary as was shown in the works [3, 14]. It has rotational symmetry which we interpret (in 4–dim limit) as U(1) global symmetry with the associated conserved number. In contrast to the one-dimensional circular extra space (which have zero Ricci scalar [15]) our configuration can lose the symmetry in early high-energetic Universe due to the metric perturbations.

To stabilize the considered extra space, the modified f(R)–gravity is used. First, the higher-dimensional action is taken in the form

$$S = \frac{m_D^{D-2}}{2} \int d^D Z \sqrt{|G|} [f(R) + L_m], \quad f(R) = \alpha R^2 + R + c. \quad (12.3)$$

Here  $D = d + 4$ ,  $m_D$  is fundamental D–dimensional Planck mass and  $L_m$  is a matter Lagrangian. A conserved number is accumulated in material fields during the stabilization of extra space. We will consider the simplest case of matter — massive scalar field:

$$L_m = \frac{1}{2} G^{MN} \partial_M \chi \partial_N \chi - V(\chi), \quad V(\chi) = \frac{1}{2} m^2 \chi^2. \quad (12.4)$$

Consider a  $D = d + 4$ –dimensional manifold with metric

$$ds^2 = G_{MN} dZ^M dZ^N = g_{\mu\nu}(x) dx^\mu dx^\nu + g_{d,mn}(x, y) dy^m dy^n, \quad (12.5)$$

here the metrics  $g_{\mu\nu}(x)$  and  $g_{d,mn}(x, y)$  corresponds to the  $M_4, K$  subspaces respectively. We will consider  $M_4$  as a common 4–dim space and  $K$  as  $d$ –dim compact extra space. The signature of D-dim metric is (+ - - ...) and the Greek indices  $\mu, \nu = 0, 1, 2, 3$  refer to common 4–dim coordinates. Latin indices  $m, n = 4, \dots, d + 3$  refer to the extra coordinates. We will use the following conventions for the Riemann tensor:  $R^D_{ABC} = \partial_C \Gamma^D_{AB} - \partial_B \Gamma^D_{AC} + \Gamma^D_{EC} \Gamma^E_{BA} - \Gamma^D_{EB} \Gamma^E_{AC}$  and for the Ricci tensor  $R_{MN} = R^A_{MAN}$ . We also use unit system  $\hbar = c = 1$ .

A time evolution of the metric  $G_{MN}(x, y)$  is determined by the f(R) Einstein’s equations and depends on initial conditions. The dissipation of energy into the 4-dim part of space  $M_4$  leads to the decrease of entropy in the compact part of space  $K$ , as was shown in [10]. As a result, a friction term appears, which stabilizes the extra metric  $g_{d,mn}(x, y)$ . In addition, the inflationary expansion strongly smooths inhomogeneity of 4-dim space:

$$g_{d,mn}(x, y) \xrightarrow{t \rightarrow \infty} g_{d,mn}(t, y). \quad (12.6)$$

Time evolution of the extra space was discussed within the Einstein’s gravity and Kaluza–Klein cosmology framework [1]. If a gravitational action has nonlinear Ricci scalar terms – f(R), the extra metric  $g_{d,mn}$  have asymptotically stationary configurations [4, 10]:

$$g_{d,mn}(t, y) \rightarrow g_{d,mn}(y). \quad (12.7)$$

See [5, 11] for more information.

For simplicity, we can assume that 4-dim space has just de-Sitter metric during inflation

$$g_{\mu\nu} = \text{diag}(1, -e^{2Ht}, -e^{2Ht}, -e^{2Ht}), \quad (12.8)$$

where  $H$  is inflationary Hubble parameter. The dynamics of inflaton field is not considered here.

To find the stationary configurations of extra space we will use the  $f(R)$  Einstein equations:

$$R_{MN}f' - \frac{1}{2}f(R)g_{d,MN} + \nabla_M \nabla_N f' - g_{d,MN} \square f' = \frac{1}{m_D^{D-2}} T_{MN}. \quad (12.9)$$

Here  $\square$  is the d'Alembertian

$$\square = \frac{1}{\sqrt{|G|}} \partial_M (G^{MN} \sqrt{|G|} \partial_N). \quad (12.10)$$

And the contribution of matter is determined by stress-energy tensor  $T_{MN}$ :

$$T_{MN} = -2 \frac{\partial L_m}{\partial G^{MN}} + G_{MN} L_m. \quad (12.11)$$

We assume that postulated 4-dim part of metric  $g_{\mu\nu}$  (12.8) satisfies the higher-dimensional Einstein equations. Next, we will assume that scalar field only depends only on the extra coordinates. It is a result of smoothing out the inhomogeneities of the 3-dim space during inflation. Equation of motion for scalar field  $\chi(x, y) = \chi(y)$  is

$$\square_d \chi = -V'(\chi), \quad (12.12)$$

where  $\square_d$  is extra dimensional part of d'Alembertian.

The very end of the process of forming a compact extra space can be considered as the relaxation of small perturbations of the metric over a stable symmetric vacuum configuration.

## 12.3 Numerical simulation

### 12.3.1 Vacuum stationary configuration

As a compact extra space (12.6), we take a 2-dimensional sphere-like manifold with the metric

$$g_{2,mn} = \begin{pmatrix} -r^2 e^{2\beta(t,\theta,\phi)} & 0 \\ 0 & -r^2 e^{2\beta(t,\theta,\phi)} \sin^2 \theta \end{pmatrix}. \quad (12.13)$$

where  $r$  is characteristic radius of the compact space and the  $\beta(t, \theta, \phi)$  is the parameterization function for extra geometry.

To begin with, we will find a vacuum stationary symmetric configuration, which will be the final stage in the evolution of extra space  $\beta(t, \theta, \phi) = \beta_{st}(\theta)$  and for the scalar field  $\chi(t, \theta, \phi) = \chi_{st}(\theta)$ . The extra metric has rotational  $U(1)$  symmetry associated the presence of Killing vector. The Killing vector field is

directed along the polar coordinate  $\phi$ . The Noether number associated with this  $U(1)$  symmetry can be interpreted as the internal polar angular momentum. A similar configuration is used for example in [3].

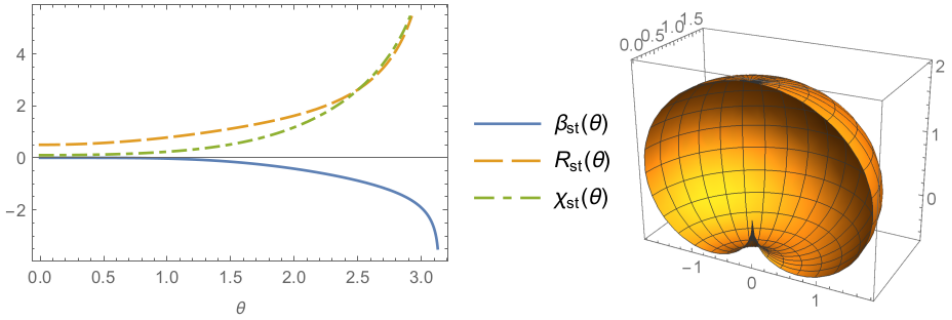


Fig. 12.1: A typical result of modeling a stationary configuration satisfying the  $f(R)$  Einstein equations (12.9). On the left: plot of the geometry parameterization function  $\beta_{st}$ , the scalar curvature  $R_{st}$  and the material scalar field  $\chi_{st}$  on the azimuthal angle  $\theta$  of compact space. On the right: visualisation of the final "apple-shape" stationary configuration of compact 2-dim manifold with metric (12.13).

### 12.3.2 Symmetrization process

Further, to consider the final stage of the relaxation process, we will simulate small perturbations of the metric parameter, scalar curvature, and material scalar field over the stable symmetric state calculated in the last paragraph:

$$\begin{aligned} \beta(t, \theta, \phi) &= \beta_{st}(\theta) + \delta\beta(t, \theta, \phi), & \delta\beta(t, \theta, \phi) &\ll \beta_{st}(\theta), \\ R(t, \theta, \phi) &= R_{st}(\theta) + \delta R(t, \theta, \phi), & \delta R(t, \theta, \phi) &\ll R_{st}(\theta), \\ \chi(t, \theta, \phi) &= \chi_{st}(\theta) + \delta\chi(t, \theta, \phi), & \delta\chi(t, \theta, \phi) &\ll \chi_{st}(\theta). \end{aligned} \tag{12.14}$$

By linearizing the Einstein's equations (12.9), and solving it [12] for natural random initial conditions, we obtain damped oscillations, which are shown in Fig.12.2. The dumping occurs for all angles  $\theta$  which shows the stability of the resulting configuration. This is due to the friction term commonly generated in the de Sitter space. The latter leads to the final stabilization to the  $U(1)$  symmetric extra space configuration.

### 12.3.3 Initial accumulation of $U(1)$ number

After the end of the relaxation processes shown in the previous subsection, a symmetric  $U(1)$  configuration is achieved. The  $U(1)$ -number associated with the

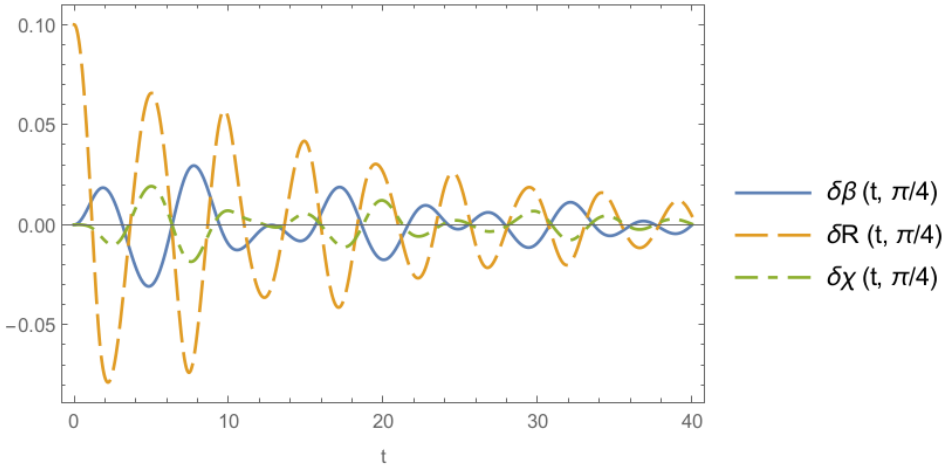


Fig. 12.2: A typical evolution of perturbations  $\delta\beta$ ,  $\delta R$ ,  $\delta\chi$  over the stable solution calculated in previous paragraph. As an example, the behavior of the polar mode  $n = 2$  is shown (standing wave along  $\phi$  coordinate). Oscillations are taken at a point  $\theta = \pi/4$ , at other points damping behaves similarly.

Noether theorem (12.2) will now be conserved. But in this section we are interested in how this number  $Q$  could have accumulated initially, until the end of the relaxation and symmetrization processes. The perturbed solutions simulated earlier allow us to compute  $Q(t)$  number. In the accompanying volume we get (from (12.2),(12.5),(12.14)):

$$\begin{aligned}
 Q(t) &= \int \partial^0 \chi \partial_\phi \chi r^2 e^{2\beta} \sin \theta d\theta d\phi = \\
 &= \int \partial^0 \delta\chi(t, \theta, \phi) \partial_\phi \delta\chi(t, \theta, \phi) r^2 e^{2(\beta_{st}(\theta) + \delta\beta(t, \theta, \phi))} \sin \theta d\theta d\phi.
 \end{aligned}
 \tag{12.15}$$

The end of inflationary process have very rapid transition to the reheating stage via the violation of the slow-roll conditions. Due to this the extra metric is quickly symmetrized (for  $H \lesssim 1/r$  extra space perturbations are rapidly suppressed), while the scalar field go into the oscillating mode. After the inflation, stationary extra metric  $\beta(t, \theta, \phi) = \beta_{st}(\theta)$  give us the equation of motion for matter (12.12) with nonperturbed symmetrical d'Alambertian. As a result, Noether's theorem starts to be fulfilled and  $Q$  ceases to depend on time. Traveling waves of the scalar field, carrying an internal angular momentum is now permanently enclosed inside extra space, since the number  $Q$  is now conserved. The initially accumulated  $Q(t)$  will now remain unchanged. The Universe enters the hot stage with a nonzero initial value of  $U(1)$  global conserved number.

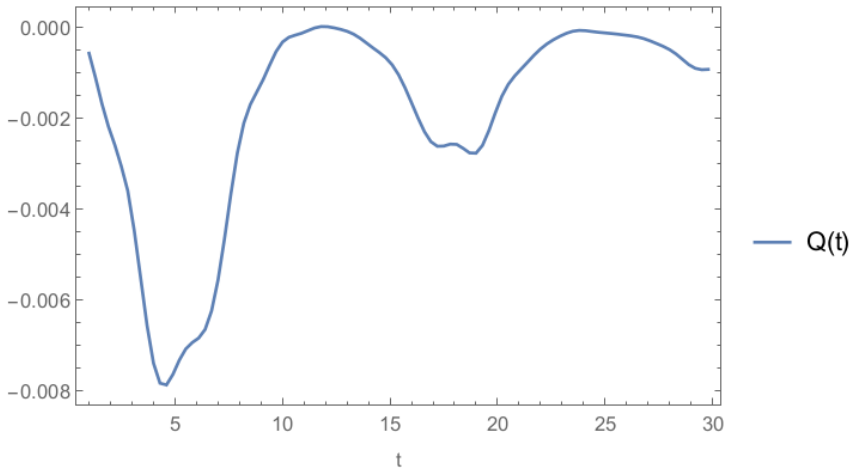


Fig. 12.3: Typical time evolution of the U(1) number  $Q(t)$  during the symmetrization of compact extra space. The number calculated numerically from (12.15).

## 12.4 Conclusion

In this research we show how the dynamics of compact extra space leads to a nonzero initial accumulation of some conserved number. Such gravitational dynamics of compact extra metric should naturally occur in the early ( $H \gg 1/r$ ) higher-dimensional Universe. The stabilization of the extra metric lead to a symmetrical stationary final configuration. We considered the case of a final U(1) rotationally symmetric state with corresponding conserved number.

Such an accumulation mechanism arising in Kaluza-Klein theories can be used to explain the origin of the cosmological baryon asymmetry [8,9]. It is known that the baryon number is described by the global U(1)-symmetry. In Kaluza-Klein theories it could be realized as the rotational symmetry of the 2-dim compact extra space (12.13). However, to transfer the baryon number, additional interaction term between the fermion and the scalar field is required (for details, see work [7]).

In future works, we plan to develop a Kaluza-Klein mechanism for transferring asymmetry into the fermions in order to explain specifically the cosmological baryon/lepton asymmetry.

## Acknowledgements

The work was supported by the Ministry of Science and Higher Education of the Russian Federation, Project "Fundamental properties of elementary particles and cosmology" No 0723-2020-0041.

## References

1. R. B. Abbott, S. M. Barr, and S. D. Ellis. Kaluza-Klein Cosmologies and Inflation. *Phys. Rev. D*, D30:720, 1984.

2. M. Blagojević, F. W. Hehl, and eds. *Gravitation and Gauge Symmetries*. Institute of Physics Publishing, Bristol, 2002.
3. K. A. Bronnikov, R. I. Budaev, A. V. Grobov, A. E. Dmitriev, and S. G. Rubin. Inhomogeneous compact extra dimensions. *Journal of Cosmology and Astroparticle Physics*, 10:001, 2017.
4. K. A. Bronnikov and S. G. Rubin. Self-stabilization of extra dimensions. *Phys. Rev. D*, 73(12):124019, 2006.
5. S. M. Carroll, J. Geddes, M. B. Hoffman, and R. M. Wald. Classical stabilization of homogeneous extra dimensions. *Phys. Rev. D*, 66(2):024036, 2002.
6. F. Cianfrani, A. Marrocco, and G. Montani. Gauge theories as a geometrical issue of a kaluza–klein framework. *International Journal of Modern Physics D*, 14(07):1195–1231, 2005.
7. A. Dolgov and J. Silk. Baryon isocurvature fluctuations at small scales and baryonic dark matter. *Phys. Rev. D*, 47:4244–4255, 1993.
8. A. D. Dolgov, M. Kawasaki, and N. Kevlishvili. Inhomogeneous baryogenesis, cosmic antimatter, and dark matter. *Nucl. Phys. B*, 807:229–250, 2009.
9. M. Y. Khlopov. Composite Dark Matter from 4-th Generation. *Pis'ma Zh. Ehksp. Teor. Fiz.*, 83:3–6, 2006.
10. A. A. Kirillov, A. A. Korotkevich, and S. G. Rubin. Emergence of symmetries. *Phys. Lett.*, B718:237–240, 2012.
11. S. Nasri, P. J. Silva, G. D. Starkman, and M. Trodden. Radion stabilization in compact hyperbolic extra dimensions. *Phys. Rev. D*, 66(4):045029, 2002.
12. V. V. Nikulin, P. M. Petriakova, and S. G. Rubin. Formation of conserved charge at the de sitter space. *Particles*, 3(2):355–363, 2020.
13. V. V. Nikulin and S. G. Rubin. Inflationary limits on the size of compact extra space. *International Journal of Modern Physics D*, 28(13):1941004, 2019.
14. S. G. Rubin. Cosmology and matter-induced branes. *Symmetry*, 12(1):45, 2020.
15. U. Sarkar. *Particle and Astroparticle physics*. CRC Press, 2007.



## 13 Sub-Planckian Evolution of the Universe

P.M. Petriakova \*

National Research Nuclear University MEPhI,  
115409, Kashirskoe shosse 31, Moscow, Russia

**Abstract.** The dynamics of a space endowed by a metric of a 3-dimensional sphere in the framework of  $f(R)$ -gravity acting in  $D = 4$  from the creation at high energies is studied.

**Povzetek.** Avtorica obravnava, v okviru  $f(R)$  gravitacije v  $D = 4$ , dinamiko prostora z metriko 3-razsežne sfere pri visokih energijah.

Keywords: three-dimensional sphere, Starobinsky model,  $f(R)$ -gravity, modified gravity.

### 13.1 Introduction

Despite the fact that we live in the era of observational cosmology and have experimental data with very good accuracy, there are a huge number of models that can satisfy the modern data, but use completely different approaches and ideologies. This is especially relevant to issues of the very early Universe: from creation to the end of inflationary stage.

The inflationary scenario firstly was detailed by Starobinsky [1], Guth [2] and after by Linde [3] and Albrecht with Steinhardt [4]. The Starobinsky model is based on gravity with added the quadratic term of scalar curvature and it is interesting that the use of such a term may be motivated by conformal anomaly considerations. In this theory the Friedmann equation is modified for large values of the Hubble parameter which leads to a cosmological solution with a scale factor growing exponentially during a certain period of evolution. This model also has a post inflationary heating up mechanism. As result of the evolution the Universe enters a hot stage. The modified gravity description of cosmological evolution of our Universe is one physically appealing theoretical framework. It can explain the various evolution eras due to providing a unified and theoretically consistent description. There exist a huge number of modified gravity models, see for example reviews [5] and [6], that can potentially describe evolution of our Universe. The most important criteria for the viability of a modified gravity theory is the compatibility of the theory with modern observations. The simplest, but being particularly favoured by present observations [7], model of the modified

---

\* E-mail: petriakovapolina@gmail.com

theory of gravity is the Starobinsky model. This model is quite successful. However, it describes evolution starting from a certain energy scale. In this paper it is proposed to study the dynamics of a three-dimensional sphere at energy scales exceeding the inflationary using  $f(R)$ -gravity with  $R^2$ -term.

We should note that many modified theories based on the consideration of a purely gravitational Lagrangian also fit into the available observable data. The tensor-to-scalar ratio in the Planck compatible region and the role of higher order curvature term for stability and the reheating dynamics for the unambiguous prediction for the number of e-foldings up to the  $R^3$ -term are discussed in [8]. Satisfying observable data, as works [9], [10] and [11] demonstrate, possible using a completely different approach: to study pure multidimensional gravity with higher derivatives. An issues of inflation model in the case of supergravity can also be found in the following works [12], [13] and [14].

### 13.2 Basic equations and initial conditions

Let us consider the theory described by the action

$$S[g_{\mu\nu}] = \frac{1}{2} M_{\text{Pl}}^2 \int d^4x \sqrt{|\det g_{\mu\nu}|} f(R). \quad (13.1)$$

The corresponding equations of motion are as follows

$$f'_R(R) R_{\mu\nu} - \frac{1}{2} f(R) g_{\mu\nu} + [\nabla_\mu \nabla_\nu - g_{\mu\nu} \square] f'_R(R) = 0, \quad \square \equiv g^{\mu\nu} \nabla_\mu \nabla_\nu. \quad (13.2)$$

Throughout this paper we use the conventions for the curvature tensor  $R^L_{MKN} = \partial_K \Gamma^L_{MN} - \partial_N \Gamma^L_{MK} + \Gamma^L_{AK} \Gamma^A_{NM} - \Gamma^L_{AN} \Gamma^A_{MK}$  and the Ricci tensor is defined as  $R_{MN} = R^K_{MKN}$ .

Taking into account the choice of the metric of a sphere

$$ds^2 = dt^2 - e^{2\alpha(t)} \left( dx^2 + \sin^2 x dy^2 + \sin^2 x \sin^2 y dz^2 \right) \quad (13.3)$$

we obtain the system of equations

$$\begin{cases} 6\dot{\alpha}(t)\dot{R}(t)f''_R(R) - 6\left(\ddot{\alpha}(t) + \dot{\alpha}^2(t)\right)f'_R(R) + f(R) = 0, \\ 2\dot{R}^2(t)f'''_R(R) + 2\left(\ddot{R}(t) + 2\dot{\alpha}(t)\dot{R}(t)\right)f''_R(R) - \\ - \left(2\ddot{\alpha}(t) + 6\dot{\alpha}^2(t) + 4e^{-2\alpha(t)}\right)f'_R(R) + f(R) = 0 \end{cases} \quad (13.4)$$

where the definition of the Ricci scalar for the used metric (13.3) is

$$R(t) = 12\dot{\alpha}^2(t) + 6\ddot{\alpha}(t) + 6e^{-2\alpha(t)}. \quad (13.5)$$

With the choice of the type of the  $f(R)$ -function as

$$f(R) = aR^2 + bR + c \quad (13.6)$$

the definition of the Ricci scalar (13.5) and the second equation of the system (13.4) with assumption (13.6) give us

$$\left\{ \begin{array}{l} \ddot{\alpha}(t) = -2\dot{\alpha}^2(t) - e^{-2\alpha(t)} + \frac{1}{6}R(t), \\ \ddot{R}(t) = -2\dot{\alpha}(t)\dot{R}(t) - \frac{1}{12}R^2(t) + \left(\dot{\alpha}^2(t) + e^{-2\alpha(t)} - \frac{b}{6a}\right)R(t) + \\ \quad + \frac{b}{2a}\dot{\alpha}^2(t) + \frac{b}{2a}e^{-2\alpha(t)} - \frac{c}{4a}. \end{array} \right. \quad (13.7)$$

After replacing  $\ddot{\alpha}(t)$  from (13.5) in the first equation (13.4) we get

$$R^2(t) - 12\left(\dot{\alpha}^2(t) + e^{-2\alpha(t)}\right)R(t) - 12\dot{\alpha}(t)\dot{R}(t) - \frac{6b}{a}\left(\dot{\alpha}^2(t) + e^{-2\alpha(t)}\right) - \frac{c}{a} = 0. \quad (13.8)$$

This expression for  $R^2(t)$  and the first equation of the system (13.7) allow us to obtain the equation of damped harmonic oscillations

$$\ddot{R}(t) + 3\dot{\alpha}(t)\dot{R}(t) + \frac{b}{6a}R(t) + \frac{c}{3a} = 0. \quad (13.9)$$

As well the same result follows from taking the trace of the system (13.2). The different modes of the solution of this equation are possible for a certain ratio between the values  $1.5\dot{\alpha}^2(t)$  and  $b/6a$ . The solution is damped oscillations under the condition  $1.5\dot{\alpha}^2(t) < b/6a$  and when this regime occurs the scalar curvature oscillations begin. Otherwise, the solution is aperiodic. The arising curvature oscillations lead to a slowdown in the growth of the value of the function  $\alpha(t)$ , i.e. the size of a sphere.

We have a system of second-order equations (13.7) in the chosen theory. It is necessary to determine the initial conditions for the values of the unknown functions  $\alpha(t)$  and  $R(t)$  and their derivatives.

Let it be given by constant

$$\alpha(0) \equiv \alpha_0, \quad \dot{\alpha}(0) \equiv \alpha_1, \quad R(0) \equiv R_0, \quad \dot{R}(0) \equiv R_1. \quad (13.10)$$

After solving the previously obtained equation (13.8) we find an expression for the function  $R(t)$  at the initial time depending on the value of other initial conditions and the parameters of the chosen  $f(R)$ -function:

$$R_0 = 6(\alpha_1^2 + e^{-2\alpha_0}) \pm \sqrt{36(\alpha_1^2 + e^{-2\alpha_0})^2 + \left(12\alpha_1 R_1 + \frac{6}{a}(\alpha_1^2 + e^{-2\alpha_0}) + \frac{c}{a}\right)}. \quad (13.11)$$

We are interested in the dynamics of a sphere starting from the sub-Planck scale. Therefore, the initial conditions on the function  $\alpha(t)$  will be near the value of the Hubble parameter at this moment

$$\alpha_0 \sim \ln H_{\text{sub-Planck}}^{-1}, \quad \alpha_1 \sim H_{\text{sub-Planck}}, \quad H_{\text{sub-Planck}} \sim 0.1. \quad (13.12)$$

Let us discuss the influence of the parameters of the  $f(R)$ -function. The value of the coefficient  $a$  allows us to adjust the moment of onset of the scalar curvature

oscillations due to mentioned  $1.5 \dot{\alpha}^2(t) < b/6a$  relation. Thus, if we want to significantly increase the size of a sphere we should have

$$a \gg \frac{2b}{27\alpha_1^2} \Big|_{b=1} \sim 10 \quad (13.13)$$

assuming the value of the coefficient  $b = 1$  without loss of generality and defining the value of  $\alpha_1$  as (13.12).

The last coefficient  $c$  in (13.6) remained undefined and we will look at the asymptotic behavior to restrict it. On the asymptotics the curvature scalar should tend to a constant  $R \rightarrow \text{const} \equiv R_c$  and following the definition (13.5) to the standard relation  $R_c = 12H_{\text{Present}}^2$  due to modern acceleration of the Universe. Then the equations of motion (13.2) at the constant scalar curvature after taking the trace are reduced to the algebraic equation

$$f'_R(R_c)R_c - 2f(R_c) = 0. \quad (13.14)$$

Solving this equation (13.14), we obtain the value of the scalar curvature on the asymptotics  $R_c = -2c$ . Therefore, we immediately come to the conditions for the value of the coefficient:  $c \sim H_{\text{Present}}^2$  and  $c < 0$ . The size of a sphere on the asymptotics will be determined from (13.5) as

$$R_c > 0 : e^{2\alpha(t)} = \frac{6}{R_c} \left| 1 + C_1 e^{t\sqrt{\frac{|R_c|}{3}}} + C_2 e^{-t\sqrt{\frac{|R_c|}{3}}} \right|, \quad (13.15)$$

$$R_c < 0 : e^{2\alpha(t)} = \frac{6}{|R_c|} \left| 1 + C_1 \cos\left(t\sqrt{\frac{|R_c|}{3}}\right) + C_2 \sin\left(t\sqrt{\frac{|R_c|}{3}}\right) \right| \quad (13.16)$$

Due to the smallness of the value  $H_{\text{Present}} \sim 10^{-61}$  at the present epoch and as consequence the last term in (13.6) we almost obtain the Starobinsky inflation model. Of course, the values of the coefficients can differ significantly at high energies, but we do not know the exact dependence of their values on the energy scale. We are going to study the dynamics of space with a fixed set of parameter values to start calculations from the sub-Planck energy scale for Starobinsky model in next section.

### 13.3 Results

Firstly, we will discuss the exact solution of the Starobinsky model. The only parameter of this model  $a = 1/6m^2$  is defined as  $m/m_{\text{Pl}} \sim 10^{-5}$  [15] and initial conditions (13.10) in this case are determined by the value of the inflationary Hubble parameter  $H_{\text{Infl}} \sim 10^{-6}$  as

$$\alpha_0 \sim \ln H_{\text{Infl}}^{-1}, \quad \alpha_1 \sim H_{\text{Infl}}, \quad R_1 = 0 \xrightarrow{(13.11)} R_+(0) = 2.9 \cdot 10^{-11}. \quad (13.17)$$

The numerical solution of the system (13.7) with given initial conditions (13.17) leads to the correctly dynamics at the inflationary and post-inflationary stages and

presented on the Fig.13.1. We see that curvature oscillations lead to a slowdown in the growth of  $\alpha(t)$ . All relevant quantities, such as: the size of a sphere  $\alpha(t)$ , the duration of the inflationary stage  $t \sim 10 \cdot 10^7$  (the beginning of the curvature  $R(t)$  oscillations) the amplitude of this oscillations, the value of the Hubble parameter i.e.  $\dot{\alpha}(t)$  are in accordance with the predictions of inflation theory and experimental data.

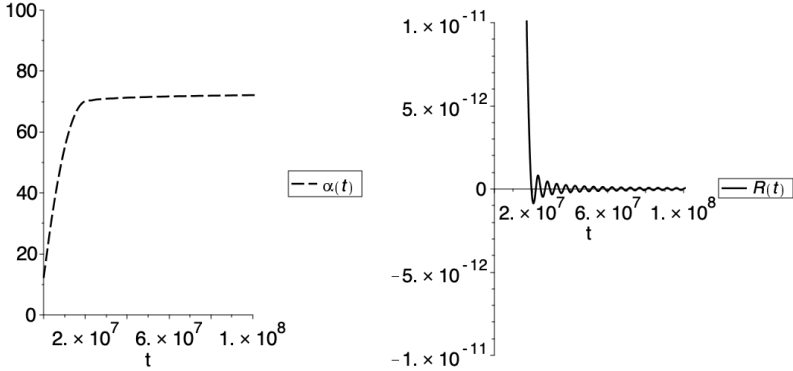


Fig. 13.1: Solution the system (13.7) with the initial conditions (13.17).

Let's continue the construction of the numerical solution up to age of the Universe  $t_{Univ} \sim 10^{61}$ . Then we get  $R(t_{Univ}) \sim 10^{-122}$ ,  $\dot{\alpha}(t_{Univ}) \sim 10^{-61}$  and ratio of sizes

$$\frac{l_{Starobinsky}}{l_{Visible}} = \frac{e^{\alpha(t_{Univ})}}{10^{61}} \sim 10^5. \tag{13.18}$$

A fundamental observational result of recent years is the fact that the spatial curvature of our Universe is very small. The main source of this fact is the study of the temperature anisotropy of the Cosmic Microwave Background (CMB). It means, at the qualitative level, that the radius of spatial curvature is much greater than the size of the observable part of the Universe, i.e. much greater than  $H_{Present}^{-1}$ . Following the fact that a topology significantly differently than Euclidean is not observed [17] obtained value (13.18) can be insufficient.

Let us solve numerically the system of equations (13.7) starting from sub-Planck energies with initial conditions (13.11) and (13.12). The result for the case of a three-dimensional sphere is shown on the left side of Fig.13.2.

We see that the principal difference with Starobinsky model is the size of the sphere formed by the end of the inflationary stage. Since we significantly (by 5 orders) change the energy scale in the initial conditions  $H_{Sub-Planck} \sim 10^5 H_{Infl}$ , we should check how an insignificant change in the only parameter of the model  $m$  will affect to the solution. We get a strong dependence on it, and it is shown on the right side of Fig.13.2. After continuing the construction of the numerical solution up to age of the Universe we get again on the asymptotic behavior correct

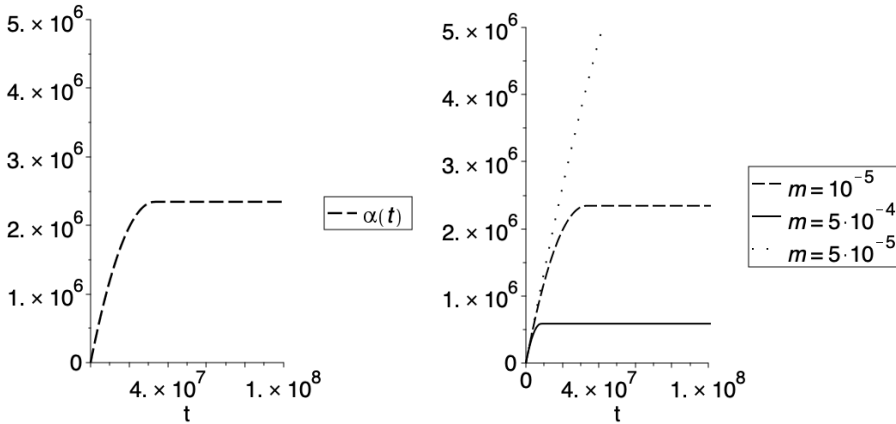


Fig. 13.2: Left side: solution the (13.7) system with the initial conditions (13.11), (13.12) and  $a = 1/6m^2$ ,  $m/m_{pl} \sim 10^{-5}$ ,  $c = -10^{-122}$ ; Right side: dependence on the coefficient  $a$  with similar (13.11), (13.12) conditions.

values  $R(t_{Univ}) \sim 10^{-122}$ ,  $\dot{\alpha}(t_{Univ}) \sim 10^{-61}$  and ratio of sizes

$$\frac{l_{\text{Starobinsky}}^{\text{sub-Planck}}}{l_{\text{Visible}}} = \frac{e^{\alpha(t_{Univ})}}{10^{61}} \sim 10^{10^{5 \div 6}}. \tag{13.19}$$

It should be noted that the growth of the sphere does not stop, but it significantly slows down on the asymptotics due to the smallness of the derivative  $\dot{\alpha}_{\text{asympt}}(t)$ . In the future, we must check that the dynamics started with high energies  $H_{\text{sub-Planck}} \sim 10^{18}\text{GeV}$  goes through the inflationary stage with all the necessary consequences.

### 13.4 Conclusion

In this work the dynamics of a three-dimensional sphere was studied in the framework of the simplest  $(R^2 + R)$  gravity. As a result starting from the sub-Planck energy scale we get the possibility to obtain space of no less than the visible part of the Universe even starting with such a small size of a sphere  $\alpha_0 \sim 2.3$  following (13.12). The next step is to study other types of modified gravity models and the effect of initial conditions on the asymptotic behavior of dynamics of space/sub-space. In future work, we are going to apply this approach in the framework of multidimensional gravity with higher derivatives and study more complex metrics in this way. The aim is to find conditions which lead to the large size of main space and small size of an extra dimensions.

### Acknowledgements

I would like to thank Prof. Maxim Yu. Khlopov for the opportunity to give a student talk at the 23rd Virtual Workshop "What Comes Beyond the Standard

Models". I am also grateful to Prof. Sergey G. Rubin for useful discussions with valuable suggestions and Prof. Arkadiy A. Popov for help. The work was supported by the Ministry of Science and Higher Education of the Russian Federation, Project "Fundamental properties of elementary particles and cosmology" N 0723-2020-0041.

## References

1. A. A. Starobinsky: A new type of isotropic cosmological models without singularity, *Phys. Lett. B* **91**, 99 (1980).
2. A.H. Guth: The Inflationary Universe: A Possible Solution to the Horizon and Flatness Problems, *Phys. Rev. D* **23**, 347 (1981).
3. A.D. Linde: A New Inflationary Universe Scenario: A Possible Solution of the Horizon, Flatness, Homogeneity, Isotropy and Primordial Monopole Problems, *Phys. Lett. B* **108**, 389 (1982).
4. A. Albrecht and P.J. Steinhardt: Cosmology for Grand Unified Theories with Radiatively Induced Symmetry Breaking, *Phys. Rev. Lett.* **48**, 1220 (1982).
5. Sh. Nojiri, S. D. Odintsov: Unified cosmic history in modified gravity: from  $F(R)$  theory to Lorentz non-invariant models, *Phys. Rept.* **505**, 59 (2011).
6. Sh. Nojiri, S. D. Odintsov: Modified Gravity Theories on a Nutshell: Inflation, Bounce and Late-time Evolution, *Phys.Rept.* **692** 1 (2017).
7. Planck Collaboration: Y. Akrami et al.: Planck 2018 results. X. Constraints on inflation, *Astron. and Astrophys.* **641**, A10 (2020).
8. Dh. Y. Cheong, S. Ch. Park: Beyond the Starobinsky model for inflation, *Phys. Lett. B*, **805**, 135453, (2020).
9. K. A. Bronnikov, S. G. Rubin, I. V. Svadkovsky: Multidimensional world, inflation and modern acceleration, *Phys. Rev. D* **81**, 084010 (2010).
10. S. V. Ketov, H. Nakada: Inflation from  $(R + \gamma R^n - 2\Lambda)$  Gravity in Higher Dimensions, *Phys. Rev. D* **95**, 103507 (2017).
11. J. C. Fabris, A. A. Popov, S. G. Rubin: Multidimensional gravity with higher derivatives and inflation, *Phys. Lett. B*, **808**, 135458, (2020).
12. S. V. Ketov, A. A. Starobinsky: Inflation and non-minimal scalar-curvature coupling in gravity and supergravity, *JCAP* **08**, 022 (2012).
13. S. V. Ketov, M. Yu. Khlopov: Extending Starobinsky inflationary model in gravity and supergravity, *Bled Workshops in Physics*, **19**, 148 (2018).
14. A. Addazi, M. Yu. Khlopov: Dark Matter and Inflation in  $R + \zeta R^2$  Supergravity, *Phys. Lett. B* **766**, 17 (2017).
15. Th. Faulkner, M. Tegmark, E. F. Bunn, Yi Mao: Constraining  $f(R)$  Gravity as a Scalar Tensor Theory, *Phys. Rev. D* **76**, 063505 (2007).
16. S. G. Rubin, A. A. Popov, P. M. Petriakova: Gravity with higher derivatives in D-dimensions, *Universe*, **6(10)**, 187, (2020).
17. N. J. Cornish, D. N. Spergel, G. D. Starkman, E. Komatsu: Constraining the Topology of the Universe, *Phys. Rev. Lett.* **92**, 201302 (2004).
18. E. V. Arbuzova, A. D. Dolgov, R. S. Singh: Distortion of the standard cosmology in  $R + R^2$  theory, *JCAP*, **2018**, (2018).



## 14 The “Dark Disk” Model in the Light of DAMPE Experiment

M.L. Solovoyov \*, M.A. Rakhimova and K.M. Belotsky

National Research Nuclear University MEPhI (Moscow Engineering Physics Institute),  
115409, Kashirskoe shosse 31, Moscow, Russia

**Abstract.** There are a lot of models considering the Dark Matter (DM) to be the origin of cosmic ray (CR) positron excess. However, they face an obstacle in the form of gamma-rays. Simple DM models tend to overproduce gamma-rays, leading to contradiction with isotropic gamma-ray background (IGRB). The “dark disk” model has been proposed to alleviate this contradiction. This work considers results of DAMPE experiment in the framework of the disk model. It is obtained that such a framework allows improving data fit considerably.

**Povzetek.** Obstaja mnogo modelov temne snovi, pri katerih je temna snov izvor presežka pozitronov v kozmičnih žarkih. Večina teh modelov napove preveč žarkov gama, ki povzročijo neizotropno ozadje žarkov gama glede na opaženja. Avtorji predlagajo svoj model “temnega” diska, ki naj bi odpravil to neskladje. Obravnavajo rezultate poskusa DAMPE v okviru tega modela in ugotovijo, da se njihov model precej bolje ujema z meritvami.

**Keywords:** Cosmic rays, cosmic ray anomalies, dark matter, gamma-ray background, dark disk

### 14.1 Introduction

During the past decade, the anomalous behaviour of CR energy spectra was brought into the light. The positron excess, found by PAMELA [1] and confirmed by AMS-02 [2, 3], the “wide” and “peak-like” excesses in electron plus positron spectrum of recent DAMPE experiment [4, 5] are amongst the most well-known ones. The simple solutions seem to not work for these puzzles, as they remain unsolved.

There are plenty of models considering DM of different nature, and there is a great freedom in defining its properties. Therefore, it is quite easy to introduce a model with decaying or annihilating DM to account for the CR puzzles. And the possibility to probe for the new physics of the Dark Matter makes these models even more appealing.

\* E-mail: max07s@mail.ru

The main alternative to DM models involves the pulsars as the cause of the excesses. Recent works in this field face the constraints [6,7] from gamma-radiation observed around the pulsars. Though attempts to solve the problems in this way continue (e.g., [8]).

However, DM models are also subject to the constraints. One of them is set by the gamma-ray data [9]. Photons are inevitably produced in the process of DM particle decay or annihilation via the final state radiation (FSR) process. And simple halo-distributed DM models dedicated to CR anomaly description tend to overproduce gammas, resulting in contradiction to Isotropic Gamma-ray Background (IGRB) data provided by Fermi-LAT [10].

To resolve it, we develop the so-called "dark disk" model with unstable DM distributed in disk [11]. This assumption helps to exclude gamma-rays from the outer regions of DM halo, that can not make a contribution to the observable charged particles fluxes.

In our previous work, we have found the IGRB data to constrain the halo models even in the case of broad electron plus positron excess in DAMPE data [12]. In this work we try to apply the "dark disk" model to this case. Sec. 14.2 provides the model description, Sec. 14.3 contains the obtained results and everything is summed up in Sec. 14.4.

## 14.2 Initial settings

We consider DM particles with mass  $m_\chi = 1800$  GeV to be able to annihilate via 3 leptonic channels ( $e^+e^-$ ,  $\mu^+\mu^-$ ,  $\tau^+\tau^-$ ) which branching ratios along with annihilation cross section  $\langle\sigma v\rangle$  are the model parameters. For DM distribution, we use two density profiles:

- Read's profile [13]

$$\rho(r, z) = \rho_{0r} \exp\left(-\frac{r}{R_R}\right) \exp\left(-\frac{z}{z_c}\right) \quad (14.1)$$

- NFW profile [14] with cut-off along the z-axis

$$\rho(r, z) = \begin{cases} \frac{\rho_{0N}}{\left(\frac{r}{R_s} + 1\right)^2}, & z \leq z_c, \\ 0, & z > z_c \end{cases} \quad (14.2)$$

where  $r$  and  $z$  are coordinates in cylindrical coordinate system,  $z_c$  is the disk half-thickness,  $\rho_{0r} = 1.32 \text{ GeV cm}^{-3}$ ,  $\rho_{0N} = 0.25 \text{ GeV cm}^{-3}$ , which corresponds to the local DM density of  $0.4 \text{ GeV cm}^{-3}$ ,  $R_R = 6.96 \text{ kpc}$ ,  $R_s = 24 \text{ kpc}$ .

We use Pythia to calculate the initial spectra of electrons, positrons and gammas. The GALPROP code is used to propagate the first two of them and obtain

their near-Earth spectra, as well as the secondary gamma flux. The prompt radiation flux is obtained by

$$\Phi_{\text{prompt}}(E_\gamma) = \frac{dN_\gamma \langle \sigma v \rangle}{dE_\gamma 4} \times \frac{1}{\Delta\Omega} \int_0^{100 \text{ kpc}} \int_{20^\circ}^{90^\circ} \int_0^{2\pi} \frac{1}{4\pi r^2} \left( \frac{\rho}{M_\chi} \right)^2 r^2 \cos(\theta) dr d\theta d\phi, \quad (14.3)$$

where  $\frac{dN_\gamma}{dE_\gamma}$  is the gamma-ray spectrum per one act of annihilation,  $M_\chi$  is the mass of DM particle,  $\Delta\Omega$  is the solid angle ( $l \in [0; 2\pi]$ ,  $b \in [20^\circ; 90^\circ]$ ) corresponding to the region of the Fermi-LAT analysis.

We use the total  $e^+e^-$  background from [15], which was obtained as the best-fit background model for a variety of cosmic-ray data.

To obtain the values of branching ratios and the process cross-section, we minimize the following expression for  $\chi^2$ :

$$\chi^2 = d^{-1} \left[ \sum_{\text{DAMPE}} \frac{(\Delta\Phi_e)^2}{\sigma_e^2} + \sum_{\text{Fermi}} \frac{(\Delta\Phi_\gamma)^2}{\sigma_\gamma^2} H(\Delta\Phi_\gamma) \right]. \quad (14.4)$$

Here  $\Delta\Phi_i \equiv \Phi_i^{(\text{th})} - \Phi_i^{(\text{obs})}$ ,  $\Phi_i$  are the predicted (*th*) and measured (*obs*) fluxes for  $i = e, \gamma$  denoting  $e^+e^-$  or gamma points respectively,  $\sigma_i$  denotes the corresponding experimental errors and  $d$  denotes the number of statistical degrees of freedom, which includes all the relevant DAMPE and Fermi-LAT data points. The first sum in Eq. (14.4) goes over the DAMPE data points and the second sum goes over the Fermi-LAT data points. DAMPE points are taken in the range  $20 \div 1600$  GeV. Since we do not try to fit the gamma-ray data, but rather not to go over the experimental limits, the terms in the second sum are non-zero only when  $\Phi_\gamma^{(\text{th})} > \Phi_\gamma^{(\text{obs})}$ , which is ensured by the Heaviside step function  $H$ .

We use two different approaches for the minimization procedure. In first, called "combined fit", we just simply minimize expression 14.4. In the second, called "e-fit", we minimize only the first sum in the expression 14.4 and only after that, using the obtained parameters, we calculate total chi-square value.

### 14.3 Results

Fig. 14.1 illustrates the correlation between  $\chi^2$  values and the disk half-width.

In the case of "e-fit" the best results are obtained with  $z_c \approx 750$  pc. However, one can clearly see that the quality of fit is still not satisfactory at all, although still better than one for the thick disks and halo. On the other hand, "combined fit" gives much better results with the minimum of  $\chi^2$  of around 1.6 for the disk half-width in the range of  $1500 \div 2000$  pc. However, in the case of AMS-02 positron fraction best fits were obtained with  $z_c = 400$  pc. Unexpectedly, the NFW density profile with cut-off produces better results, than Read's profile, over the whole considered region. We suppose it to be due to higher production of low-energy electrons and positrons for NFW, which helps it to account for the lower energy

region of the spectra. The line in the graphics breaks are mainly caused by the change of degree-of-freedom number (as we dynamically calculate it to include only those Fermi-LAT datapoints, where we have the excess) and interpolation errors.

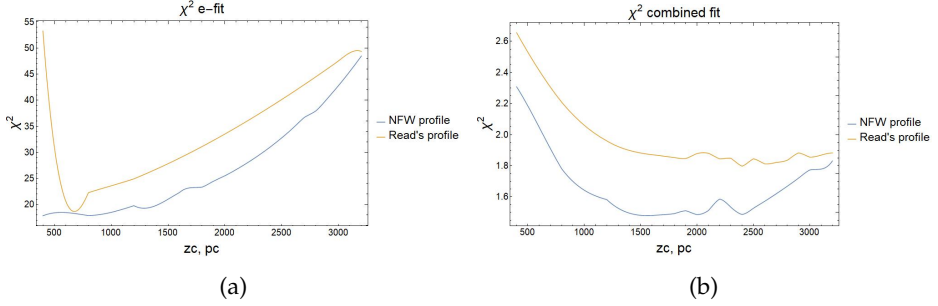


Fig. 14.1: Graphs for  $\chi^2$  values in dependence of the disk half-width in case of e-fit 14.1a and combined fit 14.1b. Blue line is used for NFW density profile, the orange one – for Read’s density profile.

Fit — Model	Halo	Disk
e-fit	203 (0.53)	17.85 (0.52)
combined fit	3.8 (2.1)	1.48 (1.20)

Table 14.1: The best-fit values of  $\chi^2$  for different DM models and approaches for the minimization procedure. The values in brackets are obtained using only electron-positron part of Eq. (14.4).

Table 14.1 contains the best-fit values of chi-square in contrast to the ones, obtained for the halo case. The comparison revealed that the dark disk model allows achieving the same accuracy in positron description, as the halo model, while giving less contradiction with IGRB. In both cases, combined fit improves the fit quality, but still not enough to overcome the discrepancy.

## 14.4 Conclusion

We continue our research of DM explanation of the CR puzzles. In this work, we have applied the “dark disk” model to the case of the wide excess of positrons plus electrons in DAMPE data. We have obtained that it helps to lessen the contradiction with cosmic gamm-ray data. However, it is achieved at the cost of thicker disk, compared to the case of low energy positron anomaly of AMS-02.

In our future works we plan to run such analysis for the different masses of initial particle, try different reaction modes and to attempt to describe AMS-02 and DAMPE data simultaneously.

## Acknowledgments

The work was supported by the Ministry of Science and Higher Education of the Russian Federation by project No 0723-2020-0040 “Fundamental problems of cosmic rays and dark matter”. Also we would like to thank R.Budaev, A.Kirillov and M.Laletin for their contribution at the early stage of this work.

## References

1. PAMELA collaboration, O. Adriani et al., *An anomalous positron abundance in cosmic rays with energies 1.5-100 GeV*, *Nature* **458** (2009) 607–609, [0810.4995].
2. AMS COLLABORATION collaboration, M. Aguilar, G. Alberti, B. Alpat, A. Alvino, G. Ambrosi, K. Andeen et al., *First result from the alpha magnetic spectrometer on the international space station: Precision measurement of the positron fraction in primary cosmic rays of 0.5-350 gev*, *Phys. Rev. Lett.* **110** (Apr, 2013) 141102.
3. AMS COLLABORATION collaboration, L. Accardo, M. Aguilar, D. Aisa, B. Alpat, A. Alvino, G. Ambrosi et al., *High statistics measurement of the positron fraction in primary cosmic rays of 0.5–500 gev with the alpha magnetic spectrometer on the international space station*, *Phys. Rev. Lett.* **113** (Sep, 2014) 121101.
4. J. Cao, X. Guo, L. Shang, F. Wang, P. Wu and L. Zu, *Scalar dark matter explanation of the DAMPE data in the minimal Left-Right symmetric model*, *Phys. Rev.* **D97** (2018) 063016, [1712.05351].
5. H.-B. Jin, B. Yue, X. Zhang and X. Chen, *Cosmic ray  $e^+e^-$  spectrum excess and peak feature observed by the DAMPE experiment from dark matter*, 1712.00362.
6. A. U. Abeysekara, A. Albert, R. Alfaro, C. Alvarez, J. D. Álvarez, R. Arceo et al., *Extended gamma-ray sources around pulsars constrain the origin of the positron flux at Earth*, *Science* **358** (Nov., 2017) 911–914, [1711.06223].
7. S.-Q. Xi, R.-Y. Liu, Z.-Q. Huang, K. Fang, H. Yan and X.-Y. Wang, *GeV observations of the extended pulsar wind nebulae challenge the pulsar interpretations of the cosmic-ray positron excess*, 1810.10928.
8. M. Linares and M. Kachelriess, *Cosmic ray positrons from compact binary millisecond pulsars*, *arXiv e-prints* (Oct., 2020) arXiv:2010.02844, [2010.02844].
9. K. Belotsky, R. Budaev, A. Kirillov and M. Laletin, *Fermi-LAT kills dark matter interpretations of AMS-02 data. Or not?*, *JCAP* **1701** (2017) 021, [1606.01271].
10. FERMI-LAT collaboration, M. Ackermann et al., *The spectrum of isotropic diffuse gamma-ray emission between 100 MeV and 820 GeV*, *Astrophys. J.* **799** (2015) 86, [1410.3696].
11. K. M. Belotsky, A. A. Kirillov and M. L. Solovyov, *Development of dark disk model of positron anomaly origin*, *Int. J. Mod. Phys.* **D27** (2018) 1841010, [1802.04678].
12. K. Belotsky, A. Kamaletdinov, M. Laletin and M. Solovyov, *The DAMPE excess and gamma-ray constraints*, *Physics of the Dark Universe* **26** (Dec, 2019) 100333, [1904.02456].
13. J. I. Read, G. Lake, O. Agertz and V. P. Debattista, *Thin, thick and dark discs in  $\Lambda$ CDM*, *Monthly Notices of the Royal Astronomical Society* **389** (sep, 2008) 1041–1057, [0803.2714].
14. J. F. Navarro, C. S. Frenk and S. D. M. White, *A Universal density profile from hierarchical clustering*, *Astrophys. J.* **490** (1997) 493–508, [astro-ph/9611107].

15. J.-S. Niu, T. Li and F.-Z. Xu, *A Simple and Natural Interpretations of the DAMPE Cosmic Ray Electron/Positron Spectrum within Two Sigma Deviations*, *Eur. Phys. J. C* **79** (2019) 125, [1712.09586].



## 15 Dynamical Evolution of a Cluster of Primordial Black Holes

V.D. Stasenko \* and A. A. Kirillov \*\*

National Research Nuclear University MEPhI (Moscow Engineering Physics Institute)

**Abstract.** Evolution of a cluster of primordial black holes in the two-body relaxation approximation based on the Fokker-Planck equation is discussed. In our calculation, we consider the self-gravitating cluster with a wide range of black holes masses from  $10^{-4}M_{\odot}$  up to  $100M_{\odot}$  and the total mass  $10^5M_{\odot}$ . Moreover, we included a massive black hole in the cluster center which determines the evolution rate of the density profile in its vicinity.

**Povzetek.** Avtorja obravnavata razvoj kopice primordialnih črnih lukenj. Uporabita Fokker-Planckove enačbe v približku dvodelčne relaksacije. Obravnavata kopico črnih lukenj z masami od  $10^{-4}M_{\odot}$  do  $100M_{\odot}$  in s skupno maso  $10^5M_{\odot}$ , ki ji dinamiko določa lastno gravitacijsko polje. V središče kopice postavita masivno črno luknjo, ki določa časovno spremembo profila gostote v njeni okolici.

Keywords: primordial black holes, clusters of primordial black holes, the Fokker-Planck equation

PACS: 04.25.dg, 05.10.Gg

### 15.1 Introduction

The hypothesis of primordial black holes (PBHs) formation was suggested in [22]. Afterward, a few scenarios of PBHs production have been developed (see reviews [7, 13]). In our work, we consider those predicting the formation of PBHs as clusters. This mechanism was proposed in [14, 17, 18] where a collapse of large closed domain walls was discussed. The produced clusters may have extended mass spectra where masses range from  $\sim 10^{17}$  g [2, 3] up to  $\sim 10^4M_{\odot}$  [11] or even more [10]. These clusters have essential consequences for shedding light on some cosmological problems. Observational manifestations of the model and smoothing of some constraints (the recent restrictions on PBHs are considered in [7]) are widely discussed in reviews [4, 5] and references within. However, finding of clusters evidences is significantly related to the mass spectrum at a specified moment of the Universe history. Therefore, understanding of cluster dynamic play an essential role and is a main research subject of this paper.

\* E-mail: StasenkoVD@gmail.com

\*\* E-mail: AAKirillov@mephi.ru

Till now, a comprehensive study of clusters evolution has not been carried out. First efforts to retrace changes of clusters mass spectra were made in [5, 9, 15, 20]. The closest physical model to a PBH cluster is a globular cluster of stars. However, it does not have a wide mass range. Therefore, globular cluster theory could not be directly extrapolated to the PBHs cluster case. Moreover, the PBHs cluster may contain a massive central black hole (CBH). In work [1], stationary distribution of stars around a massive black hole was discussed. It was established that the density obeys the law  $\rho \propto r^{-7/4}$ . However, there are a few disadvantages of this work. First, the potential from star distribution is neglected in comparison with the potential of a CBH. Second, all stars have the same mass. Besides, as was shown in [12, 19, 21], a distribution around massive black holes isn't stationary.

We focus on describing the evolution of a PBHs cluster using the orbit-averaged Fokker-Planck equation in energy space. The considered clusters have a wide mass ranges. In addition, we include in our calculations a massive BH in a cluster center which determines behaviour of density profile in a central region.

## 15.2 The Fokker-Planck equation

We study the spherically symmetric system of gravitating point masses and assume relaxation time is much longer than an orbital period, and there is no isotropy in velocity space. According to the assumptions, the distribution function (DF)  $f$  describing PBHs in a cluster depends only on energy  $E$ :  $f(\mathbf{r}, \mathbf{v}) = f(E)$ . Evolution of the DF is described by the orbit-averaged Fokker-Planck equation which in the multi-mass case has the form [8, 21]:

$$\frac{\partial N_i}{\partial t} = \frac{\partial}{\partial E} \left( m_i D_E(E, f) f_i + D_{EE}(E, f) \frac{\partial f_i}{\partial E} \right), \quad (15.1)$$

where  $m_i$ ,  $f_i$  is mass and distribution function of  $i$ -th type of PBHs, respectively, and  $N_i(E, t) = 4\pi^2 p(E) f_i(E, t)$  is number density in energy space. Expressions for the coefficients in (15.1) are

$$\begin{aligned} D_E(E, f) &= 16\pi^3 \Gamma \sum_i \int_{\phi(0)}^E m_i f_i(E') p(E') dE', \quad (15.2) \\ D_{EE}(E, f) &= 16\pi^3 \Gamma \sum_i \left( q(E) \int_E^0 m_i^2 f_i(E') dE' + \right. \\ &\quad \left. + \int_{\phi(0)}^E m_i^2 f_i(E') q(E') dE' \right), \quad (15.3) \end{aligned}$$

where the sum goes over all types of masses and  $\Gamma = 4\pi G^2 \ln \Lambda$ ,  $\ln \Lambda$  is the Coulomb logarithm.  $p(E)$  and  $q(E)$  are given by

$$\begin{aligned} p(E) &= 4 \int_0^{\phi^{-1}(E)} dr r^2 \sqrt{2(E - \phi(r))}, \\ q(E) &= \frac{4}{3} \int_0^{\phi^{-1}(E)} dr r^2 \left[ 2(E - \phi(r)) \right]^{3/2}, \end{aligned} \quad (15.4)$$

where  $\phi^{-1}(E)$  is the root of the equation  $E = \phi(r)$ . Asymptotic expressions for  $q(E)$  and  $p(E)$  in the case of the Keplerian potential  $\phi(r) = -GM_{\bullet}/r$  is:

$$p(E) = \frac{\sqrt{2}\pi(GM_{\bullet})^3}{4(-E)^{5/2}} = -\frac{3q}{2E}, \quad q(E) = \frac{\sqrt{2}\pi(GM_{\bullet})^3}{6(-E)^{3/2}}, \quad (15.5)$$

which can be used to calculate  $p(E)$  and  $q(E)$  near the CBH or at large distances from the cluster. Here,  $M_{\bullet}$  is the CBH mass.

To study evolution of a self-gravitating system, it is necessary to solve together the Fokker-Planck equation (15.1) and the Poisson equation

$$\phi(r) = -4\pi G \left( \frac{1}{r} \int_0^r dr' r'^2 \rho(r') + \int_r^{\infty} dr' r' \rho(r') \right) - \frac{GM_{\bullet}}{r}, \quad (15.6)$$

where  $\rho(r)$  is given by the expression

$$\rho(r) = 4\pi \sum_i m_i \int_{\phi(r)}^0 dE f_i(E) \sqrt{2(E - \phi(r))} = \sum_i \rho_i(r). \quad (15.7)$$

The technique of joint solution of the Poisson equation (15.6) and the Fokker-Planck equation (15.1) was described in the work [8] and improved in [21].

In practice, the density profile is initially defined, not the distribution function. In order to obtain the initial distribution function, it is necessary to use the Eddington formula [6, 16]:

$$f_i(E) = \frac{\sqrt{2}}{4\pi^2 m_i} \frac{d}{dE} \int_E^0 \frac{d\phi}{\sqrt{\phi - E}} \frac{d\rho_i}{d\phi}. \quad (15.8)$$

### 15.3 Results

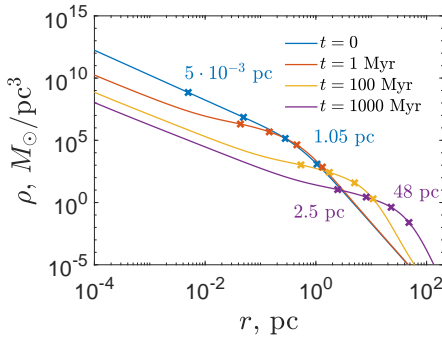
We choose the initial density profile of the cluster in the form:

$$\rho_i(r) = \rho_{0,i} \left( \frac{r}{r_0} \right)^{-2} \left[ 1 + \left( \frac{r}{r_0} \right)^2 \right]^{-3/2}, \quad (15.9)$$

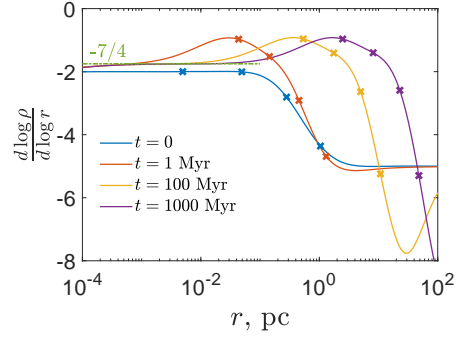
where  $\rho_{0,i}$  is the normalization factor and  $r_0 = 0.5$  pc. The mass spectrum is the same as in [5]

$$\frac{dN}{dM} \propto \frac{1}{M_{\odot}} \left( \frac{M}{M_{\odot}} \right)^{-2}, \quad (15.10)$$

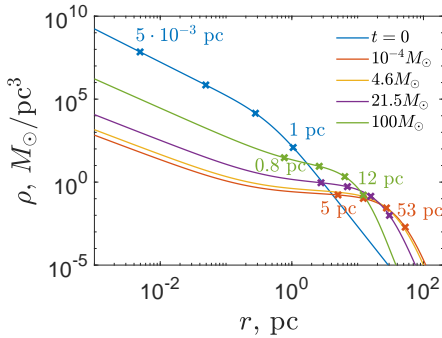
and PBHs masses range from  $10^{-4}M_{\odot}$  up to  $10^2M_{\odot}$ . We take the bin width such that the total masses of each component of PBHs are equal to each other. On a logarithmic scale, this corresponds to the same bin widths for the spectrum  $dN/dM \propto M^{-2}$ . Number of PBHs types is 10. The total mass of the cluster is  $10^5M_{\odot}$ , i.e. the total mass of each component is  $10^4M_{\odot}$ . The mass of the CBH is  $M_{\bullet} = 10^3M_{\odot}$



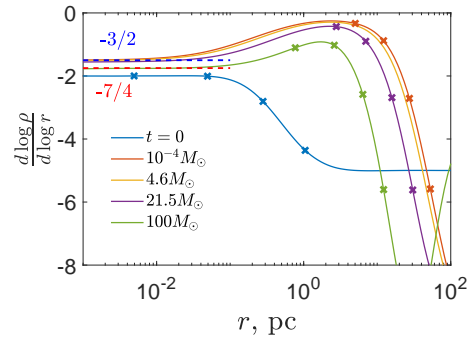
(a) The PBHs density profile in the cluster over time.



(b) The slope of the density profile.



(c) The density profiles of the different types of PBHs at the initial and the final times.



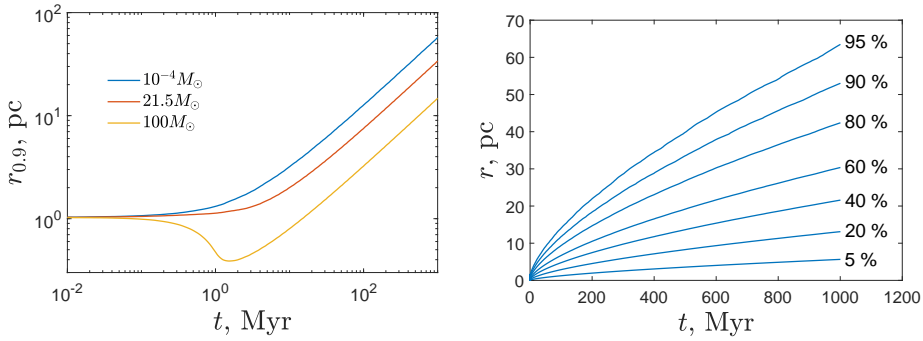
(d) The slopes of the density profiles for the different types of PBHs at the initial and the final times.

Fig. 15.1: The evolution of the mass density of PBHs in the cluster is shown. Crosses corresponds to radii containing 1, 10, 50 90 % (from left to right) of the total mass. The radius values refer to the first and the last crosses at the initial and the final ( $\sim 1$  Gyr) times.

After we define the initial density profile and mass spectrum, we could solve the equations (15.1) and (15.6). The solution technique can be found in [8,21]. Here we present the results.

Figure 15.1 shows the evolution of the total density profile of PBHs and its slope. After  $\sim 1$  Myr, the cusp  $\rho \propto r^{-7/4}$  is established in the central region, it is well known as the Bahcall-Wolf cusp [1]. Over time, the behaviour of the density profile extends to a larger values of radii. However, in figure 15.1b, one can see that only a small part of the cluster ( $< 1\%$ ) has the profile  $\rho \propto r^{-7/4}$ . It can also be seen the cluster size has grown by  $\sim 50$  times.

In figure 15.1c, it is shown that the behavior of the density profile in the central region of the cluster is determined by the most massive PBHs. Moreover, one can see heavy PBHs tend to be located near the central region of the cluster while the light ones tend to be at the periphery. Figure 15.1d presents that by the final



(a) The time dependence of the radii of the spheres containing 90% of the total mass for the different types of PBHs. (b) The evolution of the radii of the sphere containing the indicated percentage of the total cluster mass.

Fig. 15.2: The evolution of the mass distribution.

time  $\sim 1$  Gyr, the density profile of the heaviest component obtains the cusp in the central region  $\rho \propto r^{-7/4}$  and the lighter components achieve  $\rho \propto r^{-3/2}$ .

In order to show how the redistribution of masses occurs, figure 15.2a illustrates the time dependence of the radii  $r_{0.9}$  of the spheres containing 90% of masses of each component. It can be seen that at first 1 Myr, heavy PBHs are compressed toward the center of the cluster due to dynamical friction while other ones evolve in “a slow mode”. Then, the cluster begins to expand. Figure 15.2b shows the time dependence of the sphere radius for the whole cluster. Thus, one can find a significant increase in the cluster size by  $\sim 50$  times over  $\sim 1$  Gyr.

## Conclusion

In this paper, the evolution of the PBHs cluster within the Fokker-Plank framework is studied. We note the significant redistribution of the cluster structure leading heavy black holes tend to be located near the cluster center and lighter ones tend to be at the periphery. In addition, a significant increase in the cluster size by  $\sim 50$  times for a given initial density profile and mass spectrum is shown.

At the end of the conclusion, it should be noted the growth of the CBH mass due to gas accretion and capture of surrounding PBHs may change the cluster evolution rate, but it is beyond the scope of this research and should be considered separately.

## Acknowledgements

The authors are grateful to K. M. Belotsky and S. G. Rubin for useful discussions. The work was supported by the Ministry of Science and Higher Education of the Russian Federation, project “Fundamental properties of elementary particles and cosmology” No 0723-2020-0041.

## References

1. J. N. Bahcall and R. A. Wolf. Star distribution around a massive black hole in a globular cluster. *Astrophys. J.*, 209:214–232, Oct. 1976.
2. K. M. Belotsky, A. V. Berkov, A. A. Kirillov, and S. G. Rubin. Black hole clusters in our Galaxy. *Grav. Cosmol.*, 17(1):27–30, Jan. 2011.
3. K. M. Belotsky, A. V. Berkov, A. A. Kirillov, and S. G. Rubin. Clusters of black holes as point-like gamma-ray sources. *Astropart. Phys.*, 35(1):28–32, Aug. 2011.
4. K. M. Belotsky, A. E. Dmitriev, E. A. Esipova, V. A. Gani, A. V. Grobov, M. Y. Khlopov, A. A. Kirillov, S. G. Rubin, and I. V. Svadkovsky. Signatures of primordial black hole dark matter. *Mod. Phys. Lett. A*, 29(37), Nov. 2014.
5. K. M. Belotsky, V. I. Dokuchaev, Y. N. Eroshenko, E. A. Esipova, M. Y. Khlopov, L. A. Khromykh, A. e. A. Kirillov, V. V. Nikulin, S. G. Rubin, and I. V. Svadkovsky. Clusters of Primordial Black Holes. *Eur. Phys. J. C*, 79(3):246, Mar. 2019.
6. J. Binney and S. Tremaine. *Galactic Dynamics: Second Edition*. Princeton University Press, Princeton, 2008.
7. B. Carr and F. Kühnel. Primordial Black Holes as Dark Matter: Recent Developments. *Annu. Rev. Nucl. Part. Sci.*, 70(1):355–394, Oct. 2020.
8. H. Cohn. Late core collapse in star clusters and the gravothermal instability. *Astrophys. J.*, 242:765–771, Dec. 1980.
9. V. De Luca, V. Desjacques, G. Franciolini, and A. Riotto. The Clustering Evolution of Primordial Black Holes.
10. V. I. Dokuchaev, Y. N. Eroshenko, and S. G. Rubin. Quasars formation around clusters of primordial black holes. *Grav. Cosmol.*, 11:99–104, June 2005.
11. V. I. Dokuchaev, Y. N. Eroshenko, and S. G. Rubin. Early formation of galaxies induced by clusters of black holes. *Astron. Rep.*, 52(10):779–789, Oct. 2008.
12. M. J. Duncan and S. L. Shapiro. Star clusters containing massive, central black holes. IV - Galactic tidal fields. *Astrophys. J.*, 253:921–938, Feb. 1982.
13. M. Y. Khlopov. Primordial black holes. *Res. Astron. Astrophys.*, 10(6):495–528, June 2010.
14. M. Y. Khlopov, S. G. Rubin, and A. S. Sakharov. Primordial structure of massive black hole clusters. *Astropart. Phys.*, 23(2):265–277, Mar. 2005.
15. L. A. Khromykh and A. A. Kirillov. The gravitational dynamics of the primordial black holes cluster. *J. Phys. Conf. Ser.*, 1390, Nov. 2019.
16. D. Merritt. *Dynamics and Evolution of Galactic Nuclei*. Princeton University Press, Princeton, 2013.
17. S. G. Rubin, M. Y. Khlopov, and A. S. Sakharov. Primordial Black Holes from Non-Equilibrium Second Order Phase Transition. *Grav. Cosmol.*, S6:51–58, May 2000.
18. S. G. Rubin, A. S. Sakharov, and M. Y. Khlopov. The Formation of Primary Galactic Nuclei during Phase Transitions in the Early Universe. *J. Exp. Theor. Phys.*, 92(6):921–929, June 2001.
19. S. L. Shapiro. Star clusters, self-interacting dark matter halos, and black hole cusps: The fluid conduction model and its extension to general relativity. *Phys. Rev. D*, 98(2), July 2018.
20. M. Trashorras, J. García-Bellido, and S. Nesseris. The clustering dynamics of primordial black holes in N-body simulations.
21. E. Vasiliev. A New Fokker-Planck Approach for the Relaxation-driven Evolution of Galactic Nuclei. *Astrophys. J.*, 848(1):10, Oct. 2017.
22. Y. B. Zel'dovich and I. D. Novikov. The Hypothesis of Cores Retarded during Expansion and the Hot Cosmological Model. *Sov. Astron.*, 10:602, Feb. 1967.



## Poem by Astri Kleppe





## 16 Earth

Astri Kleppe

*“Did you know that the Creation begins with the seconds letter of the Hebrew alphabet? Thus you can imagine that the real beginning was not included, but gave rise to everything - by disappearing.”*

*Beginning*

A sunny summer morning,  
when the Earth  
came into being, water did not  
yet exist, and everything  
was longing for something  
like rain.

A few uncertain clouds  
eventually  
came sailing from a place  
behind the sun,  
and drops of water fell,  
and everything was drinking.  
Grass was drinking.  
Trees were drinking,  
all the thirsty  
little birds were drinking.  
But happiest of all was the enormous  
*ur-fish*, and the carps  
that all the time had longed  
for the arrival of the sea.

The water lived, it roared  
and waved with  
symmetries, no angels were  
in sight.

The ground was beaten  
by the rainfalls, under stones and rocks  
a quiet murmur from some early  
mouths was heard.  
One day a face with eyes and ears  
emerged, and soon  
a song was sung. That’s how the Earth came  
into being.





---

BLEJSKE DELAVNICE IZ FIZIKE, LETNIK 21, ŠT. 2, ISSN 1580-4992

BLED WORKSHOPS IN PHYSICS, VOL. 21, NO. 2

Zbornik 23. delavnice 'What Comes Beyond the Standard Models', Bled, 4. – 12. julij 2020 [Virtualna delavnica 6.–10. julij 2020], Vol. 2: Further Talks And Scientific Debuts

Proceedings to the 23rd workshop 'What Comes Beyond the Standard Models', Bled, July 4.–12., 2020 [Virtual Workshop, July 6.–10., 2020] Vol. 2: Further Talks And Scientific Debuts

Uredili Norma Susana Mankoč Borštnik, Holger Bech Nielsen in Dragan Lukman

Izid publikacije je finančno podprla Javna agencija za raziskovalno dejavnost RS iz sredstev državnega proračuna iz naslova razpisa za sofinanciranje domačih znanstvenih periodičnih publikacij

Brezplačni izvod za udeležence

Tehnični urednik Matjaž Zaveršnik

Založilo: DMFA – založništvo, Jadranska 19, 1000 Ljubljana, Slovenija

Natisnila tiskarna Itagraf v nakladi 130 izvodov

Publikacija DMFA številka 2123

---